

Chapter 9

100 Years of Progress in Boundary Layer Meteorology

MARGARET A. LEMONE,^a WAYNE M. ANGEVINE,^{b,c} CHRISTOPHER S. BRETHERTON,^d FEI CHEN,^a
 JIMY DUDHIA,^a EVGENI FEDOROVICH,^e KRISTINA B. KATSAROS,^f DONALD H. LENSCHOW,^a
 LARRY MAHRT,^g EDWARD G. PATTON,^a JIELUN SUN,^{a,h} MICHAEL TJERNSTRÖM,ⁱ AND JEFFREY WEIL^a

^a National Center for Atmospheric Research, Boulder, Colorado

^b CIRES, University of Colorado, Boulder, Colorado

^c NOAA ESRL, Chemical Sciences Division, Boulder, Colorado

^d Department of Atmospheric Sciences, University of Washington, Seattle, Washington

^e School of Meteorology, University of Oklahoma, Norman, Oklahoma

^f NorthWest Research Associates, Whidbey Island, Washington

^g NorthWest Research Associates, Corvallis, Oregon

^h NorthWest Research Associates, Boulder, Colorado

ⁱ Department of Meteorology, and Bolin Centre for Climate Research, Stockholm University, Sweden

ABSTRACT

Over the last 100 years, boundary layer meteorology grew from the subject of mostly near-surface observations to a field encompassing diverse atmospheric boundary layers (ABLs) around the world. From the start, researchers drew from an ever-expanding set of disciplines—thermodynamics, soil and plant studies, fluid dynamics and turbulence, cloud microphysics, and aerosol studies. Research expanded upward to include the entire ABL in response to the need to know how particles and trace gases dispersed, and later how to represent the ABL in numerical models of weather and climate (starting in the 1970s–80s); taking advantage of the opportunities afforded by the development of large-eddy simulations (1970s), direct numerical simulations (1990s), and a host of instruments to sample the boundary layer in situ and remotely from the surface, the air, and space. Near-surface flux-profile relationships were developed rapidly between the 1940s and 1970s, when rapid progress shifted to the fair-weather convective boundary layer (CBL), though tropical CBL studies date back to the 1940s. In the 1980s, ABL research began to include the interaction of the ABL with the surface and clouds, the first ABL parameterization schemes emerged; and land surface and ocean surface model development blossomed. Research in subsequent decades has focused on more complex ABLs, often identified by shortcomings or uncertainties in weather and climate models, including the stable boundary layer, the Arctic boundary layer, cloudy boundary layers, and ABLs over heterogeneous surfaces (including cities). The paper closes with a brief summary, some lessons learned, and a look to the future.

1. Introduction

How do we define the atmospheric boundary layer (ABL)? Here are some definitions from textbooks:

“that part of the troposphere that is directly influenced by the presence of the earth’s surface, and responds to surface forcings with a timescale of about an hour or less” (Stull 1988, p. 2).

“the layer of air directly above the earth’s surface in which the effects of the surface (friction, heating, and cooling) are felt directly on time scales less than a day, and in which

significant fluxes of momentum, heat, or matter are carried by turbulent motions on a scale of the order of the depth of the boundary layer or less” (Garratt 1992, p. 1).

“lowest kilometer” or “lowest portion of the atmosphere, which intensively exchanges heat as well as mass and momentum with the earth’s surface” (Sorbján 1989, p. 1).

The time scales in these definitions are fundamental, but vary by an order of magnitude, a function of context and application. On the short end, it takes minutes for air in a buoyant updraft to rise from a strongly heated surface to 1000 m above ground, where it can deposit pollutants or form a cloud; over a 24-h period, the temperature in the boundary layer varies more strongly than the air higher

Corresponding author: Margaret A. LeMone, lemone@ucar.edu

DOI: 10.1175/AMSMONOGRAPHS-D-18-0013.1

© 2019 American Meteorological Society. For information regarding reuse of this content and general copyright information, consult the [AMS Copyright Policy](https://www.ametsoc.org/PUBSReuseLicenses) (www.ametsoc.org/PUBSReuseLicenses).

up, which can lead to killer frosts on clear nights with weak wind. Fields of wind, temperature, pressure, and other flow variables in the lowest atmosphere are mostly turbulent—complex, three-dimensional, irregular, and stochastic. Turbulent motions in the ABL drive the exchange of momentum, heat, and moisture between the surface and the atmosphere, and strongly affect human activities.

“Boundary layer” has a specific meaning in theoretical and experimental fluid dynamics, and the ABL is both similar to and different from those boundary layers. It is similar in being directly affected by a surface, but different in scale (on the order of a kilometer rather than a meter or less).¹ Laboratory flows have well-defined boundary conditions, while Earth’s heterogeneous surface, variation in radiation, and weather provide conditions that are less well behaved. Nevertheless, it is convenient to divide the boundary layer into an inner layer (the “surface” layer) and outer layers, using the vertical stratification of temperature, wind, and turbulence intensity.

The textbooks provide a crude definition of the surface layer, which “occupies the lowest 10% of the whole ABL, which is about 10^0 to 10^2 m” (Sorbjan 1989); and is “the region at the bottom of the boundary layer where turbulent fluxes and stresses vary by less than 10% of their magnitude.” (Stull 1988, p. 10). The two definitions are equivalent for the commonly studied convective boundary layer (CBL), for which the fluxes vary almost linearly with height.

Here, we mostly restrict ourselves to the fair-weather ABL, following the tradition of most boundary layer research. We start with the “initial conditions,” recognizing the achievements of classical chemistry and physics, followed by those of early meteorologists often motivated by agriculture, and early fluid dynamicists who focused on turbulence and turbulent boundary layers, often in support of aircraft design, and follow with the story of the development of large-eddy simulation starting in the late 1960s. The discoveries and course corrections in our learning over the last 100 years were also enabled by development of instrumentation, both in the field and in the laboratory, and summarized in Stith et al. (2019). The material that follows is organized by topic, starting with the surface layer over land and ocean, and then moving upward to the entire ABL and its evolution under “ideal” (fair weather, no cloud) conditions. The complications of a heterogeneous surface and clouds follow, along with a description of the

boundary layer over the Arctic Ocean, because we can learn from its unique characteristics.² This is followed by a brief summary of how our knowledge of surface, boundary layer, and cloud processes is synthesized in terms of dispersion models, and the land surface and ABL parameterizations used in weather and climate models. We close with a historical synopsis, some lessons learned, and challenges and opportunities for the future.

This narrative is by its nature incomplete, reflecting the interests and backgrounds of its authors; and our identification of “first” discoveries should be taken with caution. We refer interested readers to a few books used heavily in preparation in this manuscript, in particular *A Voyage through Turbulence*, by Davidson et al. (2011), *The Climate near the Ground*, by Geiger (1966); and *Meteorology: A Historical Survey*, Vol. I, by Khrgian (1959, translated from Russian in 1970). We also consulted many textbooks along the way; most useful was *Evaporation into the Atmosphere*, by W. Brutsaert (1982), because of its emphasis on history. Finally, *The Thermal Theory of Cyclones*, by G. Kutzbach (1979) provided some surprising information about how much was known during the 1800s.

2. Historical origins

a. Early background

Our earliest knowledge of surface processes derives from agriculture. Farmers were certainly aware, for example, that killing frosts at night were more likely in low-lying areas. Indeed, McAdie (1915) discusses the association of cool air with lower elevations and the role of cold-air drainage, but more as a motivation for the real theme of his paper, entitled “The Theory and Practise (sic) of Frost Fighting.” At the same time, scientists were exploring the relationship of temperature with height at different times of the day. For example, Dines (1882) compared maximum and minimum temperatures at around 5 and 50 ft, consistently finding average 5-ft minimum temperatures about a degree Fahrenheit (°F) lower than at 50 ft, and average maximum temperatures about 0.5°–2.3°F higher, with the largest differences under clear skies. Based on observing nighttime temperature drops above and below the top of fog banks, he concluded that fog-bank tops, like grasses under clear skies, cool as a result of outgoing infrared radiation. The necessary measurements to verify this behavior were available not long after: the first longwave

¹ Readers interested in exploring the differences further are referred to Nieuwstadt (1998).

² We turn our attention to the Arctic rather than the poles because its boundary layer is over an ocean with ice as well as subject to high-latitude conditions, which makes it truly unique. Also, there appears to be far less written about the Antarctic boundary layer.

radiometers were invented in the 1890s (Hansch et al. 2006). Solar radiation was being measured by the mid-nineteenth century. Both measurements were likely used in agricultural research shortly after 1900 (Geiger 1966).

The concepts of the ideal gas law, the adiabatic process, and the release of latent heat by condensing water were all developed by 1841, when James Pollard Espy described how a plume of air, heated by Earth's surface, rises to form a cloud in his *Philosophy of Storms* (Kutzbach 1979). Described in terms familiar today, he set the stage for describing how the daytime boundary layer heats up, by pointing out that a parcel of air, rendered buoyant by heating and evaporation at the surface, cools dry adiabatically as it rises, until it reaches the condensation level, where the cooling is slowed by the release of latent heat. The onset of manned balloon flights in the 1700s and 1800s made many aware that the temperature changes with height, with more systematic measurements after around 1850–70 (Kutzbach 1979). Pomortsev used a series of manned-balloon training flights in Russia between 1885 and 1897 to document the change of wind with height until it was parallel to the isobars,³ and he associated that change with friction (proportional to the square of the wind speed). He also observed sudden changes in temperature and humidity (likely at the ABL capping inversion), and a dropoff of temperature with height at close to the adiabatic lapse rate beneath (Khrgian 1959, p. 270).

b. Early development of turbulence theory

The onset of contemporary boundary layer meteorology benefitted greatly from the developments in fluid dynamics around the beginning of the twentieth century. The term *boundary layer* was introduced by the German engineer Ludwig Prandtl (1905), who demonstrated that the flow around a solid body can be divided into two regions: a thin layer close to the body, where surface friction plays an essential role, and the external region, where the influence of the body's surface can be neglected. On the other hand, the existence of the two distinctively different types of fluid motion—laminar and turbulent—was recognized by the first half of the nineteenth century. As for the term *turbulence*, it was likely first proposed in the fluid-mechanical context in 1887 by Sir William Thomson (Lord Kelvin; Thomson 1887), a prominent British physicist and mathematician.⁴ Joseph Boussinesq, a French

mathematician and physicist, who introduced the concept of turbulent (eddy) diffusivity widely used in atmospheric boundary layer theory and modeling, described turbulent fluctuations of velocity as tumultuous motions or eddy agitations in his 1897 book (Boussinesq 1897).⁵

Foundations of modern turbulence theory were laid at the end of the nineteenth century by the British mathematician and engineer Osborne Reynolds. In his pioneering works of 1883 and 1895, Reynolds focused on conditions that determine laminar versus turbulent character of fluid flows in pipes and proposed a dimensionless parameter (Reynolds number Re , which is named after him) to be used as a criterion for dynamic similarity of viscous incompressible flows (Reynolds 1883, 1895). This number may be interpreted as the ratio of kinetic energy production by inertial forces to the energy dissipation by viscous forces and is often written as $Re = UD/\nu$, where U is a characteristic flow speed, D a characteristic flow dimension (length scale), and ν the molecular kinematic viscosity. Flows with sufficiently high Re are expected to be turbulent, and flows with sufficiently low Re are laminar. In the spirit of statistical description of turbulent flows, Reynolds also suggested separating turbulent flow variables into the slowly varying mean and highly variable fluctuating parts (components) in order to study turbulent flow in terms of mean-flow variables and statistics of turbulent fluctuations of various orders. Reynolds's original approach to evaluating turbulence statistics was based on averaging flow fields over a spatial length (or volume), according to certain rules. These rules were formulated in a way that later facilitated their implementation in the Reynolds-averaged equations of fluid dynamics extensively used in boundary layer meteorology. The presently adopted concept of turbulence averaging, which is understood as ensemble averaging, differs considerably from the averaging approach put forward by Reynolds, but remarkably preserves the Reynolds averaging properties.

The story of the publication of Reynolds's seminal 1895 paper was not as glorious as one might expect. Sir George Stokes and Dr. Horace Lamb (he was just a professor at that time), both very prominent figures in fluid dynamics in those days, were approached by the *Transactions of the Royal Society* editor Lord Rayleigh to review the article. They were rather lukewarm in their “unenthusiastic, even grudging, acquiescence to the paper's acceptance for publication” (Lauder 2015). To a great extent, this lack of appreciation is thought to

³According to Ansell et al. (2006), several sites were taking pressure measurements in the late 1800s, providing some plausibility to at least having surface pressure analyses available.

⁴Leonardo de Vinci anticipated the existence of turbulence 400 years earlier, describing flow as a “principal current” and “random and reverse motions” (Richter 1970, Plate 20 and Note 389).

⁵Oberbeck (1888) also qualitatively describes an eddy viscosity, mentioning “currents of a local nature which will increase the (internal) friction” (p. 164 of English translation), suggesting the idea was around.

be due to Reynolds's excessively wordy style of writing, his overfocus on well-established procedures and principles while leaving his novel ideas unexplained, and his tendency to use a self-invented terminology that was puzzling to the referees. The long-term effect of the paper was nevertheless tremendous, as it outlined a practical and significant approach to study turbulent flows both experimentally and theoretically.

Interestingly, during the same year Reynolds's paper on turbulence decomposition and averaging went to print, Lamb published his *Hydrodynamics* (1895), which is regarded as the first fluid-mechanics textbook. The notion of turbulent flow appears toward the very end of the book, with the author presenting a review of Reynolds's experiments in pipes and pointing to principal differences between laminar and turbulent flows, calling the latter "wildly irregular" with "interlacing and constantly varying streams, crossing and recrossing the pipe." Shortly before his death in 1934, Sir Horace Lamb wittily expressed the difficulty of explaining and studying turbulence by reportedly saying in his address to the British Association for the Advancement of Science: "*I am an old man now, and when I die and go to Heaven, there are two matters on which I hope to be enlightened. One is quantum electrodynamics, and the other is turbulence. About the former, I am really rather optimistic*" (Goldstein 1969).

The first analytical treatment of boundary layer flow in the geophysical context is attributed to Vagn Ekman (1905), a Swedish oceanographer, who employed momentum balance equations for viscous fluid to explain Fritjof Nansen's observation during the *Fram* expedition (Mohn 1905) that the surface current carried sea ice in a direction 20°–40° to the right of the prevailing wind direction. Although the problem setup was not particularly meteorological, Ekman mentioned possible atmospheric applications of his model, pointing to the analogy between the three-way balance among the pressure-gradient, Coriolis, and friction forces in the atmospheric and oceanic boundary layers. Ekman's treatment of turbulence (specifically, turbulent friction) in his equations was rather straightforward. Based on the consideration that transfer of momentum between moving layers of fluid "owing to the irregular formation of eddies" is more "intense" than "due to friction alone," he introduced a virtual viscosity with a value "much greater" than the actual molecular viscosity. (It is quite possible that Ekman was not aware of Boussinesq's introduction of eddy viscosity.) Ekman also employed the momentum balance equations in their original form, that is without applying any decomposition of flow fields in mean and fluctuating components, and without subsequent averaging of equations following Reynolds or in some other

manner. An approach very similar to that of Ekman was later used to describe atmospheric boundary layer wind profiles in the work of Filip Åkerblom (1908), another Swedish geophysicist, who never mentioned Ekman's model in his paper but cited Lamb (1895) while deriving the governing equations. Carl-Gustaf Rossby, however, states in his 1927 review article (Rossby 1927) that Åkerblom was led to his study by Ekman's (1905) paper.

The view of turbulent exchange in the atmosphere as a "process like molecular conduction but much more vigorous" was further advanced by Geoffrey Taylor, a British mathematician and physicist, in his 1915 paper about eddy motion in the atmosphere (Taylor 1915). He put forward the idea regarding "coherent fluid masses" that "move a certain distance up or down vertically carrying all their transferable properties and then mix with the surroundings in which they find themselves." The name for such a distance, the "mixture length" (it transformed with time into "mixing length" in English scientific literature) was introduced in 1925 by Ludwig Prandtl, who allegedly was not aware of Taylor's work (Wyngaard 2010). Interestingly, Taylor abandoned his own mixing-length concept in his famous 1921 paper on the nature of turbulent diffusion, where he pointed to the crucial role of covariances of turbulent fluctuations of different field variables as measures of transport of substances in a turbulent flow. In Prandtl's works, however, the notion of mixing length was exploited extensively and was used to lay the foundation for a class of approaches that we currently call semiempirical turbulence theories (Monin and Yaglom 1971). The advancement of these theories, besides Prandtl and Taylor, was strongly influenced by Prandtl's student Theodore von Kármán.

The semiempirical theories, which form the basis for the logarithmic profile developed by von Kármán (1931) to describe the flow of neutrally stratified air as a function of height and later the flux-profile relationships discussed in section 3, are based on the analogy between turbulence and random molecular motion. Besides using notions of mixing length (analogous to the molecular free path) as the turbulence length scale, and turbulent diffusivities (analogous to molecular diffusivities), semiempirical relations can be constructed between the fluxes of momentum and scalars and their corresponding gradients. These relationships have been derived from observations of turbulent flow in the laboratory and in the atmosphere, complemented with considerations of dimensionality and symmetry, plausible physical arguments, scale analysis, and similarity theories.

Semiempirical theories also played an especially important role in seeking practical solutions to the so-called turbulence closure problem as applied to the

ABL parameterization schemes discussed in [section 10](#). This problem finds its origin in the chain of differential equations for statistical moments of turbulent flow fields derived by [Keller and Friedmann \(1924\)](#), referred in the literature as Friedmann–Keller equations, in which expressions for the low-order turbulence moments unavoidably contain terms with higher-order moments. Thus, the sequence of the equations appears to be infinite, as any individual subset of these equations remains unclosed, that is, it contains more unknowns than equations available to solve for these unknowns. Semiempirical methods and hypotheses were essential in formulation of physical assumptions that enabled closing the lowest-order equations from the Friedmann–Keller set containing only first- (mean fields) and second-order (variances and covariances) turbulence statistics in terms of eddy-exchange coefficients [the so-called Reynolds-Averaged Navier–Stokes (RANS) equations].

One more group of efforts dating back to the 1920s and 1930s focused on understanding the physical mechanism of turbulence. Lewis Richardson, a British mathematician and meteorologist, hypothesized in 1922 that turbulent flows are composed of eddies of different sizes, and that kinetic energy of the flow cascades from large to small scales of motion. According to Richardson, eddies of a particular size emerge because of instability of eddies of a larger size, acquire energy from these unstable eddies, lose stability themselves, and fall apart transferring energy to the smaller eddies. The largest-scale eddies are produced as a result of the instability of the mean motion. This cascading generation of smaller and smaller eddies continues until the eddies become small enough to feel the direct effect of viscosity, which plays a stabilizing role by preventing the smallest eddies from further destruction, while the transferred energy dissipates into heat. That was a fundamental insight in the mechanism of energy transfer in the turbulent flow, although Richardson did not come up with any mathematical formulation of his theory. In 1926, Richardson made a breakthrough contribution to the theory of turbulent diffusion by establishing through physical arguments that the effective diffusion coefficient for a plume of passive constituent in developed turbulence is proportional to the four-thirds power of the characteristic length scale of the plume ([Richardson 1926](#)). Until the seminal works of Kolmogorov and Obukhov in the early 1940s (discussed below), this was the only quantitative prediction regarding the physical behavior of small-scale turbulence ([Monin and Yaglom 1971](#)). [Richardson \(1920\)](#) also developed a criterion for turbulence breakdown in sheared, stratified flows known today as the Richardson number.

Another important contribution to conceptual understanding of small-scale turbulent motions was made in 1935 by Taylor, who introduced the notion of homogeneous and isotropic turbulence, for which the probability distributions of the fluid variables are the same, regardless of translation, reflection, or orientation of the coordinate system ([Taylor 1935](#)). Under assumptions of homogeneity and isotropy, turbulent flow becomes more mathematically tractable in terms of the Friedmann–Keller equations, despite the fact that all fundamental difficulties associated with structural properties of these equations remain intact. Although the assumptions of homogenous and isotropic turbulence are never generally satisfied for any actual atmospheric turbulent flow, the mathematical tools developed for such an idealized turbulence state turned out to be useful to describe statistical turbulence structure in real flows (including atmospheric ones) at large Reynolds numbers, where small-scale turbulence may be considered locally homogeneous and locally isotropic.

The next big step in the development of turbulence theory in the first half of the twentieth century occurred when two Russian scientists—Andrey [Kolmogorov \(1941a,b\)](#) and Alexander [Obukhov \(1941\)](#)—laid the foundation for modern quantitative theory of the energy transfer processes in turbulent flows, which had paramount implications for fundamental and applied aspects of boundary layer meteorology. Kolmogorov significantly refined Richardson’s concept of the turbulence energy cascade in physical terms and put it on a solid mathematical basis. He pointed out that, no matter how inhomogeneous and anisotropic the large-scale structural flow elements are, the small-scale turbulent fluctuations in a developed turbulent flow with a very large Reynolds number would be homogeneous and isotropic. The fluctuations would also be quasi-stationary on the time scale of evolution of the mean flow. Based on such considerations, Kolmogorov formulated two hypotheses. First, that statistical properties of small-scale turbulence fluctuations are controlled by only two parameters: the kinematic viscosity of the fluid and the turbulence kinetic energy dissipation rate (which is also a measure of energy transport across the turbulence spectrum, i.e., from large to small turbulent eddies). Combinations of these two parameters provide length, velocity, and time scales of the smallest turbulent fluctuations that exist in a given turbulent flow (the so-called Kolmogorov microscales). With his second hypothesis, Kolmogorov postulated and physically substantiated the existence of the so-called inertial range of turbulence scales that are much larger than the Kolmogorov length scale, but much smaller than the scale of largest turbulent motions originating from instabilities of the mean flow. Within this range, the statistical regime

of turbulence is determined solely by the energy dissipation rate. For turbulence in the inertial range (or as we call it today, *inertial subrange*), Kolmogorov established the now famous two-thirds law for the scale dependence of the structure function of velocity fluctuations, and Obukhov derived the equivalent and even more widely known minus-five-thirds law for decay of velocity spectral density with wavenumber. This so-called $-5/3$ spectrum has since been applied in turbulence modeling, is often used to evaluate both measurements and large-eddy simulations for convective boundary layers, and provides a tool to estimate viscous dissipation.

c. Large-eddy simulation

Although the birth of large-eddy simulation (LES) occurred well into the twentieth century, its significance to boundary layer meteorology merits a brief treatment here. The eddy size in the ABL varies from a few kilometers down to a few millimeters—too much to resolve directly by even the most advanced computers today, so LES is designed to resolve a subset—the large eddies (of order of ABL depth down to tens of meters to meters)—that account for most of the turbulence kinetic energy and fluxes, while parameterizing the effects of the smaller eddies. By the middle of the twentieth century, development of electronic computers enabled the development of numerical weather prediction (NWP)⁶ and general circulation models (GCMs), (see [Randall et al. 2019](#); [Benjamin et al. 2019](#)), providing a foundation for LES development.

The ready availability of a such a powerful (for the time) computer enabled James W. Deardorff of the National Center for Atmospheric Research (NCAR) to develop the first LES in the late 1960s, with significant input from Douglas K. Lilly, who arrived at NCAR in 1964 with numerical-modeling insights he and colleagues developed at the General Circulation Laboratory (a predecessor of the Geophysical Fluid Dynamics Laboratory at Princeton; [Kanak 2004](#)). As in the case of NWP models and GCMs, the idea was to solve the rate equations for the relevant flow variables on a grid, while representing subgrid effects (smaller, unresolved scales) with some sort of parameterization. However, unlike NWP models and GCMs, the grid spacing used by LES was sufficiently fine that the simulations generated 3D time dependent random fields, that is, the LES solutions were stochastic in space and time. Early LES employed horizontal periodic boundary conditions (consistent with the assumption of horizontal homogeneity), effectively generating turbulent inflow and outflow conditions required by the computations.

Not long after, more modifications brought LES closer to the real atmosphere, with radiation included in [Deardorff \(1974a\)](#), and clouds along with the effects of horizontal advection and subsidence in [Sommeria \(1976\)](#). The domains for these early LES ranged from 2 to 5 km in the horizontal directions, and up to 2 km in the vertical direction, with horizontal grid spacing between 50 and 125 m, and the vertical spacing 50 m. Because of the finer resolutions needed to resolve the large eddies and limited computer capability, it took more than an additional decade until the first successful LES of the stable boundary layer was conducted by [Mason and Derbyshire \(1990\)](#).

One of the most challenging aspects of LES is accounting for the impacts of the subgrid-scale (SGS) eddies, those too small to be resolved. The first, and still most commonly used parameterizations assume that the SGS fluxes are proportional to the eddy-exchange coefficients for momentum K_M and heat K_H . In his early LES work, [Deardorff \(1972a\)](#) used an expression for K_M inspired by that derived by [Smagorinsky \(1963\)](#) for NWP/GCMs, with theoretical roots in the seminal work by [Lilly \(1966a\)](#). In the Smagorinsky–Lilly formulation, K_M is a function of the strain rate tensor, the grid spacing, and a constant (the “Smagorinsky constant”), with $K_H = 3K_M$, or equivalently, the turbulent Prandtl number $\text{Pr}_T \equiv K_M/K_H = 1/3$. At the lowest grid level, however, Deardorff set $\text{Pr}_T \sim 1$ based on measurements described in [Businger \(1966\)](#), an early precedent to the universal practice of requiring the near-surface flow fields in LES to match Monin–Obukhov similarity theory (see [section 3b](#)). [Lilly \(1962\)](#) included the effects of buoyancy by allowing K_M to vary with Richardson number in a simulation of a two-dimensional thermal. [Deardorff \(1980a\)](#) was the first to apply a turbulent kinetic energy (TKE) scheme⁷ for which K_M is a function of the subgrid TKE [see (9-13), [section 4](#)], thus accounting for the effects of pressure fluctuations and turbulent transport as well as buoyancy, shear, and dissipation. In this SGS model, Pr_T was weakly dependent on thermal stratification. [Deardorff \(1973\)](#) provides an insightful review of these early SGS model developments.

Most LES SGS models require that the grid size lies within the inertial subrange, so that turbulence could be treated as isotropic, something that applies best away from the lower boundary, very stable layers, or with sufficiently small grid spacing (e.g., [Sullivan et al. 1994](#) and references therein). A more fundamental problem is

⁶ Which was anticipated by [Richardson \(1922\)](#).

⁷ Called the Deardorff TKE scheme in the review of LES by [Moeng and Sullivan \(2015\)](#), which credits Deardorff with this approach, likely inspired in part by discussions with Lilly, and earlier papers by [Lilly \(1966a, 1967\)](#).

the assumption that these representations are deterministic at each point, when in fact they are deterministic only in an average (or ensemble) sense. At any given time, energy at a grid point can be transported upscale (backscattered) rather than only downscale as implied in both the Smagorinsky–Lilly and Deardorff (1980a) TKE schemes by analogy to molecular transport. Mason and Thomson (1992) addressed this problem by modifying the Smagorinsky-type SGS scheme in their LES to include stochastic upscale flow of energy (backscatter) from the subgrid to resolved scales following the ideas of Leith (1990). An alternative, more phenomenological approach was proposed by Kosović (1997).

The origin of LES has roots in the atmospheric science community, but the engineering community rapidly adopted the technique (e.g., Reynolds 1976) and started to benefit the atmospheric boundary layer community, especially in the context of representing subgrid effects.⁸ Leonard (1974) and Germano (1986), for example, provided a useful way to represent SGS parameterization for the filtered Navier–Stokes equations, by dividing the subgrid stresses into three sets of terms that are Galilean invariant and independent of the filter used to separate resolved and subgrid scales. Findikakis and Street (1979) truncated the subgrid-scale rate equations to develop a set of algebraic equations for subgrid-scale heat and momentum transport as an alternative to the eddy-diffusion models. Deardorff (1980a) refers to the Findikakis–Street paper in interpreting his LES of a stratocumulus-topped boundary layer. Likewise, Moeng (1984), in her landmark paper that develops an LES solving the horizontal equations in spectral space, notes that solving the horizontal equations in this way facilitates handling at least partially the so-called Leonard (1974) stresses in the treatment of unresolved motions. The cross-field fertilization between the geophysical and engineering communities has continued to this day. In the United States, for example, many major papers on LES have come from engineering departments at Stanford, the University of Minnesota, and Johns Hopkins, among others, and several individuals with engineering backgrounds are working on LES at atmospheric science institutions or university departments.

Moeng (1984) believed that because “the large eddies are much more important and flow dependent than the small eddies,” that LES would be “relatively insensitive to the parameterization for the small eddies,” which was verified for the CBL based on a comparison of four

different LES codes (Nieuwstadt et al. 1992). LES intercomparisons on modest meshes $\sim 100^3$ show larger differences for a neutral Ekman layer (Andr n et al. 1994) and a stable boundary layer (Beare et al. 2006); most of the differences were related to SGS parameterizations. This is of course largely because the turbulent eddies are smaller in the latter cases, so that the SGS representations are more exposed, especially near the lower boundary, where smaller eddies are more important. Sullivan and Patton (2011), using meshes of 1024^3 , find LES solutions numerically converge provided there is adequate separation between the energy containing eddies and those near the filter cutoff scale.

An alternative type of SGS scheme involves the so-called dynamic approach, in which the LES fields are filtered using two (or more) different filters and variations between the filtered fields are used to derive the subgrid fluxes. Meneveau et al. (1996), Port -Agel et al. (2000), and Bou-Zeid et al. (2005) developed a series of dynamic models using different averaging procedures in time or space to estimate the local Smagorinsky constant from the resolved-scale fields during the LES run rather than having to rely on a globally prescribed value, and Port -Agel (2004) proposed a similar treatment for K_H . Eddy-diffusion schemes, however, must produce forward scattering.⁹ This shortcoming is avoided in the dynamic reconstruction method of Chow et al. (2005), through use of the resolved subfilter scales, and by Lu and Port -Agel (2010), who develop a phenomenological dynamic approach. [For a brief discussion of some dynamic and other SGS schemes, see Shi et al. (2018b).] Ludwig et al. (2009) compared several SGS schemes for a neutral boundary layer, including some of the dynamic schemes, and found differences that show up even for the largest eddies, with the largest differences between the simple eddy-viscosity schemes and dynamic models that include backscatter, and the dynamic schemes working the best. Similarly, Shi et al. (2018a) found dynamic schemes performed better in a simulation of a stratocumulus-topped boundary layer.

Poor resolution near the surface and its potential influence of large eddies higher up spurred the LES community to increase its focus on rigorous testing of SGS schemes (e.g., Meneveau and Katz 2000 and references therein). From the atmospheric perspective, field testing emerged in the late 1990s, largely spurred on by the work of a group at Pennsylvania State University (Tong et al. 1998, 1999), who showed how ABL

⁸ And perhaps the name “large-eddy simulation” as well. It was suggested by Parvis Moin to Wyngaard (2010, footnote on p. 136) that William Reynolds of Stanford coined the term.

⁹ Calculations do, however, sometimes produce negative eddy viscosities. When this occurs, the values are typically “clipped” (set to zero or a small negative value).

turbulence-scale interaction at small scales could be studied through sampling both filter/resolved and sub-filter/subgrid scales of atmospheric variables using arrays of densely spaced instrumentation a few meters above the surface. The daunting task of setting up and maintaining the optimum arrays was beyond the reach of the early researchers, but efforts by the Pennsylvania State University group (Tong et al. 1999) and by a group from University of Minnesota and Johns Hopkins (Porté-Agel et al. 2001) were sufficiently successful to establish both the feasibility of this pioneering approach and its promise in relating filter-scale fields to subfilter fluxes (see also Higgins et al. 2003, 2004).

It was the technical staff at NCAR's Atmospheric Technology Division who enabled researchers to fully implement the design set out by Tong et al. (1998) in the first of several Horizontal Array Turbulence Study [HATS (2000); Horst et al. 2004] field campaigns, building on the contributions of Tong et al. (1999) and Porté-Agel et al. (2001). Using HATS data, Sullivan et al. (2003) found that the Smagorinsky–Lilly and Deardorff TKE schemes were adequate if the turbulence length scale corresponding to the peak in the vertical velocity w spectrum was large compared to the filter scale, but increasingly sophisticated methods using turbulence-tendency equations (e.g., Wyngaard 2004; Hatlee and Wyngaard 2007) were required as the w -peak length scale became smaller compared to the filter scale. Kleissl et al. (2004) used HATS data to show that the filter-scale dependent dynamic model of Porté-Agel et al. (2000) could reproduce the observed Smagorinsky constant and its dependence on stability and height, while scale-invariant model of Germano et al. (1991) could not.

The second HATS field campaign, the Ocean Horizontal Array Turbulence Study [OHATS (2004); Sullivan et al. 2006], revealed the need to account for impact of moving waves. Interpreting the data based on the insights provided through the direct numerical simulation (DNS) of Sullivan and McWilliams (2002), observations and wave-tank experiments by Plant (1982), and observations by Smith et al. (1992) and Grachev and Fairall (2001), Kelly et al. (2009) modified the Hatlee–Wyngaard SGS scheme to include wave effects to replicate OHATS results. Conducted over a snow field, the Sno-HATS (2006) field study (Bou-Zeid et al. 2010) provided additional data to buttress some of the HATS results in stable conditions. Canopy-HATS [CHATS (2007); Patton et al. 2011] has offered insights into exchanges in a canopy (Dupont and Patton 2012a,b; Patton et al. 2016).

In the last few decades, progress in LES and computer capabilities has enabled dealing with more realistic physical situations. The introduction of terrain at the

lower boundary in LES has contributed to studies of the impact of the surface on motions on the order of boundary layer depth and larger (section 4). LES with horizontally varying surface temperature or surface fluxes of different scales have illustrated potential influences on convective structure and fluxes through the PBL (section 7). Such treatments are benefitted by advanced methods to define the LES lower boundary through land surface models [such as in the Dutch Atmospheric Large-Eddy Simulation (DALES; Heus et al. 2010) model] and immersed-boundary methods for representing terrain (e.g., Lundquist et al. 2012) or the urban environment (e.g., Tseng et al. 2006; Giometto et al. 2016). Also, SGS treatments have been designed specifically for LES over heterogeneous surfaces (e.g., Bou-Zeid et al. 2005). Relatively recently, Sullivan et al. (2008) applied LES to the interaction between the atmosphere and nonequilibrium ocean-surface waves, for weak winds and fast-moving waves (swell). Section 8 summarizes the interplay between LES and observations in understanding boundary layers topped by clouds, especially stratocumulus. It is in these cases that representation of radiation, in conjunction with adequate SGS treatment, can have important impact (e.g., Stevens et al. 1999).

The SGS problem is avoided in DNS, for which the time and space scales of all motions are resolved, making an SGS parameterization unnecessary. This of course requires much smaller Reynolds numbers and domains. For the atmosphere, with $L \sim 1000$ m and $U \sim 1\text{--}10$ m s⁻¹, $Re = UL/\nu \sim 10^7\text{--}10^9$, since $\nu \sim 10^{-5}$ m² s⁻². As in the case of LES, the first DNS was run on a computer at NCAR, by Steven Orszag of the Massachusetts Institute of Technology and Stuart Patterson of Swarthmore College (Orszag and Patterson 1972; also see review by Fox and Lilly 1972). For this first set of DNS runs, with $Re \leq 45$, the 32^3 -grid domain was designed to simulate wind-tunnel turbulence.

With today's more powerful massively parallel computers, DNS using meshes of 2048^3 and larger, extending to $Re \sim 10^4\text{--}10^5$, has become a popular tool to study idealized atmospheric boundary flows such as turbulent Ekman layers (Shah and Bou-Zeid 2014), entrainment into dry (Garcia and Mellado 2014) or cloud-topped boundary layers (Mellado 2017), entrainment driven by shear (Jonker et al. 2013), the nocturnal jet (Fedorovich et al. 2017), katabatic flows (Shapiro and Fedorovich 2008), and turbulence “collapse” in the stable boundary layer (Ansorge and Mellado 2014). A review of the use of DNS as a research tool for turbulence can be found in Moin and Mahesh (1998).

As LESs became more sophisticated, they were increasingly used to improve the PBL parameterization

schemes employed in weather and climate models (see [section 10](#)). As an example, early tests of what later became the Mellor–Yamada–Janjić (MYJ) PBL parameterization scheme, [Yamada and Mellor \(1975\)](#) used the [Deardorff \(1974a,b\)](#) simulations of the Wangara experiment ([Clarke et al. 1971](#)); and when [Janjić \(2001\)](#) described the MYJ scheme for the modeling community, he referred to several LES papers as sources of comparison or parameterization constants. LES played an even more central role in [Nakanishi and Niino \(2009\)](#), which eventually led to the Mellor–Yamada–Nakanishi–Niino (MYNN) PBL scheme. In contrast to these models, which are based on the turbulent variance- and flux-tendency equations, the Yonsei University (YSU) scheme ([Hong et al. 2006](#)) also draws heavily on results of LES as well as observations for, among other things, profiles of K_H and K_M ([Noh et al. 2003](#)). LES has also played an important role in developing the K -profile parameterization used in ocean models ([Large et al. 1994](#)). We will see in [section 8](#) how the interplay of targeted observations and LES has led to significant progress in understanding and representing the stratocumulus-topped PBL, especially in the last two decades. Similarly, [section 10a](#) reveals the significant role of LES in dispersion studies.

Development of LES versions of mesoscale or numerical prediction models has provided additional new options for studying the evolving boundary layer over a heterogeneous surface, with a suite of physical parameterization options for clouds, radiation, the land surface, and the surface layer. Currently, many fine-grid weather or mesoscale models offer an LES option, perhaps the first of which was the Colorado State University (CSU) Regional Atmospheric Modeling System (RAMS) model ([Pielke et al. 1992](#)). Others have emerged since then, among which are the French MesonH ([Cuxart et al. 2000](#)), the British Met Office Unified model ([Beare and MacVean 2004](#)), COAMPS ([Hodur 1997](#)), the Advanced Regional Prediction System (ARPS; e.g., [Xue et al. 2001](#)), COSMO (COSMO-LES; [Loewe et al. 2017](#)), and the Weather Research and Forecasting (WRF) Model ([Mirocha et al. 2010](#)).

The limitations associated with periodic boundary conditions remain an issue, but can be addressed by selecting a domain large enough not to constrain the scales of interest (e.g., [de Roode et al. 2004](#)) or by using so-called fringe methods to generate turbulent inflow and outflow conditions ([Spalart and Watmuff 1993](#)). Not surprisingly, as computer capability has improved, large-domain LESs have emerged [e.g., 205 km × 205 km in [Khairoutdinov et al. \(2009\)](#) to enable study of maritime deep convection and its environment], but such studies could suffer from effect of still larger scales. A third approach is to nest a finer-grid LES within larger,

coarser LES domains (e.g., [Mirocha et al. 2013](#)). The next logical step—nesting down from mesoscale meshes to LES to study boundary layers influenced by real weather—is still in its infancy (see, e.g., [Moeng et al. 2007](#); [Zhu et al. 2010](#); [Mirocha et al. 2014](#); [Schalkwijk et al. 2015](#); [Muñoz-Esparza et al. 2017](#)).

3. The surface layer

As noted in the introduction, the surface layer is defined for convenience as having fluxes roughly independent of height, consistent with depths up to ~100 m in windy, convective conditions, and much shallower under stable conditions. For linear variation of fluxes with height, this amounts to about a 10% difference over the 10% of the BL depth often taken as the surface-layer depth. In the presence of surface roughness elements (stones, vegetation, buildings, waves, etc.) the surface layer lies above a roughness sublayer, where the effects of individual roughness elements are felt (e.g., [Katul et al. 1999](#); [Finnigan 2000](#)), which translates to a depth roughly 2–5 times the height of the roughness elements ([Raupach et al. 1991](#)).

a. The surface energy budget

Surface-layer and PBL stability as well as the role of water vapor in buoyancy and cloud formation are affected by the near-surface temperature T and specific humidity q and their turbulent fluxes; these are in turn influenced by the surface energy budget (SEB). Thus representing the ABL in numerical models of weather and climate ([section 10](#)) requires accurate representation of the SEB. Neglecting effects of vegetation and advection, the SEB is given by

$$Q_{R0} = Q_{H0} + Q_{E0} + Q_{G0}, \quad (9-1)$$

where the four terms are, respectively, the incoming net radiation, the sensible and latent heat flux from the surface to the air, and the heat flux into the ground (or surface), expressed in watts per meter squared. In practice, the terms are measured away from the surface and corrected to surface values assuming changes of heat and moisture content in the intervening air and soil layers are due to vertical flux divergence; with horizontal transport and vegetation effects often estimated.

By the 1920s, atmospheric radiation had been extensively studied, and people were estimating the albedo of different surfaces, and the effects of sun angle and atmospheric water vapor content were documented in the 1930s, according to [Geiger \(1966\)](#). Diurnal soil temperature variation was documented before 1900, as illustrated by [Fig. 9-1](#), and several groups were sampling soil temperatures through the year. Soil moisture was likely

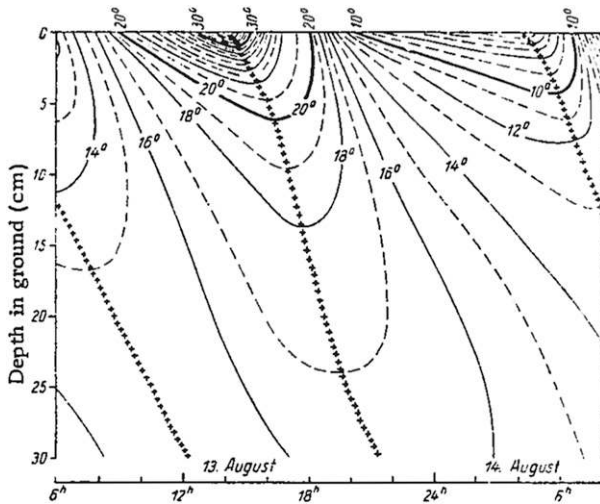


FIG. 9-1. Fair-weather diurnal soil temperature changes in Finland. Lines are isopleths of temperature ($^{\circ}\text{C}$); crosses indicate maxima and minima. [From Geiger (1966), Fig. 20 therein; redrafted from Homén (1897), Plate IV. Reprinted by permission from Springer Nature.]

estimated by drying soil samples, although de Vries (1953) attempted to estimate soil moisture from soil thermal conductivity, which was measured at Potsdam, Germany, by Albrecht (1937); and it was already recognized that both soil thermal conductivity and specific heat were functions of soil composition and water content.

The 1903 measurements of Q_{R0} and Q_{G0} at Potsdam enabled Albrecht (1940)¹⁰ to estimate Q_{H0} and Q_{E0} on a daily time scale from (9-1), quite possibly using Bowen's (1926) paper relating their ratio to vertical gradients of temperature and water vapor content. By the time of the 1953 Great Plains Turbulence field program (Lettau and Davidson 1957), better soil flux, moisture, temperature, and thermal-conductivity measurements were available and used to make estimates of soil heat flux and correct it to the surface soil heat flux Q_{G0} . Similarly, numerous radiometers sampled Q_{R0} . With these data available, Suomi used (9-1) and applied Bowen's assumptions to the vertical $\bar{\theta}$ and \bar{q} gradients to obtain Q_{H0} and Q_{E0} (Lettau 1957).

According to Lettau (1957), Halstead, on the other hand, obtained the vertical fluxes of θ and q from the bulk aerodynamic technique (e.g., Taylor 1916), which uses measurements at a single level (usually 10 m) and estimates (or measurements) of surface variables, such that turbulent fluxes $(\overline{w'\theta'})_0$, $(\overline{w'q'})_0$, and $-(\overline{u'w'})_0 \equiv u_*^2$, where q is the specific humidity, θ is temperature T corrected for height using the adiabatic lapse rate,¹¹ u_* is

called the friction velocity, and \bar{U} is the mean wind speed, are given by

$$u_*^2 = C_D \bar{U}^2, \quad (9-2a)$$

$$(\overline{w'T'})_0 = (\overline{w'\theta'})_0 = C_H (\bar{\theta}_0 - \bar{\theta}) \bar{U}, \quad \text{and} \quad (9-2b)$$

$$(\overline{w'q'})_0 = C_E (\bar{q}_0 - \bar{q}) \bar{U}, \quad (9-2c)$$

where the primes denote departures from time or horizontal averages (overbar), C_D is the drag coefficient, C_H and C_E are the exchange coefficients for heat and moisture, and the subscript 0 again indicates a "surface value" (actually a small distance above the surface, see section 3b). Halstead assumed a logarithmic \bar{U} profile, and obtained C_H and C_E from the molecular Prandtl number ($\text{Pr} \equiv C_M/C_H = 0.71$), the molecular Schmidt number ($\text{Sc} \equiv C_M/C_E = 1.64$), and C_D , which was based on drag-plate stress measurements. Unfortunately, (9-1) did not balance for Halstead.

By the 1960s, hot-wire anemometers and fine-wire resistance thermometers (e.g., Swinbank 1951); fast-response Lyman-alpha sensors, dewpoint hygrometers, and wet-bulb thermometers (Miyake and McBean 1970; Pond et al. 1971); and the development of the sonic anemometer (Schotland 1959; Barrett and Suomi 1949) made possible calculating the near-surface terms $w'T'$ and $w'q'$ directly (eddy correlation) to obtain $Q_{E0} = \bar{\rho}_0 L_e (\overline{w'q'})_0$ and $Q_{H0} = \bar{\rho}_0 c_p (\overline{w'T'})_0$, where ρ is the air density, L_e is the latent heat of vaporization, and c_p is the specific heat at constant pressure; and measurements required for estimates of Q_{G0} and Q_{R0} continued to improve. But the observed surface energy budget still failed to balance. This prompted a workshop (Foken and Oncley 1995) to examine sources of the discrepancy, including impact of sonic-anemometer flow distortion and undersampling of eddy-correlation fluxes, the sampling of different areas for the estimates of the four terms in (9-1), inherent error in the instruments involved, heat storage between the surface and flux-measurement height, storage in the soil layer, and horizontal advection. The workshop resulted in the Energy Balance Experiment (EBEX) in a periodically flooded cotton field, in which the researchers tried to minimize the known sources of error; but there was still a daytime residual of about 10% (Fig. 9-2).

How can we eliminate that last 10%? Heusinkveld et al. (2004), van de Wiel et al. (2003), Liebenthal et al. (2005), and Steeneveld et al. (2006) focused on soil measurements to improve Q_{G0} , with some success in improving balance. However, others believe that observations of Q_{H0} and Q_{E0} are the culprits, suggesting corrections by multiplying them by the factor needed to force balance (e.g., Twine et al. 2000), sampling large eddies better,

¹⁰ See Table 2 in Geiger (1966).

¹¹ If close enough to sea level, θ is approximately the potential temperature.

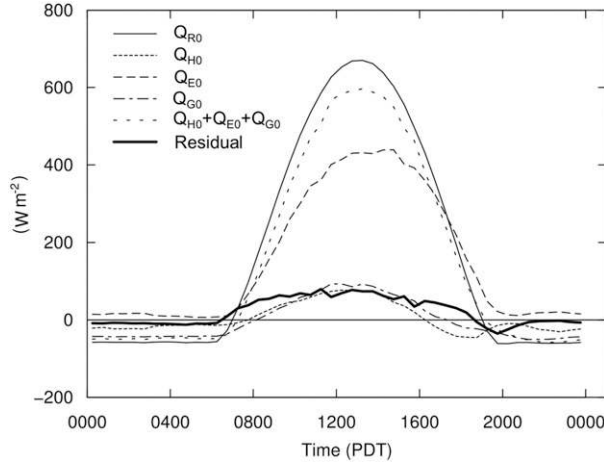


FIG. 9-2. Composite surface energy budget for flooded cotton field in EBEX. While the surface energy budget balances during the night, there is about a 10% residual during the day. [From [Oncley et al. \(2007\)](#). Reprinted by permission from Springer Nature.]

either through long averaging time ([Finnigan et al. 2003](#)) or using distributed arrays (e.g., [Engelmann and Bernhofer 2016](#)), distributing flux sites to sample different types of land cover in heterogeneous areas (e.g., [Kustas et al. 2005](#)),¹² mapping surface fluxes from aircraft ([Mauder et al. 2008](#)),¹² or performing more rigorous corrections to correct for “shadowing effects” on sonic anemometers ([Horst et al. 2015](#); [Frank et al. 2016](#)). Though some of the successes might be site or situation specific, a common theme in attempts to achieve balance is using the best instruments possible, installing them carefully, and doing thorough corrections afterward; building on the careful procedures used in EBEX.

b. Flux-profile relationships

In addition to the bulk aerodynamic technique, fluxes in the surface layer are estimated using the flux-profile technique:

$$u_*^2 = K_M \frac{\partial \bar{U}}{\partial z}, \quad (9-3a)$$

$$\overline{w'T'} = -K_H \frac{\partial \bar{\theta}}{\partial z}, \quad \text{and} \quad (9-3b)$$

$$\overline{w'q'} = -K_E \frac{\partial \bar{q}}{\partial z}. \quad (9-3c)$$

¹² Though surface energy balance was not the focus, both these papers address the problem of estimating sensible and latent heat fluxes over heterogeneous areas.

Starting in the mid-1900s, these relationships provided a theoretical basis for estimating the exchange coefficients in (9-2), drawing from the work discussed in [section 2](#). What we now call Monin–Obukhov similarity theory (MOST) was developed during and just after World War II ([Obukhov 1946, 1971](#); [Monin and Obukhov 1954](#)).¹³ [Obukhov’s \(1946\)](#) paper introduced the length scale L , given by

$$L = -\frac{u_*^3 \bar{T}}{kgw'T'}, \quad (9-4)$$

where k is the von Kármán constant and g the acceleration of gravity. The 1954 paper uses dimensional arguments¹⁴ to demonstrate that temperature and wind speed profiles are universal functions of z/L . Today, virtual temperature T_v is used instead of T . Vertical fluxes of heat and momentum are assumed constant. [Monin and Obukhov \(1954\)](#) suggested that the mean wind and temperature gradients through this layer are universal functions of z/L .¹⁵ Strictly, MOST applies for stationary, homogeneous turbulence in air over a flat surface with zero mean vertical velocity.

MOST was particularly useful because it was already realized that [von Kármán’s \(1931\)](#) logarithmic wind profile needed correction for nonneutral thermal stratification (e.g., [Rossby and Montgomery 1935](#); [Deacon 1953](#), from 1940 measurements). Many investigators participated in developing the needed functions. [Fleagle and Businger’s \(1963\)](#) text shows a conceptual derivation of the so-called KEYPS¹⁶ expression that relates the normalized vertical shear of the mean horizontal wind to thermal stratification:

$$\phi_m^4 - \gamma \frac{z}{L} \phi_m^3 = 1, \quad (9-5)$$

where $\phi_m \equiv (kz/u_*)(\partial \bar{U}/\partial z)$ and γ is a constant.

¹³ For a complete summary of M-O similarity theory, see [Foken \(2006\)](#).

¹⁴ Through applying the Buckingham Pi theorem to the relevant scales, z , u_* , $w'T'$, and g/T .

¹⁵ Apparently, Heinz [Lettau \(1949\)](#) introduced the same length scale, and Joost [Businger \(1955\)](#) independently developed the same similarity theory as part of his Ph. D. thesis, according to his résumé, which is available in the NCAR Archives; and confirmed by Businger’s son Steven (November 2018, personal communication). Also see [Businger and Yaglom \(1971\)](#).

¹⁶ An acronym based on the names Kazanski, Ellison, Yamamoto, Panofsky, and Sellers, see [Panofsky \(1963\)](#) and [Lumley and Panofsky \(1964\)](#). [Businger and Yaglom \(1971\)](#) suggested expanding to “O’KEYPS” to include Obukhov, since his 1946 paper includes a similar formula.

In the 1960s, (9-5) was modified by Businger and Dyer (Businger et al. 1971), who found from observations for unstable conditions that ϕ_m and $\phi_h = (kz/\theta_*) (\partial \bar{\theta} / \partial z)$, where $\theta_* = w' \theta' / u_*$, are given by

$$\phi_m = \left(1 - \gamma_1 \frac{z}{L}\right)^{-1/4}, \quad \text{and} \quad (9-6a)$$

$$\phi_h = \phi_{hN} \left(1 - \gamma_2 \frac{z}{L}\right)^{-1/2}, \quad (9-6b)$$

where γ_1 and γ_2 are constants to be determined, and the subscript N corresponds to neutral stratification ($z/L = 0$). The surface-stress estimates from flux plates and mean profile measurements collected near O'Neill, Nebraska, were used to test (9-6a), (e.g., Panofsky 1963).

It was the 1968 Kansas experiment (Haugen et al. 1971), during which both eddy-correlation fluxes and profiles were measured, that enabled evaluating flux-profile relationships for both temperature and momentum for stable and unstable thermal stratification. They found that $\phi_{hN} = 0.74$, $\gamma_1 = 15$, and $\gamma_2 = 19$ in (9-6a) and (9-6b) (Businger et al. 1971). For stable conditions ($L > 0$), they found

$$\phi_m = 1 + 4.7z/L, \quad \text{and} \quad (9-7a)$$

$$\phi_h = 0.74 + 4.7z/L = \phi_{hN} (1 + 6.4z/L), \quad (9-7b)$$

but there were few points beyond $z/L = 1$ on the stable side. Finally, from (9-3a) and (9-3b) and the definition of ϕ_m and ϕ_h ,

$$\frac{\phi_h}{\phi_m} = \frac{K_M}{K_H} \equiv \text{Pr}_T,$$

where the turbulent Prandtl number at neutral stratification $\text{Pr}_{TN} = 0.74$.

Subsequent international comparisons of flux measurements revealed inconsistent results, prompting improvements in sonic-anemometer design (Högström 1988) and more sophisticated corrections for flow distortion (Wieringa 1980; Wyngaard 1981). Applying both in a new set of measurements, Högström was able to update the ratio Pr_{TN} from its Kansas value of 0.74 to ~ 1 , and k from its Kansas value of 0.35 to 0.4. For $\text{Pr}_{TN} = 1$ and $k = 0.4$, more recent values of γ_1 are on the order of 16–19.3, and $\gamma_2 \sim 11$. The constant 4.7 was revised to be closer to 6 for ϕ_m and 8.2 for ϕ_h (Foken 2006). Refinements have continued for all these variables (e.g., Andreas et al. 2006).

Another important—but avoidable—difficulty in observational testing and evaluation of similarity relationships occurs when nondimensional variables containing

shared factors—such as the case for (9-6) and (9-7)—are plotted against one another. This has been called self-correlation. Self-correlation can combine with observations to either mask the physical correlation or augment the physical correlation, a problem that becomes especially serious in the very stable boundary layer (defined in section 5), where small fluxes also make observational errors relatively large. Fortunately, there are methods for assessing self-correlation (e.g., Hicks 1978; Klipp and Mahrt 2004; Baas et al. 2009; Sfyri et al. 2018) or avoiding it altogether (Anderson 2009). Large self-correlation does not necessarily negate the utility of similarity theory but it does create an observational ambiguity.

Paulson (1970) integrated (9-6), making it possible to estimate fluxes iteratively, using

$$\bar{U} = \frac{u_*}{k} \left[\ln \frac{z}{z_0} - \psi_m \left(\frac{z}{L} \right) + \psi_m \left(\frac{z_0}{L} \right) \right], \quad \text{and} \quad (9-8a)$$

$$\bar{\theta}_z - \bar{\theta}_0 = \frac{\bar{\theta}_*}{k} \left[\ln \frac{z}{z_0} - \psi_h \left(\frac{z}{L} \right) + \psi_h \left(\frac{z_0}{L} \right) \right], \quad (9-8b)$$

where the roughness length z_0 is the height at which the mean wind $\bar{U} = 0$ and $\bar{\theta} = \theta_0$, and ψ_m and ψ_h are corrections for stability. For convenience, (9-8) is written with the integrated ψ functions evaluated at z_0 and z as in Brutsaert (1982), instead of the indefinite-integral form used in Paulson's (2). Paulson also suggests that $\phi_h/\phi_{hN} = 1$ in (9-6b), based on observations at Kerang (Swinbank 1964). Typically, z_0 for a location is found empirically from (9-8a) for near-neutral conditions; it is larger for rougher surfaces. While it is implicit in (9-8b) that $\bar{\theta} = \bar{\theta}_0$ at z_0 , it was recognized earlier that it would be more appropriate to replace z_0 with z_{0m} in (9-8a) and replace z_0 in (9-8b) with z_{0h} (e.g., Chamberlain 1966). The relationship of z_{0h} to z_{0m} appears to be a function of surface cover (Zilitinkevich 1970; Chen and Zhang 2009) and time of day [Sun (1999), if $\bar{\theta}_0(z_{h0})$ is the surface radiation temperature]. Following Paeschke (1937), z is replaced with $z - d$ in the presence of tall vegetation or a canopy, where d the “displacement height” is the height of an upwardly displaced effective surface. That is, $d + z_{0m}$ is the zero intercept for a logarithmic wind profile under neutral conditions; data show $d \sim Ch_c$, where h_c is canopy height, and C is a scaling factor ranging between 0 and 1, with larger values for denser canopies. It follows that d can be a function of wind direction. Typical values for crops are between 0.6 and 0.7 (Campbell and Norman 1998; Brutsaert 1982).

The exchange coefficients for momentum and heat can be obtained by combining (9-2a) and (9-2b) with (9-8a) and (9-8b) and using the appropriate roughness lengths:

$$C_D = \frac{k^2}{\left[\ln\left(\frac{z}{z_{0m}}\right) - \psi_m\left(\frac{z}{L}\right) + \psi_m\left(\frac{z_{0m}}{L}\right) \right]^2}, \quad \text{and} \quad (9-9a)$$

$$C_H = \frac{k^2/\text{Pr}_{TN}}{\left[\ln\left(\frac{z}{z_{0m}}\right) - \psi_m\left(\frac{z}{L}\right) + \psi_m\left(\frac{z_{0m}}{L}\right) \right] \left[\ln\left(\frac{z}{z_{0h}}\right) - \psi_h\left(\frac{z}{L}\right) + \psi_h\left(\frac{z_{0h}}{L}\right) \right]}. \quad (9-9b)$$

The water vapor exchange coefficient C_E is found analogously, except that Pr_{TN} is replaced with the Schmidt number for neutral stratification Sc_{TN} . In practice, Pr_{TN} and Sc_{TN} are often set to unity. For $z = 10$ m and $z_{0m} = 0.1$ m (grass with scattered trees and houses or thick grass), $C_D \sim 0.01$ for neutral conditions ($\psi_m = 0$).

The cited work so far assumed the effect of water vapor on the buoyancy flux was negligible. To estimate surface buoyancy flux, it is often assumed that the similarity function for virtual temperature $\phi_{T_v} = \phi_h$.¹⁷ This assumption works, provided (Dias and Brutsaert 1996) that the correlation coefficient between the temperature and mixing-ratio fluctuations $R_{\theta q} \equiv \overline{T'q'}/(\sigma_T\sigma_q) \approx 1$ (-1 for stable conditions), although Larsen et al. (2014) argue that MOST relationships could be reliable for $|R_{\theta q}|$ as low as 0.5. The less stringent criterion appears to be commonly easily satisfied over land, at least to within experimental error for unstable (e.g., Swinbank and Dyer 1967) and stable (e.g., Dias and Brutsaert 1996) conditions. However, measurements over heterogeneous pine forests by Asanuma and Brutsaert (1999) and Lamaud and Irvine (2006) indicated a difference between MOST scalar similarity functions. The latter work inspired Moene and Schüttemeyer (2008) to develop a conceptual model for fluxes over heterogeneous surfaces, with updrafts carrying heterogeneous properties, and downdrafts carrying homogeneous properties. Not only did it reproduce many of Lamaud and Irvine's results, but it offered a method to estimate scalar fluxes.

Likewise, measurements in the boundary layer over the warm oceans as early as the 1970s revealed a dropoff and even a sign reversal of R_{Tq} at longer wavelengths (e.g., Phelps and Pond 1971; Donelan and Miyake 1973), resulting from both a sign reversal in $w'\theta'$ and an increase in σ_θ and σ_q near the surface. This behavior is also related to entrainment as revealed in an LES study by Cancelli et al. (2014). Both contributions are due to “nonlocal” downward heat transport by large eddies

extending through a moist mixed layer, where $\bar{\theta}$ increases with height (section 4). The success of the weaker R_{Tq} criterion even over the ocean is consistent with the satisfactory results obtained under the $\phi_{\theta_v} = \phi_h$ assumption (e.g., Fairall et al. 1996).

For wind, Panofsky et al. (1977) showed using observations that horizontal-velocity variances in the surface layer were a function of $-z_i/L$ rather than $-z/L$. Even though there are limitations associated with use of LES to evaluate MOST near the lower boundary, results in Khanna and Brasseur (1997) and Johansson et al. (2001) also point to a dependence of horizontal velocity variances on $-z_i/L$, with the latter paper suggesting a weak dependence of temperature variance as well. Finally, while Katul et al. (2011, 2013) have put ϕ_h and ϕ_m on a more rigorous basis, they have also offered insight into their limitations (because of the impact of large eddies).

c. Vegetation canopies

When the study of plant canopy turbulence was in its infancy, researchers assumed that it could be treated like boundary layer turbulence with the addition of finescale eddies generated in the wakes of the leaves, twigs, and branches. By the 1970s, it had become clear that the dominant turbulent eddies in plant canopies are much larger than plant element size. However, it took two decades to show how these eddies are generated, and another decade to develop methods to account for the associated fluxes in parameterization schemes.

1) STATISTICS

Mean profiles within a canopy (shown for neutral conditions in Fig. 9-3) are distinct from profiles in the atmospheric surface layer. The mean streamwise velocity profile follows a standard logarithmic form well above the canopy, while the profile within the canopy can be roughly described as exponential (e.g., Cionco 1965). The two types of profiles merge within the roughness sublayer (RSL) and an inflection point appears at the top of all but the sparsest canopies. The size of the most energetic eddies increases with height in the surface layer (Kaimal and Finnigan 1994). However, as will be shown below, this height dependence vanishes with descent through the

¹⁷ The research topic dealing with whether or not this, or more strictly, $\phi_T = \phi_q$ is valid is referred to as “dissimilarity.”

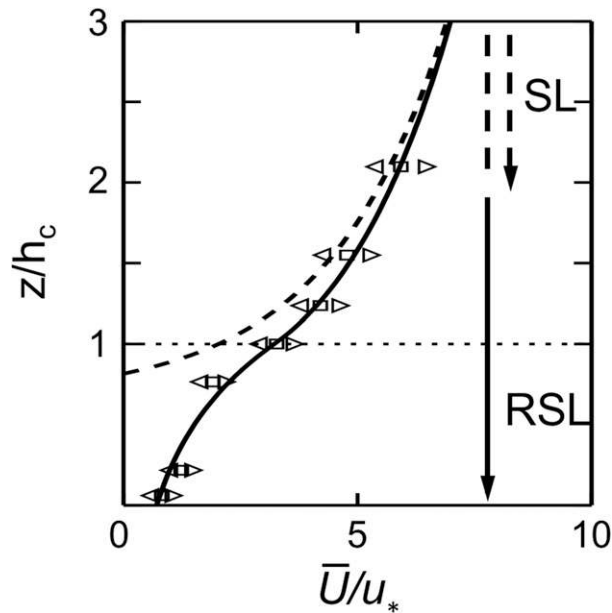


FIG. 9-3. Comparison of vertical profiles of mean wind speed \bar{U} in neutral conditions with observations from the Moga forest (rectangles, with triangles denoting one standard deviation). Dashed line: surface-layer MOST profile; $\bar{U} = 0$ at the displacement height d . Solid line: \bar{U}/u_* profile predicted by Harman and Finnigan (2007, 2008), where MOST is modified to include the influence of a vegetation canopy. The dotted line indicates the mean canopy height h_c ; SL = surface layer; RSL = roughness sublayer. The depths of these layers vary with canopy density and stability. [Adapted from Patton and Finnigan (2013). Reproduced with permission of CRC Press, Taylor & Francis Group in the format journal/magazine via Copyright Clearance Center.]

roughness sublayer, and the size of the dominant canopy eddies is height independent.

Above the canopy, momentum fluxes are nearly constant with height but rapidly decay with descent into the canopy as streamwise momentum is absorbed through canopy drag; for dense canopies $-\overline{u'w'}$ reduces nearly to zero by ground surface, indicating that nearly all downward transport of horizontal momentum has been absorbed by the canopy and therefore does not reach the underlying surface. Hence, within the canopy, the similarity scaling leading to the log-law and MOST no longer applies and the direct connection between local gradients and turbulent fluxes of scalars and momentum is lost (e.g., Denmead and Bradley 1985; Finnigan 1985), and turbulence in the RSL transports momentum and scalars more effectively than it does in the surface layer (e.g., Raupach and Thom 1981; Fazu and Schwerdtfeger 1989).

The joint probability distributions (Fig. 9-4) of the fluctuating wind components u' and w' at two heights above and within a deciduous mixed-hardwood forest

(Shaw and Patton 2003) clearly illustrate the contrast between the pattern of turbulence in the surface layer and that in the roughness sublayer. The u' and w' velocity signals near treetop level (i.e., in the RSL) reveal an increased correlation and skewness not present in the surface layer above. Turbulent momentum transport near the canopy top is by frequent upward motions bringing low-momentum air upward (Q2, ejections), with infrequent but stronger downward penetrations of high-momentum air (Q4, sweeps). Though less frequent, the sweeps contribute more to the exchange of momentum and scalars in the RSL than do the ejections (Finnigan 1979; Shaw et al. 1983; Katul et al. 1997; Finnigan et al. 2009). This is in contrast to surface-layer flows, where the contributions from sweeps and ejections are of comparable magnitude or in which ejections dominate (Raupach and Thom 1981).

In the surface layer well above the canopy, the budget of TKE [$= 1/2(\overline{u'^2} + \overline{v'^2} + \overline{w'^2})$, where v is the horizontal wind component normal to u] is generally in local equilibrium, with shear production balancing dissipation at any height under neutral conditions. However, within and just above a canopy, TKE produced in the region of high streamwise velocity shear near canopy top is exported by pressure and turbulent transport to regions away from its source. Hence at any given height within the RSL, the local rates of production and dissipation are not usually in balance, and local equilibrium is lost. All canopy second-order budgets¹⁸ lack a local balance between production and dissipation, because the dominant turbulent eddies in the canopy span most of its depth and thus can efficiently transport TKE and scalars through the entire canopy. Furthermore, the thin viscous boundary layers on the surfaces of all the canopy elements generate sufficiently abundant shear layers at the Kolmogorov microscale that the dissipation rate of turbulence within canopies can be several times higher than seen in free air flows with shear of comparable magnitude.

In canopy flows, assumptions in Kolmogorov's (1941b, 1962) theory are violated in a number of ways. First, interactions with the canopy elements act to convert mean kinetic energy into turbulent kinetic energy at scales tied to the leaves, twigs and branches; these scales usually fall at the high wavenumber (k) end of the inertial subrange. This *spectral-shortcut* process takes TKE from lower wavenumbers and injects it directly into high wavenumbers. Additionally, the work eddies do against the viscous drag of the canopy removes energy at all scales,

¹⁸ E.g., of $\overline{s'^2}$, $\overline{w's'}$, and $\overline{w'u'_i}$, where s is a scalar and $i = 1, 2, 3$ indicate the three wind components.

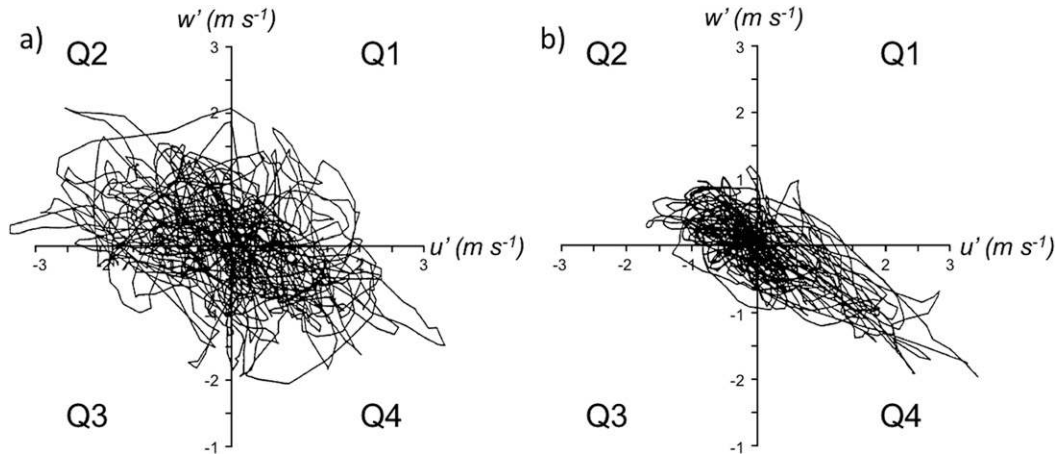


FIG. 9-4. Joint probability distribution of u' and w' , based on a 30-min time series near a deciduous mixed-hardwood forest in Camp Borden, Ontario, Canada at: (a) $z/h_c = 2.4$, and (b) $z/h_c = 0.86$. The quadrants Q2 and Q4 correspond to the ejection and sweep phases, respectively. [Adapted from [Shaw and Patton \(2003\)](#). Reprinted with permission from Elsevier.]

including inertial subrange scales. This latter process changes the overall magnitude of canopy dissipation. The net result is that within canopies $E(k)$ in the inertial subrange decreases faster than $k^{-5/3}$ at low wavenumbers and more slowly at high wavenumbers. For further discussion, see [Finnigan \(2000\)](#).

2) ORGANIZED CANOPY-INDUCED TURBULENT MOTIONS

Numerous observational studies have attempted to deduce the three-dimensional spatial flow structures underlying the observed scalar ramp patterns (e.g., [Gao et al. 1989](#); [Zhang et al. 1992](#); [Shaw et al. 1995](#); [Finnigan and Shaw 2000](#)); however, the difficulty in making the necessary observations prompted researchers to turn to LES (see [section 2c](#)). Following the pioneering studies by [Shaw and Schumann \(1992\)](#) and [Fitzmaurice et al. \(2004\)](#), [Finnigan et al. \(2009\)](#) used LES to deduce the three-dimensional structure by referencing fields to the canopy-top pressure maxima to ensemble average the flow field. They found that in neutrally stratified flow, the mean organized structure consists of a combination of “head-up” and “head-down” hairpin vortices, which are both inclined in the downstream direction ([Fig. 9-5](#)). The ejections and sweeps are flows induced between the counterrotating legs of the hairpins. The convergence region between the downstream ejection and upstream sweep produces a scalar microfront and a positive static pressure pulse.

The structures in [Fig. 9-5](#) are consistent with theory, as described in [Patton and Finnigan \(2013\)](#). First, drawing on the analogy between the canopy-top inflection point

in \bar{U} and that which develops as a resulting of mixing at the interface between two free-atmosphere layers with different wind speeds, [Raupach et al. \(1996\)](#) shows that the inviscid instability at the inflection point under neutral stratification leads to the development of

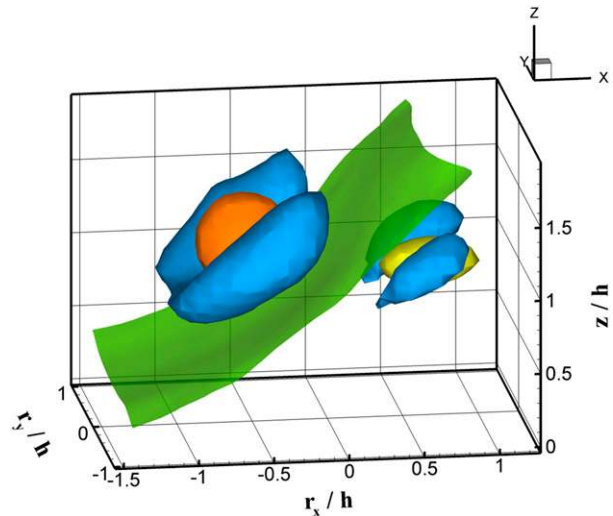


FIG. 9-5. Three-dimensional image showing the composite eddy structure from the canopy-resolving large-eddy simulation of [Finnigan et al. \(2009\)](#). The blue shapes represent the outer surfaces of the hairpin vortices, as defined by [Jeong and Hussain's \(1995\)](#) parameter $\lambda_2 = -0.77$. The green sheet, with zero scalar perturbation from the horizontal average, corresponds to the scalar microfront between the vortices. The sweep region is outlined by the orange isosurface, where $\overline{u'w'} = -0.6 \text{ m}^2 \text{ s}^{-2}$, while the ejection region is outlined by the yellow isosurface, where $\overline{u'w'} = -0.15 \text{ m}^2 \text{ s}^{-2}$. [From [Finnigan et al. \(2009\)](#). © Cambridge University Press 2009. Reprinted with permission.]

Kelvin–Helmholz (K-H) waves.¹⁹ These in turn roll up into “cat’s eye” vortex tubes (Stuart 1967). Finnigan et al. (2009) suggest that adjacent vortex tubes, in response to random turbulent perturbations, approach and rotate around each other and distort into hairpins in a process matching the helical-pairing instability of Pierrehumbert and Widnall (1982), and finally align themselves with the shear, as shown in Fig. 9-5. It should be noted that Bailey and Stoll (2016) produced a somewhat different eddy structure from a canopy LES, at least partially because their analysis includes the total streamwise velocity rather than its perturbation.

3) ROUGHNESS SUBLAYER PARAMETERIZATION

Although some details of Finnigan et al.’s (2009) theory remain speculative, it successfully explains most observations in neutrally stratified flows. Indirect evidence for the fundamental role played by this canopy-top instability comes from Harman and Finnigan’s (2007, 2008, hereafter HF) extension of MOST to the RSL, which uses the vorticity-layer thickness ($\delta_\omega = 2\langle u \rangle (\partial \langle u \rangle / \partial z)$ evaluated at canopy top, where the angle brackets represent a horizontal average, Raupach et al. 1996) associated with the K-H waves at canopy top as an additional scaling length to modify the MOST streamwise velocity (\bar{U}) profiles. The HF equation contains two sets of terms. The first is analogous to (9-8) but is rewritten such that the lower surface is at canopy height h_c rather than at the apparent sink for momentum ($d + z_{0m}$); rewriting the equation in this way eliminates z_{0m} . The second set of terms accounts for canopy-induced physics in the RSL. Key aspects of the HF parameterization include 1) d and z_{0m} are flow-dependent parameters rather than specified based on canopy structure, and 2) the formulation naturally relaxes back to standard MOST above the RSL.

The HF parameterization reproduces observed mean velocity and scalar profiles through the RSL for a wide range of canopy types and stabilities. Weligepolage et al. (2012) tested numerous canopy parameterizations against observational data collected over a fir forest and found that HF performed best. More recently, Bonan et al. (2018) implemented the HF formulation within the Community Land Model (Oleson et al. 2010) and found substantially improved skill in predicting surface exchange at a number of forest, cropland, and grassland

sites that span a broad range of canopy height, leaf area index, and climate.

4) FUTURE DIRECTIONS

Although the theory proposed by Raupach et al. (1996) and Finnigan et al. (2009) and the parameterization based on that theory by HF appear to work quite well over a range of canopies and stabilities (e.g., Bonan et al. 2018), the theory relies upon the presence of mean velocity shear at canopy top. However, under strongly stratified conditions (unstable and stable), mean shear largely vanishes. Hence, the parameterization’s applicability at stabilities far from neutral becomes suspect.

Diabatic influences on canopy-turbulence statistics are reasonably well established (e.g., Shaw et al. 1988; Fazu and Schwerdtfeger 1989; Leclerc et al. 1990; Mahrt et al. 2000; Cava et al. 2004). Under unstable conditions, turbulent scalar exchange remains vigorous even in periods with weak mean shear at canopy top (e.g., Katul et al. 1997; Dupont and Patton 2012a; Patton et al. 2016). Under strongly stable conditions, buoyancy damps vertical motions (e.g., Lee 2000; Cava et al. 2004; Vickers and Thomas 2014), and the canopy layer can decouple from the overlying ASL (e.g., Belcher et al. 2012; Thomas et al. 2013), resulting from differing efficiencies of heat versus momentum transport. While progress has been made toward characterizing buoyancy’s influence on organized canopy-scale structures (e.g., Gao et al. 1989; Cava and Katul 2008; Thomas and Foken 2007; Dupont and Patton 2012b; Shaw et al. 2013), much work remains to elucidate the turbulent eddy structure performing momentum, energy, and scalar exchange under nonneutral conditions.

In addition, this discussion has assumed that the canopy consists of horizontally homogeneously distributed elements located on flat terrain; however, these conditions are rarely found outdoors. Rather, heterogeneously distributed vegetation is the norm, whether as a result of human action through wind breaks, clear cuts, forest edges, transitions from one crop to another, etc., or through natural transitions in surface cover. Currently, there is no universal theory describing how canopy flow reacts to stratification, heterogeneity, or topography although knowledge is accumulating in incremental steps.

d. The surface layer over the ocean

1) PROBLEMS UNIQUE TO THE OCEAN SURFACE

Because the ocean is a fluid, near-surface atmospheric measurements are difficult and the physics challenging. Turbulent fluxes are a challenge to measure from a

¹⁹ The meteorological community has typically applied K-H instability to two layers of different densities moving at different speeds because of the obvious applications to billow clouds (e.g., Scorer 1978). However, the term “K-H instability” is also often applied to layers of the same density moving at different speeds (e.g., Drazin and Reid 1981, 14–22).

moving platform that is sprayed with saltwater in stronger winds. Estimating the mean quantities for the bulk aerodynamic technique (9-2) is also more difficult than over land. Since the ocean surface moves, \bar{U} in (9-2) must be relative to the surface motion, which derives not only from the great ocean currents such as the Gulf Stream, but also from the superposed Stokes drift (resulting from the net motion of the orbiting water parcels in the direction of wave propagation), and the drift current (resulting from the drag of the air on the ocean surface). Likewise, the sea surface temperature (SST) typically has been measured not at the air–sea interface, but rather at a ship’s intake or at some depth below a buoy or platform; this is called the *bulk* SST. Finally, there are waves. Waves driven by the wind (so-called wind sea) are superposed on swells from any direction. In high winds, the waves not only grow in amplitude but they also give off spray. Some or all of these phenomena affect the surface fluxes in interesting ways, many the subject of active research.

2) MEASUREMENT METHODS—A BRIEF HISTORY

(i) Bulk methods

Estimation of surface fluxes was pioneered by Montgomery using bulk methods (for more detail see Sverdrup et al. 1942), with further work by many others. The earliest estimates of sensible heat flux, evaporation, and wind stress were from research ships such as the German Research Vessel (R/V) *Meteor* (Defant 1932; Kuhlbrodt and Reger 1938). It was quickly found that the drag coefficient C_D was not a constant but increased with the 10-m wind speed \bar{U}_{10} (Montgomery 1940; Deacon et al. 1956).

Most bulk formulations have used bulk SST rather than the actual or interfacial SST, which was not available; adjustments depend on the method of measurement and the formulation used. Today, infrared (IR) and microwave sensors (on ships, aircraft, or satellites) measure the outgoing radiation from a layer just below the interface (less than 1 mm for IR, slightly farther down for microwaves) to estimate the interfacial SST; but corrections are required for atmospheric transmission, reflections of the atmospheric and cloud radiation off the sea surface, and possibly sun glint (Robinson 2004). When using the interfacial temperature, consideration should be taken of the so-called *cool film*—at least at low wind speeds, temperatures can be up to 0.2–0.3 K lower at the interface than a few millimeters below because of loss of heat from the water to the atmosphere. However, at low wind speeds and under clear, sunny skies, a *warm layer* develops in the upper ocean because of absorption of sunlight and weak mixing, and the bulk and infrared surface temperatures can

differ substantially. To relate these temperatures requires keeping track of the conditions over a period of time and preferably coupled modeling of the upper ocean and atmosphere [for reviews, see Katsaros (1980) and Fairall et al. (1996)]. Much research on the long-term bulk SST and the interfacial SST continues, because of the importance for coupled models and climate change evaluations (e.g., Donlon et al. 2007; Kent et al. 2017).

(ii) Eddy correlation

Today the preferred method to obtain fluxes in situ is by eddy correlation, which requires a stable platform or corrections for the platform motion in three dimensions. Turbulent fluxes collected by Liu et al. (1979) from a bottom-mounted mast over Lake Washington (Seattle, Washington) using this technique resulted in formulations of the exchange coefficients over water that have been used widely and extended to higher wind speeds by several field campaigns (e.g., Fairall et al. 1996, 2003; Edson et al. 2013). In addition, the “dissipation method,” which equates the turbulent dissipation at small scales with the production by eddies at larger scales, has been used (e.g., Large and Pond 1981). These methods have been compared by Donelan et al. (1997), who report good agreement for wind sea dominated conditions, but less well in the presence of swell. Turbulent fluxes have also been obtained from moored buoys, with the preferred instrumentation first being pressure sensors or propeller systems for the three-dimensional wind components (Smith 1980; Large and Pond 1981). Developments in the 1990s reduced wetting and salt-accumulation problems, allowing sonic anemometers to be operated unattended for long periods, even on autonomous buoys (Fairall et al. 1997; Edson 2009). Sonics provide reasonable measurements of sensible heat flux, but water vapor flux still suffers from contamination of humidity sensors by rain and sea spray.

Since the 1960s, the *Floating Instrument Platform (FLIP)*, a ship designed to rotate 90° from its normal position so that its bow is pointed upward, has allowed eddy correlation and other turbulence, profile, and oceanographic measurements with minimal effect from ship motion; enabling studies of sea–air interaction over the open ocean (e.g., Pond et al. 1971; Rieder et al. 1994; Hristov et al. 2003; Zappa et al. 2012). Several other stable floating platforms, extended piers away from shore, and bottom-mounted research stations in relatively shallow water have also been used extensively. An early example used successfully was the floating mast (anchored to the surface 59 m below) off Nova Scotia used by Smith (1980) to obtain wind stress by the eddy correlation method.

(iii) *Scatterometry and importance of shorter waves to stress*

Surface stress and the \bar{U} profile are expected to be related to the mean-square slope of the sea surface, which can be determined from the spread of the sun glint off the water surface, as observed from aircraft by [Cox and Munk \(1954a,b\)](#). One of the early suggestions how the roughened sea surface affects the wind stress was by [Charnock \(1955\)](#), who formulated a simple relationship between the roughness of the sea to waves based on dimensional grounds:

$$z_{0m} = \alpha \frac{u_*^2}{g}, \quad (9-10)$$

where α is the Charnock “constant,” whose value has been estimated in many publications and turns out to vary (e.g., [Komen et al. 1998](#)). This relationship led to the development of radars (scatterometers) to remotely sense the surface wind and stress over the ocean from space.

Scatterometer measurements suggest an important role of the small capillary/gravity waves in determining stress. Scatterometers receive the so-called Bragg scatter (Bragg-scattered radiation) from waves of wavelength commensurate with the radar wavelength, which was 2.1 cm (14.6 GHz) on the first scatterometer flown on the *Seasat* satellite in 1978. Other wavelengths were used on later instruments (e.g., [Robinson 2004](#)). Since the scatterometer reacts to the sea surface roughness at small scale, it is a measure of the wind stress u_* . The strength of the Bragg scatter was typically calibrated against the wind speed at 10-m height, measured from buoys and corrected to neutral stratification. This relationship is now well established for wind speeds up to about 20 m s^{-1} . Currently, it is generally thought that waves of length smaller than $\sim 10 \text{ m}$ are responsible for the bulk of the drag at winds of about 10 m s^{-1} . This is a key concept since a typical wave spectrum contains scales as large as 250 m or more. However, it is still not completely settled as to whether the few intermittent big breakers associated with longer-wavelength waves could be as important as many small microbreakers in transmitting stress from the atmosphere to the ocean, particularly in strong winds.

3) FLUXES AND THE IMPACT OF WAVES

Many aspects of the wave field—such as phase speed, slope, and peak amplitude ([Kitaigorodskii 1959](#)) and interactions across the wave spectrum ([Kitaigorodskii 1983](#), [Hasselmann et al. 1973](#))—were considered as contributors to the wave drag on the atmosphere and generating turbulence in the ocean. This has led to increasing interest in the sea state as well as the surface

stress, but typically the 1D frequency spectrum of wave height was obtained but not the directional wave spectrum. [Geernaert et al. \(1986\)](#) reported the wind stress under conditions of fully developed wind sea for measurements at the *Nordsee* platform with steady winds and a long fetch; [Donelan et al. \(1997\)](#) reported the results of the Surface Wave Dynamics Experiment (SWADE), which was aimed at measuring the effects of waves on drag. The directional wave spectrum including swell was measured during SWADE, but not the high frequency, capillary, and gravity waves ([Drennan et al. 1994](#)).

More recently, field measurements have clarified the effect of moving waves on near-surface turbulence. The OHATS ([section 2c](#)) and the Coupled Boundary Layers Air–Sea Transfer (CBLAST; [Edson et al. 2007](#)) measured the impact of fast-moving swell on air motion, scalars, and turbulence. These results clearly showed how the angle between wave motion and relative wind influences low-level turbulence and profiles, to the point that $C_D < 0$ under conditions of weak wind in the presence of swell. [Sullivan et al. \(2008\)](#) combine idealized LES simulations of the interaction between air and moving waves to CBLAST observations to isolate the mechanisms involved. These authors point out that hints of this unusual behavior can be traced back to [Harris \(1966\)](#), who found wave-driven wind in wave-tank experiments; and cite subsequent observational studies that have associated waves with unusual near-surface behavior of the atmosphere, such as unusual wind profiles and momentum fluxes not aligned with the mean wind, as well as upward momentum flux.

Recently, more focus has been on extremely high winds. For a wind sea adjusted to the wind speed, [Edson et al. \(2013\)](#), in presenting the latest version of the Coupled Ocean–Atmosphere Response Experiment (COARE) flux algorithm (version 3.5), suggest that wave influences need not be modeled separately. This is because both the influence of the wave field and the shear-induced drag are strongly correlated with the wind speed, so that both effects can be included in the formulation of the dependence of C_D on wind speed. [Figure 9-6](#) illustrates this relationship and shows the recent estimates of C_D as well as the formulation used by the coupled model at the European Centre for Medium-Range Weather Forecasts (ECMWF).

However, the individual C_D estimates at high wind speed show wide scatter, and there are some situations when the wave field is not adjusted to the wind, such as in tropical cyclones (TCs). In a moving TC, where swell and old wind sea (wind sea in equilibrium with the forcing wind) are not aligned with the rotating wind around the storm center, much more complex relationships occur. [Chen et al. \(2013\)](#) have modeled these interactions for the

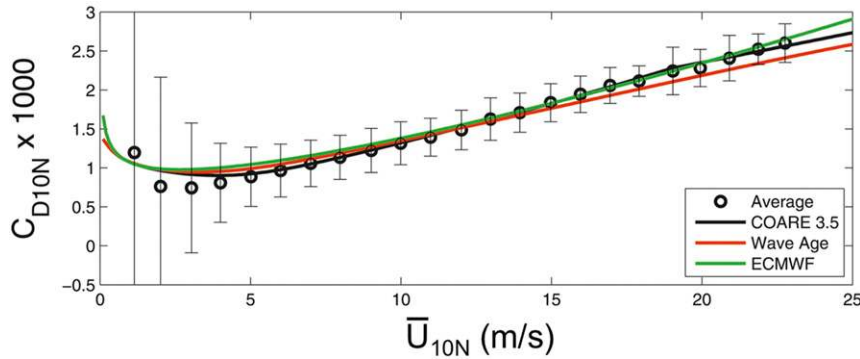


FIG. 9-6. A compilation of drag coefficient values as a function of wind speed after a reevaluation of many field programs, labeled COARE 3.5 (representing the COARE algorithm, version 3.5), where the data have been averaged over wind speed bins; it includes a curve for the case including wave age dependence and an illustration of the drag formulation used in the forecast model at ECMWF. [Figure adapted from Edson et al. (2013)].

different sections of a moving TC, showing that relationships are asymmetric between the right- and left-hand portions relative to its direction of motion.

Measurements of heat and moisture fluxes have been more difficult because of contamination from soot on ships, rain, and sea spray. Thus, acceptable values have mostly been determined under benign conditions at lower wind speeds. Based on the earliest measurements (e.g., Liu et al. 1979), the exchange coefficients C_H and C_E are constant for $\bar{U}_{10} < \sim 10 \text{ m s}^{-1}$. The Humidity Exchange over the Sea (HEXOS) field program extended this result to $U_{10} = 18 \text{ m s}^{-1}$ (DeCosmo et al. 1996). The measurements used special techniques to eliminate the sea spray from the airstream before taking measurements of temperature and humidity fluctuations (Katsaros et al. 1994). Though no profiles were obtained under spray conditions, single-height \bar{q} measurements made it clear that the reduction in surface evaporation compensated “mostly” for the addition of humidity from the evaporating spray. Later measurements of turbulent fluxes of water vapor on the outskirts of hurricanes from aircraft during CBLAST by Zhang et al. (2008) confirmed the HEXOS results and found the exchange coefficients for heat and water vapor to be constant to wind speeds as high as 25 m s^{-1} (Fig. 9-7), albeit with large scatter. This implies that in most conditions, when wind sea is in equilibrium with the wind, the effect of the waves might be incorporated in the bulk formulation for sensible heat and water vapor flux. The physics of how surface waves modify the turbulent transfer of sensible heat and water vapor is, however, still not well established.

Work continues on fluxes at extremely high winds. The effects of sea spray, though the subject of much speculation and study but few successful measurements, are still not well understood, according to a recent

review by Veron (2015), though Andreas et al. (2015) used a bulk flux algorithm to suggest some effects at high wind speeds; while Richter and Sullivan (2014) and Helgans and Richter (2016) use DNS to better understand the mechanisms involved and their net impact on heat and moisture fluxes. Other promising work at extreme wind speeds has included laboratory studies (e.g., Donelan et al. 2012; Haus et al. 2010), LES (e.g., Sullivan et al. 2014) and even a budget study to back out the exchange coefficients in two hurricanes (Bell et al. 2012). Such methods may be the only viable means to

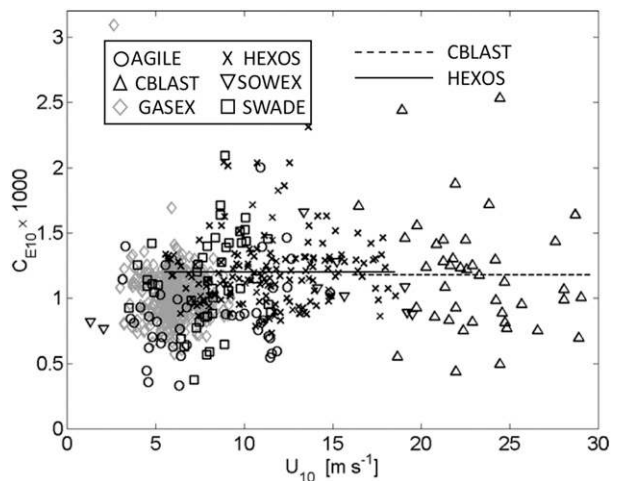


FIG. 9-7. The exchange coefficient for evaporation with results from several field experiments. The experiments all used the eddy correlation method to measure the fluxes. Non-CBLAST data are from AGILE (Donelan and Drennan 1995), HEXOS (DeCosmo et al. 1996), GASEX (McGillis et al. 2004), SOWEX (Banner et al. 1999), and SWADE (Katsaros et al. 1993). Data were corrected for density variations (Webb correction) and salinity effects using methods of Fairall et al. (2003). [Figure adapted from Drennan et al. (2007).]

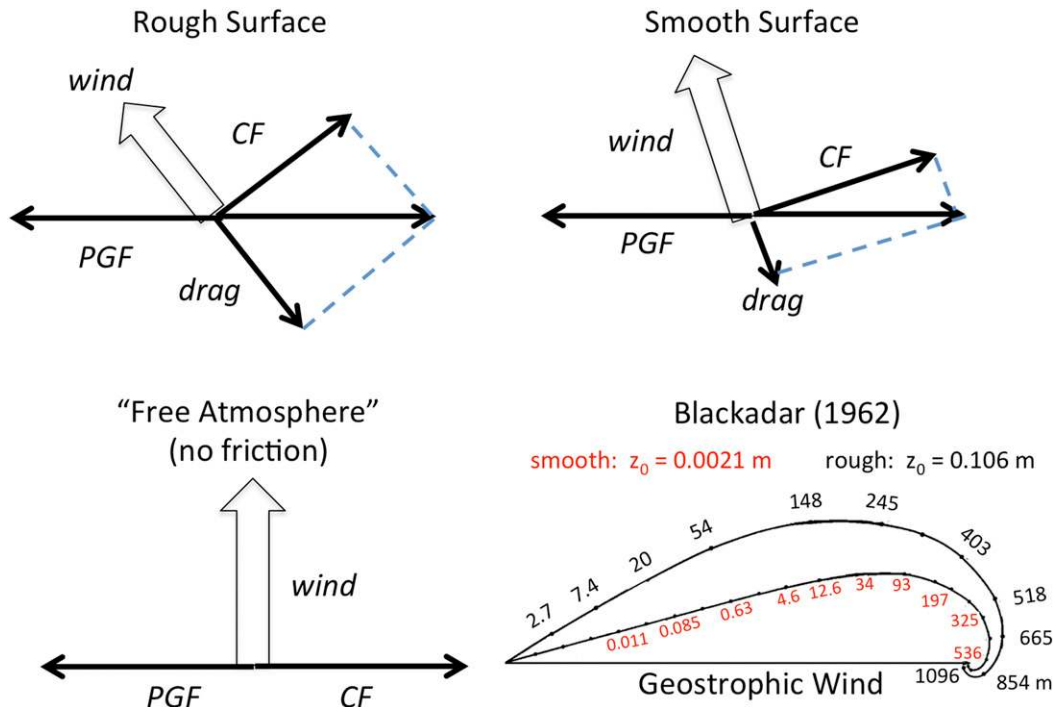


FIG. 9-8. Schematic force balance for modified Ekman wind hodograph. PGF = pressure gradient force; CF = Coriolis force; drag is a function of surface roughness z_0 as well as wind speed. [Hodograph based on Blackadar (1962).]

estimate exchange coefficients in extreme winds ($\bar{U}_{10} > 30 \text{ m s}^{-1}$), but they show large scatter of the resulting exchange coefficients and thus need verification against in situ data to wind speeds as high as can be managed. For a recent review of the coupling between surface waves and winds and currents under broad range of conditions, see Sullivan and McWilliams (2010).

4. CBL

a. Mean profiles

By the early twentieth century, dry-adiabatic lapse rates were regularly observed in daytime summer U.S. Weather Bureau (USWB) kite soundings over the center of the country, even in monthly averages (e.g., USWB 1918). As for the corresponding wind profile, many students in the midlatitudes were taught up until the 1970s that it would be similar to the “Leipzig wind profile” (Mildner 1932),²⁰ whose hodograph somewhat resembled the classic Ekman (1905) spiral. In fact, even the CBL depth was deemed proportional to the Ekman layer depth scale u_* / f (e.g.,

Tennekes 1970; Kaimal et al. 1976), even though tropical meteorologists were routinely using jumps in $\partial\theta/\partial z$ and $\partial q/\partial z$ to define boundary layer top decades earlier (e.g., Bunker et al. 1949, section 8).

While Ekman’s spiral assumed a constant K_M , the Leipzig profile K_M varied with height, reaching a maximum in the lower ABL (Lettau 1950). Following Prandtl (1932), Blackadar (1962) used $K_M = l^2 S$, where S is the magnitude of the vector shear and l is a mixing length (or characteristic turbulence length scale) that depends on height along with a characteristic eddy size λ ($\sim 150\text{--}250 \text{ m}$), to produce wind profiles whose turning angle increases with surface roughness. This length, given by the expression

$$l = kz / \left(1 + \frac{kz}{\lambda} \right), \quad (9-11)$$

is proportional to z near the surface, as postulated by Prandtl (1925) and equal to λ in the free atmosphere ($kz/\lambda \gg 1$). This relationship is still used in ABL parameterization schemes (e.g., Hong et al. 2006)

The turning of the wind with height can be explained in terms of force vectors (drag, pressure gradient force, Coriolis force) at the surface and the top of the ABL (pressure gradient force and Coriolis force) (Fig. 9-8) or mathematically by

²⁰ Even though the Leipzig wind profile was based on a set of pilot-balloon observations collected under stable conditions, according to Lettau (1950).

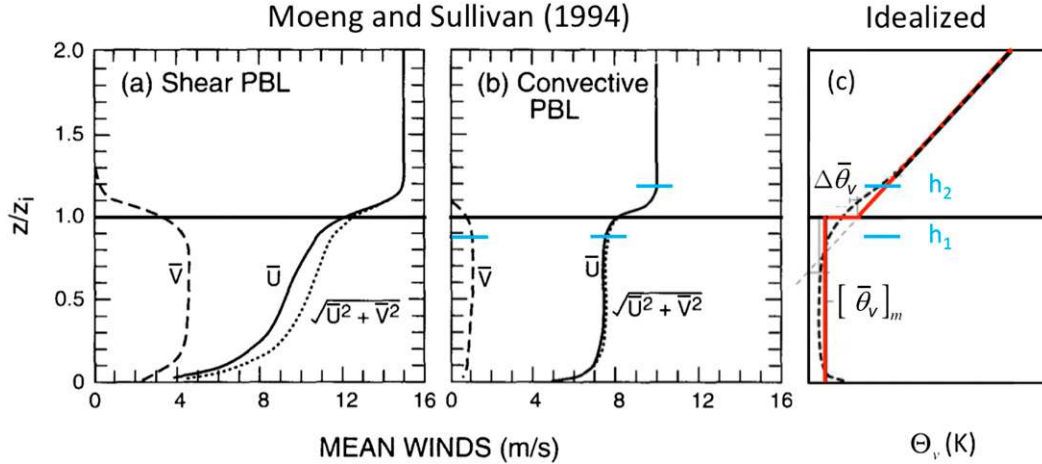


FIG. 9-9. Idealized ABL based on LES. (a),(b) Based on “Shear” and “Convective” ABL figure from [Moeng and Sullivan \(1994\)](#). Shear-driven ABL has neutral stratification; convective ABL has $-z_i/L = 18$. (c) The idealized CBL, which can be traced back to [Lilly \(1968\)](#), is based on the schematic from [Conzemius and Fedorovich \(2006b\)](#). In the right panel, the red lines correspond to the idealized mixed layer and the jump atop the mixed layer, associated with the so-called zero order or jump model; \bar{U} is along the geostrophic wind.

$$f(\bar{V} - V_g) = \frac{\partial \bar{u}'w'}{\partial z} = -K_M \frac{\partial \bar{U}}{\partial z}, \quad \text{and}$$

$$f(\bar{U} - U_g) = -\frac{\partial \bar{v}'w'}{\partial z} = +K_M \frac{\partial \bar{V}}{\partial z}, \quad (9-12)$$

where \bar{U} and \bar{V} are orthogonal horizontal wind components, the subscript g indicates geostrophic wind, and f is the Coriolis acceleration. Most observed wind profiles were not so well behaved: while veering with height was commonly observed in Northern Hemisphere soundings, the hodographs tended to be quite irregular. At about the same time, [Faller \(1963\)](#) was finding that Ekman flows in the laboratory broke down into longitudinal rolls, prompting [Faller and Kaylor \(1966\)](#) and other investigators (e.g., [Lilly 1966b](#); [Brown 1970](#)) to investigate the stability of the Ekman spiral. They found instabilities that they associated with the origin of longitudinal rolls. Brown allowed his most unstable mode to grow to equilibrium (net exchange of energy with the mean flow = 0) to produce a strongly modified hodograph with much less veering. [Brown \(1978\)](#) matched his Ekman-instability solutions to the surface layer to produce increased turning angle with roughness (surface drag) and stable thermal stratification.

The advent of LES in the early 1970s (see [section 2c](#)) led to near-universal acceptance of thermodynamic variables as the primary indicators of CBL depth (e.g., [Deardorff](#)

[1970a,b, 1974a](#)),²¹ and along with new measurement capabilities, an increased emphasis on the whole ABL. Our current picture of the fair-weather CBL appears in [Fig. 9-9](#). In the figure, the height is normalized by z_i , the top of the ABL as defined by the height of the minimum buoyancy flux $B = (g/\bar{\theta}_v)w'\theta'_v$ (see [Fig. 9-10](#)). This definition is not practical for the observed ABL, so the height of the mixed-layer top h_1 , where $\bar{\theta}$ starts to increase with height ([Fig. 9-9c](#)), is often used. In [Fig. 9-9](#), the surface layer corresponds to where $\bar{\theta}$ and the longitudinal and lateral wind components \bar{U} and \bar{V} change with height, the mixed layer has near-constant values, and the transition layer lies between h_1 and h_2 , where $\bar{\theta}$, \bar{U} , and \bar{V} reach their free-atmosphere values. While the shear-driven ABL has an Ekman-like profile, the CBL has almost no wind turning with height, except near the surface and above h_1 . This well-mixed CBL picture was reinforced by observations in the 1973 Minnesota (United States) experiment ([Kaimal et al. 1976](#)) and the observations at Wangara (Australia; [Clarke et al. 1971](#)). However, other observations (e.g., [LeMone et al. 1999](#)) and more recently LES ([Conzemius and Fedorovich 2006a](#)) reveal that these well-mixed layers are features of more slowly growing ABLs with little shear above the ABL.

b. Fluxes

1) BUOYANCY AND MOMENTUM FLUX

The vertical fluxes of buoyancy and horizontal momentum for [Moeng and Sullivan’s \(1994\)](#) convective ABL are plotted as a function of height in [Fig. 9-10](#).

²¹ Indeed, [Deardorff \(1974a, p. 96\)](#) characterizes the neutral-stratification (u_*f) formulation for CBL depth as “hopelessly inadequate.”

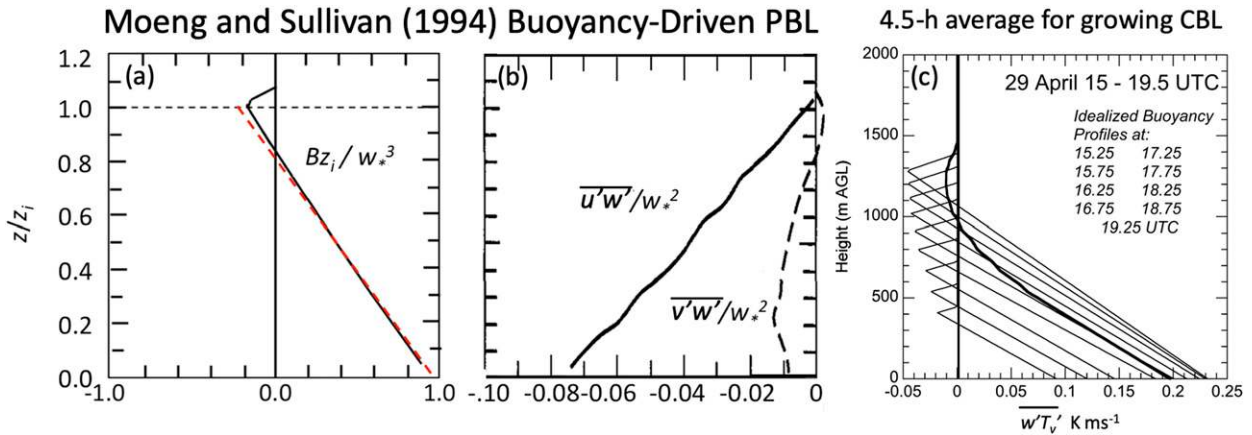


FIG. 9-10. Normalized flux profiles of (a) buoyancy and (b) momentum for convective ABL of Moeng and Sullivan (1994). The red dashed line in (a) is the idealized buoyancy flux for the zero-order CBL model. The CBL top z_i here corresponds to the minimum value of the buoyancy flux. (c) The average of half-hourly virtual-temperature flux profiles idealized using the profile at the left, based on flux and depth data for a rapidly growing CBL from the CASES-97 field program. Terms \bar{U} and \bar{V} are defined as in Fig. 9.

In the figure, the buoyancy flux B is normalized by w_*^2/z_i , where the Deardorff (1970a,b) convective velocity scale $w_* \equiv [(g/\bar{\theta}z_i)(\overline{w'T'})_0]^{1/3}$ (appropriate since $q \equiv 0$ in their simulation but now written using T'_v). Note that B is nearly linear with height up to z_i , consistent with the time rate of change of temperature being nearly independent of height but not consistent with $\partial\bar{\theta}_v/\partial z$. Such “nonlocal” fluxes²² were anticipated by Priestley and Swinbank (1947); and countergradient heat fluxes in the mixed layer were documented from aircraft data by Bunker (1956) and Telford and Warner (1964). From (9-12), the near-linear variation of $\overline{u'w'}$ with height is consistent with near-constant $\bar{V} - \bar{V}_g$ and \bar{U} within in the mixed layer, and, thus, nonlocal fluxes.

Figure 9-11 shows variances of the horizontal- and vertical-velocity components normalized by w_*^2 . In the figure, $\overline{w^2}/w_*^2$ peaks between 0.3 [Air Mass Transformation Experiment (AMTEX)] and around 0.5 (Willis and Deardorff 1974); the peak in Moeng and Sullivan (1994, not shown) is around 0.4. The variance in the horizontal wind components peaks at the surface, with a secondary maximum near ABL top in both cases. Horizontal-velocity variances for Willis and Deardorff’s (1974) laboratory model follow the same pattern. Temperature and humidity variance (not shown) also have peaks near the top and bottom of the ABL, where

$|\partial(\bar{\theta}, \bar{q})/\partial z|$ are largest; but often their peak near z_i is greater than that at the surface.

2) THE TKE BUDGET AND ENTRAINMENT

Since the 1970s, we have been able to use LES and observations to evaluate terms in the TKE budget, given by

$$\frac{\partial e}{\partial t} = \underbrace{\frac{g}{\theta_v}(\overline{w'T'_v})}_B - \underbrace{\overline{u'w'}\frac{\partial \bar{U}}{\partial z} - \overline{v'w'}\frac{\partial \bar{V}}{\partial z}}_S - \underbrace{\epsilon}_D - \underbrace{\frac{\partial(\overline{w'e'})}{\partial z}}_T - \underbrace{\frac{1}{\bar{p}}\frac{\partial(\overline{w'p'})}{\partial z}}_P. \quad (9-13)$$

where $e = \text{TKE}$, and the energy-production terms on the right side are respectively for buoyancy B and shear S (2 terms), and dissipation D . The last two terms represent vertical divergence of vertical transport of TKE T and pressure fluctuations P , respectively. Building on the work of Telford and Warner (1964), Lenschow (1970) published the first TKE budget derived from aircraft gust-probe data, which bears a strong resemblance to that for Moeng and Sullivan’s (1994) buoyancy-driven ABL (Fig. 9-12), despite his use of temperature rather than virtual temperature (implying dry air), and statistical uncertainty in the aircraft averages (see, e.g., Mann and Lenschow 1994).

A considerable amount of research has been dedicated to estimating the buoyancy flux at the BL top z_i (B_{z_i}), where the turbulent boundary layer is capturing (entraining) air from above. An entrainment ratio

²² Nonlocal fluxes are in contrast to those proportional to K times the local vertical gradient, such as those specified for the surface layer in section 3. Also called nonlocal transport. For further discussion see Deardorff (1966).

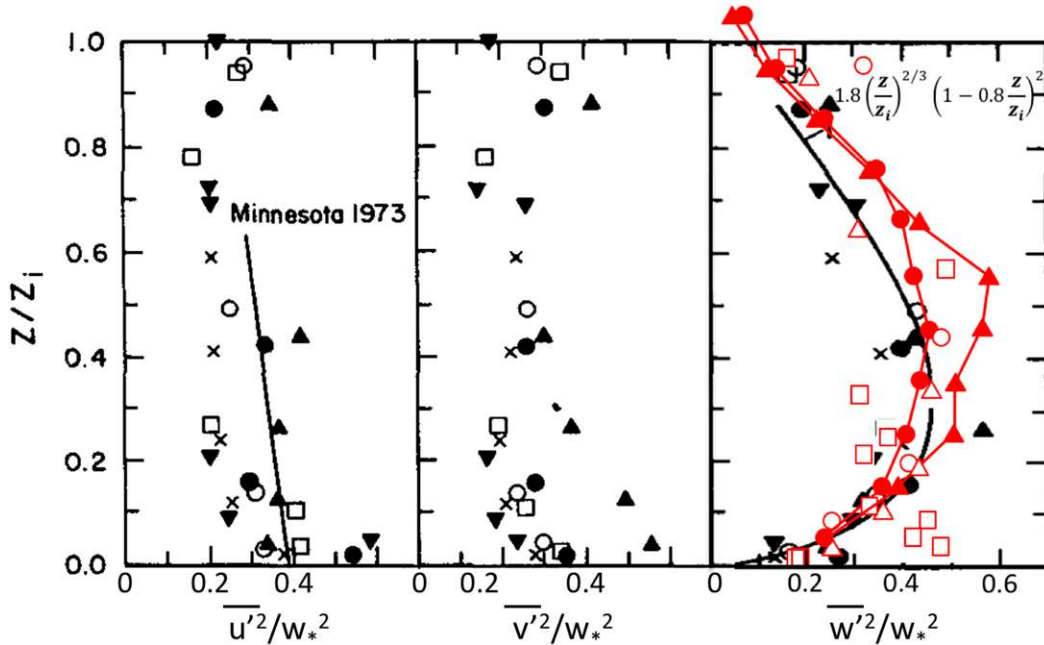


FIG. 9-11. Variances of fluctuating horizontal- and vertical-velocity components from the Air-Mass Transformation Experiment [AMTEX; black, from [Lenschow et al. \(1980\)](#)], with u in the direction of the mean wind, and from [Willis and Deardorff \(1974, Fig. 5\)](#) laboratory experiments (red). The different symbols are for different days/experiments. Idealized curves are based on the Minnesota experiment ([Kaimal et al. 1976](#)) and AMTEX (right panel). For comparison to LES see [Moeng and Sullivan \(1994\)](#).

$A_B = -B_{z_i}/B_0$, where B_0 is the surface buoyancy flux, is typically used.²³ However, since the shape of the area of negative buoyancy can vary, [Conzemius and Fedorovich \(2006a\)](#) use areas as well as A_B . A simple interpretation is that the “negative area” for B in [Fig. 9-10](#)—that area between the zero axis and the negative buoyancy fluxes, exactly balances the remaining TKE production/destruction within the CBL. Thus, for a CBL with no shear, the “negative area” would equal the integrated contribution of positive buoyancy to the TKE, minus the energy lost to dissipation. The first to estimate this ratio was [Ball \(1960\)](#), who found $A_B = 1$ assuming no shear or dissipation. With time, researchers converged on a ratio for a near-steady-state, weak-shear CBL close to 0.2 (e.g., [Stull 1976](#)). However, the negative area becomes smeared out vertically for rapidly growing CBLs, as can be seen by buoyancy profiles idealized using [Fig. 9-10a](#) as a function of height for different

times, leading to smaller values of A_B ([Fig. 9-10c](#)). One can see this smearing effect for more rapidly growing boundary layers in the classical laboratory studies of [Deardorff et al. \(1969\)](#).²⁴ Such effects, which provide strong incentive for simulating near steady-state ABLs, can mislead those doing observational studies of evolving ABLs, unless they effectively normalize by focusing on changes in the mixed layer or the entrainment layer (e.g., [Betts and Ball 1994](#); [Barr and Betts 1997](#)). For stronger winds [e.g., the [Moeng and Sullivan \(1994\)](#) shear + buoyancy ABL], the extra TKE supplied by shear production allows larger values of A_B , something confirmed by observations from the

²³ If B is used to define the entrainment ratio, use of virtual temperature or height-corrected virtual temperature will give the same answer. If, however, $w'\theta'_v$ is used, where θ_v is virtual potential temperature, A_B will be too large by a factor of roughly $[1000/P(z_i)]^{0.287}$, roughly 3% for pressure $P(z_i) = 900$ hPa for a $P_0 = 1000$ hPa.

²⁴ The more slowly growing boundary layers in [Deardorff et al. \(1969\)](#) have A_B closer to 0.2. According to [Jonker \(2018, personal communication\)](#), this turned out to be because—whether through insight or luck—their laboratory setup was in the right part of the parameter space, as defined by Prandtl, Reynolds, and Peclet numbers (the last being the heat-transfer analog to the Reynolds number). For engaging discussions of the influence of laboratory setups on entrainment results, see [Jonker et al. \(2012\)](#) and [Jonker and Jiménez \(2014\)](#). We also note that LES that use dynamic models to estimate the subgrid-scale turbulent Prandtl and Schmidt numbers are most successful in reproducing realistic results ([Shi et al. 2018a](#)). In this case, $Pr_t \sim 10$ in the cloud layer and ~ 0.5 in the air beneath.

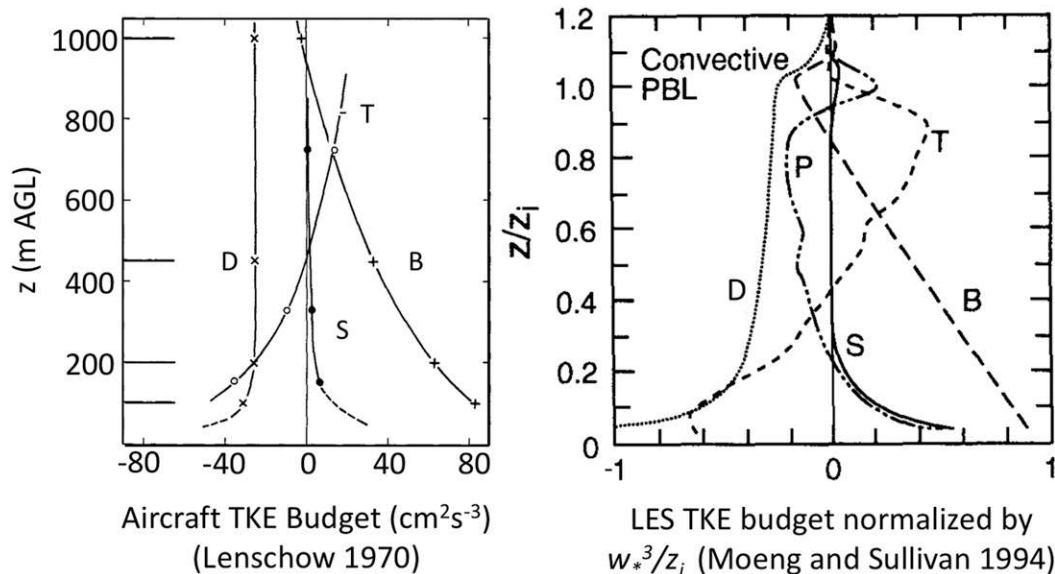


FIG. 9-12. Terms in TKE budget (9-13), based on (left) aircraft data and (right) LES. For the aircraft case, winds were on the order of $9\text{--}10\text{ m s}^{-1}$, there was scattered stratocumulus with bases just above 1000 m, and surface buoyancy fluxes were similar to those for Moeng and Sullivan. Horizontal lines mark the heights at which two sets of L-shaped patterns, 15–20 km on a side, were flown between 0942 and 1100 LST. In contrast, the corresponding shear-driven TKE budget (not shown) is mostly a balance between the shear and dissipation terms. [Adapted from Lenschow (1970) and Moeng and Sullivan (1994).]

First International Satellite Land Surface Climatology Project (ISLSCP) Field Experiment (FIFE; Betts and Barr 1996; Barr and Betts 1997). Conzemius and Fedorovich (2006b) summarize some entrainment parameterizations for ABLs with significant vertical shear.

c. Humidity and the importance of virtual temperature

So far, we have dealt with “dry” CBLs. Often, even cloudless CBLs are moist; this means that $\bar{\theta}_v$ is nearly constant in the mixed layer, with $\bar{\theta}$ increasing with height and \bar{q} decreasing with height. Such behavior is especially common over warm oceans (e.g., Bunker et al. 1949). Here, where sea–air temperature differences are often far less than over land, latent heat flux Q_{E0} is correspondingly much larger than sensible heat flux Q_{H0} . A consequence is that while $\overline{w'T'_v}$ remains positive through much of the mixed layer, $\overline{w'T'}$ is mostly negative, compensated for by large and positive $\overline{w'q'}$. Negative $\overline{w'T'}$ was observed early on. As noted in her article in *The Sea*, Malkus (1962, p. 210) found that temperature anomalies in updrafts went from positive to negative a few hundred meters above the tropical ocean; but the expected positive humidity fluctuation needed to provide buoyancy did not seem to be there—probably because the water vapor

sensor was too slow.²⁵ Not long after those observations were taken, both a wet-bulb instrument (Telford and Warner 1962, 1964) and microwave refractometer (McGavin and Vetter 1963; Bean et al. 1972) made fast water vapor measurements and thus $\overline{w'q'}$ measurements possible.

Examples of $\overline{w'T'}$, $\overline{w'q'}$, and $\overline{w'T'_v}$ profiles collected over the tropical Atlantic Ocean during GATE (1974) in Fig. 9-13 show the largest negative $\overline{w'T'}$ values corresponding to the largest upward $\overline{w'q'}$ at the top of the mixed layer, which is just below cloud base. The differences between the flux profiles (based on measurements on roughly a $30 \times 30\text{-km}$ scale) are related to the amount and vigor of cumulus cloud overhead. These differences appear to average out over larger scales, since budget studies over fair-weather domains on the order of hundreds of kilometers [Riehl et al. (1951) (see section 8c); Augstein et al. (1973) from the Atlantic Trade-wind Experiment (ATEX); Holland and Rasmusson (1973) and Esbensen (1975) from BOMEX] all find cloud-base Q_E on the order of 80%–90% of its surface value.

²⁵ This reinforced the erroneous idea that marine tropical cumulus do not have “roots,” based on aircraft subcloud turbulence observations in Bunker et al. (1949), which persisted until fast water vapor instruments were available.

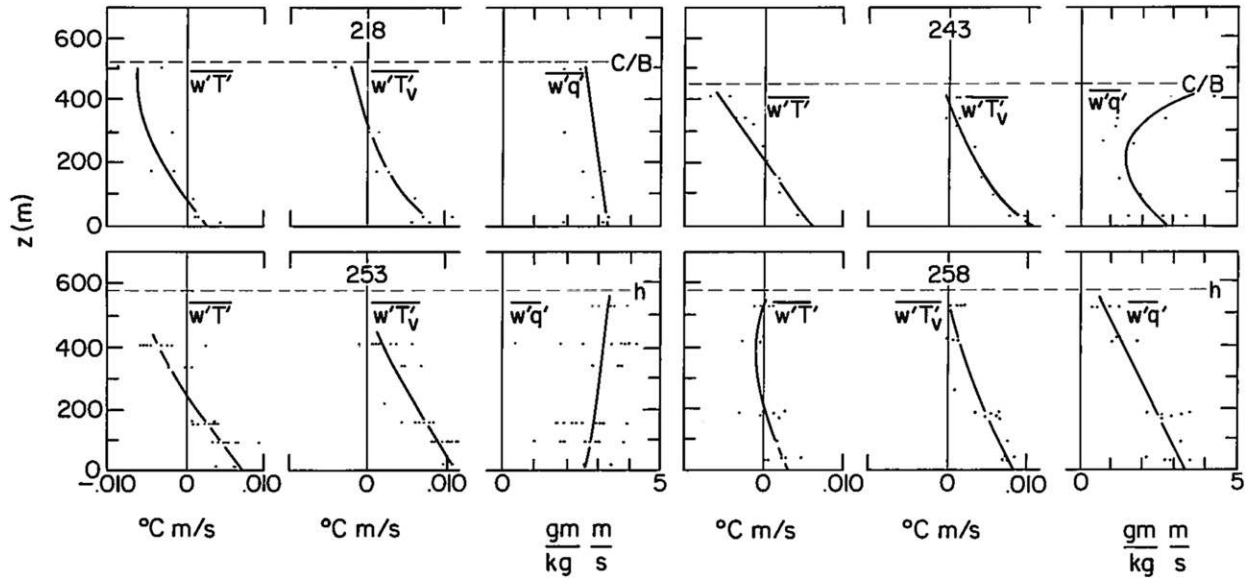


FIG. 9-13. Vertical profiles $\overline{w'T'}$, $\overline{w'q'}$, and $\overline{w'T_v}$, based on fair-weather flights during the Global Atmospheric Research Programme (GARP) Atlantic Tropical Experiment (GATE; Kuettner 1974, Kuettner and Parker 1976). Each point represents a roughly 30-km flight track either along or crosswind. There were no clouds on Julian day 258, but scattered clouds on days 218, 253, and 243. To get Q_H , multiply $\overline{w'T'}$ by 1150; to get Q_E , multiply $\overline{w'q'}$ by 2800. Note that the near-zero $\overline{w'T'}$ values in the upper half of the subcloud layer on day 258 are airplane specific, resulting from condensation on the salt-contaminated temperature sensor at the higher relative humidities. Heights were normalized by the top of the mixed layer, which was just below cloud base when clouds were present. [From Nicholls and LeMone (1980).]

If we normalize the $\overline{w'T_v}$ profiles by their surface values and combine the resulting profiles for the four days in Fig. 9-13, a linear fit yields a mixed-layer top flux about -0.17 times the surface value. While there is a strong relationship between clouds and the Q_E profiles, the cloud base acts much like the top of a cloud-free CBL.

d. Structure

Data from the Minnesota experiment (Kaimal et al. 1976) show that the peak in size for u and v eddies, though broad, is roughly constant through the ABL (Fig. 9-14) with a horizontal wavelength of about $1.5z_i$. That is, the fluctuations of the surface winds are largely determined by large eddies extending through the CBL. In contrast, w scales increase with height up to about $0.1z_i$, a consequence of updrafts associated with smaller-scale convergence and mass continuity. At smaller scales, points lie along the $-2/3$ slope associated with the frequency-weighted inertial subrange.

What do the eddies look like? As described by Woodcock (1941), circular soaring of gulls reflected columns of rising buoyant air (cells) in weak winds, while linear soaring in stronger winds reflected along-wind linear updrafts associated with helical circulations (longitudinal rolls). Kuettner (1959) suggested that cloud streets lie above roll updrafts. Hardy and Ottersten (1969) were able to document clear-air rolls and cells with radar. In the 1960s and 1970s, satellite

images and photographs by astronauts were showing cloud streets to be common, but some researchers remained skeptical about their relationship to boundary layer motions despite roll-like instabilities in boundary layers with Ekman wind profiles (e.g., Faller and Kaylor 1966; Brown 1970). This prompted LeMone and Pennell (1976) to document an example of direct association of lines of small cumulus with upwelling regions (Fig. 9-15). Weckwerth et al. (1997) used correlation functions from radar returns to determine the type of boundary layer eddies (e.g., rolls or cells, Fig. 9-16). Such echoes are common during the daytime over land when the air temperature is above about 10°C and are associated with insects. The insects do not fill the CBL because they tend to fly downward in updrafts (Geerts and Miao 2005). Further information about rolls can be found in the review paper by Young et al. (2002).

Observed rolls are roughly parallel to the mean CBL wind, and left of the geostrophic wind, as predicted for Ekman-layer rolls by Faller and Kaylor (1966), Brown (1970), and others. Deardorff (1972a) found roll-like structures in his LES for weak instability ($-z_i/L = 1.5$) but not for more unstable values, as did Moeng and Sullivan (1994) for similar values. Subsequent observational work, most recently by Weckwerth et al. (1997) suggest rolls that look like lines of cells can exist up to $-z_i/L \sim 20$, but not if $Q_H < 30\text{--}50 \text{ W m}^{-2}$, with cells occurring in weak winds. Recently, Salesky et al. (2017)

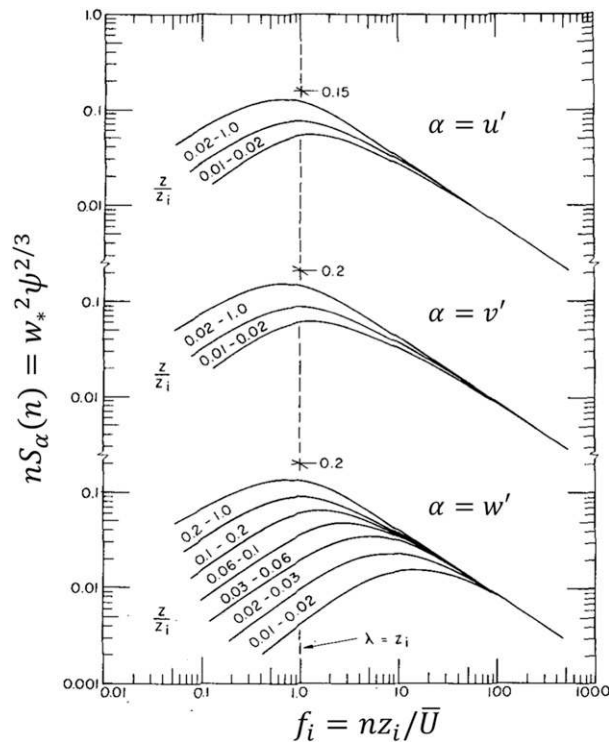


FIG. 9-14. Frequency-weighted spectra of the three velocity components, where u is in the direction of the mean wind, as a function of a dimensionless frequency that recognizes the important role of z_i . In the ordinate, ψ is normalized by the dimensionless dissipation rate, ε/B_0 . Prior to this, dimensionless frequency was typically defined by nz/\bar{U} , with \bar{U} the mean wind at height z , and n the frequency (Hz). [Adapted from Kaimal et al. (1976).]

used LES to reveal a transition of large eddies from rolls to cells as $-z_i/L$ increases from zero to ≈ 15 – 20 .²⁶ The horizontal scale for rolls and cells over land tends to be ~ 2 – $3z_i$; since rolls are aligned nearly parallel to the mean CBL wind, and cells occur in weak winds, it can take up to 30 min to an hour for either one to pass by a fixed point.²⁷ In LES, rolls are affected by periodic horizontal boundary conditions, which constrain their orientation; this problem can be dealt with by using large horizontal domains (e.g., Glendening 1996). Similarly, the choice of subfilter models can have a strong impact (Ludwig et al. 2009). While Faller, Kaylor, and Brown attribute roll formation to inflectional instability, the

²⁶ But without the clean lines-of-cells structures sometimes seen in clear-air radar echoes, probably because of a combination of LES limitations (ratio of roll width to domain size, periodic boundary conditions, grid resolution) and observational limitations (clear-air radar structures look more coherent at distances where return comes from higher in the PBL, the impact of insect behavior on clear-air radar echoes).

²⁷ For impact, see section 3a.

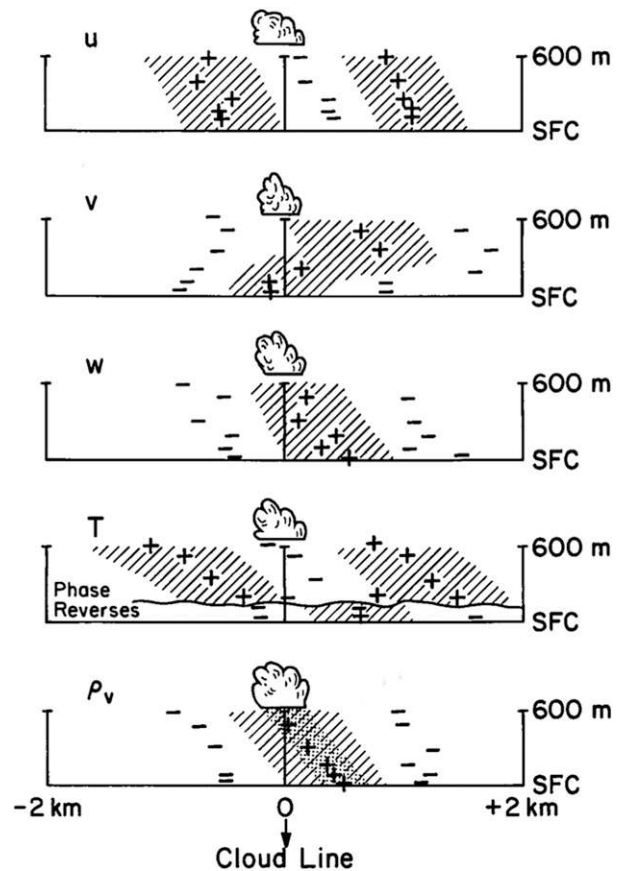


FIG. 9-15. Locations of roll-vortex extrema with respect to overhead cloud streets, illustrating a tilted roll-vortex circulation and its association with cloud streets. The wind components are in a right-handed coordinate system with u directed downwind, approximately parallel to the roll axis. Note the association of the upwelling air with low-level convergence of the cross-roll wind component v , and the association of $w > 0$ with water vapor density $\rho_v > \bar{\rho}_v$ and wind $u < \bar{u}$ through the subcloud layer. In contrast, the temperature is coolest in the roll updraft above about 200 m; above that, all positive buoyancy is from ρ_v . This is because these features were observed over the tropical ocean, where sensible heat flux is small compared to latent heat flux and mixed-layer $\bar{\theta}$ increases with height. [Figure from LeMone and Pennell (1976).]

wind profile is mostly an organizing factor: observed and LES rolls derive most of their energy from buoyancy. Moreover, shear-parallel rolls result in stability studies of constant unidirectional shear with unstable thermal stratification (e.g., Asai 1970), since shear-perpendicular rolls tend to feed energy into the mean flow.

5. Stable boundary layer

a. Introduction

While it has long been known that stable boundary layers are commonly generated during clear-sky nocturnal

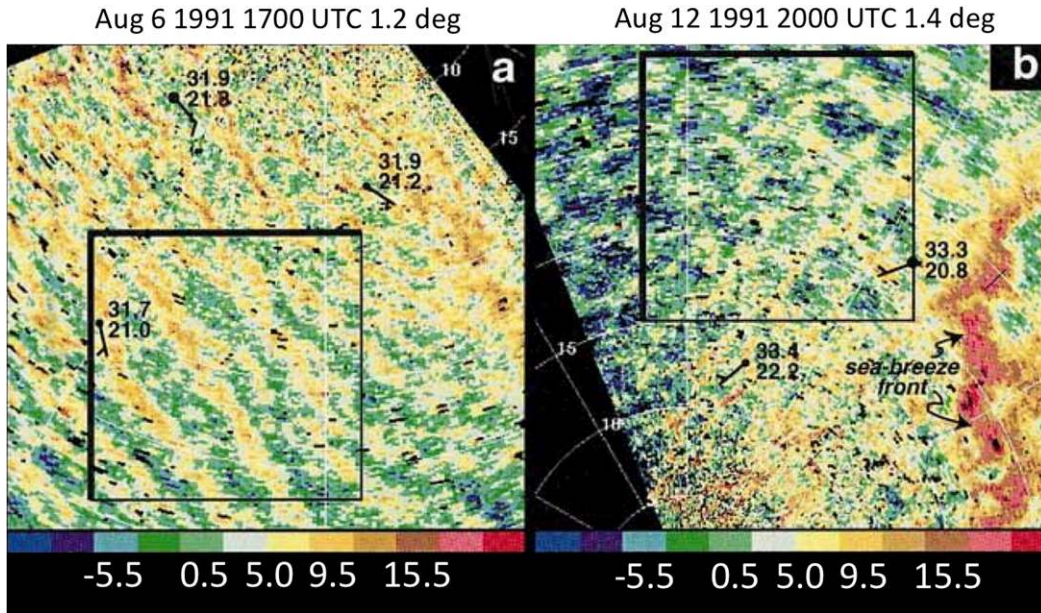


FIG. 9-16. Radar clear-air echoes showing (a) roll and (b) cell structure in the fair-weather CBL. The surface data is from NCAR portable automated mesonet stations; the squares were used for analysis. [Adapted from [Weckwerth et al. \(1997\)](#).]

conditions or with advection of warmer air over a colder surface, progress in understanding the stable boundary layer (SBL) has lagged that of the CBL because its smaller-scale and weaker turbulence, greater sensitivity to terrain, and more heterogeneous structure have made the SBL more difficult to observe (especially at night) and to simulate.

However, understanding of the SBL and particularly the nocturnal boundary layer (NBL) has increased substantially in the past two decades, especially through observational studies [e.g., CASES-99 ([Poulos et al. 2002](#)) and Surface Heat Budget of the Arctic Ocean (SHEBA; [Persson et al. 2002](#); [Grachev et al. 2005](#))]. Thanks to more powerful computers and new subgrid parameterization schemes (e.g., [Mason and Thomson 1992](#); [Sullivan et al. 1994](#); [Bou-Zeid et al. 2005](#) and references therein; [Chow et al. 2005](#)), LES have reproduced some features of NBLs with weak or moderate stability (e.g., [Kosović and Curry 2000](#); [Beare et al. 2006](#)). Newer subgrid schemes (e.g., [Zhou and Chow 2011](#)) and finer grid resolution show promise in preventing the turbulence collapse that has led to failures in LES in more stable conditions ([Jiménez and Cuxart 2005](#)). And [Sullivan et al. \(2016\)](#) simulated SBL structures for the [Beare et al. \(2006\)](#) case with L as low as 25.5 m, with careful attention to the lower boundary and using grid spacing down to 0.39 m. At the same time, observations have revealed important complications not previously recognized and noted below.

Recognizing that fluxes can vary rapidly with height in the boundary layer, [Nieuwstadt \(1984\)](#) reformulated MOST in terms of local fluxes, referred to as *local similarity theory*, where the characteristic scales are calculated locally instead of based on surface fluxes. Local similarity theory applies to the NBL above as well as within the surface layer. Local similarity theory has been evaluated by [Derbyshire \(1990\)](#), [Högström \(1996\)](#), [Basu et al. \(2006\)](#), [Steenveld et al. \(2006\)](#), and others. [Grachev et al. \(2013\)](#) verified local similarity in the surface layer for stable boundary layers after removing cases where the turbulence did not include an inertial subrange.

The turbulence in the NBL has been often classified as either weakly stable or very stable ([Mahrt 2014](#), and citations therein). [Van de Wiel et al. \(2003\)](#) successfully partitioned the NBL into a turbulent regime (roughly weakly stable), an intermittent regime, and a radiative regime where the turbulence remained extremely weak (a subset of the very stable class). A number of modeling studies have found transitions between weakly stable and very stable boundary layers to be dynamically unpredictable (e.g., [McNider et al. 1995](#); [Derbyshire 1999a](#)), which might be partly related to thermal interaction with the ground surface and vegetation ([van de Wiel et al. 2002](#)). We organize our thinking by contrasting the weakly stable and very stable boundary layers, with the understanding that such a classification greatly oversimplifies the physics of SBLs.

b. Weakly stable boundary layers

The weakly stable NBL is well defined, with turbulence decreasing with height to near zero, often at a local wind maximum, which may also correspond to the top of the nocturnal inversion (e.g., Blackadar 1957), all of which have been used to identify the NBL top. The weakly stable boundary layer is associated with significant winds and/or cloudy skies, and can reach hundreds of meters in depth.

The weakly stable NBL can be vertically partitioned into the roughness sublayer, the surface layer and the outer layer, the first two of which have been discussed in section 3. The *outer layer* extends from the surface layer top to the NBL top. Boundary layers that are relatively stationary for extended periods can occur during the polar night and be described by Ekman dynamics in the outer layer (Grachev et al. 2005). Turbulence in the outer layer may also follow Rossby similarity theory (Sorbjan 1989). Nonetheless, the role of the Coriolis parameter in the nocturnal boundary layer has been generally difficult to establish from observations.

With weakly stable conditions, the interior of the outer layer may be nearly well mixed, but the surface layer and the top of the boundary layer remain stably stratified. Turbulence may be driven partly by a nocturnal jet. Such jets are sometimes driven by inertial effects (Blackadar 1957), baroclinity associated with cooling over sloped terrain (Holton 1967), or a combination of the two (Du and Rotunno 2014; Shapiro et al. 2016). Lundquist (2003), Banta et al. (2006), Cuxart (2008), van de Wiel et al. (2010), Fedorovich et al. (2017), and others provide additional insight into the evolution of the nocturnal jet. The turbulence can become weak or nearly vanish at the nose of the jet where the speed shear vanishes. Turbulence may also be generated by shear above the jet (Conangla and Cuxart 2006).

With winds sufficiently strong, and terrain sufficiently gentle, airflow follows the surface without changing potential temperature, implying continued coupling between the surface and atmosphere (LeMone et al. 2003). For slightly weaker winds, airflow is coupled to the higher terrain features but more detached from lower-elevation sites (Acevedo and Fitzjarrald 2001; Fiebrich and Crawford 2001).

c. Very stable boundary layers

The very stable NBL results from weak large-scale flow and clear skies and remains poorly understood. The boundary layer top can be difficult to define and the zone of strongest generation of turbulence can be semi-detached from the surface or occur in layers (Balsley et al. 2003). Very stable boundary layers are generally quite

thin such that the fluxes may vary significantly between the surface and typical observation levels.

The vertical divergence of the radiative flux (clear air) can become important (Edwards 2009), and fog formation is common at some geographical locations. Typical nonstationarity of the very stable regime prevents physical description by similarity theory (Derbyshire 1999b; Mahrt 1999). Such nonstationarity is partly due to *submeso*²⁸ motions on scales just larger than the turbulence and includes wavelike motions, microfronts, quasi-horizontal meandering motions (Mortarini et al. 2016), and more complex modes. Examples are shown in Fig. 9-17. Because the wind direction cannot be predicted even on short time scales, dispersion models can be of limited skill in the very stable boundary layer. Unfortunately, these are the situations where the concentration of contaminants may be greatest.

The scale of submeso eddies can actually overlap with the largest turbulent eddies, compromising efforts to separate the turbulence from submeso motions in time series. Submeso motions nominally extend up to horizontal length scales of 2 km (the smallest mesoscale motion) although this partitioning is not based on any physics. A number of recent studies have made progress in understanding the different types of turbulent eddies and their relationship to submeso motions (Vercauteren and Klein 2015; Kang et al. 2015; Vercauteren et al. 2016), although a unified theory has yet to emerge.

The intermittency of the turbulence in very stable conditions is generally related to submeso motions or local shear instability. With increasing numerical resources, shear instability and resulting intermittency has become a growing area of research activity (e.g., Flores and Riley 2011; Anson and Mellado 2014; Sullivan et al. 2016).

Even shallow slopes or weak surface heterogeneity, of little consequence with more significant winds, can strongly affect the flow with large stability when the turbulent eddies are weak and of particularly small scale. In this regard, most of Earth's land surface becomes heterogeneous in strongly stable conditions. Thin drainage flows down local slopes can lead to a wind maximum only a few meters above the surface, such that the vertical gradients of wind speed and momentum flux can reverse sign near the surface. The vertical profile of the turbulence intensity may have a minimum at the wind maximum even close to the surface (Horst and Doran 1988; Grisogono et al. 2007; Mahrt et al. 2014).

²⁸ The term may have first been used in an atmospheric science context by Mestayer and Anquetin (1995), but it was later defined to be between turbulence and smallest mesoscales (e.g., see review of the SBL by Mahrt 2014).

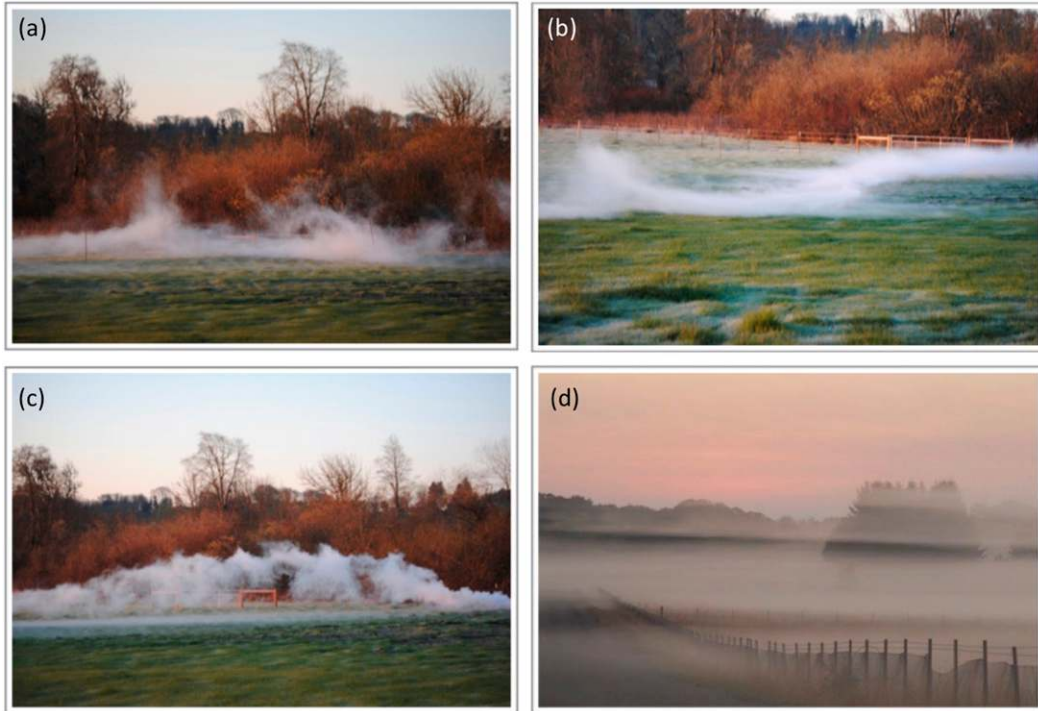


FIG. 9-17. Four examples of frequently observed structures in the weak-wind stably stratified boundary layer as revealed by machine-generated fog, namely: (a) an upward ejection of near-surface fluid, which often coincides with the greatest upward displacement in shallow wave-like modes, plus a transverse eddy overturning, (b) meandering of the wind vector and a small upward ejection, apparently part of a wave-like motion, (c) nearly one cycle of a wave-like mode with transverse instability occurring on a horizontal scale of at least one order of magnitude smaller, and (d) striated natural fog where the turbulence is limited to fine scales that lead to only slow diffusion of the striations. (Photos courtesy of Larry Mahrt.)

Such thin drainage flows are characterized by relatively large stress divergence below their wind maxima (Nadeau et al. 2013).

Most of Earth's surface is characterized by surface heterogeneity that occurs simultaneously on different horizontal scales. Horizontal temperature advection may be locally important with low wind speeds (Cuxart et al. 2016). Cold pools can form even in gentle terrain, and commonly form in valleys with shallow down-valley slope. The resulting horizontal temperature variance in larger watersheds (airsheds) can increase through the night to values much larger than those for the weakly stable ABL over flat terrain (Fig. 9-18). In such weak winds, the long-known dependence of air temperature on surface cover (e.g., Cornford 1938) would be expected to be stronger. The time required after sunset to reach maximum horizontal variation of observed 2-m temperature at well-exposed sites is a function of array width, horizontal variation of even mild terrain, and station siting. For example, the timing of maximum variability at well-exposed sites in Fig. 9-18 (top) is linked to the travel time of horizontal drainage winds

from the edges of the Walnut River watershed. In contrast, low-lying sites sheltered from the wind are influenced more by radiative cooling. Local (of scale < 1 km) cold pools with shallow slopes are often intermittent (Geiss and Mahrt 2015). Cold pools are better defined and thus better understood in uncommon completely enclosed depressions (Whiteman et al. 2004).

d. Representing the SBL in models

Models accommodate uniform parameterizations (such as existing similarity theory) better than class-dependent parameterizations. However, similarity theory suffers from lack of understanding of the underlying basic physics for the SBL. Specification of the turbulent Prandtl number Pr_T as a function of stability as defined by the gradient Richardson number,

$$Ri_g = \frac{g}{\theta_v} \frac{\partial \bar{\theta}_v}{\partial z} \left(\left[\frac{\partial \bar{U}}{\partial z} \right]^2 + \left[\frac{\partial \bar{V}}{\partial z} \right]^2 \right)^{-1},$$

is one example of this difficulty. Some insight is provided by the equation for total turbulent energy that combines

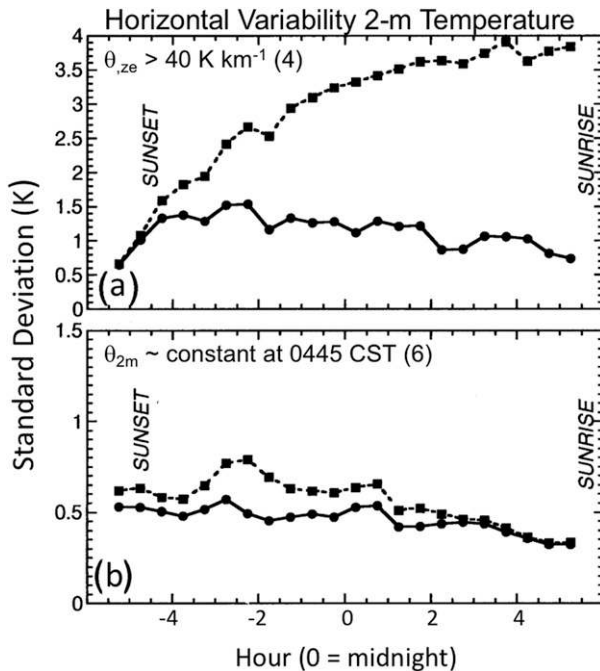


FIG. 9-18. Average horizontal variability in 0.5-h average 2-m $\bar{\theta} = \bar{\theta}_{2m}$ through the night for ABLs that are mostly (a) very stable ($\bar{\theta}_{ze} > 40 \text{ K km}^{-1}$) and (b) weakly stable ($\bar{\theta}_{2m} = \text{const}$), based on 0.5-h averages between 0430 and 0500 local standard time, using CASES-97 (LeMone et al. 2000) data. Numbers in parentheses are the number of nights represented. For the nights included, the dashed line in each panel gives the average of the standard deviations relative to the mean of the surface sites for each time. The solid line is found by first finding the least squares best-fit line relating $\bar{\theta}_{2m}$ to site elevation z_e for each time, and then computing the standard deviation relative to that line. In (a) $\bar{\theta}_{ze} \equiv \partial \bar{\theta}_{2m} / \partial z_e$ increases with (but is less than) the radiosonde-based vertical gradient $\bar{\theta}_{ze} \equiv \partial \bar{\theta} / \partial z$. The good linear relationship of 2-m temperature to elevation just before sunrise was related to drainage winds from the watershed boundaries reaching all the surface towers. [Adapted from LeMone et al. (2003).]

turbulent kinetic energy and turbulent potential energy $[= (1/2)\sigma_{\theta_v}^2 (g/\theta_v) N^{-2}$, where the Brunt–Väisälä frequency $N = [(g/\theta_v)(\partial \theta_v / \partial z)]^{1/2}$; Mauritsen et al. 2007; Zilitinkevich et al. 2013]. This approach is no longer constrained by a critical Richardson number for differentiating between turbulence and laminar flow but rather leads to a transition Richardson number that divides the weakly stable and strongly stable regimes.

Some higher-order ABL models (e.g., Mauritsen et al. 2007; Zilitinkevich et al. 2013; Sukoriansky and Galperin 2013) predict that Pr_T increases with Ri_g , which has some observational support (e.g., Strang and Fernando 2001; Yague et al. 2006) and has been attributed to inclusion of internal gravity waves. However, there is considerable uncertainty, since gravity wave scales present multiple sampling problems (see Acevedo and Mahrt 2010 and references therein). In addition, the time series near the surface

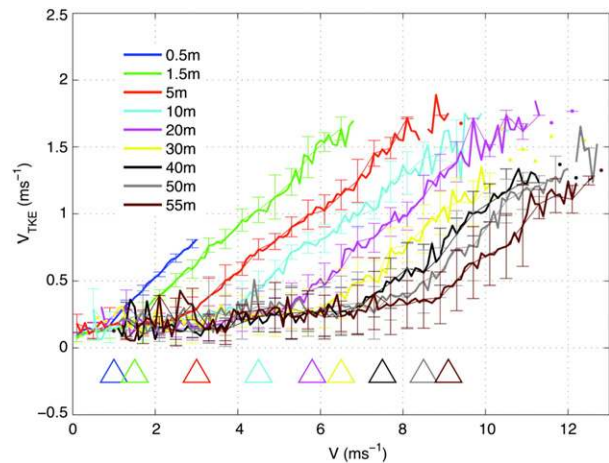


FIG. 9-19. Shown is $V_{\text{TKE}} = (\text{TKE})^{1/2}$ as a function of mean wind at different heights on a 60-m tower, based on all nighttime data from CASES-99 (Poulos et al. 2002), showing that V_{TKE} is a linear function of wind above a certain threshold wind speed V_s , which is indicated by the large triangles. For $V > V_s$ (regime 2) eddy size is independent of height; for $V < V_s$ (regime 1), eddy size increases with height. [Adapted from Fig. 1 of Sun et al. (2012).]

show a complex mix of motions, and clean monochromatic waves are uncommon (Sun et al. 2015). Although self-correlation predicts that Pr_T increases with Ri_g , Anderson (2009) developed an approach that mitigates the effects of self-correlation and still found that Pr_T increases with Ri_g .

As noted by Grachev et al. (2007), the influence of other factors such as radiative flux divergence needs to be investigated. Alternatively, modeling approaches, such as that of Li et al. (2015), which emphasizes the physics behind the relationship between Pr_T and Ri_g , including the different relaxation times for the heat and momentum fluxes and their dependence on scale, are needed.

The turbulence in the weakly stable boundary layer is generally considered to be more or less continuous and to satisfy similarity theory, but this has become increasingly challenged. Sun et al. (2016), for example, used CASES-99 data to show that fluxes are poorly predicted using MOST for their Regime 2 (Fig. 9-19), which roughly corresponds to the weakly stable NBL, where fluxes are determined by large eddies sensing gradients over their depth (Sun et al. 2012). This regime corresponds to the strong-wind part of the “hockey stick” dependence of u_* or V_{TKE} on the wind speed, which has been found in numerous other studies. For a few examples, see Andreas et al. (2012) over a sea surface, Vignon et al. (2017) over the Antarctic plateau, and Acevedo et al. (2016) over complex terrain.

6. The diurnal cycle

Many studies of the CBL and NBL have been limited to near-steady state, or at least slow evolution, by the

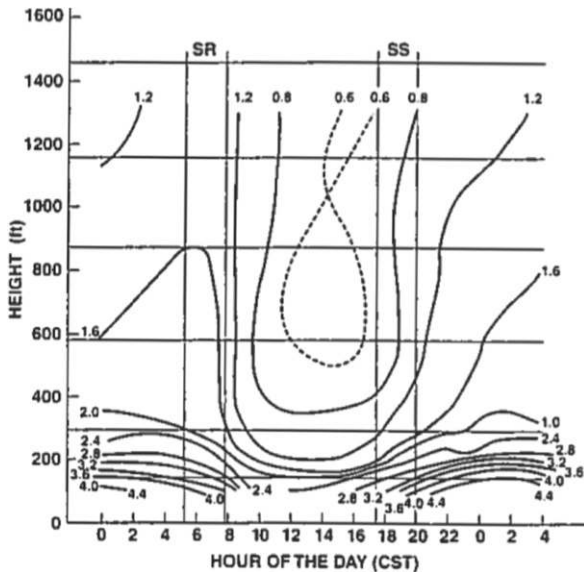


FIG. 9-20. Average diurnal cycle of vertical wind shear [$\text{kt} (100 \text{ ft})^{-1}$, which corresponds to $1.7 \text{ m s}^{-1} (100 \text{ m})^{-1}$], from one year of data from the KTVY-TV tower in Oklahoma City, which was instrumented by the National Severe Storms Laboratory. [From Crawford and Hudson (1970).]

requirement for sufficient statistics to document the contributions of turbulence. As research topics, transitions between states have received attention only relatively recently, despite their recognized importance to many applications. While near steady-state CBLs can exist over the ocean, and weakly stable boundary layers can reach near steady state over the Arctic, the CBLs and SBLs described above are in reality special or end states within the diurnal cycle over land. Transitions take several hours of the diurnal cycle even in rather simple situations. Figure 9-20 indicates, for example, that fully convective low-shear boundary layers typically occur within the 2–4 h after local noon in the Midwestern United States.

Over land, the rising and setting of the sun drives a diurnal cycle of temperature and boundary layer depth. The amplitude of the cycle depends on season, latitude, surface type, land use and soil moisture; it interacts with clouds. Geiger (1966) has examples of documented diurnal $\bar{\theta}$ variation prior to the twentieth century and discoveries of greater frequency of calm winds at night in the early twentieth century. The diurnal variation of \bar{q} has been less studied, but Geiger (1966, p. 107) shows a graph from Frankenberger (1955) of the “well known” \bar{q} diurnal variation, with peaks during the early morning and evening resulting from evapotranspiration into a shallow boundary layer.

In the classical picture (Ball 1960; Lilly 1968; Garratt 1990), the growth of the boundary layer in the morning

is determined by competition between surface buoyancy flux, entrainment of air into the growing boundary layer, and subsidence. From section 4b(2), the entrainment ratio A_B was often assumed to be constant, neglecting shear effects. However, Angevine et al. (2001) found that after sunrise, the air below 50 m warmed to form a nascent boundary layer *before* B_0 became positive, with the CBL growing much faster than suggested for buoyancy-driven growth with $A_B = 0$, indicating the need to account for shear-driven mixing and its role in entrainment. During this “morning transition,” the boundary layer is in a “mixed CBL–SBL state” both vertically, as revealed in LES by Beare (2008) and—in even mildly varying terrain—horizontally, as shown in observations by Lenschow et al. (1979). Only by mid-to-late morning does the buoyancy-driven CBL achieve the entrainment ratios produced by LES of buoyancy-driven CBLs. While direct heating of the air by radiation was recognized as being a factor in daytime warming, its effect over land is often fairly small (e.g., Deardorff 1974a; Angevine et al. 1998).

During the afternoon and evening, the boundary layer was found to undergo “transition” and “collapse” of turbulence by early researchers. The associated reduction in near-surface thermal instability, followed by onset of a nocturnal inversion resulting from radiative cooling on clear nights, has been documented for a century or more (Geiger 1966). Now we have a richer picture of coevolution of turbulence and mean profiles during late afternoon and evening. As the sun moves lower in the sky through the afternoon, the surface cools more rapidly than the air a few meters above the surface, making the air less unstable. Therefore, thermals weaken. They rise through an approximately neutral layer, so even these weaker thermals can reach the same height as earlier; but eventually other processes become important, and most of these processes tend to warm and stabilize the upper BL (e.g., Grant 1997). For example, shear-driven entrainment and direct radiative heating both warm the upper BL. Subsidence also drives the BL top downward. The result is that the CBL depth as defined by an increase in $\partial\bar{\theta}_v/\partial z$ stays roughly constant or decreases in the afternoon, with the $w'\theta'_v$ -defined depth (top of radar-sensed plumes, since Ri higher up indicates little local mixing) decreasing even faster on many occasions. Grimsdell and Angevine (2002) were the first to describe an afternoon transition in these terms, drawing from in situ flux profiles (e.g., Grant 1997). Figure 9-21 shows an example of this evolution. The afternoon weakening of turbulence and decline of the BL top can occur slowly enough that statistical stationarity still applies.

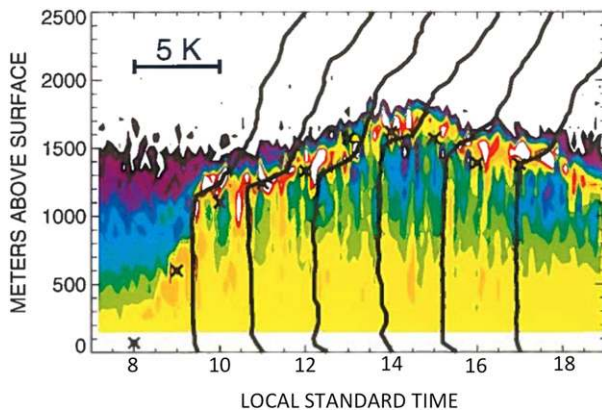


FIG. 9-21. Evolution of the CBL based on radar wind profiler signal-to-noise ratio (SNR) and sequential radiosondes released from Beaumont, Kansas, during CASES-97. Note the descent of the CBL top after 1400 LST and the continuing evidence of thermals in the late afternoon, even though they tend to be weaker and shallower. ABL stands for Argonne Boundary Layer Experiments; operated by Argonne National Laboratory. Colors going from small to large SNR are white, black, violet, dark blue, blue-green, green, light green, yellow, orange, red, and white. [Adapted from Fig. 12 of LeMone et al. (2000).]

Eventually, $\bar{\theta}_{v0}$ falls below $\bar{\theta}_{v,air}$, making the surface layer stable. As a result, $w'\theta'_v$ becomes negative and the winds decelerate as downward momentum mixing decreases; these changes coincide with the onset of the evening transition. Businger (1973) argued that this cooling can make the air stable enough that turbulence is suppressed—the so-called collapse. This situation tends to be temporary, since turbulence persists at higher altitudes, resulting in an increase in near-surface wind and thus a resumption of near-surface turbulence once the vertical shear becomes sufficient for turbulence to be re-established. As shown by van de Wiel et al. (2002, 2003), this process can repeat through the night.

The Boundary Layer Late Afternoon and Sunset Turbulence project (BLLAST; Lothon et al. 2014) was dedicated to deeper understanding of these processes. On the modeling side, the Global Energy and Water Cycle Experiment (GEWEX) Atmospheric Boundary Layer Study (GABLS) GABLS2 and GABLS3 single-column modeling comparisons included full diurnal cycles (Bosveld et al. 2014; Svensson et al. 2011). In both studies, the various models produced quite different responses, especially in the evening. Recently, Basu et al. (2008), Kumar et al. (2006, 2010), and Sharma et al. (2017) have conducted LES of the diurnal cycle, providing reasonable matches to observations. Such studies are rare, mainly because of the need for finer grids and sophisticated subfilter-scale representations needed for stable stratification.

7. Impact of horizontal heterogeneity

Any time airflow encounters an abrupt change in surface characteristics, the boundary layer will be out of equilibrium and a circulation will develop. The sea breeze is the best-known example, but horizontal heterogeneities also matter over land. From the early twentieth century, researchers have documented the influence of vegetation or soil properties on near-surface temperature, humidity, and wind (Geiger 1966). Starting in the late 1950s, researchers began to examine internal boundary layers resulting from a change in surface roughness; first, for the simple case of neutrally stratified flow, but later examining the effects of abrupt changes in surface flux and temperature (Garratt 1990). Such information was helpful in figuring out just where to measure a surface flux representative of, say, a large cornfield; but for flux measurements from a moving platform like an aircraft, the problem is turned around: just which surface contributed to the measured fluxes?

As can be seen from Fig. 9-22, there is a qualitative relationship of fluxes to surface properties beneath and upstream of the aircraft track, but more quantitative information is desirable for testing surface-flux models. The contribution of the upstream surface to the fluxes measured at a point is determined in terms of a so-called footprint, which is a function of height, stratification, and wind speed. Schuepp et al. (1990, 1992) refined a “footprint” function, derived for diffusion applications by Pasquill and Smith (1983) to address this question, and applied it to aircraft data from FIFE (Sellers et al. 1992). Davis et al. (2003) used the Weil and Horst (1992) footprint formulation to show that the fetch is on the order of 10 times the measurement height during convective conditions, with this increasing significantly during stable conditions. Thus, for a surface-level measurement, a 100–200-m fetch is recommended. If one can model the surface fluxes for each surface type contributing to the measured flux using its flux footprint (e.g., Anderson et al. 2004), then the model can then be applied to similar parcels of land to “scale up” the fluxes over a region (e.g., Anderson et al. 2007), sometimes referred to as the tile approach.

Fluxes over a heterogeneous area can also be computed applying MOST to roughness lengths that apply to the area (Wieringa 1976). These regional or effective roughness lengths apply above a so-called blending height—where the fluxes from the nonuniform surface become blended—but still within the surface layer; that is, the blending height must be low (In the case of Anderson et al. 2004, about 50 m). Estimates of the effective roughness length z_{0m}^{eff} were perhaps first made when Fiedler and Panofsky (1972) applied a simple

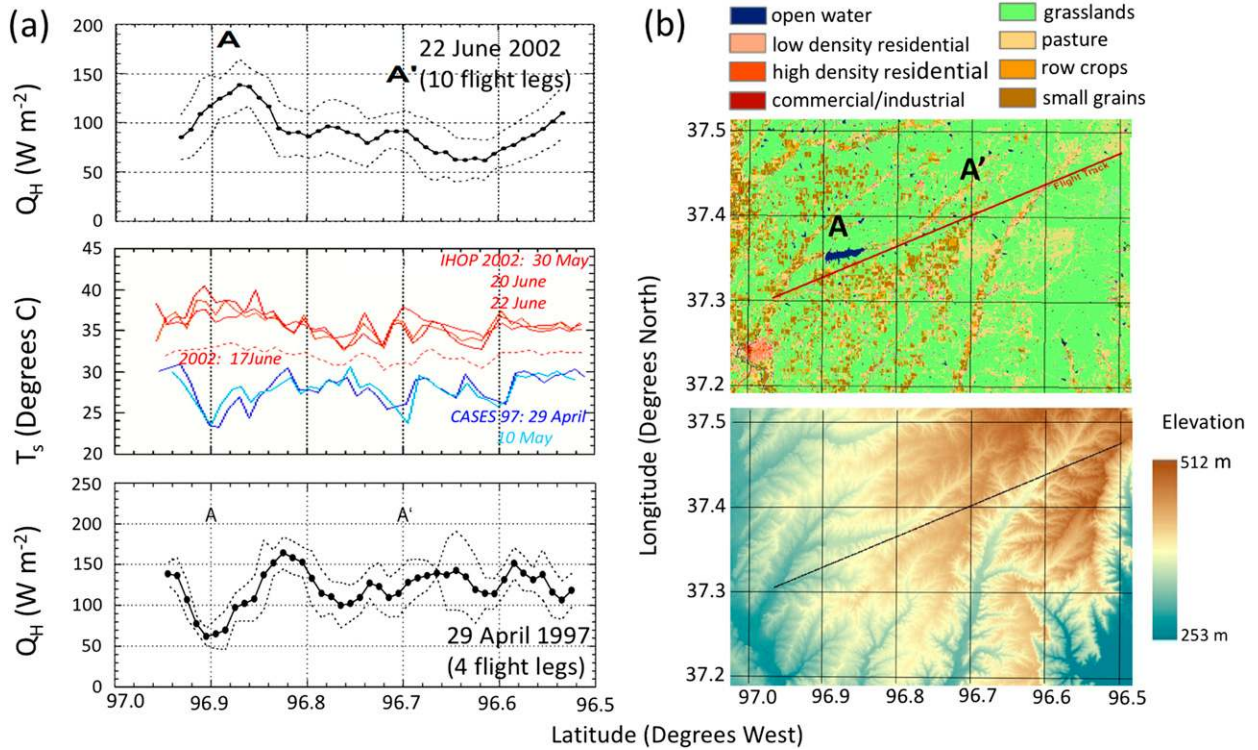


FIG. 9-22. (a) The influence of surface properties on sensible heat flux Q_H , based on aircraft data collected at 65 m AGL, (b) along a track flown during the spring (CASES-97; dormant grass and growing winter wheat) and summer [IHOP_2002, Weckwerth et al. (2004); senescent/harvested winter wheat and green grass]. Fluxes are averages over N flight legs, of 4-km running-mean averages of instantaneous values of Q_H based on departures of θ and w from their linear trends along each leg. Dashed lines are $\pm\sigma[(N-1)/N]^{0.5}$, where σ is standard deviation. Wind direction is from the south. [Panel (a) and top of (b) are adapted from Figs. 5–7 of LeMone et al. (2007).]

equation relating the ageostrophic wind to boundary layer fluxes using aircraft wind and turbulence data collected at 75 and 225 m AGL. Ironically, this was the same year that Pasquill (1972) introduced the blending-height concept. Since weather and climate models compute fluxes over grid areas that typically encompass a nonuniform surface, z_{0m}^{eff} and its heat-flux and moisture-flux counterparts z_{0h}^{eff} and z_{0q}^{eff} are needed on a routine basis (Beljaars and Holtslag 1991). The blending height has been estimated as proportional to the scale of the heterogeneity (Mason 1988), and varies with stability, wind speed, and surface properties (e.g., Wood and Mason 1991; Mahrt 1996).

Beljaars (1988, see Beljaars and Bosveld 1997) estimated z_{0m}^{eff} as a function of fetch and season for the 200-m Cabauw tower in the Netherlands and found it to be larger than that at the tower itself; this work was refined using an expanded dataset by Verkaik and Holtslag (2007). Kustas et al. (2005) obtained z_{0m}^{eff} for the CBL over an area with corn and soybean fields both by using aircraft data collected above the blending height and by aggregating the roughness lengths of the fields in the aircraft flux footprint following Mason (1988)

and found that the aggregated value—and therefore the associated flux—was too small. However, they successfully managed to replicate heat and moisture fluxes. They concluded that the too-small z_{0m}^{eff} was related to flow over sharp boundaries between fields, such as created by shelterbelts, edges of roadways, or the height differences between the two crops, as well as upstream buildings and other obstacles not accounted for. A number of years earlier, an LES study of a neutrally stratified BL by Albertson and Parlange (1999b) revealed that the edges of patches with different roughness contributed to the total surface stress, with stress larger for more, smaller patches. More recently, Bou-Zeid et al. (2004) performed a series of neutral-boundary layer LES for a similar range of patch sizes to develop relationships between patch size, blending height, and z_{0m}^{eff} .

As for z_{0h}^{eff} , Wood and Mason (1991) and Beljaars and Holtslag (1991) both showed that it can be significantly different from local values in the CBL. For a weakly stable BL with continuous turbulence, over a surface with streamwise horizontally varying temperature, Stoll and Porté-Agel (2009) suggest that the scalar fluxes

found from averaging MOST-derived fluxes for individual patches (\sim one-half to twice PBL depth) grossly underestimate the actual heat flux, unless local similarity theory is used. For further information on blending-height theory and related concepts, see [Mahrt \(2000\)](#).

Relating fluxes to surface properties is made possible by databases for land cover and soil properties, which are heavily dependent on satellite remote sensing. This of course required translating measurements at different wavelengths into vegetation properties, such as the leaf area index (LAI, leaf area per unit surface area, estimated first by [Jordan 1969](#)), and the normalized differential vegetation index ([Rouse et al. 1974](#)), a measure of vegetation greenness. The first land-use satellite (Landsat) was launched in 1972; the first global land-cover database was completed in the 1990s (<https://archive.usgs.gov/archive/sites/landcover.usgs.gov/globalandcover.html>; also see [Loveland et al. 1995](#)). In the United States, two commonly used land surface datasets are based on Advanced Very High Resolution Radiometer (AVHRR) data, provided by the U.S. Geological Survey, and the Moderate Resolution Imaging Spectroradiometer (MODIS). Soil moisture and temperature are found through use of land surface models (see [section 10](#)).

There emerged in the 1980s an increased interest in the impact of surface heterogeneity on boundary layer structure. Horizontal nonuniformity in soil moisture and land cover and even modest changes in elevation lead to mesoscale circulations that are more than curiosities: they can initiate development of thunderstorms (e.g., [Pielke et al. 1997](#); [Fig. 9-23](#)). Such an association was anticipated in idealized mesoscale simulations by [Ookouchi et al. \(1984\)](#). Numerous other authors have examined the impact of horizontal nonuniformities using mesoscale models ([Yan and Anthes 1988](#)), LES ([Walko et al. 1992](#)), and LES and DNS ([Krettenauer and Schumann 1992](#)). These circulations vary in horizontal extent from ~ 5 km ([Mahrt et al. 1994](#)) to ~ 100 km ([Chen and Avissar 1994b](#)). Observations are scarce, although [Physick and Tapper \(1990\)](#) document diurnal circulations around a ~ 8 -km diameter salt pan in Australia, [LeMone et al. \(2002\)](#) find 60-km circulations for a summer day when dormant (warm) vegetation at higher elevations reinforced terrain effects in forcing the circulations, and [Mahrt and Ek \(1993\)](#) found evidence of “forest breezes,” in HAPEX-MOBILHY in France, almost 100 years after they were first reported ([Schmauss 1920](#); see [Geiger 1966](#)).

How do these structures impact fluxes and profiles? Numerous LES studies have addressed the impact of surface heterogeneity and associated circulations on regional boundary layer statistics. Comparing a simulated CBL over a uniform surface to one with imposed

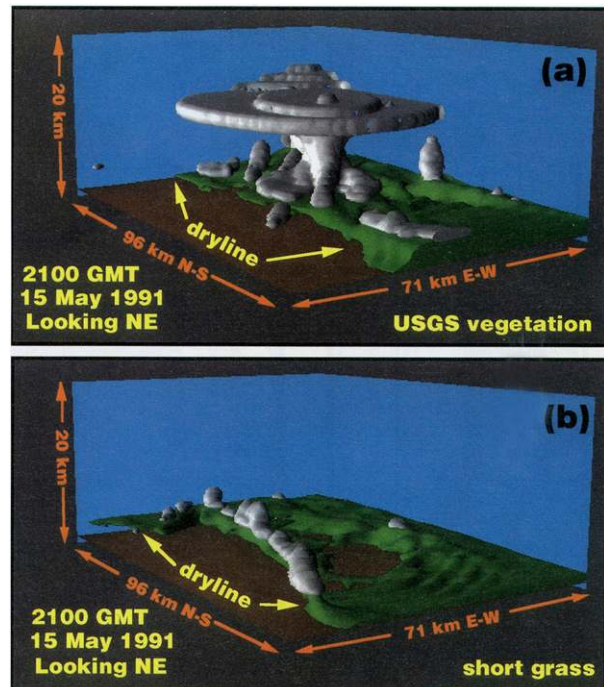


FIG. 9-23. Impact of horizontal variability on development of precipitation, based on RAMS simulations for United States Geological Survey (USGS) (top) vegetation and (bottom) short grass only. [From [Pielke et al. \(1997\)](#). © 1997 Ecological Society of America.]

realistic surface temperature variations of scale 450–900 m to represent the surface over which observations were taken, [Hechtel et al. \(1990\)](#) found little difference between simulated boundary layer evolution and horizontally averaged variances θ , q , and w , buoyancy flux, q flux and TKE, which, they noted could partially result from a $\sim 5 \text{ m s}^{-1}$ wind. [Avissar and Schmidt \(1998\)](#) found that idealized but realistic heat-flux patchiness of scale < 5 – 10 km had little effect on the average CBL θ and q statistics, but they did find impact for larger scales and winds $< 5 \text{ m s}^{-1}$. Similarly, [Albertson and Parlange \(1999a\)](#) find the blending-height concept to be useful for imposed heat and moisture fluxes on scales on the order of PBL depth owing to mixing by PBL eddies of comparable scale to z_i , especially for mean profiles of θ and q .

Cities are important sources of horizontal heterogeneity throughout the boundary layer. [Oke \(1982\)](#) traced our awareness of urban–rural differences in near-surface temperature back to the early 1800s but notes the absence of systematic investigation going beyond mere statistical association until around 1970. By the 1980s, a number of studies (e.g., [Bornstein 1968](#), [Changnon 1981](#)) revealed that, compared to the surrounding rural areas, cities at night tend to be warmer near the surface,

with $\bar{\theta}$ less stratified; while during the day, the urban CBL tends to be deeper. Oke attributed these changes not only to the impact of different structure and composition of cities on heating, cooling, and momentum exchange, but also to release of heat from buildings, factories, cars, and even people. [Fernando \(2010\)](#) and [Barlow \(2014\)](#) provide more recent reviews of the effects of cities on the ABL.

8. Cloud-topped boundary layers

a. Introduction

Cloud-topped boundary layers (CTBLs), especially over the oceans, have developed into one of the most important topics in boundary layer meteorology because of their extensive coverage and climate impact. Clouds strongly interact with solar and infrared radiation and they can precipitate; consequently, they affect and are affected by the surface energy balance as well as the ABL turbulence structure. They also strongly impact ABL aerosols and chemical composition. Overall, they significantly impact Earth's radiation balance and general circulation. The response of boundary layer clouds to anthropogenic greenhouse gases and aerosols are two of the key modeling uncertainties in projecting climate change ([IPCC 2013](#), chapter 7). CTBLs are ubiquitous: based on routine surface observations compiled in the Warren cloud atlas ([Warren et al. 1986, 1988](#)), on average over 47% of the globe (55% of the ocean and 26% of the land), is covered by low-lying cloud cover with a base below 1 km ([Hahn and Warren 1999](#); Fig. 3 in [Park and Bretherton 2009](#)), most of which is likely rooted in the ABL.

While interest in the tropical marine CTBL can be traced back to the 1930s, research on CTBLs picked up during the 1980s, as a natural next step after rapid progress on the clear-air CBL ([section 4](#)). The timing was good, since NWP and climate models were just beginning to predict cloud development. This effort was supported by a series of international field programs with a focus on cloud-topped boundary layers, taking advantage of the latest developments in remote sensing, surface flux, and aircraft turbulence and microphysics measurement technology. Also, starting in 1992 with the Atmospheric Radiation Measurement (ARM) Program Southern Great Plains (SGP) facility, a series of surface “supersites” in different parts of the world became available to provide valuable surface-based observations to complement such field efforts. The GEWEX project began to foster a series of LES and single-column model (SCM) studies of significant CTBL regimes and processes sampled in field campaigns, some

initiated by the climate community. Thanks in large part to this synergy, LES technology improved to the point that it could be used as a benchmark for developing CTBL parameterization schemes for increasingly complex scenarios.

b. Cumulus-topped boundary layers

Kite soundings from the *Meteor* cruises of the 1930s ([von Ficker 1936](#)) established the vertical wind and temperature structure of the Atlantic trade winds. After World War II, airborne meteorological research focused on the relatively benign nonprecipitating trade wind–cumulus boundary layer regimes that were accessible over the island-dotted Caribbean and west Pacific. [Stommel \(1947\)](#) was the first to quantitatively estimate the rate of lateral mixing of air into a shallow cumulus cloud. [Bunker et al. \(1949\)](#), [Malkus \(1958\)](#), and [Malkus and Riehl \(1964\)](#) distilled aircraft observations to document the vertical structure of trade wind–cumulus boundary layers and noted their mesoscale organization into rows and clusters.

As noted in [section 4](#), ATEX, BOMEX, and GATE in the 1960s and 1970s documented profiles and fluxes for several shallow-cumulus CTBLs, which formed the basis for studies using the emerging LES technology. [Sommeria \(1976\)](#) showed realistic cloud profiles and turbulence statistics in a pioneering LES of nonprecipitating shallow cumulus clouds idealized from BOMEX and other contemporary field studies; and did a reasonable job of reproducing subcloud fluxes and structure for a fair-weather trade–cumulus case sampled north of Puerto Rico ([Sommeria and LeMone 1978](#)). Indeed, BOMEX measurements for 22–26 June 1969 featured a quasi-steady nonprecipitating trade cumulus boundary layer that was used as a GEWEX Cloud System Study (GCSS) benchmark case for testing models and parameterizations in this regime ([Siebesma et al. 2003](#)). As in the case of the [Moeng and Sullivan \(1994\)](#) LES clear-air buoyancy-driven CBL in [Fig. 9-10](#), $A_B \approx 0.2$ in their simulation if one uses cloud base height as z_i . In an LES of a small-Cu case with geostrophic wind $\sim 10 \text{ m s}^{-1}$ over Oklahoma, [Brown et al. \(2002\)](#) obtain $A_B \approx 0.15$. This is also true for the GATE cases ([Fig. 9-13](#)), for which $A_B = 0.17$ and the GATE TKE budget ([Fig. 4](#) in [LeMone 1980](#)) resembles the buoyancy-driven CBL TKE budgets in [Fig. 9-12](#). Thus, despite the presence of cloud “roots” ([Fig. 9-15](#)) and the strong association of $w'q'$ and $w'\theta'$ profiles with cumulus cloudiness ([Fig. 9-13](#)), the CBL TKE budget in the presence of weak nonprecipitating trade cumuli is to a good approximation decoupled from the clouds.

For more intense clouds and/or on larger scale, coupling between clouds and the subcloud layer starts to manifest itself at least in terms of mesoscale structure.

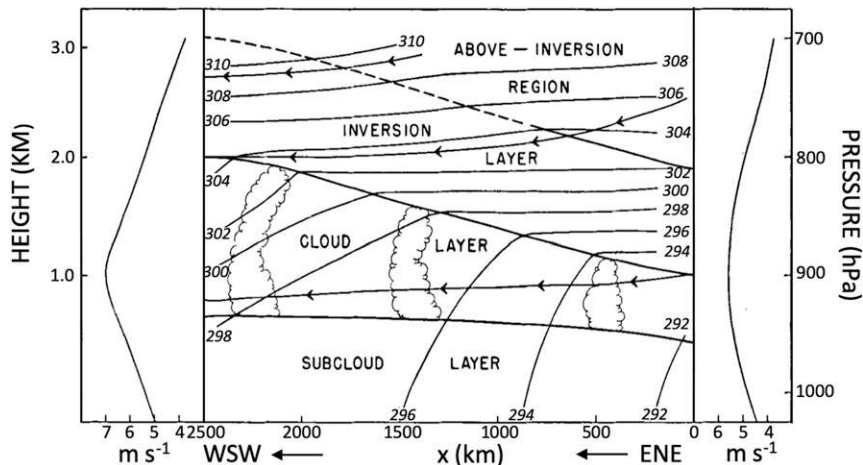


FIG. 9-24. Summertime ABL cross section adapted from Malkus (1956), based on analysis of Riehl et al. (1951). Note that this cross section starts more than 1000 km southwest of San Francisco and ends near Pearl Harbor, Hawaii. Along-section wind profiles are for the (right) beginning and (left) end of the cross-section. [© 1956 Joanne Starr Malkus. Published by Taylor and Francis Group LLC. CC BY 4.0 (<https://creativecommons.org/licenses/by/4.0>).]

LeMone and Meitin (1984) used GATE aircraft data to document mesoscale patches and bands of concentrated shallow to moderate cumulus 10–30 km across that lay above moister regions in the subcloud layer. Balaji et al. (1993) later associated the cumulus bands for one of the cases with modulation of the CBL by tropospheric gravity waves, launched as “convection waves” over the boundary layer clouds but eventually assuming a wavelength consistent with their stable environment, as described in Clark et al. (1986). Their flatness (band spacing several times ABL depth) is consistent with the cold-air outbreak “longitudinal rolls” at lower latitudes in Fig. 6 of Miura (1986) and the “sea cold-air outbreak” rolls in Fig. 4 of Young et al. (2002). Melfi and Palm (2012) postulate the same mechanism for such cloud bands in a cold-air outbreak over the North Atlantic. These broad cloud bands are not to be confused with the more closely spaced cloud streets observed over the tropical ocean, which lie above the clear-air convective rolls discussed in section 4. However, our knowledge of boundary layers with convective clouds of intermediate development remains the most incomplete, largely because such BLs are so difficult to sample and precipitation becomes more significant.

c. Stratocumulus-topped ABLs

1) ENTRAINMENT AND THE STRATOCUMULUS–CUMULUS TRANSITION

Radiosonde data collected from three weather ships stationed between the U.S. West Coast and Hawaii

during World War II provided Riehl et al. (1951) the opportunity to document the downstream development of the northeast Pacific CTBL between the cool waters off California and the warmer waters near Hawaii. They noticed a close connection between the vertical structure of the CTBL and the associated cumulus clouds (Fig. 9-24), and mentioned the stratiform clouds closer to the California coast. Using the along-cross-section wind divergence to estimate the mean vertical motion in this region, they demonstrated that free-tropospheric air must be descending through the inversion and becoming turbulently mixed or entrained into the cloud layer, weakening the inversion toward the west and increasing its height. A similar result was obtained by Neuberger et al. (1961), who used radiosonde data from postwar research cruises to map out the offshore increase in inversion height and decrease in horizontal divergence under summertime conditions. For more detail of the history of marine stratocumulus experiments off the California coast, see Kloesel (1992).

Intrigued by the shallow stratocumulus-topped boundary layers capped by a strong sharp inversion, which is prominent in summertime radiosonde observations along the California coast, Lilly (1968) developed a seminal mixed-layer model, based on the insight that the turbulence that mixes moisture upward to form clouds was driven by infrared-radiation cooling at cloud top. The turbulence also induces entrainment of warm, dry air from above that regulates the cloud thickness and boundary layer depth. Lilly’s model demonstrated for the first time the tight feedbacks among clouds,

radiation, turbulence and surface fluxes characteristic of many CTBLs. His paper used the TKE budget drawing on concepts introduced by Ball (1960) to address the difficult problem of entrainment closure, which has remained a theme of stratocumulus-topped boundary layer research for the subsequent 50 years.

The 1976 Marine Stratocumulus Experiment (Wakefield and Schubert 1976; Brost et al. 1982a,b; Albrecht et al. 1985) utilized an aircraft off the California coast in the first extensive observational test of Lilly’s mixed-layer model. Wakefield and Schubert (1981) applied a slightly generalized form of the Lilly model to the Lagrangian evolution of stratocumulus (Sc) along typical summertime boundary layer trajectories and found that the Sc layer tended to thicken indefinitely downstream. Thus, this model could not explain the Sc–cumulus (Cu) transition. Randall (1980) and Deardorff (1980b) proposed that the Sc–Cu transition was due to cloud-top entrainment instability, a runaway feedback between entrainment-induced evaporative cooling and turbulence production in a Sc cloud layer; radiosonde measurements taken as part of the First ISCCP Radiation Experiment (FIRE; Albrecht et al. 1988) disproved the original criterion (Kuo and Schubert 1988), but more restrictive versions are plausible (e.g., Lock 2009).

Given the important role of entrainment in Sc evolution, observational estimation of the small (typically less than 1 cm s^{-1}) but important entrainment rate and its relation to other cloud and boundary layer properties became a priority. Nicholls and Turton (1986) and others inferred entrainment rate from airborne measurements using a humidity flux/jump method, and suggested a relationship between entrainment and turbulence within the Sc layer; uncertainties were too large to rule out other possible entrainment relationships, however. Airplane observations from the Dynamics and Chemistry of Marine Stratocumulus (DYCOMS)-I in 1985 (Lenschow et al. 1988) demonstrated the applicability of trace species (e.g., ozone) for measuring entrainment (Kawa and Pearson 1989), and later, dimethyl sulfide (DMS) during DYCOMS-II (Faloona et al. 2005). As described in the review article by Mellado (2017) and more recent papers by, for example, Shi et al. (2018a,b) and van Hooft et al. (2018), advanced DNS and LES should provide further insight into entrainment at the top of stratocumulus clouds.

2) DIURNAL CHANGES

Using summertime aircraft observations over the North Sea, Nicholls (1984) showed that daytime in-cloud solar heating tends to stratify a stratocumulus-topped boundary layer, leading it to “decouple” into

separate layers, one surface-driven and the other driven by cloud-top longwave cooling. The two layers can then “recouple” into a single mixed layer overnight.

Since low-level aircraft flights were made mostly during daylight, surface-based remote sensing opened new windows on the diurnal cycle of stratocumulus. Tethered balloon studies of nocturnal stratocumulus over the United Kingdom elucidated the strong vertical gradients in turbulence, cloud properties, and thermodynamic structure near the capping inversion (Roach et al. 1982; Caughey et al. 1982). During FIRE in June 1987, a laser ceilometer, a microwave radiometer, and an acoustic sounder on an island off the California coast documented the diurnal cycle of cloud, boundary layer depth, and daytime boundary layer decoupling (Albrecht et al. 1990). During the June 1992, Atlantic Stratocumulus Transition Experiment (ASTEX; Albrecht et al. 1995), millimeter-wavelength cloud radars on two islands revealed surprising prevalence of drizzle from stratocumulus, especially at night (Miller and Albrecht 1995; Frisch et al. 1995).

3) DECOUPLING AND THE STRATOCUMULUS–CUMULUS TRANSITION

In the early 1990s, an alternative to the Wakefield–Schubert Sc–Cu transition hypothesis was developed, inspired by Nicholls’s work on diurnal decoupling. It was based on turbulence closure modeling (Bretherton 1991) and mixed layer modeling (Bretherton and Wyant 1997) of the Lagrangian evolution of the Sc layer as it moved over warmer waters, and later, two-dimensional LES-like simulations of this multiday transition (Krueger et al. 1995a,b; Wyant et al. 1997). As a Sc-capped mixed layer moves over warmer waters, the capping inversion weakens, leading to more entrainment and a rising capping inversion. The increased entrainment ultimately causes the Sc mixed layer to decouple from the surface. Cumulus clouds form on top of the resulting surface mixed layer, and rise up into the overlying Sc mixed layer. As the inversion rises, the cumulus clouds become deeper and more vigorous, and their overshooting tops entrain increasingly more air across the inversion. This disrupts the stratocumulus layer, ultimately leaving behind only a trade cumulus layer over warm waters (Wyant et al. 1997). Another contributing factor to the stratocumulus dissipation may be the humidity jump between the stratocumulus and the dry overlying air, which becomes increasingly large over warmer water and may contribute to an evaporative enhancement of the efficiency of entrainment (Lock 2009). ASTEX pioneered multiday airborne Lagrangian sampling of the Sc–Cu transition (Bretherton et al. 1995a,b), creating unique datasets that

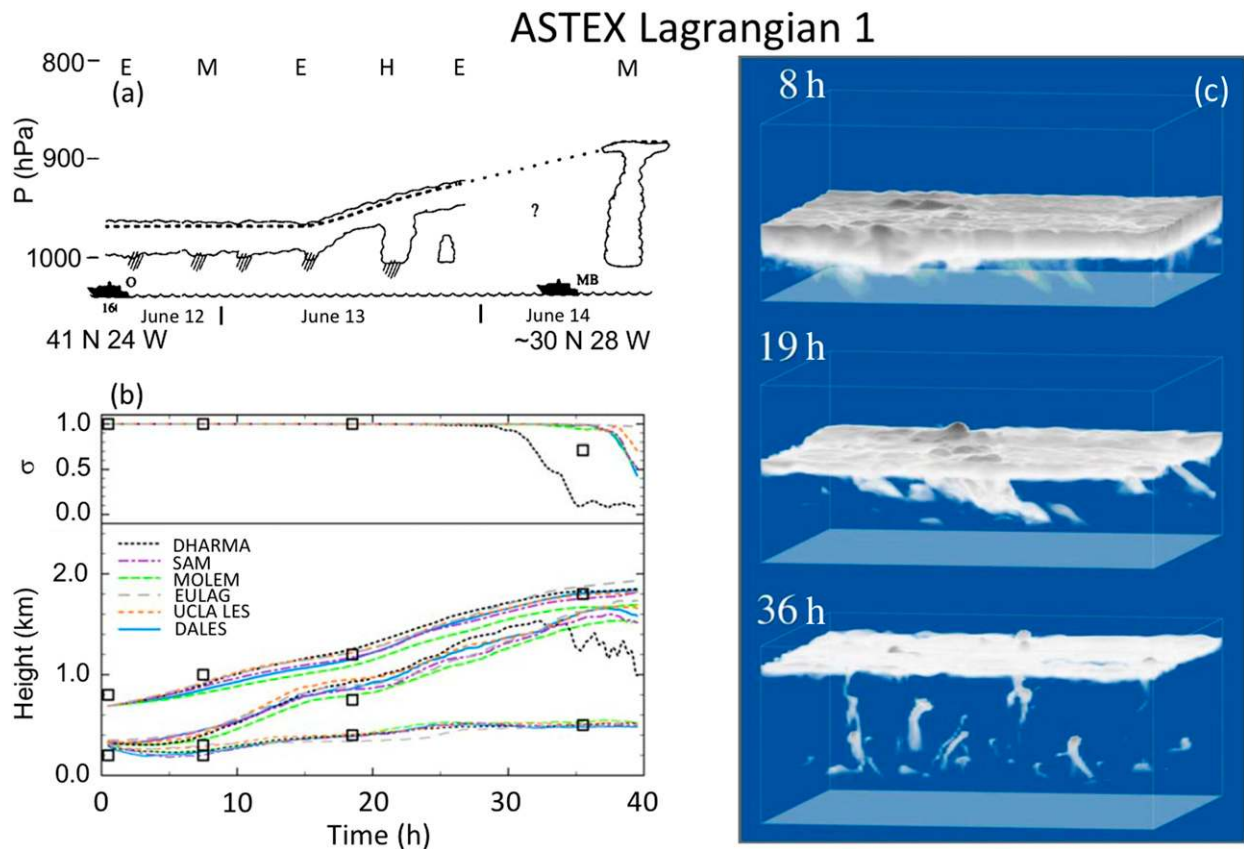


FIG. 9-25. For ASTEX Lagrangian 1 trajectory (a) schematic of clouds along trajectory. Letters indicate aircraft (E = NCAR Electra, M = U.K. Meteorological Research Flight C130, H = University of Washington C131) or ships (O = Woods Hole R/V *Oceanus*; MB = R/V *Malcolm Baldrige*). Latitudes and longitudes of beginning and end of trajectory are approximate. (b) Simulation of cloud cover in the top panel and inversion base (cloud top), mean cloud base, and minimum cloud base in the bottom panel, from various LES. (c) Snapshots of water content from DALES at 8, 19, and 36 h; cloud liquid water q_L varies from white, becoming darker at larger values. The pale blue plane is the surface. [Panel (a) is adapted from Bretherton and Pincus (1995); (b) and (c) are adapted from van der Dussen et al. (2013).]

largely confirmed this new hypothesis (Fig. 9-25), and which are still invaluable for process and LES intercomparisons (Bretherton et al. 1999a; van der Dussen et al. 2013).

4) CLOUDS, AEROSOLS, AND PRECIPITATION

Early field studies of marine boundary layer clouds frequently encountered drizzle and rain showers even from clouds only a few hundred meters thick (e.g., DYCOMS-I; Lenschow et al. 1988), and sampled heavier precipitation on the windward side of islands in the trades like Hawaii [e.g., the 1990 Hawaiian Rainband Project (HaRP); Paluch et al. 1994]. Likewise, precipitation was a common feature of trade wind CTBLs in ASTEX (Albrecht et al. 1995).

In the first airborne deployment of a Doppler cloud radar and lidar, Vali et al. (1998) found extensive precipitation in a marine Sc layer less than 300 m thick off

the Oregon coast. Ship-based cloud radar over the southeast Pacific stratocumulus region in the East Pacific Investigation of Climate (EPIC; Bretherton et al. 2004b) and airborne cloud-radar observations during the June–July 2001 DYCOMS-II (Stevens et al. 2003), together with satellite-based estimates of droplet size, suggested that regions of broken Sc within solid Sc decks, called “pockets of open cells” (POCs) or “rifts,” were regions of more cumuliform and heavily precipitating cloud with lower aerosol concentrations (Fig. 9-26; Stevens et al. 2005b). Penetrations of numerous POCs in the VAMOS Ocean Cloud Atmosphere Land Study (VOCALS) Regional Experiment (2008; Wood et al. 2011b) confirmed this view and documented an “ultraclean layer” of highly depleted aerosol and very low cloud droplet concentrations just below the trade inversion base, maintained by precipitation scavenging of aerosol (Wood et al. 2011a;

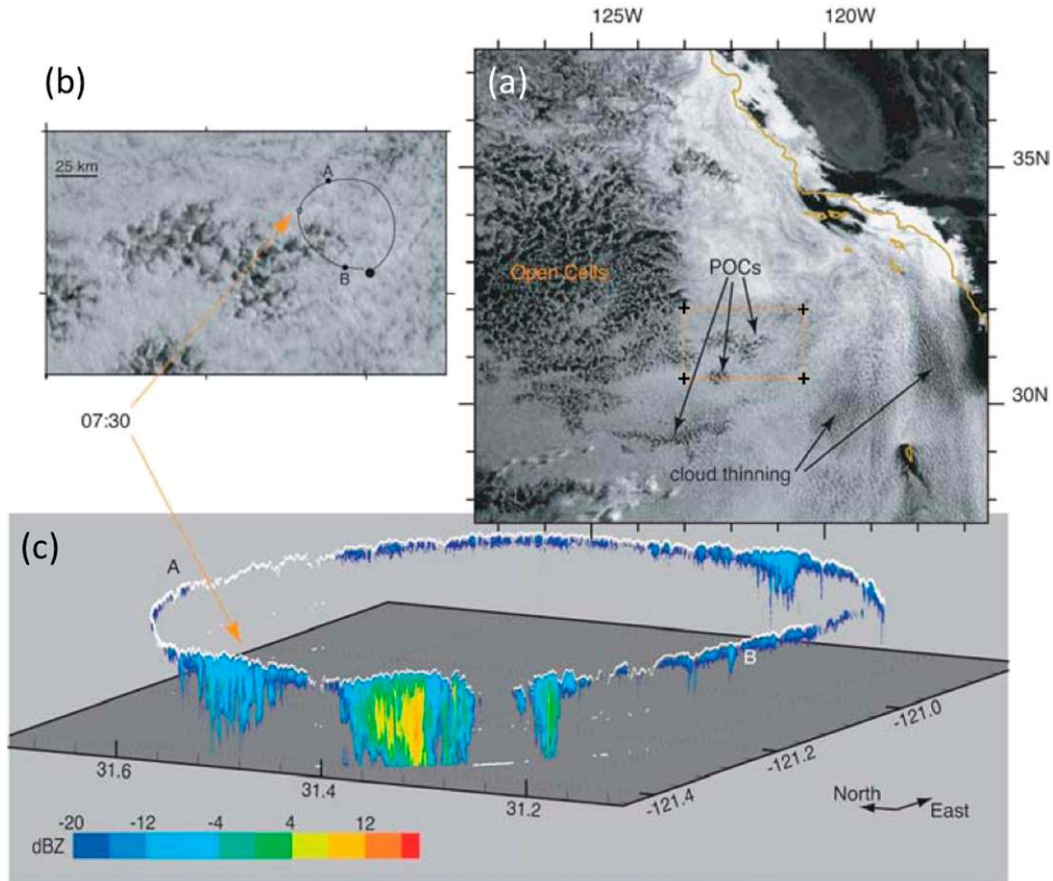


FIG. 9-26. (a) GOES-10 channel I ($0.6 \mu\text{m}$) reflectance over the northeast Pacific at 0730 LST (1430 UTC), 11 Jul 2002; (b) as in (a), but for the outlined box in (a), plus the circular segment of Flight RF02 spanning the time of (a). Note the tilde-shaped POC, which lasted for at least 10 h. (c) Circular cross section from downward-looking radar and lidar, with color the radar reflectivity and the white line indicating cloud top; white at the surface indicates no cloud. Orange arrows indicate the aircraft position at 0730 LST. [Adapted from Stevens et al. (2005b).]

Terai et al. 2014). LES in mesoscale domains showed the importance of cloud–aerosol–precipitation–dynamics interaction in maintaining long-lived POCs embedded in solid stratocumulus (Wang et al. 2010; Kazil et al. 2011; Berner et al. 2013).

In January–February 2005, the Rain in Cumulus over the Ocean experiment (RICO; Rauber et al. 2007), focused on precipitation formation in tropical Atlantic shallow cumulus clouds and its interplay with cloud organization, boundary layer depth, and aerosols. GEWEX Cloud System Study (GCSS) LES intercomparison studies of both precipitating stratocumulus (Ackerman et al. 2009) and shallow cumulus (van Zanten et al. 2010) showed considerable sensitivity of simulated precipitation and cloud properties to the choice of microphysics parameterizations; this remains a key uncertainty in LES and SCM of precipitating boundary layer clouds and their response to aerosol

perturbations. LES suggests that precipitation may often control the depth of trade cumulus boundary layers (Blossey et al. 2013; Seifert et al. 2015).

5) COLD-AIR OUTBREAKS

AMTEX (Lenschow and Agee 1976) documented air mass modification and cloud structure in midlatitude oceanic cold-air outbreaks, another key marine boundary layer regime. Using ships, buoys, aircraft and carefully collocated satellite imagery, open and closed mesoscale cellular cloud organization (Agee et al. 1973) were sampled and related to the associated boundary layer profiles and turbulent moisture and buoyancy fluxes (Burt and Agee 1977; Rothermel and Agee 1980). As was the case for the trade-cumulus BL, The AMTEX TKE budget (Lenschow et al. 1980) resembled the Moeng and Sullivan (1994) budget for a buoyancy-driven CBL (Fig. 9-12), despite the presence of

scattered-to-broken stratocumulus clouds and strong baroclinity.

Recent GCMs produce systematic cloud biases around midlatitude oceanic cyclones, with too little cloud in their cold sectors, which are dominated by boundary layer stratus cloud transitioning into shallow cumuli (Bodas-Salcedo et al. 2014). A Global Atmospheric System Study (GASS) intercomparison based on a North Atlantic cold-air outbreak (Field et al. 2017) showed that LES and 1-km grid regional models also have these biases. One issue may be premature glaciation and rapid dissipation of supercooled liquid stratus cloud,²⁹ possibly in association with excessive ice nucleation. Parameterization changes inhibiting cloud glaciation at higher temperatures have been developed to control this bias; boundary layer observations in this regime were taken in the January–February 2018 Southern Ocean Cloud Radiation Aerosol Transport Experimental Study (SOCRATES) south of Tasmania to test if other microphysical, aerosol, or boundary layer processes are also important.

d. Improved representation of marine boundary layer clouds in global models

GCSS was started in 1992 (GEWEX Cloud System Science Team 1993; Randall et al. 2003) in order to more effectively use observations to improve large-scale and process models. The GCSS Boundary Layer Cloud working group designed a series of intercomparisons for LES and SCM versions of weather and climate prediction models, distilled from observational case studies. After a first nocturnal stratocumulus case with discouragingly divergent results between models (Moeng et al. 1996), cases were chosen to isolate important modeling issues, initially numerical algorithms and grid resolution, while using idealized formulations of other physical processes such as radiative cooling that could be standardized across models. A “smoke cloud” case (Bretherton et al. 1999b) inspired by Lilly (1968) was even compared with a laboratory experiment rather than field observations

By the early 2000s, LES representation of observed CTBLs was getting good enough that they could realize their potential as benchmarks for informing parameterization development. GCSS successfully tackled a shallow cumulus development over land (Brown et al. 2002) idealized from a June 1997 case over the ARM SGP site. In both this and the earlier BOMEX case, different LES run at the same grid resolution gave

generally similar results. However, GCSS intercomparisons showed that more sophisticated advection schemes and 5–10-m grids were necessary to avoid overentrainment and premature breakup of Sc clouds, not a surprising result since DYCOMS-I observations by Lenschow et al. (2000) indicated that the discontinuity in thermodynamic variables at cloud top could be less than 1 m thick. With a 5-m vertical grid near the inversion, a subset of LES reasonably matched the observed Sc thickness, entrainment rate, and turbulence characteristics for a nonprecipitating Sc-capped mixed-layer case study in DYCOMS-II (Stevens et al. 2005a; Zhu et al. 2005). More recent and comprehensive studies have shown that LES with 5-m vertical grid, interactive radiation, microphysics and surface flux parameterizations, and accurate large-scale forcing can also skillfully represent observed cloud and boundary layer characteristics in the subtropical Sc–Cu transitions (van der Dussen et al. 2013; McGibbon and Bretherton 2017).

In the GCSS stratocumulus and shallow cumulus studies, SCMs showed a broad range of behaviors. This, together with the large marine boundary layer cloudiness biases in global and regional models, motivated intensive work on marine boundary layer parameterization development, leading to improved simulations of stratocumulus and shallow cumulus regimes in weather and climate models (e.g., Lock et al. 2000; Golaz et al. 2002; Bretherton et al. 2004a; Siebesma et al. 2007; Bretherton and Park 2009; Park and Bretherton 2009; Neggers et al. 2009; Köhler et al. 2011).

9. Boundary layer over the Arctic Ocean

While the physics governing the Arctic atmospheric boundary layer (AABL) is fundamentally the same as everywhere else, the AABL is set apart from ABLs at lower latitudes by a unique combination of forcings as a consequence of its high latitudes, and a strong influence of snow and ice at the surface. The inaccessibility and harsh conditions of this remote region combine to make field work in the Arctic difficult. Consequently, fewer AABL observations are available than for ABLs at lower latitudes.

a. A brief look back in time

The history of AABL research goes back to the late 1800s and early 1900s, when the early explorers were interested in the atmosphere because of its influence on the polar ocean and in particular the sea ice. While many of these expeditions, like Fritjof Nansen’s *Fram* expedition, only took standard surface observations (Mohn 1905), these were of sufficiently high quality to be used today. Some early expeditions, such as Amundsen’s 1918–21 expedition on the *Maud*, also took vertical profiles using

²⁹ A problem also in modeling of Arctic stratocumulus (e.g., Prenni et al. 2007; Pithan et al. 2014).

balloons or kites. As described by Sverdrup (1922), Amundsen's aim was to drift across the Arctic Ocean, like Nansen on the *Fram*. While forced to spend three winters in the Arctic because of difficult ice conditions, they took observations during the whole expedition, including vertical profiles that revealed the strong surface temperature inversions that sometimes occur in winter (Sverdrup 1922, 1925). All the data from the expedition were delivered intact once the *Maud* returned. However, an attempt to safeguard observations after the first winter by sending copies overland led to the deaths of the two men carrying the data (Sverdrup 1922). This illustrates both the dedication of these early explorers and the harsh and unpredictable conditions they encountered.

After the early explorers, the literature reveals little activity during the first half of the twentieth century. The expeditions that were deployed usually had little or no atmospheric component. Although not being an AABL project per se, the manned Russian Drifting Stations, also called Ice-islands or "North Pole" (NP) stations (Romanov et al. 1997), deserve attention. These stations were launched annually between 1937 and 1991; the program was resurrected in 2004 but ended again in 2015. The NP stations performed regular soundings that today form a backbone for our knowledge about the vertical structure of the AABL (e.g., Kahl et al. 1996, 1999).

Even as late as the 1970s the primary goal for micrometeorological observations during the Arctic Ice Dynamics Joint Experiment (AIDJEX; Untersteiner 1979) was to determine how momentum flux from the atmosphere caused sea ice to move around and deform (Maykut et al. 1972; Arya 1973). While AIDJEX was primarily a sea ice experiment, several AABL observations were taken, including surface-layer temperature profiles, wind speed profiles, and eddy-correlation fluxes, mostly to derive formulations for z_{0m} and C_D for Arctic sea ice. AIDJEX was also one of the first experiments deploying research aircraft in the Arctic and one of the first focusing on AABL clouds. Several smaller aircraft-based observation campaigns followed, for example the Arctic Stratus Experiment in 1980 (e.g., Curry and Herman 1985) and the Lead Experiment (LEADDEX; Morison et al. 1993) in the early 1990s, marking a shift in emphasis from sea ice to the AABL itself. For example, LEADDEX studied the spectacular turbulent fluxes over open water leads in winter. Several aircraft-supported experiments studied the AABL transition in the marginal ice zone (MIZ) in on- and off-ice flow, including the 1983–84 Marginal Ice Zone experiment in 1984 (Morison et al. 1987; Kellner et al. 1987), the 1991 and 1993 Radiation and Eddy Flux Experiments (REFLEX; Hartmann et al. 1992; Kottmeier et al. 1994), and the 1997–2000 Arctic Radiation and

Turbulent Interaction Study (ARTIST; Hartmann et al. 1999).

An exciting new observing platform was introduced in 1980 with an international expedition based on the Swedish icebreaker *Ymer*, which provided a safe platform for staff as well as expensive, sensitive, and heavy instruments that did not need to be deployed on the ice. Organized in commemoration of Nordenskjöld's voyage through the Northeast Passage (e.g., Schytt 1983), the expedition's measurements included atmospheric chemistry and aerosols, with AABL observations made both onboard, and by a shore team on Spitsbergen. Shorter-term icebreaker-based research is typically conducted in summer or autumn, when the ice is easier to navigate. Since the early 1990s, several such AABL campaigns were undertaken with the Swedish icebreaker *Oden* (e.g., Leck et al. 1996, 2001; Tjernström et al. 2004, 2014; Sotiropoulou et al. 2016) and the German icebreaker *Polarstern* (e.g., Driemel et al. 2016; Lüpkes et al. 2010). The Canadian icebreaker *Amundsen* has also been involved, for example, the 2007–08 Circumpolar Flaw Lead Study (Barber et al. 2010), however, with only a modest AABL component.

Some more recent Arctic field campaigns have had a strong focus on the AABL. Perhaps the most significant to date is the 1997–98 SHEBA campaign (Uttal et al. 2002; Persson et al. 2002), when the Canadian icebreaker *Des Groseilliers* was frozen into the ice north of Alaska and drifted with it for a full year. While SHEBA was multidisciplinary, its substantial AABL program has become a gold standard for AABL studies, with eddy-correlation flux measurements, mean profiles, soundings, and remote sensing observations of AABL clouds. Indeed, SHEBA generated an extensive record of stably stratified turbulence, providing insight for similar conditions also outside of the Arctic (e.g., Grachev et al. 2005; Mauritsen and Svensson 2007; Holtslag et al. 2013, also see section 5). During the 2007–08 International Polar Year, the schooner *Tara* drifted across the Arctic, Nansen-style, as part of the Developing Arctic Modelling and Observing Capabilities for Long-term Environmental Studies (DAMOCLES) project (Gascard et al. 2008, 2015); but its yearlong AABL program suffered from winter data gaps because of damage to instrumentation from ice deformation. During spring 2008, scientists flew in and collected boundary layer profiles with a tethered balloon and surface-flux observations (e.g., Vihma et al. 2008).

b. Developing a scientific understanding

Two principal factors contribute to shaping the AABL. First—and perhaps most obvious—is the relatively smaller role of solar radiation in the local surface

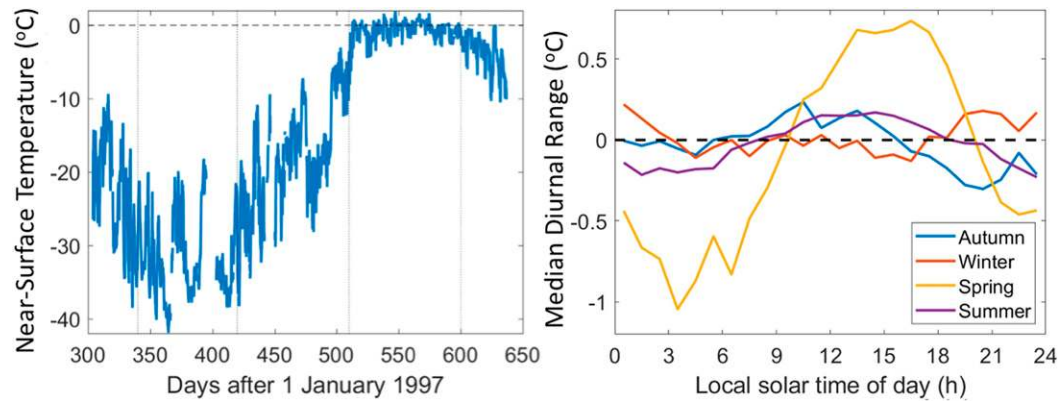


FIG. 9-27. Comparison of annual and diurnal cycles in the Arctic, based on SHEBA temperature data. (left) Near-surface temperature and (right) the median diurnal cycle based on local solar time.

energy budget, compared to lower latitudes. For large parts of winter, the sun is absent; in summer it is above the horizon all day, but at large solar zenith angles and often in combination with a high surface albedo. Hence, there is typically a much-reduced diurnal cycle in the AABL, but a very strong annual cycle (Persson et al. 2002); see Fig. 9-27. This leaves a proportionally larger role for longwave radiation processes in determining the AABL stability and structure, and also provides a favorable setting for persistent conditions; low-level clouds, strongly modulating both short- and longwave radiation, are frequent in the Arctic.

The second factor is the thermodynamics of phase change (Persson 2012; Persson and Vihma 2017). In winter, the snow surface in the Arctic can become quite cold, especially in cloud-free conditions, while the ocean beneath the sea ice remains at the freezing point, $\sim -1.8^\circ\text{C}$. Heat conduction through the ice, from the ocean to the atmosphere, keeps the ice surface warmer than the adjacent land, while heat loss at the surface is translated to growing ice thickness since the temperature at the bottom of the ice remains at the freezing point. In spring and summer, solar radiation raises the surface temperature but only to the melting point, where it stays as long as significant amounts of melting snow and ice remain. Hence there is little or no diurnal cycle in summer and winter. Only when solar radiation is present and the surface temperature is well below the melting point can there be any diurnal cycle; even then it is not very pronounced. In the absence of nearby open water, the static stability of the AABL over ice is instead determined by clouds or advection of warm air from lower latitudes.

1) SURFACE-LAYER TURBULENCE

The first attempts to determine the surface momentum flux over sea ice were aimed at understanding how

winds force the motion and deformation of the sea ice. Early investigators measured wind speed profiles on homogeneous sea ice, using similarity theory to determine roughness length z_{0m} or the drag coefficient C_D . Although low masts were used ($< 2\text{ m}$; Untersteiner and Badgley 1965) to ensure a small footprint to more easily sample homogeneous conditions, they still found large variability, with $z_{0m} \sim 10^{-5}\text{--}10^{-3}\text{ m}$. Already during AIDJEX, it was realized that large part of the atmospheric forcing came from form drag associated with pressure ridges in the ice (e.g., Arya 1973). This has since been verified from several field experiments [e.g., Arctic Ocean Experiment 2001 (AOE-2001); Tjernström 2005]. Momentum flux from the atmosphere contributes to such deformation of the ice, thereby modifying the surface drag, in turn changing the forcing. Roughness length is also influenced by the fraction of ice upstream as illustrated by Arctic Summer Cloud Ocean Study (ASCOS) observations from the edge of an open lead (Fig. 9-28). Note how z_{0m} varies for different sectors, being smallest for homogeneous sea ice or open water fetch, but orders of magnitude larger for fetch over broken ice. Flux estimates using measurements from more complex locations, by open leads, and from moving platforms (ships and aircraft) have established that z_{0m} for partial ice cover has a strongly nonlinear relationship with sea ice concentration, with the largest z_0 for 40%–70% ice cover and the reason is—again—form drag, this time coming from many small ice edges between the ice floes (e.g., Schröder et al. 2003; Lüpkes et al. 2012).

Very special conditions develop when a lead in the ice opens up in winter. Open water at the freezing point ($\sim -1.8^\circ\text{C}$) is then exposed to air temperatures easily several tens of degrees below zero, leading to dramatically large surface heat fluxes (e.g., Andreas 1980;

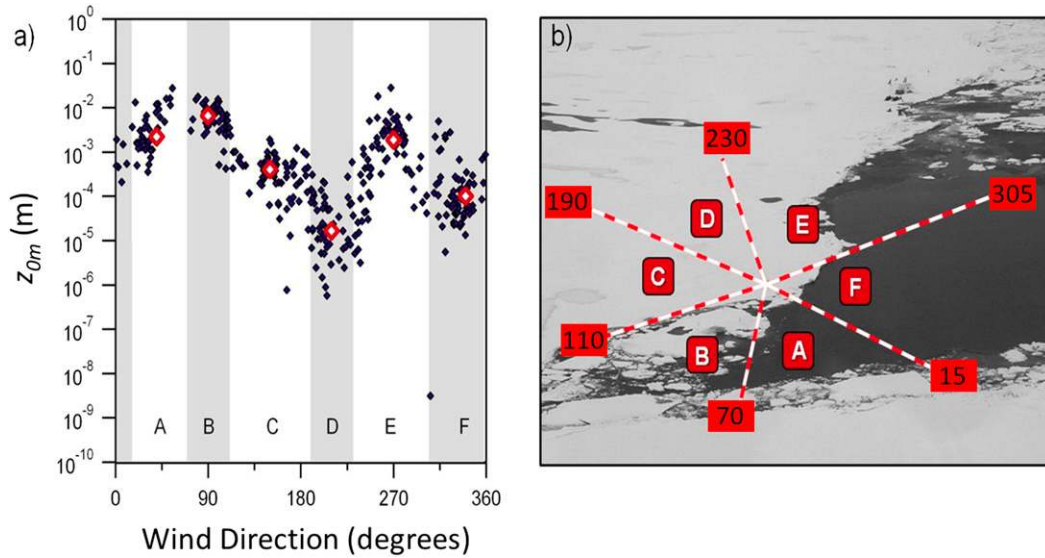


FIG. 9-28. (a) Surface roughness length as a function of fetch over sectors (letters) with different characteristics as shown in the photograph in (b). Numbers in squares are the upwind (fetch) directions (in degrees); i.e., north is to the right in the photograph. [Adapted from Held et al. (2011). © 2011 A. Held, I. M. Brooks, C. Leck, and M. Tjernström. CC BY 3.0 (<https://creativecommons.org/licenses/by/3.0/>).]

Morison et al. 1993; Ruffieux et al. 1995), followed by a rapid formation of new ice. This process was a focus of some field campaigns (e.g., LEADDEX); modeling (e.g., Mauritsen et al. 2005; Lüpkes et al. 2008) suggests an AABL impact far downwind. Aside from leads, early interest for turbulent heat fluxes was small, but this changed with a growing interest in climate change and its impact on sea ice. Thus SHEBA was designed to address the surface energy budget with turbulent surface heat fluxes as an important component. These fluxes were found to be typically small over sea ice: Fig. 9-29a shows sensible heat flux was most often close to zero, varying between ~ -30 and $+20 \text{ W m}^{-2}$, while the latent

heat flux was even smaller in magnitude and rarely downward. However, the frequency and magnitude of downward latent heat flux may be underestimated since ice is more likely to form on the sensors, which disrupts the observations under conditions with downward water vapor transport.

2) ARCTIC BOUNDARY LAYER CLOUDS AND SURFACE RADIATION

Surface and ABL energy budgets are driven by radiation; the main modulator for both shortwave and longwave radiation in the Arctic is cloudiness. Clouds are ubiquitous in the Arctic; the summer cloud fraction

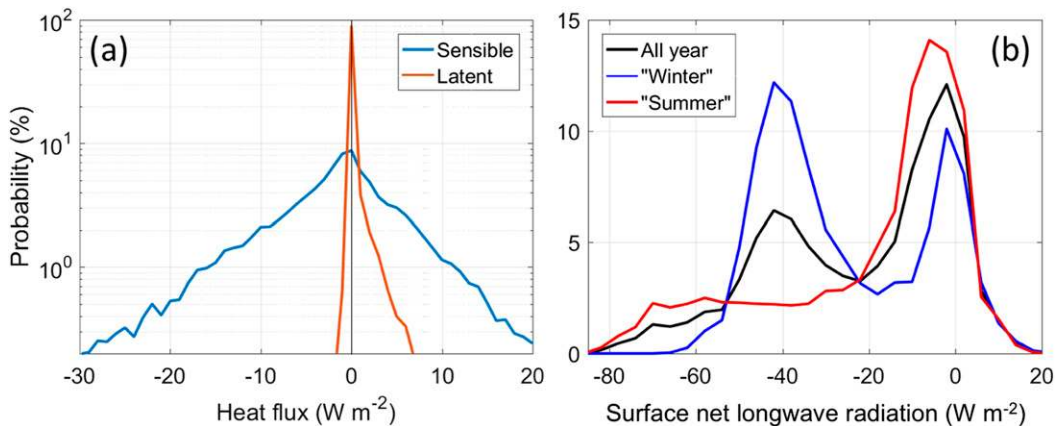


FIG. 9-29. From SHEBA, frequency of occurrence for (a) sensible heat flux and latent heat flux for the year and (b) the surface net longwave radiation for all year, winter (October–March), and summer (April–September).

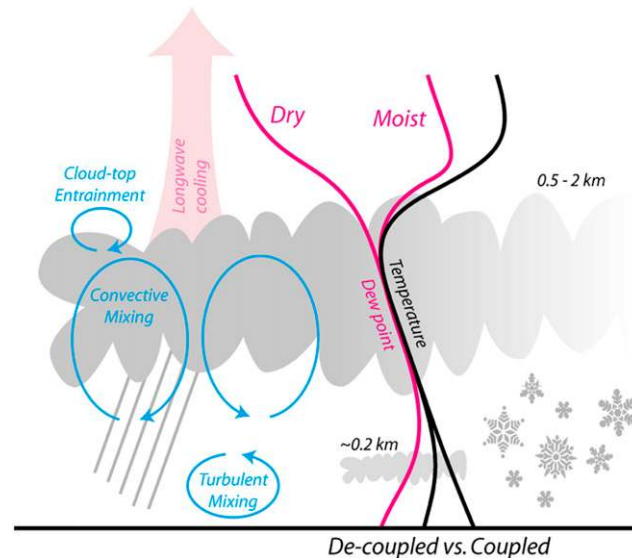


FIG. 9-30. Schematic illustrating the role of mixed-phase stratocumulus in the ABL. [From Brooks et al. (2017).]

is typically >90%, dropping to 60%–80% in winter, and most of the clouds are AABL clouds (Shupe 2011).

The first studies of Arctic clouds came as spin-off from research flights during AIDJEX and focused on radiation (e.g., Herman 1977), followed by more focused aircraft campaigns, such as the 1980 Arctic Stratus Experiment (e.g., Curry and Herman 1985). Modeling came into play relatively early and one focus was the observed “layering” of Arctic clouds. Herman and Goody (1976) used model calculations of AABL clouds to infer the physics behind this layering, while manipulating turbulent mixing and the cloud’s radiative properties. As most of these earlier studies were either directly or indirectly based on observations from research aircraft, focus was on the summer, and clouds were generally assumed to contain only liquid water. Curry (1986), who provided an important review of the relevant processes and their interactions, was one of the first to point out the moisture inversion at cloud top, which leads to entrainment of moist air, and thus contributes to cloud maintenance and high AABL relative humidity, usually close to 100% in summer.

The study of AABL clouds took a giant leap forward with SHEBA along with a supplementary aircraft campaign targeting clouds and aerosols in spring 1998 (FIRE-Arctic; Curry et al. 2000). Perhaps the most important result was the observation that AABL clouds mainly consist of a mixture of ice particles and liquid droplets even in summer, and that a liquid-droplet layer can remain with cloud-top temperatures as low as -34°C (Intrieri et al. 2002b). This has a tremendous impact on

the AABL energy budget and on its vertical structure. In contrast to ice clouds, which interact only weakly with infrared radiation, a liquid-water layer keeps the net surface longwave radiation near zero during overcast conditions; otherwise it is large and negative (upward). The transition between cloud-free or optically thin clouds and radiatively active clouds is often abrupt, tied to intrusions of warm and moist air from the south (e.g., Persson et al. 2002; Morrison et al. 2011). Stramler et al. (2011) showed how this leads to the now famous bimodal distribution of the surface net longwave radiation in Fig. 9-29b. With a sufficiently high surface albedo and large solar zenith angle, data taken during the summer (ASCOS) indicate that clouds can increase the surface net longwave radiation more than they reduce the net surface solar radiation (e.g., Sedlar et al. 2011). Intrieri et al. (2002a) showed that AABL clouds during SHEBA had a net warming effect at the surface most of the year, except for a short period in summer when the surface albedo was reduced; this effect is very sensitive to surface albedo (Sedlar et al. 2011; Intrieri et al. 2002b).

Clouds thus have a tremendous impact on the stability of the AABL, and hence on its surface turbulent fluxes and its vertical structure, as shown in Fig. 9-30. In essence, AABL clouds move the large upward surface net longwave radiation to the cloud top, where it generates cloud-top cooling, negative buoyancy, and hence turbulent mixing, as in the subtropical stratocumulus described in section 8 but without a substantial diurnal cycle (e.g., Tjernström 2007). This generates a cloud mixed layer, which often extends below the cloud.

Cloud-driven mixing appears to be a main factor for mixing the AABL, often more efficient than the surface mixing (Brooks et al. 2017). The cloudy turbulent layer is often decoupled from the surface (Shupe et al. 2013; Sotiropoulou et al. 2014; Brooks et al. 2017); limited observations, mostly from summer, indicate that this happens about two-thirds of the time.

AABL mixed-phase clouds are characterized by a thin supercooled liquid layer that constantly precipitates ice crystals. This has generated substantial interest, both in a cloud microphysical context and for its effects on AABL vertical structure and stability. A series of field campaigns was devoted to AABL mixed-phase clouds: FIRE-Arctic (Curry et al. 2000), Mixed-Phase Arctic Cloud Experiment (M-PACE; Verlinde et al. 2007), and Indirect and Semi-Direct Aerosol Campaign (ISDAC; McFarquhar et al. 2011). Although many of these campaigns were primarily focused on cloud microphysics, the results confirm that cloud-driven turbulent mixing in the AABL plays a crucial role in maintaining both cloudiness and AABL turbulence, as summarized in a review paper by Morrison et al. (2011). Sublimation/evaporation of ice particles/drizzle from the cloud layer and evaporation from the surface may saturate the lower layer; in that case fog often develops.

3) VERTICAL STRUCTURE OF THE AABL

The scarce early observations suggested that the Arctic AABL is usually stably stratified; but is this correct? Already Sverdrup (1925), while analyzing the temperature profiles from the *Maud* expedition, concluded that the temperature structure over the Arctic Ocean was different from that over the continent in that “every wind generally also brings an increase in temperature with height.” Since then many papers have discussed various aspects of the “stable Arctic boundary layer” without distinguishing whether the inversion is elevated or at the surface. Some, however, seem to have understood this distinction. In the 1950s, Webster (1954, p. 77), in a review of measurements from the Russian ice-drift stations, questions Sverdrup and writes, “The lower boundary of the layer of inversion is marked by turbulence which causes a vertical distribution of temperatures characteristic of unstable air masses. The so-called ‘cold layer’ would be better named the ‘unstable layer.’” Although the word “unstable” is perhaps unfortunate in a boundary layer context, since the AABL is seldom truly convective, it is clear that he was referring to the shallow well-mixed inversion-capped AABL. Interestingly, Webster also discussed the advection of warm air into the Arctic: “These masses often disperse above the 100–200 m cold earth layer throughout

the troposphere to a height of 7–8 km.” Although not strictly a boundary layer-meteorology feature, and hence not further discussed here, it is notable that this advection contributes to maintaining and strengthening the deep AABL-capping inversion and may also explain the moisture inversion. It is also among the most discussed issues in Arctic meteorology today.

Several papers in the early 1990s used soundings from combinations of coastal stations, aircraft dropsondes, and the Russian NP stations (Kahl et al. 1999) to explore the stratification in the Arctic lower troposphere, and concluded that inversions were frequent (Kahl 1990; Serreze et al. 1992) and their strength was increasing (Kahl et al. 1996). Based on the year of high-resolution SHEBA soundings, Tjernström and Graversen (2009) showed that a lower-troposphere inversion was almost always present. Considering only boundary layer inversions, they found that the mean inversion base height was typically 100–400 m from April through September, while surface inversions were most common from December through February. These inversions were commonly 500–700 m thick from November through March, and thinner (200–400 m) though much of spring and summer (Fig. 9-31). While surface inversions were present less than 10% of the time during spring and summer, they occurred slightly over half the time during autumn and winter, making the dominant AABL stratification during SHEBA nearly neutral.

Based on the foregoing, the main reason for the predominantly well-mixed AABL structure is the presence of AABL clouds. Whenever these are present, the combination of cloud-driven mixing and mechanical mixing at the surface keep the AABL nearly neutrally stratified, in summer as well as in winter. When the clouds disappear, the surface energy budget is dominated by strong negative net longwave radiation flux, the temperature drops, and a surface inversion forms. This effect is most pronounced in winter, when the presence of clouds seems to be governed by large-scale advection, explaining the persistence of both regimes and the rapid transitions between them (Morrison et al. 2011). During the SHEBA winter, the free troposphere temperature was systematically higher in cloudy than in clear conditions (O. Persson 2018, personal communication). Unlike in the nocturnal continental SBL in lower latitudes, the stably stratified AABL is rarely capped by a near neutrally stratified residual layer, so that vertically propagating gravity waves in the free troposphere can reach the surface (Persson and Vihma 2017), where they can break and contribute to AABL turbulence. In summer, however, AABL clouds are common and persistent and therefore surface inversions are rare. Hence the conceptual model in Fig. 9-30 can serve as a

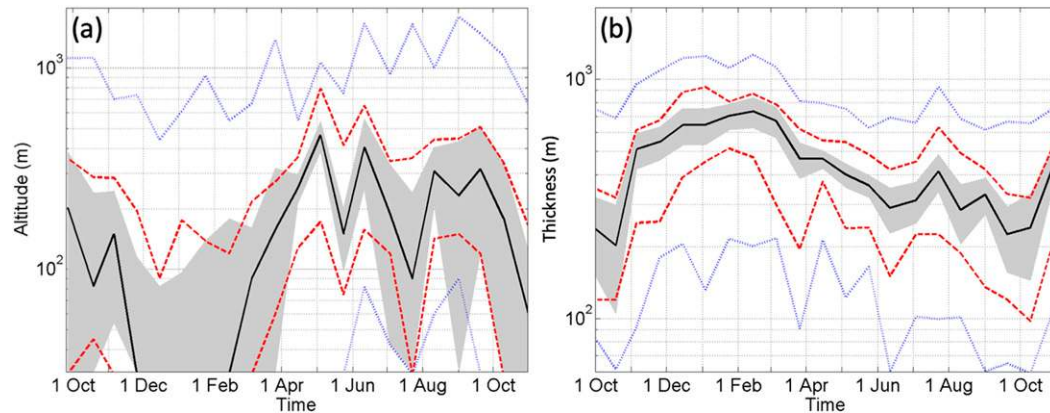


FIG. 9-31. Annual statistics of for (a) lowest inversion base and (b) lowest inversion thickness, showing the median (black), the 25th and 75th percentiles (dashed red line), and the 5th and 95th percentiles (dotted blue line). The gray shading indicates the 95% confidence interval based on a double-sided Student's t test. [Adapted from Tjernström and Graversen (2009). © Royal Meteorological Society.]

zeroth-order description of the AABL, almost all the time in summer and almost half the time in winter.

c. Modeling and the future

Given the lack of initialization and verification data, our still emerging knowledge of the dominating physics, and the strong feedbacks between clouds and fluxes, it is not surprising that numerical models have difficulty replicating the complex behavior of the AABL. Sorteberg et al. (2007) tried to make up for the data deficiency by comparing surface fluxes in climate models to those from reanalysis, essentially performing a model-to-model intercomparison. Comparing with actual data, Tjernström et al. (2005) found that models did poorly in replicating sensible and latent heat fluxes from SHEBA, with too many extreme values of both signs. Momentum flux was better, but with too many cases with large values and too few with small. Similarly, Tjernström et al. (2008) and Wyser et al. (2008) showed that regional climate models systematically produced winter AABL clouds that were too optically thin (mostly being ice clouds), and summer clouds that were too optically thick. Consequently, surface net longwave radiation flux was much too small in winter, while surface solar forcing was too low in summer (e.g., Prenni et al. 2007). Besides affecting the AABL itself, all these biases have severe consequences in coupled modeling because of the sensitivity of the sea ice to atmospheric forcing.

10. Representing the ABL in models

This section describes how the knowledge gained over the last 100 years and earlier has been synthesized into

atmospheric dispersion models, land surface models, and ABL parameterization schemes. Dispersion models provide us with tools for predicting the spread and concentration of contaminants. Land surface models account for the strong influence of the surface and its heterogeneity on the ABL, while ABL parameterization schemes account for boundary layer effects in weather and climate models.

a. Dispersion models

Progress in dispersion understanding is paced by our knowledge of the ABL and its turbulence. Here, we review the key dispersion-modeling developments in mostly chronological order for 1) the early period (prior to 1960–70), 2) the “explosive period” (from 1970 to ~1990) with main achievements for convective and stable ABLs, and 3) progress on other topics (from ~1990 to present)—(i) LES of dispersion, (ii) Lagrangian particle models, (iii) concentration fluctuations, and (iv) urban dispersion.

1) EARLY PERIOD: EDDY DIFFUSION, LAGRANGIAN SIMILARITY, AND STATISTICAL THEORIES

Early dispersion research was restricted to heights less than ~100 m because of limited turbulence and wind information. Dispersion was modeled using eddy-diffusion methods, Lagrangian similarity theories (LSTs), statistical theories (e.g., Pasquill and Smith 1983), and analytical methods. In principle, eddy diffusion or “ K ” theory is limited to problems where the local plume depth (e.g., vertical dispersion σ_z) is of the same order or larger than the characteristic eddy size (e.g., Weil 2013). Short-range dispersion from a surface

release satisfied this limitation, and the two-dimensional diffusion equation with an appropriate K was used to model the crosswind-integrated concentration (CWIC C^y) from a surface source. This was done with Roberts's (unpublished) analytical solution (Calder 1949) and power-law profiles of wind and diffusivity, and achieved partial agreement with observations. Vertical dispersion also was modeled with LST (Monin 1959; Gifford 1962), which assumed that the Lagrangian velocity of "particles" depends on the same variables, u_* , θ_* , buoyancy, etc., as given by the Eulerian statistics and MOST. However, LST gave no real advantage over K theory and has seen little use since the 1980s.

For statistical theory, two key developments took place both for homogeneous turbulence and based on Lagrangian formulations: 1) Taylor's (1921) results on mean dispersion in a fixed (Eulerian) system, and 2) Batchelor's (1950) theory on relative dispersion, that is, dispersion about the local plume centerline [see section 10a(3)(iii)]. Taylor's analysis predicted the root-mean-square (rms) vertical dispersion to vary as $\sigma_z = \sigma_w t$ for short times $t < T_L$ and as $\sigma_z = (2\sigma_w^2 T_L t)^{1/2}$ for long times $t > T_L$, where σ_w is the standard deviation of w , and T_L is the Lagrangian integral time scale or "memory time" of the dispersion process. The short-time result is sometimes called a "ballistic" limit because the particle paths are essentially straight lines, whereas the long-time result is consistent with K theory, that is, a diffusive ($t^{1/2}$) limit or "random walk," with a vertical diffusivity $K_z = \sigma_w^2 T_L$. Similar results apply to other directions. This theory has withstood the test of time, being relevant today in providing 1) theoretical limits for new models, 2) dispersion predictions for convective and stable ABLs, and 3) expressions for applied dispersion models based on parameterized turbulence profiles (Hanna and Paine 1989; Carruthers et al. 1994; Cimorelli et al. 2005; see also Haupt et al. 2019).

2) EXPLOSIVE PERIOD: CONVECTIVE AND STABLE BOUNDARY LAYERS

The "explosive period" is so labeled because of the rapid and significant progress in the understanding of ABL turbulence, structure, and dispersion that was achieved through laboratory experiments, numerical simulations, and field observations. For dispersion from surface sources, Nieuwstadt and van Ulden (1978) extended the "early period" work by solving the diffusion equation numerically using MOST profiles for mean wind and turbulence, and van Ulden (1978) obtained an analytical solution based on an extension of Roberts's work to include the MOST profiles. These models were applied to both convective and stable surface layers using the MOST similarity function for heat $\phi_h(z/L)$

(section 3b). CWIC results from the models agreed well with the Prairie Grass data (Barad 1958), which are considered the "gold standard" for surface releases. Related modeling was conducted by Gryning et al. (1983) for surface deposition and Horst (1979).

Venkatram (1992) provided further understanding by deriving simple analytical expressions for σ_z and the surface CWIC in very unstable and stable conditions using the long-time limit of statistical theory $d\sigma_z^2/dt = K_z(t)$ and the MOST results for heat, $K_z = K_H(z/L)$. By evaluating K_H at $z = \sigma_z$, he obtained $\sigma_z \propto x^2/|L|$ and the surface $C^y \propto Q_S(|L|)/(u_* x^2)$, in very unstable conditions, with $\sigma_z \propto L^{2/3} x^{1/3}$ and $C^y \propto Q_S/(u_* L^{1/3} x^{2/3})$ in very stable conditions, where Q_S is source strength and x is the downwind distance. The downwind dependence on x in Venkatram's expressions matched van Ulden's (1978) curves and explicitly showed the variation of σ_z and C^y with x , L , and u_* .

(i) CBL

Convective scaling (Willis and Deardorff 1976) was a major advance in understanding of dispersion throughout the CBL and enabled the comparison of laboratory, numerical, and field-data results in simple dimensionless coordinates. The key length, velocity, and time scales for turbulence and dispersion were z , w_* , and the eddy turnover time z_i/w_* , where $T_L \propto z_i/w_*$ for the large eddies. In strong convection ($-z_i/L \gg 1$), the mean wind \bar{U} is nearly uniform in the upper CBL and thus the plume travel time $t \approx x/\bar{U}$. Willis and Deardorff proposed that the dimensionless CWIC, $C^y \bar{U} z_i / Q_S = f_1(z/z_i, X, z_s/z_i)$, where $X = w_* x / (\bar{U} z_i)$ is the dimensionless distance or travel time, z_s is the source height, and f_1 is some functional form. Here, $C^y \bar{U} z_i / Q_S$ is the ratio of the local CWIC C^y to the well-mixed value $Q_S / (\bar{U} z_i)$ attained far downstream ($X \sim 3$).

Figure 9-32 shows contours of the dimensionless CWIC from the Willis and Deardorff (1976, 1978) laboratory experiments as a function of dimensionless height and distance in strong convection ($-z_i/L \gg 1$). For a near-surface source, the average plume centerline (as defined by maximum CWIC) ascends after a short distance, whereas an elevated source centerline descends until it reaches the surface. These behaviors were explained by the vertical-velocity skewness and the release of material into updrafts and downdrafts (Lamb 1982; Weil 1988), which have different areal fractions. More area (60%) is covered by downdrafts, and thus for the elevated source, there is a higher probability of material being emitted into downdrafts and then being carried down toward the surface. The results have been supported by field observations (Nieuwstadt 1980; Briggs 1993) and numerical simulations (e.g., Lamb

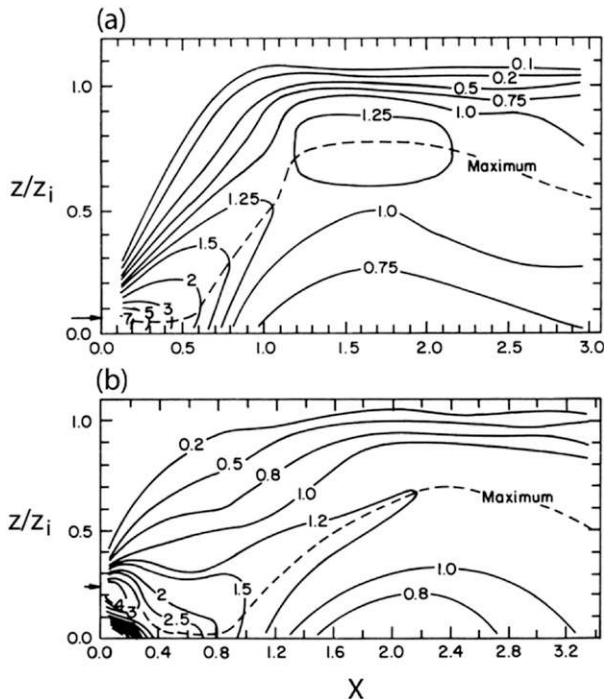


FIG. 9-32. Laboratory convection tank results showing contours of dimensionless crosswind-integrated concentration as a function of dimensionless distance X and height z/z_i for sources at two heights in the CBL: (a) $z_s/z_i = 0.067$ and (b) $z_s/z_i = 0.24$. [Panel (a) is from Willis and Deardorff (1976); © Royal Meteorological Society. Panel (b) is from Willis and Deardorff (1978); reprinted with permission from Elsevier.]

1978, 1982; Baerentsen and Berkowicz 1984; Weil et al. 2012). They differed substantially from the standard Gaussian plume model of the time, which predicted a horizontal centerline.

The elevated source experiment referred to above was motivated by Lamb's (1978) numerical simulation using a Lagrangian particle dispersion model (LPDM) driven by LESs. Lamb (1978) first predicted the descending plume centerline for the elevated release, which was later confirmed by experiment (Fig. 9-32b) and field observations (Briggs 1993).

Comparisons of statistical theory with observations and convective scaling have been made for elevated sources in the CBL (Nieuwstadt 1980; Briggs 1988, 1993; Weil 1988); the theory is applicable because the mean wind and turbulence are quasi-homogeneous in the upper CBL. Figure 9-33a shows that crosswind dispersion (σ_y) observations from the Convective Diffusion Observed with Remote Sensors (CONDORS) experiment (Briggs 1993) in dimensionless form agree with the statistical theory prediction, $\sigma_y/z_i = 0.6X$, which holds for $X < \sim 0.7$; beyond this X , the observations suggest that long-time ($t > T_L$) memory effects may be important with $\sigma_y \propto t^{1/2}$.

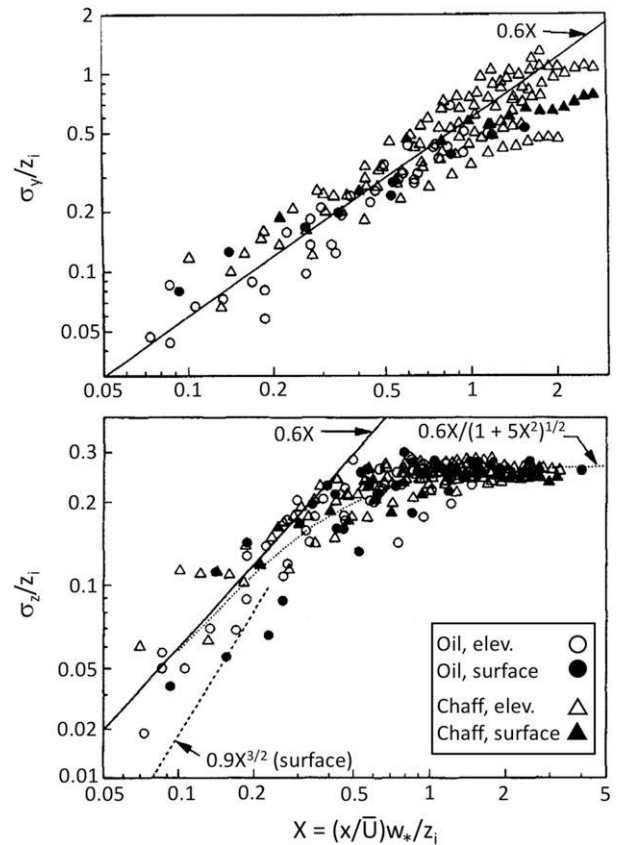


FIG. 9-33. Dimensionless (a) crosswind σ_y/z_i and (b) vertical dispersion σ_z/z_i as a function of the dimensionless distance X , from the CONDORS experiment; the rms lateral and vertical turbulence velocities used in the statistical theory predictions (solid lines) are $\sigma_v = \sigma_w = 0.6w_*$. "Oil" = oil fog generated from food-grade oil. [Adapted from Briggs (1993).]

For vertical dispersion (Fig. 9-33b), the data support the short-time prediction for $X < 0.5$, but beyond that distance, they converge toward $\sigma_z/z_i = 0.27$. The latter is due to plume trapping by the elevated inversion and a tendency toward a vertically well-mixed distribution by $X = 2$ or 3. Results from the Willis and Deardorff (1976, 1978, 1981) experiments and Lamb's numerical simulations (Lamb 1978, 1982) are similar to the observations.

These results motivated a new type of dispersion model—an approach based on the probability density function (PDF) of w in the CBL (Misra 1982; Venkatram 1983; Weil 1988). The PDF is non-Gaussian, consistent with the Fig. 9-32 results, and is typically modeled with a bi-Gaussian distribution. It has been included in applied dispersion models (e.g., Cimorelli et al. 2005; Carruthers et al. 1994; Hanna and Paine 1989).

The above results pertained to strong convection, but data were sorely needed for the more common weaker convective regime ($-z_i/L \ll \sim 20$). Dosio et al. (2003)

used LES to explore dispersion in this regime and found reduced vertical dispersion with lower mean plume heights versus X , surface CWIC versus X profiles shifted downstream, and increased lateral dispersion (σ_y); this was attributed to the greater TKE dissipation rate near the surface and shorter time scales T_L for weaker convection. Another extension of the CBL work was to buoyant plume dispersion, pursued in part using LES (van Haren and Nieuwstadt 1989), but mostly explored in convection tank experiments (Willis and Deardorff 1983, 1987; Weil et al. 2002). The experiments provided new insights into highly buoyant plumes that loft at the CBL top and resist downward mixing, and exhibit an enhanced lateral spread because of their buoyancy. The enhanced lateral spreading was successfully predicted using a gravity-current model (e.g., Simpson 1982).

(ii) SBL

For elevated sources in the SBL, the short-time vertical dispersion is given by statistical theory, but the long-time dispersion can range between a classical diffusion limit ($\sigma_z \propto t^{1/2}$; Venkatram et al. 1984) and a constant vertical thickness or “pancake limit” (Pearson et al. 1983); the latter was observed by Hilst and Simpson (1958). The “statistical theory” case was modeled using an interpolation expression of the form, $\sigma_z = \sigma_w t / (1 + 0.5t/T_L)^{1/2}$, which satisfied both the short and long time limits. In addition, Venkatram et al. (1984) parameterized T_L using “neutral” and “stable” forms applicable near the surface and in the upper SBL, respectively, as given by Brost and Wyngaard (1978). Their model was supported by dispersion measurements downwind of a ~ 50 -m tall source.

Pearson et al. (1983) predicted the long-time dispersion to range from a constant σ_z to the classical behavior ($\propto t^{1/2}$) depending on the value of a “molecular mixing” parameter γ . For zero or small γ , a constant pancake-like plume is attained with $\sigma_z \propto \sigma_w/N$, where the Brunt-Väisälä frequency N depends on the local stratification. That is, if $\gamma = 0$, a fluid particle moving about in a stratified turbulent flow retains its initial density and moves through a vertical distance $\sim \sigma_w/N$ before the buoyancy force returns it to its original height. However, if $\gamma > 0$, the particle can be warmed or cooled by molecular diffusion if moving up or down, weakening the buoyancy force; the particle is then displaced a distance greater than σ_w/N . With a moderate to large γ , the classical behavior is recovered. The Pearson et al. (1983) model was supported by observations, including field data in the Venkatram et al. (1984) study (see Weil 2013).

The classical dispersion limit would be expected in a weakly stable boundary layer (WSBL) with continuous turbulence, whereas the pancake limit may apply to a

very stable boundary layer with weak, intermittent or “wavylike” turbulence in the upper SBL. Further support for the classical σ_z behavior was given by dispersion simulations using the coupled LPDM-LES for a WSBL (Kemp and Thomson 1996). Recent LESs of a moderately stable boundary layer have been conducted for fine grid spacings (0.39–12.5 m) (Beare et al. 2006; Huang and Bou-Zeid 2013; Sullivan et al. 2016), with those by Sullivan et al. conducted for the finest grid spacings. Their results for $z_i/L = 6$ show a region of relatively weak turbulence ($\sigma_w \approx 0.01 \text{ m s}^{-1}$) in the uppermost 30% of the SBL, which offers the potential for finding the pancake-like dispersion behavior using an LPDM driven by LES.

Lateral dispersion can be determined from statistical theory, but parameterization of σ_v in terms of the micrometeorological variables u_* , L , etc. is problematic because of contributions from large-scale meandering, especially in weak winds. Mahrt et al. (2001) found that the source of meandering was ill defined. Hence, Vickers et al. (2008) used data from a 7-tower network over a small domain to measure the spatially and temporally varying wind field along with an added stochastic component to predict “particle” dispersion and interesting horizontal concentration contour patterns. The latter consist of “spokelike” or “jagged” crosswind concentration profiles because of localized peaks of wind-direction probability rather than a smoothly varying wind-direction probability. Similar work was done by Anfossi et al. (2006), who compared their concentration results with observations. One potential source of the meander could be the ubiquitous random turbulent structures and fronts in the SBL surface layer (Adrian 2007; Sullivan et al. 2016).

3) PROGRESS ON OTHER TOPICS

Over the past three decades, large-eddy simulation has gained much use in dispersion modeling mainly because of its success in ABL research. Here, we discuss this LES application as well as Lagrangian particle modeling, concentration fluctuations, and urban dispersion.

(i) LES of dispersion

The application of LES to dispersion modeling has followed two main approaches: 1) Eulerian methods in which the scalar diffusion equation is added to the LES model, and 2) Lagrangian techniques wherein “passive” particles from a source are tracked using the LES velocity fields [see sections 10a(2) and 10a(3)(ii)]. Here, the focus is on the Eulerian approach in which early contributions were made by Sykes and Henn (1992) and Henn and Sykes (1992) for neutral and convective ABLs, respectively. For mean concentrations, their

results were in fair-to-good agreement with experiments in a neutral wind-tunnel flow (Fackrell and Robins 1982) and a convection tank (Willis and Deardorff 1978, 1981). Their computed concentration fluctuations for the CBL, including variances and PDFs, were some of the first from an LES and demonstrated the LES potential. However, their modeled fluctuations were typically only 60% of the tank data values possibly because of the small number of grid cells ($80 \times 80 \times 72$), the large source size modeled, and the neglect of SGS fluctuations; these problems have been overcome with a Lagrangian two-particle model driven by LES [see Weil et al. 2017; section 10a(3)(ii)]. The Eulerian approach also was adopted in studies of CBL stability effects on dispersion [Dosio et al. 2003; see section 10a(2)] as well as dispersion statistics and concentration fluctuations (Dosio and de Arellano 2006), which matched the tank fluctuation data much better than Henn and Sykes (1992). This was likely due to the much greater number of grid cells ($512 \times 512 \times 128$) used by Dosio and de Arellano (2006) than by Henn and Sykes (1992).

In addition, the LES Eulerian approach has been applied to 1) pollen dispersion in a neutral ABL over a crop field (Chamecki et al. 2009), 2) fumigation of pollutants trapped in an elevated inversion into the CBL mixed layer (Cai and Luhar 2002), and 3) dispersion in a regular array of urban block buildings for both a neutral LES flow (Boppana et al. 2010; Tseng et al. 2006) and a stably stratified flow for a similar building configuration (Tomas et al. 2016).

(ii) LPDMs

Over the past 30 years, Lagrangian particle dispersion models have seen greater use because of 1) their capability of handling turbulence complexities such as spatial inhomogeneity, non-Gaussianity, and a large T_L , and 2) the substantial increase in computing power. In an LPDM, one computes “passive” particle trajectories given the random velocity field with the mean concentration found from the particle position PDF, which is obtained by tracking tens to hundreds of thousands of particles. The velocities are determined either from 1) a purely stochastic approach—a Lagrangian stochastic model (LSM), or 2) LES using the resolved LES velocities plus a random subfilter-scale (SFS) velocity obtained from an LSM. In a landmark paper, Thomson (1987) gave a rigorous basis for an LSM construct, using two criteria: 1) the “well mixed” condition that assumes that particles initially uniformly distributed in phase space must remain so, and 2) the Fokker–Planck equation that governs the evolution of the joint PDF of particle position and velocity. Thomson’s approach corrected some problems of earlier models and has been adopted in most currently used

LSMs. Some examples include dispersion in the CBL (Luhar and Britter 1989; Weil 1990), which requires a skewed w PDF, fumigation into a coastal internal boundary layer (Luhar and Sawford 1995), and dispersion from surface sources over a range of stability (Du and Venkatram 1997). Much of this work was reviewed by Wilson and Sawford (1997), who reported problems for strongly stratified turbulence, which remains a key issue for ABL research. The review led Das and Durbin (2005) to develop a new approach that improved the LSM agreement with experiments on stable flows.

In pioneering work, Lamb (1978, 1982) developed the LPDM-LES approach and simulated dispersion in the CBL, finding good agreement of dispersion statistics and concentration fields with the Willis and Deardorff (1976, 1978) tank experiments. Weil et al. (2004) adapted a more detailed LSM (Thomson 1987) for the SFS velocities and a finer LES grid and also obtained agreement with the Willis and Deardorff data; they also demonstrated the need for a realistic SFS model to predict surface concentrations for near-surface sources. Other ABL applications include 1) fumigation in a CBL (Kim et al. 2005), 2) dispersion in the SBL (Kemp and Thomson 1996), 3) dispersion in the evening transition layer (Taylor et al. 2014), and 4) statistical variability of dispersion in the CBL based on LPDM-LES modeling and observations (Weil et al. 2012).

The LSM and LPDM-LES methods also have been used for determining flux footprints—the contribution of upwind surface emission elements to the measured vertical scalar flux at some height. They have both a “forward” formulation from source to receptor and a “backward” version. LSM applications for the forward case include 1) the atmospheric surface layer (Horst and Weil 1992; Leclerc and Thurtell 1990; Schmid 1994), 2) the CBL (Weil and Horst 1992; Kljun et al. 2004), and 3) flows within and above canopies (Baldochi 1997). The backward LSM has the advantage of being applicable to nonhomogeneous surfaces and has been used by Flesch et al. (1995) and Kljun et al. (2002, 2004).

(iii) Concentration fluctuations

Concentration fluctuations result from the stochastic nature of turbulence and dispersion, and are important for estimating the concentration variance, PDF, and peak values (Csanady 1973; Chatwin 1982). The fluctuations at a point are characterized by σ_c or the fluctuation intensity, σ_c/\bar{C} , where \bar{C} is the ensemble mean concentration at that point; for an elevated source the intensity can range from 1 to 10 at short downwind distances, with the high values caused by large-scale plume meandering. Several approaches have been pursued for predicting the fluctuations and σ_c : 1) models

based on Gifford's (1959) "meandering plume" approach and extensions using LSMs (Franzese 2003; Luhar et al. 2000), 2) Lagrangian two-particle stochastic models that predict the relative dispersion and σ_c (Thomson 1990), 3) micromixing models that describe the time variation of a "particle's" concentration with coupling to LPDMs for concentration statistics (Sawford 2004; Cassiani et al. 2005; Luhar and Sawford 2005), 4) second-order closure models (Sykes et al. 1984), and 5) LES coupled with the diffusion equation (Dosio and de Arellano 2006; Henn and Sykes 1992; Sykes and Henn 1992) and more recently LES coupled with a Lagrangian two-particle dispersion model (L2PDM; Weil et al. 2017).

The above approaches either explicitly model the relative dispersion σ_r about the plume centroid at a given distance from its source with Batchelor's (1950) theory or use the theory for estimating key variables such as the micromixing time scale (e.g., Cassiani et al. 2005). For short times, $\sigma_r \propto t^{3/2}$ and at long times, $\sigma_r \propto t^{1/2}$. The models have been tested with laboratory data for the CBL (e.g., Deardorff and Willis 1984; Weil et al. 2002) and a neutral boundary layer (Fackrell and Robins 1982).

(iv) Urban dispersion

Understanding of dispersion in urban areas has progressed substantially over the past 25 years through the combined work of modeling and simulations, laboratory experiments, and field observations. Urban dispersion is often classified in 1) four horizontal-scale regimes—regional ($x < 200$ km), city ($< \sim 20$ km), neighborhood ($x < \sim 2$ km), and street ($x < \sim 200$ m); and 2) four vertical sublayers analogous to those considered in section 3—urban canopy layer (UCL; $z/h_B < 1$), RSL ($z/h_B < 2$ or 3), inertial sublayer ($z/h_B > 2$ or 3), and outer layer; here h_B is the mean building height. Recent reviews by, for example, Britter and Hanna (2003), Belcher (2005), Fernando (2010), and Belcher et al. (2013) discuss this progress in detail. They show that the coordinated efforts of theoretical and numerical modeling (e.g., Coceal et al. 2014; Tomas et al. 2016), wind-tunnel studies (e.g., Kastner-Klein et al. 2004; Castro et al. 2006), and field observations (e.g., Davidson et al. 1995; Hanna et al. 2007) have improved knowledge. The urban flow field is marked by increased turbulence, mainly in the UCL and RSL, because of flow about the buildings and surface warming, while the mean wind is reduced because of building drag. Vertically, the effects are greatest in the UCL and RSL, and horizontally on the neighborhood and street scales. Studies show that 1) the locations of shear layers and "dividing streamlines" in the UCL control the mixing and transport (Belcher

2005), and 2) lateral dispersion varies initially as $\sigma_y \propto x$ and then as $\sigma_y \propto x^{1/2}$ because of "topological dispersion" or wind-direction changes from flow impingement on buildings in an array (Davidson et al. 1995; Jerram et al. 1995). In addition, an isolated tall building in an urban area greatly enhances the upward transport of polluted UCL air because of the low pressure and corner vortices on the building lee side (Heist et al. 2009).

An unresolved issue is the net effect of urban roughness on maximum concentrations from surface sources due to the competing effects of increased turbulence and reduced winds, which lead to lower and higher concentrations, respectively. Some small-scale field and laboratory experiments show little net effect (Britter and Hanna 2003), whereas field observations and modeling demonstrate a net concentration reduction (Britter and Hanna 2003; Delle Monache et al. 2009).

b. Land surface modeling in weather and climate models

To a large degree, the ABL is driven by surface fluxes, which in turn result from the exchange of energy and water fluxes across the land (or water)–atmosphere interface, as described in section 3a. The exchanges over the oceans are described in section 3d. Here are described the much more complex exchanges over land, as represented in land surface models (LSMs), which follow the flow of moisture and heat from the subsurface, through the surface, its vegetation, (and sometimes built structure), and snow/ice into the atmospheric surface layer, where the fluxes are linked to ABL parameterization schemes through MOST functions. Land surface processes play an important role in both GCMs (e.g., Mintz 1982; Rowntree and Bolton 1983), and regional and mesoscale atmospheric models (Ookouchi et al. 1984; Mahfouf et al. 1987; Chen and Avissar 1994a,b; Pielke et al. 1997; Rasmussen et al. 2011).

In NWP and climate models prior to the 1960s, the description of land surface processes was either absent or oversimplified with a prescribed diurnal cycle of surface heat fluxes and surface temperature. The first interactive model concept was perhaps the work of Budyko (1956), which used a simple "bucket" model to calculate surface evaporation as a function of soil moisture. That concept was perhaps first adapted for use in a climate model by Manabe (1969) and then for an interactive soil model in a mesoscale weather model by Physick (1976). McCumber and Pielke (1981) coupled a mesoscale model with a soil model in which the surface heat fluxes depended on the soil moisture and temperature.

Undoubtedly, introducing a vegetation foliage layer (the so-called big leaf model) by Deardorff (1978) was a major milestone in land surface modeling. The concept

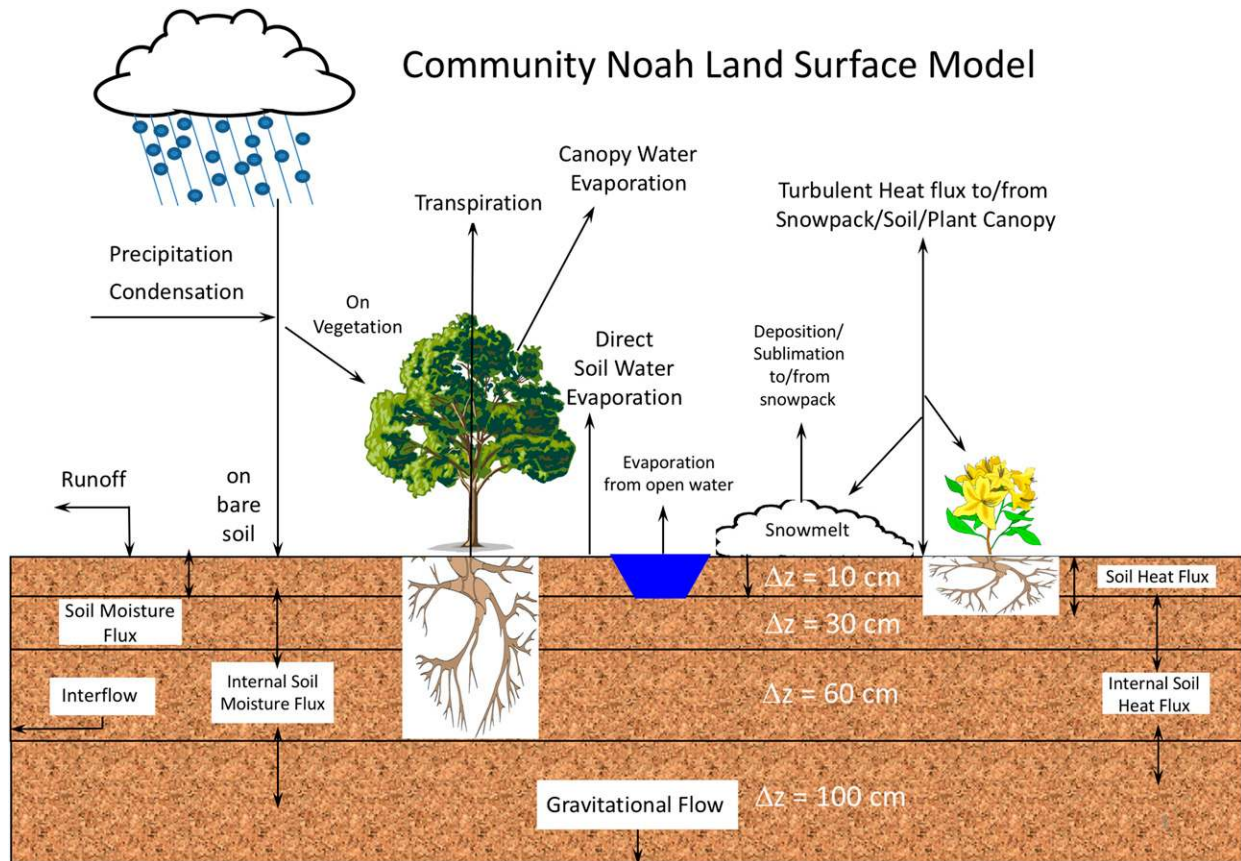


FIG. 9-34. Schematic representation of processes represented in the community Noah land model. [Adapted from [Chen and Dudhia \(2001\)](#).]

of explicitly treating the plant canopy with simplifications was later adopted in land surface models (e.g., [Pan and Mahrt 1987](#); [Noilhan and Planton 1989](#)) or enhanced with more complex biophysical processes ([Dickinson 1984](#); [Sellers et al. 1986](#)) and hydrological processes (e.g., [Entekhabi and Eagleson 1989](#); [Wood et al. 1992](#)).

In the 1990s, the availability of long-term field data such as HAPEX-MOBILHY ([André et al. 1986](#)), Cabauw ([Beljaars and Bosveld 1997](#)), and FIFE ([Sellers et al. 1992](#)) promoted further development of LSMs, their systematic evaluations through initiatives such as the Project for the Intercomparison of Land-Surface Parameterization Schemes (PILPS; [Henderson-Sellers et al. 1993](#); [Wood et al. 1998](#)), and their implementation in NWP models (e.g., [Noilhan and Planton 1989](#); [Chen et al. 1997](#); [Smirnova et al. 1997](#); [Viterbo and Beljaars 1995](#); [Chen and Dudhia 2001](#)). Figure 9-34 shows processes included in the Noah model, typical for an LSM used in NWP models.

In the context of the longer-time-scale Earth system models, such as the NCAR Earth System model and its

LSM, the Community Land Model (CLM; [Oleson et al 2013](#); [Lawrence et al. 2012](#)), development today deals in greater depth with much broader topics, such as the spatial distribution of soil characteristics, vegetation, the use of remote sensing data, and the initialization of soil moisture and snow depth. This includes human impacts, such as urbanization ([Best 2005](#); [Oleson et al. 2008](#); [Chen et al. 2011](#)) and agricultural management ([Levis et al. 2012](#); [Liu et al. 2016](#); [Leng et al. 2017](#)). Developers continue to add more complexity and physical realism to LSMs, while starting to explore incorporating horizontal complexities such as subgrid-scale land-cover heterogeneity for large-scale models (e.g., [Oleson et al. 2010](#); [Li et al. 2013](#)) and applying subgrid-scale methods developed for LES to heterogeneous surfaces at larger scales ([Passalacqua et al. 2006](#)). In particular, more LSMs include lateral surface and subsurface hydrologic flows at the grid or subgrid scales (e.g., [Seuffert et al.; 2002](#); [Maxwell and Miller 2005](#); [Miguez-Macho et al. 2007](#); [Gochis et al. 2013](#); [Barlage et al. 2015](#)), additions that have had major impact on simulated surface heat and moisture fluxes, regional weather, and climate.

This increased complexity invites more uncertainty because of our incomplete knowledge of the physics, the inherent assumptions in model structures and parameterization schemes (Rosero et al. 2009, etc.), and the large set of imperfectly specified physical parameters used (Chen and Dudhia 2001). Mitigating these uncertainties requires more systematic evaluation and benchmarking of LSMs (e.g., Koster et al. 2004; Luo et al. 2012; Best et al. 2015; Newman et al. 2017). Thus, new frameworks have been developed for testing working hypotheses and parameterizations (e.g., Clark et al. 2011). The community Noah LSM with multi-parameterization options (Noah-MP; Niu et al. 2011) and the Structure for Unifying Multiple Modeling Alternatives (SUMMA; Clark et al. 2015) LSM are two prominent examples. Recent studies (e.g., Zhang et al. 2016) illustrate how incorporation of different parameterization schemes for key physical processes provides the opportunity to interpret modeling results for a given subprocess through the use of physics-ensemble simulations in the same model framework.

Last, it would not make much sense to implement a sophisticated LSM in weather models without a proper soil-state initialization procedure. However, there are no routine soil moisture and soil temperature observations over the large spatial domains typically spanned by weather models. Moreover, LSMs may have different soil moisture dynamic ranges because of different approaches to treating evaporation and runoff (Koster and Milliman 1997), and the soil types used as input are only approximate. It is therefore important to recognize that the soil state calculated for a given atmospheric forcing depends on the model and input. The soil moisture and temperature fields from the traditional four-dimensional data assimilation (4DDA) systems of coupled land/atmosphere models often suffer substantial errors and drift owing to precipitation, temperature, and radiation biases in the coupled system. Such errors and drift often necessitate the application of soil moisture nudging techniques in coupled 4DDA systems (Mahfouf 1991; Douville et al. 2000). But the nudging approach may fail in situations where the soil moisture is insensitive to atmospheric conditions such as under cloudy and windy conditions. The combination of remotely sensed surface temperature and soil moisture, and the development of ensemble Kalman filter and variational methods enable large-scale land data assimilation (Maggioni and Houser 2017).

An alternative strategy is to utilize available observations (precipitation, surface solar insolation, and meteorological analysis) to drive an LSM in offline mode and use the results to initiate the model. This need was met by the development of the North American Land Data Assimilation System (NLDAS; Mitchell et al. 2004),

the Global Land Data Assimilation System (GLDAS; Rodell et al. 2004), and the high-resolution land data assimilation system (HRLDAS; Chen et al. 2007).

c. Evolution of ABL parameterization in weather and climate models

Since the 1970s, operational and research NWP and climate models have become increasingly sophisticated, and this has included the treatment of the ABL, especially under convective conditions. Early models, especially global models, had low vertical resolutions with the lowest layers several hundred meters thick, thus representing the boundary layer as a whole rather than a separate thin surface layer for which similarity theory could be used. These thicker layers required so-called bulk ABL parameterizations and bulk exchange coefficients to derive surface fluxes from lowest-level atmospheric fields. The methods were typically simple with empirical heat and momentum exchange coefficients, as used in early mesoscale models (e.g., Anthes and Warner 1978). Phillips (1986) had a bulk mixed-layer scheme to redistribute surface fluxes in a boundary layer of several levels in the National Meteorological Center's (NMC's) global and regional Nested Grid Model (NGM) and Regional Analysis and Forecast System (RAFS) models.

Already in the 1970s, boundary layers in models were represented with higher resolution and vertical diffusion with mixing length theory, using enhanced mixing lengths in the boundary layer to account for eddy scales larger than the vertical grid size. O'Brien's (1970) K profile, a cubic function of z , was adopted by Tapp and White (1976) in the Met Office mesoscale model, while Busch et al. (1976) had a prognostic length scale that had a similar shape and was used in early versions of the Pennsylvania State University mesoscale model (Anthes and Warner 1978). This latter model also adopted the Deardorff (1972b) countergradient term to allow vertical heat fluxes even in well-mixed conditions. This term was to mimic the effect of deep surface-based eddies that transported heat nonlocally, that is, in a way that was independent of the local vertical gradient, and it allowed a neutral stratification to develop, while one without such a term would remain unstable and could never reach neutrality when driven by surface fluxes alone. Zhang and Anthes (1982) presented a successor to the Pennsylvania State University high-resolution ABL scheme, following the ideas of Blackadar (1979), which represented direct transport by thermals between the surface layer and all other CBL layers, an early example of a nonlocal mass-flux approach. It also included an entrained buoyancy flux equal to -0.2 times the surface buoyancy flux.

In the 1970s and 1980s, turbulence modeling also increasingly turned to so-called higher-order closure, inspired by the seminal paper on the hierarchy of turbulence closures by Mellor and Yamada (1974). Computational power was increasing rapidly in the 1970s, so there was a general belief that the number of prognostic equations for turbulence statistics could be increased, thereby pushing uncertain closure assumptions to even higher moments, where they either would either be simplified or at least not be so critical. For example, André et al. (1978) presented a model with prognostic equations for both second- and third-order correlations, which was tested against the Wangara data. Eventually, however, it was realized that little was gained, the closure assumptions for higher moments were more complicated than expected, negative variances resulted (Wyngaard 1988), and results were poor for the CBL (Moeng and Wyngaard 1989). Moreover, some of the hybrid schemes, like the Mellor–Yamada Level 3 scheme, were not fully realizable (e.g., André 1990).

Nevertheless, the so-called 1.5-order schemes, which predicted TKE as an extra second-order variable, started to become popular in the early 1990s. Such a scheme was adopted for the regional Eta model at NMC (Janjić 1990) based on the ideas of Mellor and Yamada (1982). Together with a diagnosed vertical length scale, TKE could be used to compute the vertical K coefficients. A prognostic TKE approach could be applied to the whole column, handling elevated turbulence as well as boundary layer turbulence, while maintaining a memory of the turbulence even after surface forcing ceases. French global and regional NWP models [ARPEGE, ALADIN, Applications of Research to Operations at Mesoscale (AROME)], and the European HIRLAM model consortium also adopted such approaches (e.g., Bougeault and Lacarrere 1989; Cuxart et al. 2000); the various TKE approaches mostly differ by how they compute the length scales and stability effects. The Bougeault–Lacarrere approach also adopts Deardorff's (1972b) countergradient term. TKE approaches have also been adopted for the German model, COSMO (Baldauf et al. 2011), the Japanese NHM model (Saito et al. 2006), the U.S. Navy COAMPS (Hodur 1997), and the U.S. Rapid Update Cycle model (RUC), initially using the Burk and Thompson (1989) TKE scheme.

Another trend in the 1990s among the K diffusion schemes was the increasing use of enhanced K -profile methods (similar to O'Brien 1970) along with a nonlocal or countergradient term in the vertical heat transport (similar to Deardorff 1972b). The ideas of Troen and Mahrt (1986) helped to quantify these terms as a function of surface heat flux and an ABL depth defined in terms of a bulk Richardson number. Holtslag and

Boville (1993) applied this approach to replace the local scheme in the U.S. climate model, second version (CCM2), and Hong and Pan (1996) similarly replaced a local scheme in the U.S. global weather prediction model, MRF, with one that includes a countergradient term and enhanced K profile.

At the Met Office, Lock et al. (2000) also adopted countergradient term plus K -profile methods for the dry CBL and extended the boundary layer scheme to cover cloud-topped boundary layers, enhanced entrainment, and so-called top-down mixing driven by cloud-top radiative cooling. This marked the beginning of a trend to include shallow clouds in ABL schemes.

In the 2000s, the eddy-diffusion mass-flux (EDMF) approach started to be used in NWP models. This method combines local methods for vertical diffusion, either TKE based or diagnostic- K based, with a mass-flux treatment of CBL thermals using a one-dimensional plume model with a nonlocal mass flux between the surface and the thermal top (Soares et al. 2004). The ECMWF model switched from a local- K scheme to a cubic K profile, similar to those mentioned earlier with enhanced values in the middle of the ABL, plus a separate mass-flux term represented by an entraining and detraining plume transporting surface air upward (Siebesma et al. 2007). In the French models, the local vertical diffusion scheme continued to use the TKE approach, but a mass-flux plume was added (Pergaud et al. 2009), which could also handle shallow clouds. Neggers et al. (2009) also treated dry and cloud-topped thermals separately in their EDMF scheme; this was tested by ECMWF (Köhler et al. 2011) and later adopted. Following a related but different approach, the U.S. climate model Mean Climate of the Community Atmosphere Model (CAM4) adopted Bretherton and Park's (2009) CAM University of Washington (UW) ABL scheme, which included a diagnostic TKE and a generalized nonlocal vertical turbulence term that allows deeper moist and dry layers to mix. The CAM4 physics also considers shallow clouds separately (Park and Bretherton 2009) and includes top-down mixing.

Since 2000, the YSU ABL scheme (Hong et al. 2006), commonly used in WRF simulations, added explicit entrainment to the MRF ABL countergradient scheme modifying the K profile to stop at the top of the neutral layer and adding a term proportional to surface heat flux in an entrainment layer above. Pleim (2007) extended the Zhang and Anthes (1982) nonlocal upward transport to add a local downward flux in a so-called asymmetric convective model. Meanwhile NCEP's rapid refresh models [RAP, High-Resolution Rapid Refresh (HRRR)] switched to another Mellor–Yamada-based TKE scheme with more sophisticated length scales (Nakanishi and Niino 2006).

Since 2010, in more recent developments the YSU ABL scheme added a top-down enhanced mixing profile driven by radiative cooling at fog (or cloud) top (Wilson and Fovell 2018), the U.S. Rapid Refresh model has been enhancing their Nakanishi–Niino TKE scheme to include an EDMF nonlocal part and shallow convection, and the GFS (formerly MRF) ABL scheme has moved from a purely countergradient nonlocal term to a hybrid countergradient and EDMF scheme based on the amount of instability (Han et al. 2016).

At present, mesoscale numerical models at fine resolution (horizontal grid spacing on the order of a few kilometers), especially if using ABL schemes with local diffusivity alone, produce enticingly realistic but only partially resolved rolls and cells to make up for the “lost” transport (e.g., Ching et al. 2014; Zhou et al. 2014). Properly representing boundary layer processes in a mesh with subkilometer-scale horizontal spacing [the PBL–LES “grey zone” or Wyngaard’s (2004) “Terra Incognita”] remains an active area of research, and several investigators are using LES (e.g., Honnert et al. 2011; Beare 2014; Shin and Dudhia 2016) or refined grids in mesoscale models (Zhou et al. 2017) to address this problem.

In conclusion, there has been a general trend from very simple dry local mixing approaches in earlier models to ABL schemes that represent nonlocal transport by thermals, cloud effects, top-down mixing, etc., thus including the full spectrum of ABL types within a single parameterization scheme and enabling improvements in representing the evolution of low cloud cover. The idea that ABL schemes should be unified with shallow cumulus schemes has been gaining popularity together with the concept of top-down radiatively driven mixing influencing both the boundary layer growth and shallow cloud development.

11. Discussion and synthesis

a. Historic synthesis

One hundred years ago, many scientists recognized that the winds in the boundary layer could be represented by some form of the Ekman spiral; that the virtual potential temperature $\bar{\theta}_v$ was well mixed during the day, and that radiative cooling at night led to a deepening temperature inversion. Surface maps were becoming routine, as were kite soundings. As measuring techniques improved to allow sampling of turbulence quantities, we were able to quantify vertical transport of heat and momentum so that, by midcentury, Monin–Obukhov similarity theory provided a framework under which we could relate those fluxes to their corresponding mean profiles.

In the 1970s, ABL knowledge expanded rapidly as research emphasis shifted from the surface layer to the entire CBL, thanks to the emergence of LES, laboratory studies, and the ability to measure water vapor fluxes as well as heat and momentum fluxes from aircraft. Satellite images of cumulus clouds, tower measurements, and boundary layer clear-air radar reflectivity patterns revealed CBL rolls and cells, which were replicated in LES and explained in theoretical studies. The development of numerical models of weather and climate prompted scientists to design ambitious field studies to systematically understand the exchanges of energy and moisture at the surface and through the boundary layer under a variety of conditions. These early studies included ATEX (February 1969), BOMEX (June–July 1969), GATE (June–September 1974), and AMTEX (February 1976). We drew extensively from classical turbulence and fluid dynamics to interpret the data from these field campaigns, LES, and laboratory studies. The early boundary layer parameterizations, first driven by observations and later increasingly by LES, drew in varying degrees from “higher order” modeling, using the classical Friedmann–Keller equations (see section 2b).

The 1980s and 1990s saw increased emphasis on interaction of the boundary layer with the surface and with clouds. *Seasat*, launched in 1978, enabled surface-stress and wind estimates over the ocean. Progress in understanding and simulating land surface processes was greatly enhanced by documentation of soil and vegetation characteristics, much of which was satellite based. Comparison of different land surface schemes soon followed under the auspices of GEWEX as part of the PILPS (1992). Understanding of the roughness sublayer associated with canopies, ocean waves, and cities was starting to be enhanced by LES and DNS. Much of the landscape today consists of crops and urban development. Thus, it is not surprising that crop-specific surface characteristics are available as input for land surface models, or that development urban-specific and crop-specific land surface models received increased emphasis.

Cloud processes were introduced into LES in the mid-1970s; with LES of observed case studies by the early 1980s supplementing knowledge gained in aircraft observations over the tropical oceans dating back to the 1940s; and improved aircraft instrumentation enabled estimates of entrainment into stratus-topped boundary layers. While the stratus-to-cumulus transition in the tropics had been studied as far back as 1950, this became an intense area of research in the 1990s. Through GEWEX, international LES and single-column-model comparisons were started to figure out what was needed to accurately replicate observations of different types of cloud-topped boundary layers, with the goal of improving LES to the point that they could be reliable benchmarks

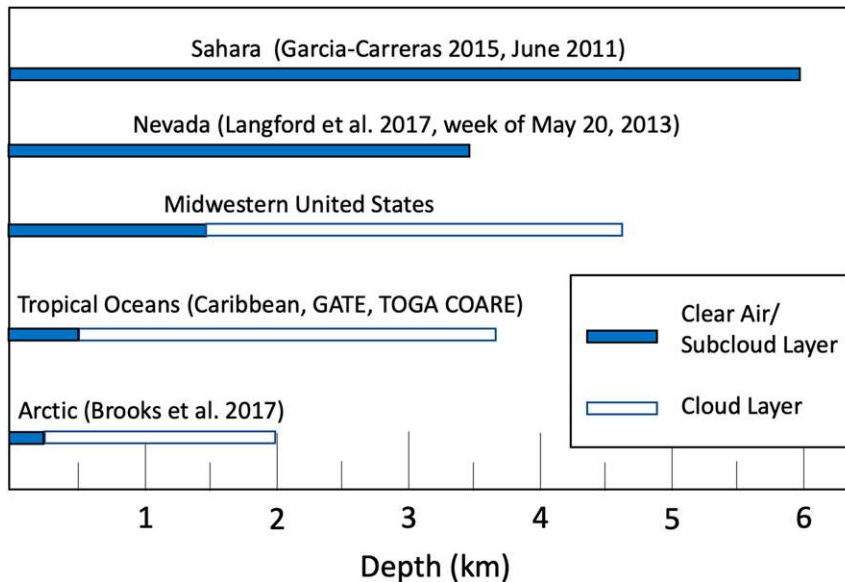


FIG. 9-35. Range of warm-season fair-weather maximum CBL depth as defined by subcloud layer top (roughly mixed-layer top) and top of cloud (typically cumulus) layer, based on Garcia-Carreras et al. (2015), Langford et al. (2017), Brooks et al. (2017), and the foregoing discussion. For Midwest (Oklahoma), see Liu and Liang (2010); Lareau et al. (2018) has a deeper subcloud layer; for TOGA COARE, see Johnson et al. (2001). Caribbean and GATE references are in sections 4 and 8, along with more Midwest references.

in the development of parameterization schemes in weather and climate models. These efforts became more successful with time, thanks to careful case selection, improvements in LES, SCMs, and measurement technology, which, by the 1990s and 2000s, included cloud radars, Doppler and aerosol lidars, and ground-based radiometers, acoustic sounders, and Doppler radars.

The 1990s and 2000s saw significant progress in sampling the surface layer over the ocean, aided by field campaigns and the ability to measure fluxes from autonomous buoys. The impact of waves on fluxes, the subject of research in the 1950s and earlier, was being more directly addressed, both in the field (e.g., SWADE, HEXOS), and ocean-specific surface-layer models were being developed to estimate fluxes, drawing from TOGA COARE and other field programs. Flux-profile relationships were extended to increasingly strong winds, based on measurements, laboratory results, and LES. Faced with considerable scatter in experimental results in high-wind regimes, researchers focused more on the study of wave fields not in equilibrium with the wind, such as occurs in tropical cyclones.

Studies of the stable boundary layer lagged far behind, owing to difficulties in observation and LES in addition to its inherent complexity. It can be argued that there was early progress: the famous Leipzig wind profile was sampled on a weakly stable day; however, modern progress perhaps began with observations in the Arctic of a weakly stable boundary layer and its subsequent simulation. In

parallel, LES at higher resolution and with more sophisticated subfilter-scale parameterizations are becoming capable of simulating more stable stratification. The SBL was the subject of a number of field programs starting in the 1990s; an Arctic program [the 1994 Beaufort Arctic Stratus Experiment (BASE)] provided the basis for an international LES comparison (Beare et al. 2006). However, these approaches continue to be limited by intermittency and even tiny surface nonuniformities.

Like the SBL, progress in understanding the evolving boundary layer has come much later. Our understanding is partially hampered by difficulties in sampling evolving boundary layers, and partially by the fact that our conception of the boundary layer has been driven by steady-state idealizations. Continued development of ABL parameterizations, elements of which are based on steady-state observations or LES, needs to be informed by comparison to observed or simulated evolving boundary layers.

b. Some lessons learned: Parameter space

1) CBL DEPTH

One kilometer is a good order-of-magnitude estimate for the depth of the CBL, but this mostly applies to the eastern United States and much of Europe in the summertime. Indeed, the daytime CBL can vary by nearly a factor of 10 in both directions, as illustrated a sampling of the literature in Fig. 9-35. Not surprisingly,

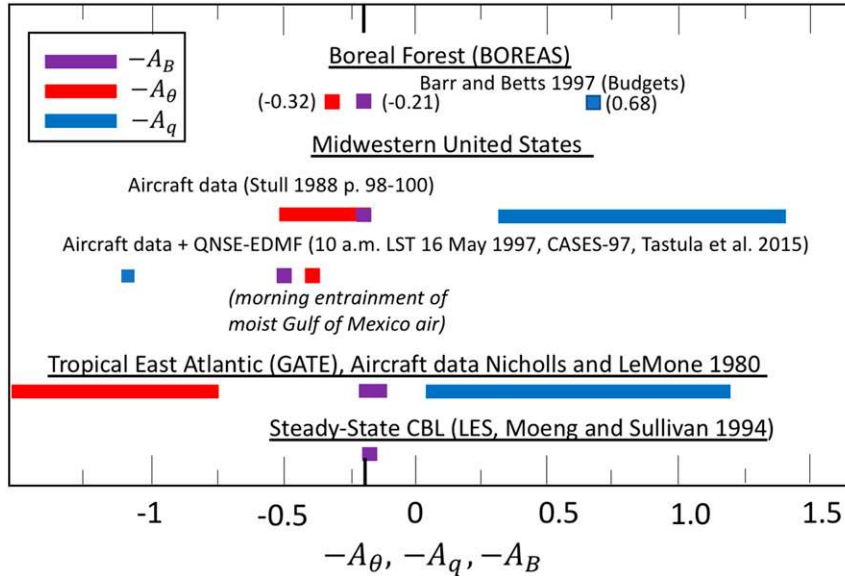


FIG. 9-36. CBL entrainment ratios for $\overline{w'T'}$, $\overline{w'q'}$, and $\overline{w'T'_v}$ to illustrate variation in fluxes producing $-A_B \approx -0.2$, (Barr and Betts 1997; Stull 1988; Nicholls and LeMone 1980; Moeng and Sullivan 1994) plus the case with negative moisture flux at CBL top (Tastula et al. 2015). Bold ticks indicate the ratio -0.2 . Note that the mixed-layer top (just below cloud base when there are clouds) is used for the tropical ratios. Negative ratios are plotted to have the same sign as fluxes at CBL top. Numbers for the top region are averages.

given strong surface heating and very dry conditions (hence few or no surface-based clouds), desert locations have the deepest boundary layers. Conversely, with weak surface heating, the Arctic CBL is shallow, its turbulence typically driven by shear near the surface and cloud-top cooling, and it is thus frequently transformed into two layers by decoupling of the cloud layer from the surface. In the middle are CBLs that are most often sampled and studied, which reach depths of ~ 1 km, with clouds in fair weather possibly extending a few kilometers more. Somewhat surprisingly, the *composite* mixed-layer top (not shown) reached 2 km and more over the boreal forest during BOREAS (May–August) at about 55°N (Barr and Betts 1997). This results from a combination of the length of day compensating for the large zenith angle to make total insolation not that much lower than the tropics (List 1963, Table 134) a low albedo, (Betts and Ball 1997), and high Bowen ratios (Barr and Betts 1997).

2) ENTRAINMENT (SECTIONS 4 AND 6)

Our survey of the literature reveals strong departures of the buoyancy entrainment ratio A_B from 0.2 in the early morning, when there is strong wind (or shear near CBL top); late afternoon, when surface buoyancy flux weakens and processes local to the CBL top become important; and during times of rapid change, when

simply averaged negative buoyancy flux is smeared vertically. What is not always appreciated is the enormous variability of the entrainment ratios for temperature and mixing ratio even when $A_B = 0.2$ as illustrated in Fig. 9-36, for situations when the “negative buoyancy flux area” is sufficiently well behaved that A_B based on single-height buoyancy fluxes has meaning. From the figure, $-A_\theta = (\overline{w'\theta'})_{z_i}/(\overline{w'\theta'})_0$ has been observed to have values as low as -1.5 , a reflection of important role of water vapor fluxes in moist CBLs like those over the tropical ocean. Similarly, large $-A_q = (\overline{w'q'})_{z_i}/(\overline{w'q'})_0$ values have been observed both over land and the tropical ocean; and *negative* values—indicating moister air being entrained into the CBL—have been observed in the Arctic (section 9), and over the central United States when southerlies are transporting moist air from the Gulf of Mexico.

c. Some lessons learned: Physical models

Just as limited knowledge of the ABL parameter space can be a hindrance, blind use of physical models can lead to trouble. For example, flux-profile relationships rely on parameters inspired by molecular theory, where fluxes are related to local gradients: the eddy-exchange coefficients (K_M , K_H , etc), and the turbulent Prandtl number Pr_T . Yet nonlocal fluxes have been documented in both the CBL (large eddies) and SBL

(gravity waves, the eddies in Regime 2 of Sun et al. 2012). The K problem is propagated further in application of the higher-order equations, which, despite some disillusionment in the 1980s, are still being used today. In CBL parameterizations, use of K and higher-order models has been supplemented by, for example, adding a plume model. The picture is muddled in the case of the turbulent Prandtl number $Pr_T = K_M/K_H$, the ratio of two ill-defined functions. In the SBL (including the inversion at the top of the CBL), inclusion of gravity waves can change the trend of Pr_T with stability. Similarly, several shortcomings of MOST have been enumerated, some also traced to nonlocal fluxes. Even the von Kármán constant has been the subject of vigorous debate. We can be reassured by the fact that all of these concepts have been successful to some degree; and that, by treating them with appropriate caution and respect, future researchers can develop improvements or new approaches altogether.

d. Some lessons learned: Common misconceptions or sources of confusion

Real boundary layers usually differ from the simple, quasi-steady-state boundary layers we often document or simulate. Direct heating and cooling of the air by radiation and the impact of horizontal advection are too often neglected: even when such effects are small, they can be important from a climate perspective if they are common. Likewise, CBL profiles of mean quantities often depart from their idealized forms in evolving boundary layers. Finally, whole bodies of research can be lost when phenomena are renamed—sometimes more than once, a significant problem now that researchers use key words in Internet literature searches. For example, large CBL eddies associated with strong winds have been called “longitudinal vortex rolls” (Kaimal et al. 1972), “roll vortices” (section 4), “horizontal convective rolls (HCRs)” (e.g., Weckwerth et al. 1997), and a subclass of the “turbulent organized structures (TOS)” (Kanda et al. 2004).

e. Lack of awareness and rediscovery

Lack of awareness leads to error and “firsts” that were not. Khrgian (1959, p. 226) describes two scientists in the late 1800s who, knowing from manned balloon flights that the air got colder higher up but who were unaware of adiabatic compression (discovered in the early 1800s), thought that cold air associated with winter anticyclones originated from the upper

atmosphere! In the process of researching this paper, we discovered two other researchers who came close to independently deriving MOST, and one of the authors had heard of a third.³⁰ A more current example is the rediscovery of the importance of water vapor to buoyancy. Even though known early—Espy wrote of this in 1841 and McAdie in 1915—its effects were ignored during the development of MOST and in the Businger et al. (1971) Kansas experiment paper, likely because the authors thought the effects were small. However, the same omission was made in some of the papers cited in Stull’s (1976) review paper on the entrainment ratio, where it is likely not negligible. However, measurements in AMTEX (1974) and GATE (1974) were reminders of its importance, and Brutsaert included the effects of water vapor in his definition of L in his 1982 text.

f. Challenges and opportunities for the future

1) REPRESENTING SURFACE FLUXES

For the last 50–60 years, MOST has formed the basis for study of the lowest 5%–15% of the ABL; indeed, the definition of the surface layer is intimately tied to MOST. Yet shortcomings have emerged, particularly in the presence of nonlocal fluxes, in the presence of a canopy or built environment, and in the presence of ocean waves, particularly wave fields not in equilibrium with the wind (sections 3 and 5).

2) LARGE EDDIES

Above the surface layer, a significant amount of vertical transport is by eddies spanning the CBL. These eddies, with horizontal scales from 1.5 to several times the depth of the CBL, are due to flow instability, surface horizontal heterogeneity, or interaction of the CBL with tropospheric gravity waves (sections 4, 7, and 8). Their presence could make estimates of the surface-energy budget difficult. Large eddies are both difficult to document in observations, and to represent in NWP and climate models because they are only partially resolved. What representations will work for what applications?

3) CLOUDS

Theory, numerical modeling, and observations in concert have pushed forward our knowledge of the linkages between the boundary layer and low clouds. Understanding and representing the interplay between microphysics, turbulence, and dynamics involved in weakly to strongly coupled cloud-boundary layer systems remains a challenge (sections 8 and 9).

³⁰This likely resulted from the interruption of scientific communication during World War II.

4) NUMERICAL MODELING

Discovery, description, and modeling of boundary layer processes has benefitted from tools that we have barely touched on. From the modeling point of view, LES is benefitting from larger domains, finer resolution, the inclusion of more refined radiation and cloud-microphysics schemes, and subfilter parameterization schemes. Very high resolution LES and DNS are enhancing our understanding of near-surface and entrainment processes, and instrumental in studies of finescale processes such as airflow around cities or entrainment. Adaptive-grid methodologies (e.g., van Hooft et al. 2018) are being developed that will increase the flexibility and efficiency in studies of entrainment and evolving boundary layers. Use of immersed-boundary methods and inclusion of land surface models in LES is advancing studies of the interaction with heterogeneous surfaces. In addition, LES are now nested in mesoscale numerical models, which provides a ready-made environment for studies of surface-atmosphere interactions. These numerical approaches can enable deeper understanding of the evolving boundary layer, and the role of synoptic-scale processes, clouds, and radiation. However, LES nested in mesoscale models is in its infancy, and verification of leading-edge simulations with observations and laboratory work is essential.

5) OBSERVATIONS

Improvements in remote sensing of air motion, temperature, water vapor, trace gases, aerosols, and clouds have the potential to better sample turbulence structure and evaluate fluxes of momentum and scalars and thus increase understanding of evolving clear-air and cloud-topped boundary layers. Likewise, in situ sensing systems for measuring fluxes (including radiation), cloud particles, and aerosols, as well as new platforms like unattended aerial vehicles (UAVs), provide detail at smaller scales and at heights not always accessible by aircraft or remote sensing devices.

Older systems that have sometimes fallen into disuse are seeing new life. For example, in recent years scintillometers using temperature and water vapor-sensitive wavelengths can be combined to estimate water vapor (Meijninger et al. 2002a) and heat (Meijninger et al. 2002b) fluxes with reasonable accuracy. Similarly, data from older devices such as sodars can be used in new ways, such as interpreting profile data collected from collocated tethered or nontethered balloon platforms (e.g., Anderson 2003).

These platforms can be complemented by distributed surface sites sampling immediately above the surface,

through the surface, and through the layers beneath the surface, sometimes using wireless networks of high density to sample microstructure structure in the atmosphere, the atmosphere-soil interface, and the soils. Supplementary observations and reanalysis products provide the context for a complete description of the ABL. Boundary layer scientists should look for existing observational networks, and opportunities to collaborate with citizen scientists, which often provides easier access to observational sites and maintaining and protecting instruments as well as providing extra observations. Finally, increased access of archived datasets dating back decades through online platforms offers an opportunity to test new ideas for multiple sites.

6) LABORATORY

Laboratory work has had an important role in advancing studies of dispersion and growing, entraining boundary layers. As noted in section 4, the mixed results of laboratory entrainment results are traced to a complex parameter space; such work points to the need of much larger (swimming-pool-size convection) tanks to address the entrainment problem in greater detail (Jonker and Jiménez 2014).

Acknowledgments. In a paper like this, the credit has to be shared. Thus we recognize those who drafted the individual sections. Wayne Angevine wrote the introduction (section 1) with input from Margaret LeMone. Evgeni Fedorovich wrote section 2b on early work on turbulence and fluid dynamics, with technical assistance from Elizabeth Smith; while LeMone wrote section 2a, and, with input from three informal reviewers, Peter Sullivan, Fedorovich, and Branko Kosović, section 2c on LES. LeMone and Jielun Sun wrote section 3a on the surface energy budget, LeMone wrote section 3b on the surface layer, Edward Patton wrote section 3c on canopies, and Kristina Katsaros wrote section 3d on sea-air exchanges. LeMone wrote section 4 on the CBL, Larry Mahrt wrote section 5 on the SBL, Wayne Angevine wrote section 6 on the diurnal cycle, LeMone wrote section 7 on the impact of horizontal heterogeneity, Christopher Bretherton and Don Lenschow wrote section 8 on cloud-topped boundary layers, and Michael Tjernström wrote section 9 on the boundary layer over the Arctic Ocean. For the section on representing the boundary layer in models, Jeffrey Weil wrote section 10a on dispersion, Fei Chen discussed land surface models used in weather and climate models in section 10b, and Jimy Dudhia discussed ABL parameterization schemes for weather and climate models in section 10c. Wayne Angevine worked with LeMone on section 11, which is based on impressions from the earlier sections

and the cited literature. LeMone and Angevine merged the sections into a single document; some material was moved from one section or another, and some was added; and many of the other authors reviewed other sections. In addition, Peter Sullivan provided material for the ocean discussion and Chris Fairall reviewed it. Sullivan also provided material for the LES section. Joseph Alfieri and Larry Mahrt offered advice on the horizontal heterogeneity section. Ola Persson provided useful input to the Arctic discussion. Jim Fleming supplied us with some references from around 1900 describing early work on the boundary layer and provided us with a copy of his recent book, *Inventing Atmospheric Science* (MIT Press, 2016), which provided useful context for us. Finally we thank Sukanta Basu and the three other reviewers for useful input, which enabled broadening and deepening the discussion in useful ways. Dudhia, Sun, and Patton are supported by NCAR, which is sponsored by the National Science Foundation; LeMone, Lenschow, and Weil are funded by TIAA/CREF with office support from NCAR; Katsaros is funded by TIAA/CREF, Fedorovich by the University of Oklahoma; Tjernström is funded by the University of Stockholm; Angevine is funded by NOAA ESRL CSD; Bretherton is funded by NSF Grant AGS-1660604; Chen is funded by the NCAR Water System, USDA NIFA Grants 2015-67003-23508 and 2015-67003-23460, NSF Grant 1739705, and NOAA OAR Grant NA18OAR4590381; and Mahrt is funded by NSF Grant AGS-1614345.

REFERENCES

- Acevedo, O. C., and D. R. Fitzjarrald, 2001: The early evening transition: Temporal and spatial variability. *J. Atmos. Sci.*, **58**, 2650–2667, [https://doi.org/10.1175/1520-0469\(2001\)058<2650:TEESLT>2.0.CO;2](https://doi.org/10.1175/1520-0469(2001)058<2650:TEESLT>2.0.CO;2).
- , and L. Mahrt, 2010: Systematic vertical variation of mesoscale fluxes in the nocturnal boundary layer. *Bound.-Layer Meteor.*, **135**, 19–30, <https://doi.org/10.1007/s10546-010-9465-4>.
- , —, F. S. Puhales, F. D. Costa, L. E. Medeiros, and G. A. Degrazia, 2016: Contrasting structures between the decoupled and coupled state of the stable boundary layer. *Quart. J. Roy. Meteor. Soc.*, **142**, 693–702, <https://doi.org/10.1002/qj.2693>.
- Ackerman, A. S., and Coauthors, 2009: Large-eddy simulations of a drizzling, stratocumulus-topped marine boundary layer. *Mon. Wea. Rev.*, **137**, 1083–1110, <https://doi.org/10.1175/2008MWR2582.1>.
- Adrian, R. J., 2007: Hairpin vortex organization in wall turbulence. *Phys. Fluids*, **19**, 041301, <https://doi.org/10.1063/1.2717527>.
- Agee, E. M., T. S. Chen, and K. E. Dowell, 1973: A review of mesoscale cellular convection. *Bull. Amer. Meteor. Soc.*, **54**, 1004–1012, [https://doi.org/10.1175/1520-0477\(1973\)054<1004:AROMCC>2.0.CO;2](https://doi.org/10.1175/1520-0477(1973)054<1004:AROMCC>2.0.CO;2).
- Åkerblom, F., 1908: Recherches sur les courants les plus bas de l'atmosphère au-dessus de Paris. *Nova Acta Regiae Soc. Sci. Ups.*, **II**, 1–45.
- Albertson, J. D., and M. B. Parlange, 1999a: Natural integration of scalar fluxes from complex terrain. *Adv. Water Resour.*, **23**, 239–252, [https://doi.org/10.1016/S0309-1708\(99\)00011-1](https://doi.org/10.1016/S0309-1708(99)00011-1).
- , and —, 1999b: Surface length scales and shear stress: Implications for land-atmosphere interaction over complex terrain. *Water Resour. Res.*, **35**, 2121–2132, <https://doi.org/10.1029/1999WR900094>.
- Albrecht, F., 1937: Messgeräte des Wärmehaushalts an der Erdoberfläche als Mittel der bioklimatischen Forschung. *Meteor. Z.*, **54**, 471–475.
- , 1940: *Untersuchungen über den Wärmehaushalt der Erdoberfläche in verschiedenen Klimagebieten*. Springer, 81 pp., <https://doi.org/10.1007/978-3-662-42530-5>.
- Albrecht, B. A., R. S. Penc, and W. H. Schubert, 1985: An observational study of cloud-topped mixed layers. *J. Atmos. Sci.*, **42**, 800–822, [https://doi.org/10.1175/1520-0469\(1985\)042<0800:AOSOCT>2.0.CO;2](https://doi.org/10.1175/1520-0469(1985)042<0800:AOSOCT>2.0.CO;2).
- , D. A. Randall, and S. Nicholls, 1988: Observations of marine stratocumulus during FIRE. *Bull. Amer. Meteor. Soc.*, **69**, 618–626, [https://doi.org/10.1175/1520-0477\(1988\)069<0618:OOMSCD>2.0.CO;2](https://doi.org/10.1175/1520-0477(1988)069<0618:OOMSCD>2.0.CO;2).
- , C. W. Fairall, D. W. Thomson, A. B. White, J. B. Snider, and W. H. Schubert, 1990: Surface-based remote sensing of the observed and the adiabatic liquid water content of stratocumulus clouds. *Geophys. Res. Lett.*, **17**, 89–92, <https://doi.org/10.1029/GL017i001p00089>.
- , C. S. Bretherton, D. Johnson, W. Schubert, and A. S. Frisch, 1995: The Atlantic Stratocumulus Transition Experiment (ASTEX). *Bull. Amer. Meteor. Soc.*, **76**, 889–903, [https://doi.org/10.1175/1520-0477\(1995\)076<0889:TASTE>2.0.CO;2](https://doi.org/10.1175/1520-0477(1995)076<0889:TASTE>2.0.CO;2).
- Anderson, P. S., 2003: Fine-scale structure observed in a stable atmospheric boundary layer by sodar and kite-borne tether-sonde. *Bound.-Layer Meteor.*, **107**, 323–351, <https://doi.org/10.1023/A:1022171009297>.
- , 2009: Measurement of Prandtl Number as a function of Richardson Number avoiding self-correlation. *Bound.-Layer Meteor.*, **131**, 345–362, <https://doi.org/10.1007/s10546-009-9376-4>.
- Anderson, M. C., J. M. Norman, J. R. Mecikalski, R. D. Torn, W. P. Kustas, and J. B. Basara, 2004: A multiscale remote sensing model for disaggregating regional fluxes to micrometeorological scales. *J. Hydrometeorol.*, **5**, 343–363, [https://doi.org/10.1175/1525-7541\(2004\)005<0343:AMRSMF>2.0.CO;2](https://doi.org/10.1175/1525-7541(2004)005<0343:AMRSMF>2.0.CO;2).
- , —, —, J. A. Otkin, and P. P. Kustas, 2007: A climatological study of evapotranspiration and moisture stress across the continental United States based on thermal remote sensing: 1. Model formulation. *J. Geophys. Res.*, **112**, D10117, <https://doi.org/10.1029/2006JD007506>.
- André, J. C., G. De Moor, P. P. Lacarrère, G. Thery, and R. du Vachat, 1978: Modelling the 24-hour evolution of the mean and turbulent structures in the planetary boundary layer. *J. Atmos. Sci.*, **35**, 1861–1883, [https://doi.org/10.1175/1520-0469\(1978\)035<1861:MTHEOT>2.0.CO;2](https://doi.org/10.1175/1520-0469(1978)035<1861:MTHEOT>2.0.CO;2).
- , J. P. Goutorbe, and A. Perrier, 1986: HAPEX-MOBLIHY: A hydrologic atmospheric experiment for the study of water budget and evaporation flux at the climatic scale. *Bull. Amer. Meteor. Soc.*, **67**, 138–144, [https://doi.org/10.1175/1520-0477\(1986\)067<0138:HAHAEF>2.0.CO;2](https://doi.org/10.1175/1520-0477(1986)067<0138:HAHAEF>2.0.CO;2).
- Andreas, E. L., 1980: Estimation of heat and mass fluxes over Arctic leads. *Mon. Wea. Rev.*, **108**, 2057–2063, [https://doi.org/10.1175/1520-0493\(1980\)108<2057:EOHAMF>2.0.CO;2](https://doi.org/10.1175/1520-0493(1980)108<2057:EOHAMF>2.0.CO;2).
- , K. J. Claffey, R. E. Jordan, C. W. Fairall, P. S. Guest, P. O. G. Persson, and A. A. Grachev, 2006: Evaluations of the von Kármán

- constant in the atmospheric surface layer. *J. Fluid Mech.*, **559**, 117–149, <https://doi.org/10.1017/S0022112006000164>.
- , L. Mahrt, and D. Vickers, 2012: A new drag relation for aerodynamically rough flow over the ocean. *J. Atmos. Sci.*, **69**, 2520–2537, <https://doi.org/10.1175/JAS-D-11-0312.1>.
- , —, and —, 2015: An improved bulk air–sea surface flux algorithm, including spray-mediated transfer. *Quart. J. Roy. Meteor. Soc.*, **141**, 642–654, <https://doi.org/10.1002/qj.2424>.
- Andr n, A., 1990: Evaluation of a turbulence closure scheme suitable for air-pollution applications. *J. Appl. Meteor.*, **29**, 224–239, [https://doi.org/10.1175/1520-0450\(1990\)029<0224:EOATCS>2.0.CO;2](https://doi.org/10.1175/1520-0450(1990)029<0224:EOATCS>2.0.CO;2).
- , A. R. Brown, J. Graf, P. J. Mason, C.-H. Moeng, F. T. M. Nieuwstadt, and U. Schumann, 1994: Large-eddy simulation of a neutrally stratified boundary layer: A comparison of four computer codes. *Quart. J. Roy. Meteor. Soc.*, **120**, 1457–1484, <https://doi.org/10.1002/qj.49712052003>.
- Anfossi, D., S. Alessandrini, S. T. Castell , E. Ferrero, D. Oetli, and G. Degrazia, 2006: Tracer dispersion simulation in low wind speed conditions with a new 2D Langevin equation system. *Atmos. Environ.*, **40**, 7234–7245, <https://doi.org/10.1016/j.atmosenv.2006.05.081>.
- Angvine, W. M., A. W. Grimmsdell, and S. A. McKeen, 1998: Entrainment results from the Flatland boundary layer experiments. *J. Geophys. Res.*, **103**, 13 689–13 701, <https://doi.org/10.1029/98JD01150>.
- , H. K. Baltink, and F. C. Bosveld, 2001: Observations of the morning transition of the convective boundary layer. *Bound.-Layer Meteor.*, **101**, 209–227, <https://doi.org/10.1023/A:1019264716195>.
- Ansell, T. J., and Coauthors, 2006: Daily mean sea-level pressure reconstructions for the European–North America region for the period 1850–1903. *J. Climate*, **19**, 2717–2742, <https://doi.org/10.1175/JCLI3775.1>.
- Ansorge, C., and J. P. Mellado, 2014: Global intermittency and collapsing turbulence in the stratified planetary boundary layer. *Bound.-Layer Meteor.*, **153**, 89–116, <https://doi.org/10.1007/s10546-014-9941-3>.
- Anthes, R. A., and T. T. Warner, 1978: Development of hydrodynamic models suitable for air pollution and other micrometeorological studies. *Mon. Wea. Rev.*, **106**, 1045–1078, [https://doi.org/10.1175/1520-0493\(1978\)106<1045:DOHMSF>2.0.CO;2](https://doi.org/10.1175/1520-0493(1978)106<1045:DOHMSF>2.0.CO;2).
- Arya, S. P. S., 1973: Air friction and form drag on Arctic sea ice. *AIDJEX Bull.*, **19**, 45–57.
- Asai, T., 1970: Three-dimensional features of thermal convection in a plane Couette flow. *J. Meteor. Soc. Japan*, **48**, 129–139, https://doi.org/10.2151/jmsj1965.48.2_129.
- Asanuma, J., and W. Brutsaert, 1999: Turbulence variance characteristics of temperature and humidity in the unstable atmospheric surface layer above a variable pine forest. *Water Resour. Res.*, **35**, 515–521, <https://doi.org/10.1029/1998WR900051>.
- Augstein, E., H. Riehl, F. Ostapoff, and V. Warner, 1973: Mass and energy transports in an undisturbed Atlantic trade-wind flow. *Mon. Wea. Rev.*, **101**, 101–111, [https://doi.org/10.1175/1520-0493\(1973\)101<0101:MAETIA>2.3.CO;2](https://doi.org/10.1175/1520-0493(1973)101<0101:MAETIA>2.3.CO;2).
- Avissar, R., and T. Schmidt, 1998: An evaluation of the scale at which ground-surface heat flux patchiness affects the convective boundary layer using large-eddy simulations. *J. Atmos. Sci.*, **55**, 2666–2689, [https://doi.org/10.1175/1520-0469\(1998\)055<2666:AEOTSA>2.0.CO;2](https://doi.org/10.1175/1520-0469(1998)055<2666:AEOTSA>2.0.CO;2).
- Baas, P., F. C. Bosveld, H. K. Baltink, and A. A. M. Holtslag, 2009: A climatology of nocturnal low-level jets at Cabauw. *J. Appl. Meteor.*, **48**, 1627–1642, <https://doi.org/10.1175/2009JAMC1965.1>.
- Baerentsen, J. H., and R. Berkowicz, 1984: Monte Carlo simulation of plume dispersion in the convective boundary layer. *Atmos. Environ.*, **18**, 701–712, [https://doi.org/10.1016/0004-6981\(84\)90256-7](https://doi.org/10.1016/0004-6981(84)90256-7).
- Bailey, B. N., and R. Stoll, 2016: The creation and evolution of coherent structures in plant canopy flows and their role in turbulent transport. *J. Fluid Mech.*, **789**, 425–460, <https://doi.org/10.1017/jfm.2015.749>.
- Balaji, V., J.-L. Redelsperger, and G. P. Klaassen, 1993: Mechanisms for the mesoscale organization of tropical cloud clusters in GATE Phase III: Part I: Shallow cloud bands. *J. Atmos. Sci.*, **50**, 3571–3589, [https://doi.org/10.1175/1520-0469\(1993\)050<3571:MFTMOO>2.0.CO;2](https://doi.org/10.1175/1520-0469(1993)050<3571:MFTMOO>2.0.CO;2).
- Baldauf, M., A. Seifert, J. F rstner, D. Majewski, M. Raschendorfer, and T. Reinhardt, 2011: Operational convective-scale numerical weather prediction with the COSMO model: Description and sensitivities. *Mon. Wea. Rev.*, **139**, 3887–3905, <https://doi.org/10.1175/MWR-D-10-05013.1>.
- Baldocchi, D., 1997: Flux footprints within and over forest canopies. *Bound.-Layer Meteor.*, **85**, 273–292, <https://doi.org/10.1023/A:1000472717236>.
- Ball, F. K., 1960: Control of inversion height by surface heating. *Quart. J. Roy. Meteor. Soc.*, **86**, 483–494, <https://doi.org/10.1002/qj.49708637005>.
- Balsley, B., R. Frehlich, M. Jensen, and Y. Meillier, 2003: Extreme gradients in the nocturnal boundary layer: Structure, evolution and potential causes. *J. Atmos. Sci.*, **60**, 2496–2508, [https://doi.org/10.1175/1520-0469\(2003\)060<2496:EGITNB>2.0.CO;2](https://doi.org/10.1175/1520-0469(2003)060<2496:EGITNB>2.0.CO;2).
- Banner, M. L., W. Chen, E. J. Walsh, J. B. Jensen, S. Lee, and C. Fandry, 1999: The Southern Ocean Waves Experiment. Part I: Overview and mean results. *J. Phys. Oceanogr.*, **29**, 2130–2145, [https://doi.org/10.1175/1520-0485\(1999\)029<2130:TSOWEP>2.0.CO;2](https://doi.org/10.1175/1520-0485(1999)029<2130:TSOWEP>2.0.CO;2).
- Banta, R. M., Y. L. Pichugina, and W. Brewer, 2006: Turbulent velocity-variance profiles in the stable boundary layer generated by a nocturnal low-level jet. *J. Atmos. Sci.*, **63**, 2700–2719, <https://doi.org/10.1175/JAS3776.1>.
- Barad, M. L., 1958: Project Prairie Grass. A Field Program in Diffusion. Geophysical Research Paper 59, Vols. I and II, AFCRF-TR-235, Air Force Cambridge Research Center, 489 pp.
- Barber, D. G., M. G. Asplin, Y. Gratton, J. V. Lukovich, R. J. Galley, R. L. Raddatz, and D. Leitch, 2010: The International Polar Year (IPY) Circumpolar Flaw Lead (CFL) system study: Overview and the physical system. *Atmos.–Ocean*, **48**, 225–243, <https://doi.org/10.3137/OC317.2010>.
- Barlage, M., M. Tewari, F. Chen, G. Miguez-Macho, Z. L. Yang, and G. Y. Niu, 2015: The effect of groundwater interaction in North American regional climate simulations with WRF/Noah-MP. *Climatic Change*, **129**, 485–498, <https://doi.org/10.1007/s10584-014-1308-8>.
- Barlow, J. F., 2014: Progress in observing and modelling the urban boundary layer. *Urban Climate*, **10**, 216–240, <https://doi.org/10.1016/j.uclim.2014.03.011>.
- Barr, A. G., and A. K. Betts, 1997: Radiosonde boundary layer budgets over a boreal forest. *J. Geophys. Res.*, **102**, 29 205–29 212, <https://doi.org/10.1029/97JD01105>.
- Barrett, E., and V. E. Suomi, 1949: Preliminary report on temperature measurements by sonic means. *J. Meteor.*, **6**, 273, [https://doi.org/10.1175/1520-0469\(1949\)006<0273:PROTMB>2.0.CO;2](https://doi.org/10.1175/1520-0469(1949)006<0273:PROTMB>2.0.CO;2).

- Basu, S., F. Porté-Agel, E. Foufoula-Georgiou, J.-F. Vinuesa, and M. Pahlow, 2006: Revisiting the local scaling hypothesis in stably stratified atmospheric boundary layer turbulence: An integration of field and laboratory measurements with large-eddy simulations. *Bound.-Layer Meteor.*, **119**, 473–500, <https://doi.org/10.1007/s10546-005-9036-2>.
- , J.-F. Vinuesa, and A. Swift, 2008: Dynamic LES modeling of a diurnal cycle. *J. Appl. Meteor. Climatol.*, **47**, 1156–1174, <https://doi.org/10.1175/2007JAMC1677.1>.
- Batchelor, G. B., 1950: The application of the similarity theory of turbulence to atmospheric dispersion. *Quart. J. Roy. Meteor. Soc.*, **76**, 133–146, <https://doi.org/10.1002/qj.49707632804>.
- Bean, B. R., R. Gilmer, R. L. Grossman, and R. McGavin, 1972: An analysis of airborne measurements of vertical water vapor flux during BOMEX. *J. Atmos. Sci.*, **29**, 860–869, [https://doi.org/10.1175/1520-0469\(1972\)029<0860:AAOAMO>2.0.CO;2](https://doi.org/10.1175/1520-0469(1972)029<0860:AAOAMO>2.0.CO;2).
- Beare, R. J., and Coauthors, 2006: An intercomparison of large-eddy simulations of the stable boundary layer. *Bound.-Layer Meteor.*, **118**, 247–272, <https://doi.org/10.1007/s10546-004-2820-6>.
- , 2008: The role of shear in the morning transition boundary layer. *Bound.-Layer Meteor.*, **129**, 395–410, <https://doi.org/10.1007/s10546-008-9324-8>.
- , 2014: A length scale defining partially-resolved boundary-layer turbulence simulations. *Bound.-Layer Meteor.*, **151**, 39–55, <https://doi.org/10.1007/s10546-013-9881-3>.
- , and M. K. MacVean, 2004: Resolution sensitivity and scaling of large-eddy simulations of the stable boundary layer. *Bound.-Layer Meteor.*, **112**, 257–281, <https://doi.org/10.1023/B:BOUN.0000027910.57913.4d>.
- Belcher, S. E., 2005: Mixing and transport in urban areas. *Philos. Trans. Roy. Soc.*, **363A**, 2947–2968, <https://doi.org/10.1098/rsta.2005.1673>.
- , I. N. Harman, and J. J. Finnigan, 2012: The wind in the willows: Flows in forest canopies in complex terrain. *Annu. Rev. Fluid Mech.*, **44**, 479–504, <https://doi.org/10.1146/annurev-fluid-120710-101036>.
- , O. Coceal, J. Hunt, D. Carruthers, and A. Robins, 2013: A review of urban dispersion modelling. Tech. Rep. ADMLC-R7, 96 pp.
- Beljaars, A. C. M., 1988: The measurements of gustiness at routine wind stations: A review. Instruments and Observing Methods, WMO Rep. 31, 52 pp., https://library.wmo.int/pmb_ged/iom_31.pdf.
- , and F. C. Bosveld, 1997: Cabauw data for the validation of land surface parameterization schemes. *J. Climate*, **10**, 1172–1193, [https://doi.org/10.1175/1520-0442\(1997\)010<1172:CDFTVO>2.0.CO;2](https://doi.org/10.1175/1520-0442(1997)010<1172:CDFTVO>2.0.CO;2).
- , and A. A. M. Holtslag, 1991: Flux parameterization over land surfaces for atmospheric models. *J. Appl. Meteor.*, **30**, 327–341, [https://doi.org/10.1175/1520-0450\(1991\)030<0327:FPOLSF>2.0.CO;2](https://doi.org/10.1175/1520-0450(1991)030<0327:FPOLSF>2.0.CO;2).
- Bell, M. M., M. T. Montgomery, and K. A. Emanuel, 2012: Air–sea enthalpy and momentum exchange at major hurricane wind speeds observed during CBLAST. *J. Atmos. Sci.*, **69**, 3197–3222, <https://doi.org/10.1175/JAS-D-11-0276.1>.
- Benjamin, S., J. Brown, G. Brunet, P. Lynch, K. Saito, and T. W. Schlatter, 2019: 100 years of progress in forecasting and NWP applications. *A Century of Progress in Atmospheric and Related Sciences: Celebrating the American Meteorological Society Centennial*. Meteor. Monogr., No. 59, Amer. Meteor. Soc., <https://doi.org/10.1175/AMSMONOGRAPHS-D-18-0020.1>.
- Berner, A. H., C. S. Bretherton, R. Wood, and A. Mühlbauer, 2013: Marine boundary layer cloud regimes and POC formation in an LES coupled to a bulk aerosol scheme. *Atmos. Chem. Phys.*, **13**, 12 549–12 572, <https://doi.org/10.5194/acp-13-12549-2013>.
- Best, M. J., 2005: Representing urban areas within operational numerical weather prediction models. *Bound.-Layer Meteor.*, **114**, 91–109, <https://doi.org/10.1007/s10546-004-4834-5>.
- , and Coauthors, 2015: The plumbing of land surface models: Benchmarking model performance. *J. Hydrometeorol.*, **16**, 1425–1442, <https://doi.org/10.1175/JHM-D-14-0158.1>.
- Betts, A. K., and J. H. Ball, 1994: Budget analysis of FIFE 1987 sonde data. *J. Geophys. Res.*, **99**, 3655–3666, <https://doi.org/10.1029/93JD02739>.
- , and —, 1997: Albedo over the boreal forest. *J. Geophys. Res.*, **102**, 28 901–28 909, <https://doi.org/10.1029/96JD03876>.
- , and A. G. Barr, 1996: First international land surface climatology field experiment 1987 sonde budget revisited. *J. Geophys. Res.*, **101**, 23 285–23 288, <https://doi.org/10.1029/96JD02247>.
- Blackadar, A. K., 1957: Boundary-layer wind maxima and their significance for the growth of nocturnal inversions. *Bull. Amer. Meteor. Soc.*, **38**, 283–290, <https://doi.org/10.1175/1520-0477-38.5.283>.
- , 1962: The vertical distribution of wind and turbulent exchange in a neutral atmosphere. *J. Geophys. Res.*, **67**, 3095–3102, <https://doi.org/10.1029/JZ067i008p03095>.
- , 1979: High resolution models of the planetary boundary layer. *Advances in Environmental Science and Engineering*, Vol. 1, J. Pfafflin and E. Ziegler, Eds., Gordon and Breach, 50–85.
- Blossey, P. N., and Coauthors, 2013: Marine low cloud sensitivity to an idealized climate change: The CGILS LES intercomparison. *J. Adv. Model. Earth Syst.*, **5**, 234–258, <https://doi.org/10.1002/jame.20025>.
- Bodas-Salcedo, and Coauthors, 2014: Origins of the solar radiation biases over the Southern Ocean in CFMIP2 models. *J. Climate*, **27**, 41–56, <https://doi.org/10.1175/JCLI-D-13-00169.1>.
- Bonan, G. B., E. G. Patton, I. N. Harman, K. W. Oleson, J. J. Finnigan, Y. Lu, and E. A. Burakowski, 2018: Modeling canopy-induced turbulence in the Earth system: A unified parameterization of turbulent exchange within plant canopies and the roughness sublayer (CLM-ml v0). *Geosci. Model Dev.*, **11**, 1467–1496, <https://doi.org/10.5194/gmd-11-1467-2018>.
- Boppa, V. B. L., Z.-T. Xie, and I. P. Castro, 2010: Large-eddy simulation of dispersion from surface sources in arrays of obstacles. *Bound.-Layer Meteor.*, **135**, 433–454, <https://doi.org/10.1007/s10546-010-9489-9>.
- Bornstein, R. D., 1968: Observations of the urban heat island effect in New York City. *J. Appl. Meteor.*, **7**, 575–582, [https://doi.org/10.1175/1520-0450\(1968\)007<0575:OOUTUHI>2.0.CO;2](https://doi.org/10.1175/1520-0450(1968)007<0575:OOUTUHI>2.0.CO;2).
- Bosveld, F., and Coauthors, 2014: The third GABLS intercomparison case for evaluation studies of boundary-layer models. Part B: Results and process understanding. *Bound.-Layer Meteor.*, **152**, 157–187, <https://doi.org/10.1007/s10546-014-9919-1>.
- Bougeault, P., and P. Lacarrere, 1989: Parameterization of orography-induced turbulence in a mesobeta-scale model. *Mon. Wea. Rev.*, **117**, 1872–1890, [https://doi.org/10.1175/1520-0493\(1989\)117<1872:POOITI>2.0.CO;2](https://doi.org/10.1175/1520-0493(1989)117<1872:POOITI>2.0.CO;2).
- Boussinesq, J., 1897: *Théorie de L'écoulement Tourbillonnant et Tumultueux des Liquides dans les Lits Rectilignes a Grande Section*. Gauthier-Villars et fils, 64 pp.

- Bou-Zeid, E., C. Meneveau, and M. Parlange, 2004: Large-eddy simulation of neutral atmospheric boundary layer flow over heterogeneous surfaces: Blending height and effective surface roughness. *Water Resour. Res.*, **40**, W02505, <https://doi.org/10.1029/2003WR002475>.
- , —, and —, 2005: A scale-dependent Lagrangian dynamic model for large eddy simulation of complex turbulent flows. *Phys. Fluids*, **17**, 025105, <https://doi.org/10.1063/1.1839152>.
- , C. Higgins, H. Huwald, C. Meneveau, and M. B. Parlange, 2010: Field study of the dynamics and modelling of subgrid-scale turbulence in a stable atmospheric surface layer over a glacier. *J. Fluid Mech.*, **665**, 480–515, <https://doi.org/10.1017/S0022112010004015>.
- Bowen, I. S., 1926: The ratio of heat losses by conduction and by evaporation from any water surface. *Phys. Rev.*, **27**, 779–787, <https://doi.org/10.1103/PhysRev.27.779>.
- Bretherton, C. S., 1991: Modelling the Lagrangian evolution of cloud-topped boundary layers. *Physical Processes in Atmospheric Models*, D. R. Sikka and S. S. Singh, Eds., 97–119.
- , and R. Pincus, 1995: Cloudiness and marine boundary layer dynamics in the ASTEX Lagrangian experiments. Part I: Synoptic setting and vertical structure. *J. Atmos. Sci.*, **52**, 2707–2723, [https://doi.org/10.1175/1520-0469\(1995\)052<2707:CAMBLD>2.0.CO;2](https://doi.org/10.1175/1520-0469(1995)052<2707:CAMBLD>2.0.CO;2).
- , and M. C. Wyant, 1997: Moisture transport, lower tropospheric stability and decoupling of cloud-topped boundary layers. *J. Atmos. Sci.*, **54**, 148–167, [https://doi.org/10.1175/1520-0469\(1997\)054<0148:MTL TSA>2.0.CO;2](https://doi.org/10.1175/1520-0469(1997)054<0148:MTL TSA>2.0.CO;2).
- , and S. Park, 2009: A new moist turbulence parameterization in the Community Atmosphere Model. *J. Climate*, **22**, 3422–3448, <https://doi.org/10.1175/2008JCLI2556.1>.
- , P. Austin, and S. T. Siems, 1995a: Cloudiness and marine boundary layer dynamics in the ASTEX Lagrangian experiments. Part II: Cloudiness, drizzle, surface fluxes and entrainment. *J. Atmos. Sci.*, **52**, 2724–2735, [https://doi.org/10.1175/1520-0469\(1995\)052<2724:CAMBLD>2.0.CO;2](https://doi.org/10.1175/1520-0469(1995)052<2724:CAMBLD>2.0.CO;2).
- , E. Klinker, J. Coakley, and A. K. Betts, 1995b: Comparison of ceilometer, satellite, and synoptic measurements of boundary-layer cloudiness and the ECMWF diagnostic cloud parameterization scheme during ASTEX. *J. Atmos. Sci.*, **52**, 2736–2751, [https://doi.org/10.1175/1520-0469\(1995\)052<2736:COCSAS>2.0.CO;2](https://doi.org/10.1175/1520-0469(1995)052<2736:COCSAS>2.0.CO;2).
- , S. K. Krueger, M. C. Wyant, P. Bechtold, E. van Meijgaard, B. Stevens, and J. Teixeira, 1999a: A GCSS boundary layer model intercomparison study of the first ASTEX Lagrangian experiment. *Bound.-Layer Meteor.*, **93**, 341–380, <https://doi.org/10.1023/A:1002005429969>.
- , and Coauthors, 1999b: An intercomparison of radiatively-driven entrainment and turbulence in a smoke cloud, as simulated by different numerical models. *Quart. J. Roy. Meteor. Soc.*, **125**, 391–423, <https://doi.org/10.1002/qj.49712555402>.
- , J. R. McCaa, and H. Grenier, 2004a: A new parameterization for shallow cumulus convection and its application to marine subtropical cloud-topped boundary layers. Part I: Description and 1D results. *Mon. Wea. Rev.*, **132**, 864–882, [https://doi.org/10.1175/1520-0493\(2004\)132<0864:ANPFSC>2.0.CO;2](https://doi.org/10.1175/1520-0493(2004)132<0864:ANPFSC>2.0.CO;2).
- , T. Uttal, C. W. Fairall, S. E. Yuter, R. A. Weller, D. Baumgardner, K. Comstock, and R. Wood, 2004b: The EPIC 2001 stratocumulus study. *Bull. Amer. Meteor. Soc.*, **85**, 967–977, <https://doi.org/10.1175/BAMS-85-7-967>.
- Briggs, G. A., 1988: Analysis of diffusion field experiments. *Lectures on Air Pollution Modeling*, A. Venkatram and J. C. Wyngaard, Eds., Amer. Meteor. Soc., 64–117.
- , 1993: Plume dispersion in the convective boundary layer. Part II: Analyses of CONDORS field experiment data. *J. Appl. Meteor.*, **32**, 1388–1425, [https://doi.org/10.1175/1520-0450\(1993\)032<1388:PDITCB>2.0.CO;2](https://doi.org/10.1175/1520-0450(1993)032<1388:PDITCB>2.0.CO;2).
- Britter, R. E., and S. R. Hanna, 2003: Flow and dispersion in urban areas. *Annu. Rev. Fluid Mech.*, **35**, 469–496, <https://doi.org/10.1146/annurev.fluid.35.101101.161147>.
- Brooks, I. M., and Coauthors, 2017: The turbulent structure of the Arctic summer boundary layer during the Arctic Summer Cloud-Ocean Study. *J. Geophys. Res. Atmos.*, **122**, 9685–9704, <https://doi.org/10.1002/2017JD027234>.
- Brost, R. A., and J. C. Wyngaard, 1978: A model study of the stably stratified planetary boundary layer. *J. Atmos. Sci.*, **35**, 1427–1440, [https://doi.org/10.1175/1520-0469\(1978\)035<1427:AMSOTS>2.0.CO;2](https://doi.org/10.1175/1520-0469(1978)035<1427:AMSOTS>2.0.CO;2).
- , D. H. Lenschow, and J. C. Wyngaard, 1982a: Marine stratocumulus layers: Part I: Mean conditions. *J. Atmos. Sci.*, **39**, 800–817, [https://doi.org/10.1175/1520-0469\(1982\)039<0800:MSLPMC>2.0.CO;2](https://doi.org/10.1175/1520-0469(1982)039<0800:MSLPMC>2.0.CO;2).
- , —, and —, 1982b: Marine stratocumulus layers: Part II: Turbulence budgets. *J. Atmos. Sci.*, **39**, 818–836, [https://doi.org/10.1175/1520-0469\(1982\)039<0818:MSLPIT>2.0.CO;2](https://doi.org/10.1175/1520-0469(1982)039<0818:MSLPIT>2.0.CO;2).
- Brown, R. A., 1970: A secondary flow model for the planetary boundary layer. *J. Atmos. Sci.*, **27**, 742–757, [https://doi.org/10.1175/1520-0469\(1970\)027<0742:ASFMT>2.0.CO;2](https://doi.org/10.1175/1520-0469(1970)027<0742:ASFMT>2.0.CO;2).
- , 1978: Similarity parameters from first-order closure. *Bound.-Layer Meteor.*, **14**, 381–396, <https://doi.org/10.1007/BF00121047>.
- Brown, A. R., and Coauthors, 2002: Large eddy simulation of the diurnal cycle of shallow cumulus convection over land. *Quart. J. Roy. Meteor. Soc.*, **128**, 1075–1093, <https://doi.org/10.1256/003590002320373210>.
- Brutsaert, W., 1982: *Evaporation into the Atmosphere: Theory, History, and Applications*. Springer, 302 pp.
- Budyko, M. I., 1956: The heat balance of the earth's surface. *Gidrometeoizdat*, **2**, 3–13, <https://doi.org/10.1080/00385417.1961.10770761>.
- Bunker, A., 1956: Measurements of counter-gradient heat flows in the atmosphere. *Aust. J. Phys.*, **9**, 133–143, <https://doi.org/10.1071/PH560133>.
- , B. Haurwitz, J. S. Malkus, and H. Stommel, 1949: Vertical distribution of temperature and humidity over the Caribbean Sea. *Papers in Physical Oceanography and Meteorology*, Vol. 11, No. 1, MIT/WHOI, 82 pp.
- Burk, S. D., and W. T. Thompson, 1989: A vertically nested regional numerical weather prediction model with second-order closure physics. *Mon. Wea. Rev.*, **117**, 2305–2324, [https://doi.org/10.1175/1520-0493\(1989\)117<2305:AVNRNW>2.0.CO;2](https://doi.org/10.1175/1520-0493(1989)117<2305:AVNRNW>2.0.CO;2).
- Burt, W. V., and E. M. Agee, 1977: Buoy and satellite observations of mesoscale cellular convection during AMTEX 75. *Bound.-Layer Meteor.*, **12**, 3–24, <https://doi.org/10.1007/BF00116395>.
- Busch, N. E., S. W. Chang, and R. A. Anthes, 1976: A multi-level model of the planetary boundary layer. *J. Appl. Meteor.*, **15**, 909–919, [https://doi.org/10.1175/1520-0450\(1976\)015<0909:AMLMOT>2.0.CO;2](https://doi.org/10.1175/1520-0450(1976)015<0909:AMLMOT>2.0.CO;2).
- Businger, J. A., 1955: On the structure of the atmospheric surface layer. *J. Meteor.*, **12**, 553–561, [https://doi.org/10.1175/1520-0469\(1955\)012<0553:OTSOTA>2.0.CO;2](https://doi.org/10.1175/1520-0469(1955)012<0553:OTSOTA>2.0.CO;2).
- , 1966: Transfer of momentum and heat in the planetary boundary layer. *Proc. Symp. Arctic Heat Budget and Atmospheric Circulation*, Lake Arrowhead, CA, Rand Corp., RM-5233-NSF, 305–322.

- , 1973: Turbulent transfer in the atmospheric surface layer. *Workshop on Micrometeorology*, D. A. Haugen, Ed., Amer. Meteor. Soc., 67–100.
- , and A. M. Yaglom, 1971: Introduction to Obukhov's paper on 'Turbulence in an atmosphere with a non-uniform temperature.' *Bound.-Layer Meteor.*, **2**, 3–6, <https://doi.org/10.1007/BF00718084>.
- , J. C. Wyngaard, Y. Izumi, and E. F. Bradley, 1971: Flux-profile relationships in the atmospheric surface layer. *J. Atmos. Sci.*, **28**, 181–189, [https://doi.org/10.1175/1520-0469\(1971\)028<0181:FPRTA>2.0.CO;2](https://doi.org/10.1175/1520-0469(1971)028<0181:FPRTA>2.0.CO;2).
- Cai, X. M., and A. K. Luhar, 2002: Fumigation of pollutants in and above the entrainment zone into a growing convective boundary layer: A large-eddy simulation. *Atmos. Environ.*, **36**, 2997–3008, [https://doi.org/10.1016/S1352-2310\(02\)00240-6](https://doi.org/10.1016/S1352-2310(02)00240-6).
- Calder, K. L., 1949: Eddy diffusion and evaporation in flow over aerodynamically smooth and rough surfaces: A treatment based on laboratory laws of turbulent flow with special reference to conditions in the lower atmosphere. *Quart. J. Mech. Appl. Math.*, **2**, 153–176, <https://doi.org/10.1093/qjmath/2.2.153>.
- Campbell, G. S., and J. M. Norman, 1998: *An Introduction to Environmental Biophysics*. Springer Verlag, 286 pp.
- Cancelli, D. M., M. Chamecki, and N. L. Dias, 2014: A large-eddy simulation study of scalar dissimilarity in the convective atmospheric boundary layer. *J. Atmos. Sci.*, **71**, 3–15, <https://doi.org/10.1175/JAS-D-13-0113.1>.
- Carruthers, D. J., D. R. J. Holroy, J. C. R. Hunt, W. S. Weng, A. G. Robins, D. D. Apsley, D. J. Thomson, and F. B. Smith, 1994: UK-ADMS—A new approach to modeling dispersion in the Earth's atmospheric boundary layer. *J. Wind Eng. Ind. Aerodyn.*, **52**, 139–153, [https://doi.org/10.1016/0167-6105\(94\)90044-2](https://doi.org/10.1016/0167-6105(94)90044-2).
- Cassiani, M., P. Franzese, and U. Giostra, 2005: A PDF micromixing model of dispersion for atmospheric flow. Part II: Application to the convective boundary layer. *Atmos. Environ.*, **39**, 1471–1479, <https://doi.org/10.1016/j.atmosenv.2004.11.019>.
- Castro, I. P., H. Cheng, and R. Reynolds, 2006: Turbulence over urban-type roughness: Deductions from wind-tunnel measurements. *Bound.-Layer Meteor.*, **118**, 109–131, <https://doi.org/10.1007/s10546-005-5747-7>.
- Caughey, S. J., B. A. Crease, and W. T. Roach, 1982: A field study of nocturnal stratocumulus: II. Turbulence structure and entrainment. *Quart. J. Roy. Meteor. Soc.*, **108**, 125–144, <https://doi.org/10.1002/qj.49710845508>.
- Cava, D., and G. G. Katul, 2008: Spectral short-circuiting and wake production within the canopy trunk space of an alpine hardwood forest. *Bound.-Layer Meteor.*, **126**, 415–431, <https://doi.org/10.1007/s10546-007-9246-x>.
- , U. Giostra, M. Siqueira, and G. Katul, 2004: Organised motion and radiative perturbations in the nocturnal canopy sublayer above an even-aged pine forest. *Bound.-Layer Meteor.*, **112**, 129–157, <https://doi.org/10.1023/B:BOUN.0000020160.28184.a0>.
- Chamberlain, A. C., 1966: Transfer of gases to and from grass and grass-like surfaces. *Proc. Roy. Soc. London*, **290A**, 236–265, <https://doi.org/10.1098/rspa.1966.0047>.
- Chamecki, M., C. Meneveau, and M. B. Parlange, 2009: Large eddy simulation of pollen transport in the atmospheric boundary layer. *J. Aerosol Sci.*, **40**, 241–255, <https://doi.org/10.1016/j.jaerosci.2008.11.004>.
- Changnon, S. A., 1981: *METROMEX: A Review and Summary*. Meteor. Monogr., No. 40, Amer. Meteor. Soc., 181 pp.
- Charnock, H., 1955: Wind stress on a water surface. *Quart. J. Roy. Meteor. Soc.*, **81**, 639–640, <https://doi.org/10.1002/qj.49708135027>.
- Chatwin, P. C., 1982: The use of statistics in describing and predicting the effects of dispersing gas clouds. *J. Hazard. Mater.*, **6**, 213–230, [https://doi.org/10.1016/0304-3894\(82\)80041-1](https://doi.org/10.1016/0304-3894(82)80041-1).
- Chen, F., and R. Avissar, 1994a: Impact of land-surface moisture variability on local shallow convective cumulus and precipitation in large-scale models. *J. Appl. Meteor.*, **33**, 1382–1401, [https://doi.org/10.1175/1520-0450\(1994\)033<1382:IOLSMV>2.0.CO;2](https://doi.org/10.1175/1520-0450(1994)033<1382:IOLSMV>2.0.CO;2).
- , and —, 1994b: The impact of land-surface wetness heterogeneity on mesoscale heat fluxes. *J. Appl. Meteor.*, **33**, 1323–1340, [https://doi.org/10.1175/1520-0450\(1994\)033<1323:TIOLSW>2.0.CO;2](https://doi.org/10.1175/1520-0450(1994)033<1323:TIOLSW>2.0.CO;2).
- , and J. Dudhia, 2001: Coupling an advanced land surface–hydrology model with the Penn State–NCAR MM5 modeling system. Part I: Model implementation and sensitivity. *Mon. Wea. Rev.*, **129**, 569–585, [https://doi.org/10.1175/1520-0493\(2001\)129<0569:CAALSH>2.0.CO;2](https://doi.org/10.1175/1520-0493(2001)129<0569:CAALSH>2.0.CO;2).
- , and Y. Zhang, 2009: On the coupling strength between the land surface and the atmosphere: From viewpoint of surface exchange coefficients. *Geophys. Res. Lett.*, **36**, L10404, <https://doi.org/10.1029/2009GL037980>.
- , Z. Janjić, and K. Mitchell, 1997: Impact of atmospheric surface-layer parameterizations in the new land-surface scheme of the NCEP mesoscale Eta model. *Bound.-Layer Meteor.*, **85**, 391–421, <https://doi.org/10.1023/A:1000531001463>.
- , and Coauthors, 2007: Description and evaluation of the characteristics of the NCAR high-resolution land data assimilation system. *J. Appl. Meteor. Climatol.*, **46**, 694–713, <https://doi.org/10.1175/JAM2463.1>.
- , and Coauthors, 2011: The integrated WRF/urban modelling system: Development, evaluation, and applications to urban environmental problems. *Int. J. Climatol.*, **31**, 273–288, <https://doi.org/10.1002/joc.2158>.
- Chen, S. S., W. Z. Hao, M. A. Donelan, and H. L. Tolman, 2013: Directional wind–wave coupling in fully coupled atmosphere–wave–ocean models: Results from CBLAST-Hurricane. *J. Atmos. Sci.*, **70**, 3198–3215, <https://doi.org/10.1175/JAS-D-12-0157.1>.
- Ching, J., R. Rotunno, M. LeMone, A. Martilli, B. Kosović, P. A. Jiménez, and J. Dudhia, 2014: Convectively induced secondary circulations in fine-grid mesoscale numerical prediction models. *Mon. Wea. Rev.*, **142**, 3284–3302, <https://doi.org/10.1175/MWR-D-13-00318.1>.
- Chow, F., R. L. Street, M. Xue, and J. Ferziger, 2005: Explicit filtering and reconstruction turbulence modeling for large-eddy simulation of neutral boundary layer flow. *J. Atmos. Sci.*, **62**, 2058–2077, <https://doi.org/10.1175/JAS3456.1>.
- Cimorelli, A. J., and Coauthors, 2005: AERMOD: A dispersion model for industrial source applications. Part I: General model formulation and boundary characterization. *J. Appl. Meteor.*, **44**, 682–693, <https://doi.org/10.1175/JAM2227.1>.
- Cionco, R. M., 1965: A mathematical model for air flow in a vegetative canopy. *J. Appl. Meteor.*, **4**, 517–522, [https://doi.org/10.1175/1520-0450\(1965\)004<0517:AMMFAF>2.0.CO;2](https://doi.org/10.1175/1520-0450(1965)004<0517:AMMFAF>2.0.CO;2).
- Clark, M. P., D. Kavetski, and F. Fenicia, 2011: Pursuing the method of multiple working hypotheses for hydrological modeling. *Water Resour. Res.*, **47**, W09301, <https://doi.org/10.1029/2010WR009827>.
- , and Coauthors, 2015: A unified approach to process-based hydrologic modeling: 1. Modeling concept. *Water Resour. Res.*, **51**, 2498–2514, <https://doi.org/10.1002/2015WR017198>.
- Clark, T. L., T. Hauf, and J. P. Kuettner, 1986: Convectively forced internal gravity waves: Results from two-dimensional experiments. *Quart. J. Roy. Meteor. Soc.*, **112**, 899–926, <https://doi.org/10.1002/qj.49711247402>.

- Clarke, J. R., A. J. Dyer, R. R. Brook, D. G. Reid, and A. J. Troup, 1971: The Wangara Experiment: Boundary layer data. CSIRO Division of Meteorological Physics Tech. Paper 19, 340 pp.
- Coccal, O., E. V. Goulart, S. Branford, T. G. Thomas, and S. E. Belcher, 2014: Flow structure and near-field dispersion in arrays of building-like structures. *J. Wind Eng. Ind. Aerodyn.*, **125**, 52–68, <https://doi.org/10.1016/j.jweia.2013.11.013>.
- Conangla, L., and J. Cuxart, 2006: On the turbulence in the upper part of the low-level jet: An experimental and numerical study. *Bound.-Layer Meteor.*, **118**, 379–400, <https://doi.org/10.1007/s10546-005-0608-y>.
- Conzemius, R. J., and E. Fedorovich, 2006a: Dynamics of sheared convective boundary layer entrainment. Part I: Methodological background and large-eddy simulation. *J. Atmos. Sci.*, **63**, 1151–1178, <https://doi.org/10.1175/JAS3691.1>.
- , and —, 2006b: Dynamics of sheared convective boundary layer entrainment. Part II: Evaluation of bulk model predictions of entrainment flux. *J. Atmos. Sci.*, **63**, 1179–1199, <https://doi.org/10.1175/JAS3696.1>.
- Cornford, C. E., 1938: Katabatic winds and the prevention of frost damage. *Quart. J. Roy. Meteor. Soc.*, **64**, 553–591, <https://doi.org/10.1002/qj.49706427702>.
- Cox, C. S., and W. H. Munk, 1954a: Statistics of the sea surface derived from sun glitter. *J. Mar. Res.*, **13**, 198–227.
- , and —, 1954b: Measurements of the roughness of the sea surface from photographs of the sun glitter. *J. Opt. Soc. Amer.*, **44**, 838–850, <https://doi.org/10.1364/JOSA.44.000838>.
- Crawford, K. C., and H. R. Hudson, 1970: Behavior of winds in the lower 1500 feet in Central Oklahoma: June 1966–May 1967. National Severe Storms Laboratory Tech. Memo. ERLTM-NSSL 48, 57 pp.
- Csanady, G. T., 1973: *Turbulent Diffusion in the Environment*. Reidel, 248 pp.
- Curry, J. A., 1986: Interactions among turbulence, radiation and microphysics in Arctic stratus clouds. *J. Atmos. Sci.*, **43**, 90–106, [https://doi.org/10.1175/1520-0469\(1986\)043<0090:IATRAM>2.0.CO;2](https://doi.org/10.1175/1520-0469(1986)043<0090:IATRAM>2.0.CO;2).
- , and G. F. Herman, 1985: Infrared properties of summertime Arctic stratus clouds. *J. Appl. Meteor. Climatol.*, **24**, 525–538, [https://doi.org/10.1175/1520-0450\(1985\)024<0525:IRPOSA>2.0.CO;2](https://doi.org/10.1175/1520-0450(1985)024<0525:IRPOSA>2.0.CO;2).
- , and Coauthors, 2000: FIRE Arctic Clouds Experiment. *Bull. Amer. Meteor. Soc.*, **81**, 5–30, [https://doi.org/10.1175/1520-0477\(2000\)081<0005:FACE>2.3.CO;2](https://doi.org/10.1175/1520-0477(2000)081<0005:FACE>2.3.CO;2).
- Cuxart, J., 2008: Nocturnal basin low-level jets: An integrated study. *Acta. Geophys.*, **56**, 100–113, <https://doi.org/10.2478/s11600-007-0042-2>.
- , P. Bougeault, and J.-L. Redelsperger, 2000: A turbulence scheme allowing for mesoscale and large-eddy simulations. *Quart. J. Roy. Meteor. Soc.*, **126**, 1–30, <https://doi.org/10.1002/qj.49712656202>.
- , and Coauthors, 2016: Estimation of the advection affects induced by heterogeneities in the surface energy budget. *Atmos. Chem. Phys.*, **16**, 9489–9504, <https://doi.org/10.5194/acp-16-9489-2016>.
- Das, S. K., and P. A. Durbin, 2005: A Lagrangian stochastic model for dispersion in stratified turbulence. *Phys. Fluids*, **17**, 025109, <https://doi.org/10.1063/1.1849184>.
- Davidson, M. J., K. R. Mylne, C. D. Jones, J. C. Phillips, R. J. Perkins, J. C. H. Fung, and J. C. R. Hunt, 1995: Plume dispersion through large groups of obstacles—A field investigation. *Atmos. Environ.*, **29**, 3245–3256, [https://doi.org/10.1016/1352-2310\(95\)00254-V](https://doi.org/10.1016/1352-2310(95)00254-V).
- Davidson, P. A., Y. Kaneda, K. Moffatt, and K. R. Sreenivasan, 2011: *A Voyage through Turbulence*. Cambridge University Press, 434 pp.
- Davis, K., P. S. Bakwin, C. Yi, B. W. Berger, C. Zhao, R. M. Teclaw, and J. G. Isebrands, 2003: The annual cycles of CO₂ and H₂O exchange over a northern mixed forest as observed from a very tall tower. *Global Change Biol.*, **9**, 1278–1293, <https://doi.org/10.1046/j.1365-2486.2003.00672.x>.
- Deacon, E. L., 1953: *Vertical Profiles of Mean Wind in the Surface Layers of the Atmosphere*. Geophysical Memoirs, Vol. 91, Met Office, 68 pp.
- , P. A. Sheppard, and E. K. Webb, 1956: Wind profiles over the sea and the drag at the sea surface. *Aust. J. Phys.*, **9**, 511–541, <https://doi.org/10.1071/PH560511>.
- Deardorff, J. W., 1966: The counter-gradient heat flux in the lower atmosphere and in the laboratory. *J. Atmos. Sci.*, **23**, 503–506, [https://doi.org/10.1175/1520-0469\(1966\)023<0503:TCGHFI>2.0.CO;2](https://doi.org/10.1175/1520-0469(1966)023<0503:TCGHFI>2.0.CO;2).
- , 1970a: Preliminary results from numerical integrations of the unstable planetary boundary layer. *J. Atmos. Sci.*, **27**, 1209–1211, [https://doi.org/10.1175/1520-0469\(1970\)027<1209:PRFNIO>2.0.CO;2](https://doi.org/10.1175/1520-0469(1970)027<1209:PRFNIO>2.0.CO;2).
- , 1970b: Convective velocity and temperature scales for the unstable boundary layer and for Rayleigh convection. *J. Atmos. Sci.*, **27**, 1211–1213, [https://doi.org/10.1175/1520-0469\(1970\)027<1211:CVATSF>2.0.CO;2](https://doi.org/10.1175/1520-0469(1970)027<1211:CVATSF>2.0.CO;2).
- , 1972a: Numerical investigation of neutral and unstable planetary boundary layers. *J. Atmos. Sci.*, **28**, 91–115, [https://doi.org/10.1175/1520-0469\(1972\)029<0091:NIONAU>2.0.CO;2](https://doi.org/10.1175/1520-0469(1972)029<0091:NIONAU>2.0.CO;2).
- , 1972b: Parameterization of the planetary boundary layer for use in general circulation models. *Mon. Wea. Rev.*, **100**, 93–106, [https://doi.org/10.1175/1520-0493\(1972\)100<0093:POTPBL>2.3.CO;2](https://doi.org/10.1175/1520-0493(1972)100<0093:POTPBL>2.3.CO;2).
- , 1973: Three-dimensional numerical modeling of the planetary boundary layer. *Workshop on Micrometeorology*, D. A. Haugen, Ed. Amer. Meteor. Soc., 271–305.
- , 1974a: Three-dimensional numerical study of the height and mean structure of a heated planetary boundary layer. *Bound.-Layer Meteor.*, **7**, 81–106, <https://doi.org/10.1007/BF00224974>.
- , 1974b: Three-dimensional numerical study of turbulence in an entraining mixed layer. *Bound.-Layer Meteor.*, **7**, 199–206, <https://doi.org/10.1007/BF00227913>.
- , 1978: Efficient prediction of ground surface temperature and moisture, with inclusion of a layer of vegetation. *J. Geophys. Res.*, **83**, 1889–1903, <https://doi.org/10.1029/JC083iC04p01889>.
- , 1980a: Stratocumulus-capped mixed layers derived from a three-dimensional model. *Bound.-Layer Meteor.*, **18**, 495–527, <https://doi.org/10.1007/BF00119502>.
- , 1980b: Cloud top entrainment instability. *J. Atmos. Sci.*, **37**, 131–147, [https://doi.org/10.1175/1520-0469\(1980\)037<0131:CTEI>2.0.CO;2](https://doi.org/10.1175/1520-0469(1980)037<0131:CTEI>2.0.CO;2).
- , and G. E. Willis, 1984: Groundlevel concentration fluctuations from a buoyant and a non-buoyant source within a laboratory convectively mixed layer. *Atmos. Environ.*, **18**, 1297–1309, [https://doi.org/10.1016/0004-6981\(84\)90039-8](https://doi.org/10.1016/0004-6981(84)90039-8).
- , —, and D. K. Lilly, 1969: Laboratory investigation of non-steady penetrative convection. *J. Fluid Mech.*, **35**, 7–31, <https://doi.org/10.1017/S0022112069000942>.
- DeCosmo, J., K. B. Katsaros, S. D. Smith, R. J. Anderson, W. A. Oost, K. Bumke, and H. Chadwick, 1996: Air-sea exchange of water vapor and sensible heat: The Humidity Exchange Over

- the Sea (HEXOS) results. *J. Geophys. Res.*, **101**, 12 001–12 016, <https://doi.org/10.1029/95JC03796>.
- Defant, A., 1932: Die Gezeiten und inneren Gezeitenwellen der Atlantischen Ozeans. German Atlantic Expedition *Meteor* 1925–1927, Wissenschaftliche Ergebnisse (Scientific Results), Vol. 7, Part 1, Walter de Gruyter, 318 pp.
- Delle Monache, L., J. Weil, M. Simpson, and M. Leach, 2009: A new urban boundary layer and dispersion parameterization for an emergency response modeling system: Tests with the Joint Urban 2003 data set. *Atmos. Environ.*, **43**, 5807–5821, <https://doi.org/10.1016/j.atmosenv.2009.07.051>.
- Denmead, O. T., and E. F. Bradley, 1985: Flux-gradient relationships in a forest canopy. *The Forest–Atmosphere Interaction*, B. A. Hutchison and B. B. Hicks, Eds., D. Reidel, 421–442, https://doi.org/10.1007/978-94-009-5305-5_27.
- Derbyshire, S. H., 1990: Nieuwstadt’s stable boundary layer revisited. *Quart. J. Roy. Meteor. Soc.*, **116**, 127–158, <https://doi.org/10.1002/qj.49711649106>.
- , 1999a: Boundary-layer decoupling over cold surfaces as a physical boundary instability. *Bound.-Layer Meteor.*, **90**, 297–325, <https://doi.org/10.1023/A:1001710014316>.
- , 1999b: Stable boundary layer modelling: Established approaches and beyond. *Bound.-Layer Meteor.*, **90**, 423–446, <https://doi.org/10.1023/A:1001749007836>.
- de Roode, S. R., P. G. Dunkerke, and H. J. J. Jonker, 2004: Large-eddy simulation: How large is large enough? *J. Atmos. Sci.*, **61**, 403–421, [https://doi.org/10.1175/1520-0469\(2004\)061<0403:LSHLIL>2.0.CO;2](https://doi.org/10.1175/1520-0469(2004)061<0403:LSHLIL>2.0.CO;2).
- de Vries, D. A., 1953: Some results of field determinations of the moisture content of soil from thermal conductivity measurements. *Neth. J. Agric. Sci.*, **1**, 115–121.
- Dias, N. L., and W. Brutsaert, 1996: Similarity of scalars under stable conditions. *Bound.-Layer Meteor.*, **80**, 355–373, <https://doi.org/10.1007/BF00119423>.
- Dickinson, R. E., 1984: Modeling evapotranspiration for three-dimensional global climate models. *Climate Processes and Climate Sensitivity*, *Geophys. Monogr.*, Vol. 29, Amer. Geophys. Union, 58–72.
- Dines, G., 1882: On difference of temperature with elevation. *Quart. J. Roy. Meteor. Soc.*, **8**, 189–197, <https://doi.org/10.1002/qj.4970084303>.
- Donelan, M. A., and M. Miyake, 1973: Spectra and fluxes in the boundary layer of the trade-wind zone. *J. Atmos. Sci.*, **30**, 444–464, [https://doi.org/10.1175/1520-0469\(1973\)030<0444:SAFITB>2.0.CO;2](https://doi.org/10.1175/1520-0469(1973)030<0444:SAFITB>2.0.CO;2).
- , and W. M. Drennan, 1995: Direct field measurements of the flux of carbon dioxide. *Air–Water Gas Transfer*, B. Jähne and E. C. Monahan, Eds., Aeon-Verlag, 677–683.
- , —, and K. B. Katsaros, 1997: The air–sea momentum flux conditions of wind sea and swell. *J. Phys. Oceanogr.*, **27**, 2087–2099, [https://doi.org/10.1175/1520-0485\(1997\)027<2087:TASMFI>2.0.CO;2](https://doi.org/10.1175/1520-0485(1997)027<2087:TASMFI>2.0.CO;2).
- , M. Curcic, S. S. Chen, and A. K. Magnusson, 2012: Modeling waves and wind stress. *J. Geophys. Res.*, **117**, C00J23, <https://doi.org/10.1029/2011JC007787>.
- Donlon, C., and Coauthors, 2007: The Global Ocean Data Assimilation Experiment High-resolution Sea Surface Temperature Pilot Project. *Bull. Amer. Meteor. Soc.*, **88**, 1197–1213, <https://doi.org/10.1175/BAMS-88-8-1197>.
- Dosio, A., and J. V.-G. de Arellano, 2006: Statistics of absolute and relative dispersion in the atmospheric convective boundary layer: A large-eddy simulation study. *J. Atmos. Sci.*, **63**, 1253–1272, <https://doi.org/10.1175/JAS3689.1>.
- , —, and A. A. M. Holtslag, 2003: Dispersion of a passive tracer in buoyancy- and shear-driven boundary layers. *J. Appl. Meteor.*, **42**, 1116–1130, [https://doi.org/10.1175/1520-0450\(2003\)042<1116:DOAPTI>2.0.CO;2](https://doi.org/10.1175/1520-0450(2003)042<1116:DOAPTI>2.0.CO;2).
- Douville, H., P. Viterbo, J. F. Mahfouf, and C. Beljaars, 2000: Evaluation of the optimum interpolation and nudging techniques for soil moisture analysis using FIFE data. *Mon. Wea. Rev.*, **128**, 1733–1756, [https://doi.org/10.1175/1520-0493\(2000\)128<1733:EOTOIA>2.0.CO;2](https://doi.org/10.1175/1520-0493(2000)128<1733:EOTOIA>2.0.CO;2).
- Drazin, P. G., and W. H. Reid, 1981: *Hydrodynamic Stability*. Cambridge University Press, 525 pp.
- Drennan, W. M., M. A. Donelan, N. Madsen, K. B. Katsaros, E. A. Terray, and C. N. Flagg, 1994: Directional wave spectra from a SWATH ship at sea. *J. Atmos. Oceanic Technol.*, **11**, 1109–1116, [https://doi.org/10.1175/1520-0426\(1994\)011<1109:DWSFAS>2.0.CO;2](https://doi.org/10.1175/1520-0426(1994)011<1109:DWSFAS>2.0.CO;2).
- , J. A. Zhang, J. R. French, C. McCormick, and P. G. Black, 2007: Turbulent fluxes in the hurricane boundary layer. Part II: Latent heat flux. *J. Atmos. Sci.*, **64**, 1103–1115, <https://doi.org/10.1175/JAS3889.1>.
- Driemel, A., B. Loose, H. Grobe, R. Sieger, and G. König-Langlo, 2016: 30 years of upper air soundings on board of R/V POLARSTERN. *Earth Syst. Sci. Data*, **8**, 213–220, <https://doi.org/10.5194/essd-8-213-2016>.
- Du, S., and A. Venkatram, 1997: A parameterization of vertical dispersion of ground-level releases. *J. Appl. Meteor.*, **36**, 1004–1015, [https://doi.org/10.1175/1520-0450\(1997\)036<1004:APOVDO>2.0.CO;2](https://doi.org/10.1175/1520-0450(1997)036<1004:APOVDO>2.0.CO;2).
- Du, Y., and R. Rotunno, 2014: A simple analytical model of the nocturnal low-level jet over the Great Plains of the United States. *J. Atmos. Sci.*, **71**, 3674–3683, <https://doi.org/10.1175/JAS-D-14-0060.1>.
- Dupont, S., and E. G. Patton, 2012a: Influence of stability and seasonal canopy changes on micrometeorology within and above an orchard canopy: The CHATS experiment. *Agric. For. Meteorol.*, **157**, 11–29, <https://doi.org/10.1016/j.agrformet.2012.01.011>.
- , and —, 2012b: Momentum and scalar transport within a vegetation canopy following atmospheric stability and seasonal canopy changes: The CHATS experiment. *Atmos. Chem. Phys.*, **12**, 5913–5935, <https://doi.org/10.5194/acp-12-5913-2012>.
- Edson, J., 2009: Sensors for micrometeorological and flux measurements. *A Derivative of Encyclopedia of Ocean Sciences: Measurement Technology, Sensors and Platform*, 2nd ed. J. H. Steele, S. A. Thorpe, and K. K. Turekian, Eds., Academic Press, 651 pp.
- , and Coauthors, 2007: The Coupled Boundary Layers and Air–Sea Transfer Experiment in low winds (CBLAST_Low). *Bull. Amer. Meteor. Soc.*, **88**, 341–356, <https://doi.org/10.1175/BAMS-88-3-341>.
- , and Coauthors, 2013: On the exchange of momentum over the open ocean. *J. Phys. Oceanogr.*, **43**, 1589–1610, <https://doi.org/10.1175/JPO-D-12-0173.1>.
- Edwards, J. M., 2009: Radiative processes in the stable boundary layer. Part I: Radiative aspects. *Bound.-Layer Meteor.*, **131**, 105–126, <https://doi.org/10.1007/s10546-009-9364-8>.
- Ekman, V. W., 1905: On the influence of Earth’s rotation on ocean currents. *Ark. Mat. Astron. Fys.*, **2**, 1–51.
- Engelmann, C., and C. Bernhofer, 2016: Exploring eddy-covariance measurements using a spatial approach: The eddy matrix. *Bound.-Layer Meteor.*, **161**, 1–17, <https://doi.org/10.1007/s10546-016-0161-x>.

- Entekhabi, D., and P. S. Eagleson, 1989: Land surface hydrology parameterization for atmospheric general circulation models including subgrid scale spatial variability. *J. Climate*, **2**, 816–831, [https://doi.org/10.1175/1520-0442\(1989\)002<0816:LSHPFA>2.0.CO;2](https://doi.org/10.1175/1520-0442(1989)002<0816:LSHPFA>2.0.CO;2).
- Esbensen, S., 1975: An analysis of subcloud-layer heat and moisture budgets in the western Atlantic trades. *J. Atmos. Sci.*, **32**, 1921–1933, [https://doi.org/10.1175/1520-0469\(1975\)032<1921:AAOSLH>2.0.CO;2](https://doi.org/10.1175/1520-0469(1975)032<1921:AAOSLH>2.0.CO;2).
- Fackrell, J. E., and A. G. Robins, 1982: Concentration fluctuations and fluxes in plumes from point sources in a turbulent boundary layer. *J. Fluid Mech.*, **117**, 1–26, <https://doi.org/10.1017/S0022112082001499>.
- Fairall, C. W., E. F. Bradley, D. P. Rogers, J. B. Edson, and G. S. Young, 1996: Bulk parameterizations of air-sea fluxes for Tropical Ocean-Global Atmosphere Coupled-Ocean Atmosphere Response Experiment. *J. Geophys. Res.*, **101**, 3747–3764, <https://doi.org/10.1029/95JC03205>.
- , A. B. White, J. B. Edson, and J. E. Hare, 1997: Integrated shipboard measurements of the marine boundary layer. *J. Atmos. Oceanic Technol.*, **14**, 338–35, [https://doi.org/10.1175/1520-0426\(1997\)014<0338:ISMOTM>2.0.CO;2](https://doi.org/10.1175/1520-0426(1997)014<0338:ISMOTM>2.0.CO;2).
- , E. F. Bradley, J. E. Hare, A. A. Grachev, and J. B. Edson, 2003: Bulk parameterization of air-sea fluxes and verification for the COARE algorithm. *J. Climate*, **16**, 571–591, [https://doi.org/10.1175/1520-0442\(2003\)016<0571:BPOASF>2.0.CO;2](https://doi.org/10.1175/1520-0442(2003)016<0571:BPOASF>2.0.CO;2).
- Faller, A. J., 1963: An experimental study of the instability of the laminar Ekman boundary layer. *J. Fluid Mech.*, **15**, 560–576, <https://doi.org/10.1017/S0022112063000458>.
- , and R. E. Kaylor, 1966: A numerical study of the laminar Ekman layer. *J. Atmos. Sci.*, **23**, 466–480, [https://doi.org/10.1175/1520-0469\(1966\)023<0466:ANSOTI>2.0.CO;2](https://doi.org/10.1175/1520-0469(1966)023<0466:ANSOTI>2.0.CO;2).
- Faloona, I., and Coauthors, 2005: Observations of entrainment in eastern Pacific stratocumulus using three conserved scalars. *J. Atmos. Sci.*, **62**, 3268–3285, <https://doi.org/10.1175/JAS3541.1>.
- Fazu, C., and P. Schwerdtfeger, 1989: Flux-gradient relationships for momentum and heat over a rough natural surface. *Quart. J. Roy. Meteor. Soc.*, **115**, 335–352, <https://doi.org/10.1002/qj.49711548607>.
- Fedorovich, E., J. Gibbs, and A. Shapiro, 2017: Numerical study of idealized nocturnal low-level jets over gently sloping terrain. *J. Atmos. Sci.*, **74**, 2813–2834, <https://doi.org/10.1175/JAS-D-17-0013.1>.
- Fernando, H. J. S., 2010: Fluid dynamics of urban atmospheres in complex terrain. *Annu. Rev. Fluid Mech.*, **42**, 365–389, <https://doi.org/10.1146/annurev-fluid-121108-145459>.
- Fiebrich, C. A., and K. C. Crawford, 2001: The impact of unique meteorological phenomena detected by the Oklahoma Mesonet and ARS Micronet on Automated Quality Control. *Bull. Amer. Meteor. Soc.*, **82**, 2173–2187, [https://doi.org/10.1175/1520-0477\(2001\)082<2173:TIOUMP>2.3.CO;2](https://doi.org/10.1175/1520-0477(2001)082<2173:TIOUMP>2.3.CO;2).
- Fiedler, F., and H. A. Panofsky, 1972: The geostrophic drag and the ‘effective’ roughness length. *Quart. J. Roy. Meteor. Soc.*, **98**, 213–220, <https://doi.org/10.1002/qj.49709841519>.
- Field, P. R., and Coauthors, 2017: Exploring the convective grey zone with regional simulations of a cold air outbreak. *Quart. J. Roy. Meteor. Soc.*, **143**, 2537–2555, <https://doi.org/10.1002/qj.3105>.
- Findikakis, A. N., and R. L. Street, 1979: An algebraic model for sub-grid-scale turbulence in stratified flow. *J. Atmos. Sci.*, **36**, 1934–1949, [https://doi.org/10.1175/1520-0469\(1979\)036<1934:AAMFSS>2.0.CO;2](https://doi.org/10.1175/1520-0469(1979)036<1934:AAMFSS>2.0.CO;2).
- Finnigan, J. J., 1979: Turbulence in waving wheat. I. Mean statistics and honami. *Bound.-Layer Meteor.*, **16**, 181–211.
- , 1985: Turbulent transport in flexible plant canopies. *The Forest-Atmosphere Interaction*, B. A. Hutchison and B. B. Hicks, Eds., D. Reidel, 443–480, https://doi.org/10.1007/978-94-009-5305-5_28.
- , 2000: Turbulence in plant canopies. *Annu. Rev. Fluid Mech.*, **32**, 519–571, <https://doi.org/10.1146/annurev.fluid.32.1.519>.
- , and R. H. Shaw, 2000: A wind-tunnel study of airflow in waving wheat: an EOF analysis of the structure of the large-eddy motion. *Bound.-Layer Meteor.*, **96**, 211–255, <https://doi.org/10.1023/A:1002618621171>.
- , R. Clement, Y. Malhi, R. Leuning, and H. A. Cleugh, 2003: A re-evaluation of long-term flux measurement techniques. Part I: Averaging and coordinate rotation. *Bound.-Layer Meteor.*, **107**, 1–48, <https://doi.org/10.1023/A:1021554900225>.
- , R. H. Shaw, and E. G. Patton, 2009: Turbulence structure above a vegetation canopy. *J. Fluid Mech.*, **637**, 387–424, <https://doi.org/10.1017/S0022112009990589>.
- Fitzmaurice, L., R. H. Shaw, K. T. Paw U, and E. G. Patton, 2004: Three-dimensional scalar microfront systems in a large-eddy simulation of vegetation canopy flow. *Bound.-Layer Meteor.*, **112**, 107–127, <https://doi.org/10.1023/B:BOUN.0000020159.98239.4a>.
- Fleagle, R. G., and J. A. Businger, 1963: *An Introduction to Atmospheric Physics*. Academic Press, 346 pp.
- Flesch, T. K., J. D. Wilson, and E. Yee, 1995: Backward-time Lagrangian stochastic models and their application to estimate gaseous emissions. *J. Appl. Meteor.*, **34**, 1320–1332, [https://doi.org/10.1175/1520-0450\(1995\)034<1320:BTLSDM>2.0.CO;2](https://doi.org/10.1175/1520-0450(1995)034<1320:BTLSDM>2.0.CO;2).
- Flores, O., and J. Riley, 2011: Analysis of turbulence collapse in the stably stratified surface layer using direct numerical simulation. *Bound.-Layer Meteor.*, **139**, 241–259, <https://doi.org/10.1007/s10546-011-9588-2>.
- Foken, T., 2006: 50 years of the Monin–Obukhov similarity theory. *Bound.-Layer Meteor.*, **119**, 431–447, <https://doi.org/10.1007/s10546-006-9048-6>.
- , and S. P. Oncley, 1995: Results of the workshop “Instrumental and methodical problems of land surface flux measurements.” *Bull. Amer. Meteor. Soc.*, **76**, 1191–1193, <https://doi.org/10.1175/1520-0477-76.7.1191>.
- Fox, D. G., and D. K. Lilly, 1972: Numerical simulation of turbulent flows. *Rev. Geophys. Space Phys.*, **10**, 51–72, <https://doi.org/10.1029/RG010i001p00051>.
- Frank, J. M., W. J. Massman, E. Swiatek, H. Zimmerman, and B. E. Ewers, 2016: All sonic anemometers need to correct for transducer and structural shading in their velocity measurements. *J. Atmos. Oceanic Technol.*, **33**, 149–167, <https://doi.org/10.1175/JTECH-D-15-0171.1>.
- Frankenberger, E., 1955: Über vertikale Temperatur-, Fuchte- und Windgradienten in den untersten 7 Dekametern der Atmosphäre, den Vertikalaustausch und den Wärmehaushalt an Wiesenboden bei Quickborn/Holstein 1953/4. *Berichte des Deutschen Wetterdienstes* 3, No. 20, 40 pp., https://www.dwd.de/DE/leistungen/pfbf_verlag_berichte/pdf_einzelbaende/20_pdf.pdf?__blob=publicationFile&v=3.
- Franzese, P., 2003: Lagrangian stochastic modelling of a fluctuating plume in the convective boundary layer. *Atmos. Environ.*, **37**, 1691–1701, [https://doi.org/10.1016/S1352-2310\(03\)00003-7](https://doi.org/10.1016/S1352-2310(03)00003-7).
- Frisch, A. S., C. W. Fairall, and J. B. Snider, 1995: Measurements of stratus cloud and drizzle parameters in ASTEX with a K_z -band Doppler radar and a microwave radiometer.

- J. Atmos. Sci.*, **52**, 2788–2799, [https://doi.org/10.1175/1520-0469\(1995\)052<2788:MOSCAD>2.0.CO;2](https://doi.org/10.1175/1520-0469(1995)052<2788:MOSCAD>2.0.CO;2).
- Gao, W., R. H. Shaw, and K. T. Paw U, 1989: Observation of organized structure in turbulent flow within and above a forest canopy. *Bound.-Layer Meteor.*, **47**, 349–377, <https://doi.org/10.1007/BF00122339>.
- Garcia, J. R., and J. P. Mellado, 2014: The two-layer structure of the entrainment zone in the convective boundary layer. *J. Atmos. Sci.*, **71**, 1935–1955, <https://doi.org/10.1175/JAS-D-13-0148.1>.
- Garcia-Carreras, L., and Coauthors, 2015: The turbulent structure and diurnal growth of the Saharan atmospheric boundary layer. *J. Atmos. Sci.*, **72**, 693–713, <https://doi.org/10.1175/JAS-D-13-0384.1>.
- Garratt, J. R., 1990: The internal boundary layer—A review. *Bound.-Layer Meteor.*, **50**, 171–203, <https://doi.org/10.1007/BF00120524>.
- , 1992: *The Atmospheric Boundary Layer*. Cambridge Atmospheric and Space Science Series, Cambridge University Press, 316 pp.
- Gascard, J.-C., and Coauthors, 2008: Exploring Arctic transpolar drift during dramatic sea ice retreat. *Eos, Trans. Amer. Geophys. Union*, **89**, 21–22, <https://doi.org/10.1029/2008EO030001>.
- , T. Vihma, and R. Döscher, 2015: General introduction to the DAMOCLES special issue. *Atmos. Chem. Phys.*, **15**, 5377–5379, <https://doi.org/10.5194/acp-15-5377-2015>.
- Geernaert, G. L., K. B. Katsaros, and K. Richter, 1986: Variation of the drag coefficient and its dependence on sea state. *J. Geophys. Res.*, **91**, 7667–7679, <https://doi.org/10.1029/JC091iC06p07667>.
- Geerts, B., and Q. Miao, 2005: A simple numerical model of the flight behavior of small insects in the atmospheric convective boundary layer. *Environ. Entomol.*, **34**, 353–360, <https://doi.org/10.1603/0046-225X-34.2.353>.
- Geiger, R., 1966: *The Climate near the Ground*. Rev. ed. Harvard University Press, 611 pp.
- Geiss, A., and L. Mahrt, 2015: Decomposition of spatial structure of nocturnal flow over gentle terrain. *Bound.-Layer Meteor.*, **156**, 337–347, <https://doi.org/10.1007/s10546-015-0043-7>.
- Germano, M., 1986: A proposal for a redefinition of the turbulent stresses in the filtered Navier-Stokes equations. *Phys. Fluids*, **29**, 2323–2324, <https://doi.org/10.1063/1.865568>.
- , U. Piomelli, P. Moin, and W. H. Cabot, 1991: A dynamic subgrid-scale eddy viscosity model. *Phys. Fluids*, **3A**, 1760–1765, <https://doi.org/10.1063/1.857955>.
- GEWEX Cloud System Science Team, 1993: The GEWEX Cloud System Study. *Bull. Amer. Meteor. Soc.*, **74**, 387–399, [https://doi.org/10.1175/1520-0477\(1993\)074<0387:TGCSS>2.0.CO;2](https://doi.org/10.1175/1520-0477(1993)074<0387:TGCSS>2.0.CO;2).
- Gifford, F. A., 1959: Statistical properties of a fluctuating plume dispersion model. *Advances in Geophysics*, Vol. 6, Academic Press, 117–138.
- , 1962: Diffusion in the diabatic surface layer. *J. Geophys. Res.*, **67**, 3207–3212, <https://doi.org/10.1029/JZ067i008p03207>.
- Giometto, M., A. Christen, C. Meneveau, J. Fang, M. Krafczyk, and M. Parlange, 2016: Spatial characteristics of roughness sublayer mean flow and turbulence over a realistic urban surface. *Bound.-Layer Meteor.*, **160**, 425–452, <https://doi.org/10.1007/s10546-016-0157-6>.
- Glendening, J. W., 1996: Lineal eddy features under strong shear conditions. *J. Atmos. Sci.*, **53**, 3430–3449, [https://doi.org/10.1175/1520-0469\(1996\)053<3430:LEFUSS>2.0.CO;2](https://doi.org/10.1175/1520-0469(1996)053<3430:LEFUSS>2.0.CO;2).
- Gochis, D. J., W. Yu, and D. N. Yates, 2013: The WRF-Hydro Model technical description and user's guide, version 1.0. NCAR Tech. Doc., 120 pp., http://www.ral.ucar.edu/projects/wrf_hydro/.
- Golaz, J.-C., V. E. Larson, and W. R. Cotton, 2002: A PDF based model for boundary layer clouds. Part I: Method and model description. *J. Atmos. Sci.*, **59**, 3540–3551, [https://doi.org/10.1175/1520-0469\(2002\)059<3540:APBMFB>2.0.CO;2](https://doi.org/10.1175/1520-0469(2002)059<3540:APBMFB>2.0.CO;2).
- Goldstein, S., 1969: Fluid mechanics in the first half of this century. *Annu. Rev. Fluid Mech.*, **1**, 1–29, <https://doi.org/10.1146/annurev.fl.01.010169.000245>.
- Grachev, A., and C. W. Fairall, 2001: Upward momentum transfer in the marine boundary layer. *J. Phys. Oceanogr.*, **31**, 1698–1711, [https://doi.org/10.1175/1520-0485\(2001\)031<1698:UMTITM>2.0.CO;2](https://doi.org/10.1175/1520-0485(2001)031<1698:UMTITM>2.0.CO;2).
- , C. W. Fairall, P. Persson, E. Andreas, and P. Guest, 2005: Stable boundary-layer scaling regimes: The SHEBA data. *Bound.-Layer Meteor.*, **116**, 201–235, <https://doi.org/10.1007/s10546-004-2729-0>.
- , E. Andreas, C. Fairall, P. Guest, and P. Persson, 2007: On the turbulent Prandtl number in the stable atmospheric boundary layer. *Bound.-Layer Meteor.*, **125**, 329–341, <https://doi.org/10.1007/s10546-007-9192-7>.
- , —, C. Fairall, P. Guest, and P. Persson, 2013: The critical Richardson number and limits of applicability of local similarity theory in the stable boundary layer. *Bound.-Layer Meteor.*, **147**, 51–82, <https://doi.org/10.1007/s10546-012-9771-0>.
- Grant, A. L. M., 1997: An observational study of the evening transition boundary layer. *Quart. J. Roy. Meteor. Soc.*, **123**, 657–677, <https://doi.org/10.1002/qj.49712353907>.
- Grimsdell, A. W., and W. M. Angevine, 2002: Observations of the afternoon transition of the convective boundary layer. *J. Appl. Meteor.*, **41**, 3–11, [https://doi.org/10.1175/1520-0450\(2002\)041<0003:OOTATO>2.0.CO;2](https://doi.org/10.1175/1520-0450(2002)041<0003:OOTATO>2.0.CO;2).
- Grisogono, B., L. Kraljević, and J. Jericević, 2007: The low-level katabatic jet height versus Monin–Obukhov height. *Quart. J. Roy. Meteor. Soc.*, **133**, 2133–2136, <https://doi.org/10.1002/qj.190>.
- Gryning, S. E., A. P. van Ulden, and S. Larsen, 1983: Dispersion from a continuous ground-level source investigated by a *K* model. *Quart. J. Roy. Meteor. Soc.*, **109**, 355–364, <https://doi.org/10.1002/qj.49710946008>.
- Hahn, C. J., and S. G. Warren, 1999: Extended edited cloud reports from ships and land stations over the globe, 1952–1996. Numerical Data Package NDP-026C, Carbon Dioxide Information Analysis Center, Department of Energy, 79 pp., <http://cdiac.ess-dive.lbl.gov/ftp/ndp026c/ndp026c.pdf>.
- Han, J., M. L. Witek, J. Teixeira, R.-Y. Sun, H.-L. Pan, J. K. Fletcher, and C. S. Bretherton, 2016: Implementation in the NCEP GFS of a hybrid eddy-diffusivity mass-flux (EDMF) boundary layer parameterization with dissipative heating and modified stable boundary layer mixing. *Wea. Forecasting*, **31**, 341–352, <https://doi.org/10.1175/WAF-D-15-0053.1>.
- Hanna, S. R., and R. J. Paine, 1989: Hybrid plume dispersion model (HPDM) development and evaluation. *J. Appl. Meteor.*, **28**, 206–224, [https://doi.org/10.1175/1520-0450\(1989\)028<0206:HPDMA>2.0.CO;2](https://doi.org/10.1175/1520-0450(1989)028<0206:HPDMA>2.0.CO;2).
- , J. White, and Y. Zhou, 2007: Observed winds, turbulence, and dispersion in built-up downtown areas of Oklahoma City and Manhattan. *Bound.-Layer Meteor.*, **125**, 441–468, <https://doi.org/10.1007/s10546-007-9197-2>.

- Hansch, T. W., S. Leschiutta, and A. J. Wallard, Eds., 2006: Meteorology and Fundamental Constants, Course CLXVI. IOS Press, 649 pp.
- Hardy, K. R., and H. Ottersten, 1969: Radar investigations of convective patterns in the clear atmosphere. *J. Atmos. Sci.*, **26**, 666–672, [https://doi.org/10.1175/1520-0469\(1969\)26<666:RIOCP1>2.0.CO;2](https://doi.org/10.1175/1520-0469(1969)26<666:RIOCP1>2.0.CO;2).
- Harman, I. N., and J. J. Finnigan, 2007: A simple unified theory for flow in the canopy and roughness sublayer. *Bound.-Layer Meteor.*, **123**, 339–363, <https://doi.org/10.1007/s10546-006-9145-6>.
- , and —, 2008: Scalar concentration profiles in the canopy and roughness sublayer. *Bound.-Layer Meteor.*, **129**, 323–351, <https://doi.org/10.1007/s10546-008-9328-4>.
- Harris, D. L., 1966: The wave-driven wind. *J. Atmos. Sci.*, **23**, 688–693, [https://doi.org/10.1175/1520-0469\(1966\)023<0688:TWDW>2.0.CO;2](https://doi.org/10.1175/1520-0469(1966)023<0688:TWDW>2.0.CO;2).
- Hartmann, J., C. Kottmeier, and C. Wamser, 1992: *Radiation and Eddy Flux Experiment 1991 (REFLEX I)*. Reports on Polar Research, Vol. 105, Alfred Wegener Institute, 72 pp.
- , and Coauthors, 1999: *Arctic Radiation and Turbulence Interaction Study*. Reports on Polar Research, Vol. 305, Alfred Wegener Institute, 81 pp.
- Hasselmann, K., and Coauthors, 1973: Measurements of wind-wave growth and swell decay during the Joint North Sea Wave Project (JONSWAP). *Dtsch. Hydrogr. Z.*, **12A**, 95 pp.
- Hatlee, S. C., and J. C. Wyngaard, 2007: Improved subfilter-scale models from the HATS field data. *J. Atmos. Sci.*, **64**, 1694–1705, <https://doi.org/10.1175/JAS3909.1>.
- Haugen, D. A., J. C. Kaimal, and E. F. Bradley, 1971: An experimental study of Reynolds stress and heat flux in the atmospheric surface layer. *Quart. J. Roy. Meteor. Soc.*, **97**, 168–180, <https://doi.org/10.1002/qj.49709741204>.
- Haupt, S. E., S. Hanna, M. Askelson, M. Shepherd, M. A. Fragomeni, N. Debbage, and B. Johnson, 2019: Progress in applied meteorology. Part II: Applications that address growing populations. *A Century of Progress in Atmospheric and Related Sciences: Celebrating the American Meteorological Society Centennial*, Meteor. Monogr., No. 59, Amer. Meteor. Soc., <https://doi.org/10.1175/AMSMONOGRAPHS-D-18-0007.1>.
- Haus, B. K., L. K. Shay, P. A. Work, G. Voulgaris, R. J. Ramos, and J. Martinez-Pedraja, 2010: Wind speed dependence of single-site wave-height retrievals from high-frequency radars. *J. Atmos. Oceanic Technol.*, **27**, 1381–1394, <https://doi.org/10.1175/2010JTECH0730.1>.
- Hechtel, L. M., C.-H. Moeng, and R. B. Stull, 1990: The effects of nonhomogeneous surface fluxes on the convective boundary layer: A case study using large-eddy simulation. *J. Atmos. Sci.*, **47**, 1721–1741, [https://doi.org/10.1175/1520-0469\(1990\)047<1721:TEONSF>2.0.CO;2](https://doi.org/10.1175/1520-0469(1990)047<1721:TEONSF>2.0.CO;2).
- Heist, D. K., L. A. Brixey, J. Richmond-Bryant, G. E. Bowker, S. G. Perry, and R. W. Wiener, 2009: The effect of a tall tower on flow and dispersion through a model urban neighborhood, Part 1. Flow characteristics. *J. Environ. Monit.*, **11**, 2163–2170, <https://doi.org/10.1039/b907135k>.
- Held, A., I. M. Brooks, C. Leck, and M. Tjernström, 2011: On the potential contribution of open lead particle emissions to the central Arctic aerosol concentration. *Atmos. Chem. Phys.*, **11**, 3093–3105, <https://doi.org/10.5194/acp-11-3093-2011>.
- Helgans, B., and D. H. Richter, 2016: Turbulent latent and sensible heat transfer in the presence of evaporative droplets. *Int. J. Multiphase Flow*, **78**, <https://doi.org/10.1016/j.ijmultiphaseflow.2015.09.010>.
- Henderson-Sellers, A., Z. L. Yang, and R. E. Dickinson, 1993: The project for intercomparison of land-surface parameterization schemes. *Bull. Amer. Meteor. Soc.*, **74**, 1335–1349, [https://doi.org/10.1175/1520-0477\(1993\)074<1335:TPFIOL>2.0.CO;2](https://doi.org/10.1175/1520-0477(1993)074<1335:TPFIOL>2.0.CO;2).
- Henn, D. S., and R. I. Sykes, 1992: Large-eddy simulation of dispersion in the convective boundary layer. *Atmos. Environ.*, **26A**, 3145–3159, [https://doi.org/10.1016/0960-1686\(92\)90471-V](https://doi.org/10.1016/0960-1686(92)90471-V).
- Herman, G. F., 1977: Solar radiation in summertime Arctic stratus clouds. *J. Atmos. Sci.*, **34**, 1423–1432, [https://doi.org/10.1175/1520-0469\(1977\)034<1423:SRISAS>2.0.CO;2](https://doi.org/10.1175/1520-0469(1977)034<1423:SRISAS>2.0.CO;2).
- , and R. Goody, 1976: Formation and persistence of summertime Arctic stratus clouds. *J. Atmos. Sci.*, **33**, 1537–1553, [https://doi.org/10.1175/1520-0469\(1976\)033<1537:FAPOSA>2.0.CO;2](https://doi.org/10.1175/1520-0469(1976)033<1537:FAPOSA>2.0.CO;2).
- Heus, T., and Coauthors, 2010: Formulation of the Dutch Atmospheric Large-Eddy Simulation (DALES) and overview of its applications. *Geosci. Model Dev.*, **3**, 415–444, <https://doi.org/10.5194/gmd-3-415-2010>.
- Heusinkveld, B. G., A. F. G. Jacobs, A. A. M. Holtslag, and S. M. Berkowicz, 2004: Surface energy balance closure in an arid region. *Agric. For. Meteorol.*, **122**, 21–37, <https://doi.org/10.1016/j.agrformet.2003.09.005>.
- Hicks, B., 1978: Some limitations of dimensional analysis and power laws. *Bound.-Layer Meteorol.*, **14**, 567–569, <https://doi.org/10.1007/BF00121895>.
- Higgins, C. W., M. B. Parlange, and C. Meneveau, 2003: Alignment trends of velocity gradients and subgrid-scale fluxes in the turbulent atmospheric boundary layer. *Bound.-Layer Meteorol.*, **109**, 59–83, <https://doi.org/10.1023/A:1025484500899>.
- , —, and —, 2004: The heat flux and the temperature gradient in the lower atmosphere. *Geophys. Res. Lett.*, **31**, L22105, <https://doi.org/10.1029/2004GL020053>.
- Hilst, G. R., and C. I. Simpson, 1958: Observations of vertical diffusion rates in stable atmospheres. *J. Meteorol.*, **15**, 125–126, [https://doi.org/10.1175/1520-0469\(1958\)015<0125:OOVDRI>2.0.CO;2](https://doi.org/10.1175/1520-0469(1958)015<0125:OOVDRI>2.0.CO;2).
- Hodur, R., 1997: The Naval Research Laboratory's Coupled Ocean/Atmosphere Mesoscale Prediction System (COAMPS). *Mon. Wea. Rev.*, **125**, 1414–1430, [https://doi.org/10.1175/1520-0493\(1997\)125<1414:TNRLSC>2.0.CO;2](https://doi.org/10.1175/1520-0493(1997)125<1414:TNRLSC>2.0.CO;2).
- Högström, U., 1988: Non-dimensional wind and temperature profiles in the atmospheric surface layer: A re-evaluation. *Bound.-Layer Meteorol.*, **42**, 55–78, <https://doi.org/10.1007/BF00119875>.
- , 1996: Review of some basic characteristics of the atmospheric surface layer. *Bound.-Layer Meteorol.*, **78**, 215–246, <https://doi.org/10.1007/BF00120937>.
- Holland, J. Z., and E. M. Rasmusson, 1973: Measurements of the atmospheric mass, moisture and momentum budgets over a 500-kilometer square of tropical ocean. *Mon. Wea. Rev.*, **101**, 44–55, [https://doi.org/10.1175/1520-0493\(1973\)101<0044:MOTAME>2.3.CO;2](https://doi.org/10.1175/1520-0493(1973)101<0044:MOTAME>2.3.CO;2).
- Holton, J. R., 1967: The diurnal boundary layer wind oscillation above sloping terrain. *Tellus*, **19A**, 199–205, <https://doi.org/10.1111/j.2153-3490.1967.tb01473.x>.
- Holtslag, A. A. M., and Coauthors, 2013: Stable atmospheric boundary layers and diurnal cycles: Challenges for weather and climate models. *Bull. Amer. Meteor. Soc.*, **94**, 1691–1706, <https://doi.org/10.1175/BAMS-D-11-00187.1>.
- , and B. A. Boville, 1993: Local versus nonlocal boundary-layer diffusion in a global climate model. *J. Climate*, **6**, 1825–1842, [https://doi.org/10.1175/1520-0442\(1993\)006<1825:LVNBLD>2.0.CO;2](https://doi.org/10.1175/1520-0442(1993)006<1825:LVNBLD>2.0.CO;2).

- Homén, T., 1897: Der tägliche Wärmeumsatz im Boden und die Wärmestralung zwischen Himmel und Erde. Societatus Scientiarum Fennicae Special Publ. Vol. 23, No. 3, Wilhelm Engelmann, 148 pp.
- Hong, S.-Y., and H.-L. Pan, 1996: Nonlocal boundary layer vertical diffusion in a medium-range forecast model. *Mon. Wea. Rev.*, **124**, 2322–2339, [https://doi.org/10.1175/1520-0493\(1996\)124<2322:NBLVDI>2.0.CO;2](https://doi.org/10.1175/1520-0493(1996)124<2322:NBLVDI>2.0.CO;2).
- , Y. Noh, and J. Dudhia, 2006: A new vertical diffusion package with an explicit treatment of entrainment processes. *Mon. Wea. Rev.*, **134**, 2318–2341, <https://doi.org/10.1175/MWR3199.1>.
- Honnert, R., V. Masson, and F. Couvreur, 2011: A diagnostic for evaluating the representation of turbulence in atmospheric models at kilometeric scale. *J. Atmos. Sci.*, **68**, 3112–3131, <https://doi.org/10.1175/JAS-D-11-061.1>.
- Horst, T. W., 1979: Lagrangian similarity modeling of vertical diffusion from a ground-level source. *J. Appl. Meteor.*, **18**, 733–740, [https://doi.org/10.1175/1520-0450\(1979\)018<0733:LSMOVD>2.0.CO;2](https://doi.org/10.1175/1520-0450(1979)018<0733:LSMOVD>2.0.CO;2).
- , and J. C. Doran, 1988: The turbulence structure of nocturnal slope flow. *J. Atmos. Sci.*, **45**, 605–616, [https://doi.org/10.1175/1520-0469\(1988\)045<0605:TTSONS>2.0.CO;2](https://doi.org/10.1175/1520-0469(1988)045<0605:TTSONS>2.0.CO;2).
- , and J. C. Weil, 1992: Footprint estimation for scalar flux measurements in the atmospheric surface layer. *Bound.-Layer Meteor.*, **59**, 279–296, <https://doi.org/10.1007/BF00119817>.
- , J. Kleissl, D. H. Lenschow, C. Meneveau, C.-H. Moeng, M. B. Parlange, P. P. Sullivan, and J. C. Weil, 2004: HATS: Field observations to obtain spatially filtered turbulence fields from crosswind arrays of sonic anemometers in the atmospheric surface layer. *J. Atmos. Sci.*, **61**, 1566–1581, [https://doi.org/10.1175/1520-0469\(2004\)061<1566:HFOTOS>2.0.CO;2](https://doi.org/10.1175/1520-0469(2004)061<1566:HFOTOS>2.0.CO;2).
- , S. R. Semmer, and G. Maclean, 2015: Correction of a non-orthogonal, three-component sonic anemometer for flow distortion by transducer shadowing. *Bound.-Layer Meteor.*, **155**, 371–395, <https://doi.org/10.1007/s10546-015-0010-3>.
- Hristov, T. S., S. D. Miller, and C. A. Friehe, 2003: Dynamic coupling of wind and ocean waves through wave-induced air flow. *Nature*, **422**, 55–58, <https://doi.org/10.1038/nature01382>.
- Huang, J., and E. Bou-Zeid, 2013: Turbulence and vertical fluxes in the stable atmospheric boundary layer. Part I: A large-eddy simulation study. *J. Atmos. Sci.*, **70**, 1513–1527, <https://doi.org/10.1175/JAS-D-12-0167.1>.
- Intrieri, J. M., M. D. Shupe, T. Uttal, and B. J. McCarty, 2002a: An annual cycle of Arctic cloud characteristics observed by radar and lidar at SHEBA. *J. Geophys. Res.*, **107**, 8030, <https://doi.org/10.1029/2000JC000423>.
- , C. W. Fairall, M. D. Shupe, P. O. G. Persson, E. L. Andreas, P. S. Guest, and R. E. Moritz, 2002b: An annual cycle of Arctic surface cloud forcing at SHEBA. *J. Geophys. Res.*, **107**, 8039, <https://doi.org/10.1029/2000JC000439>.
- IPCC, 2013: *Climate Change 2013: The Physical Science Basis*. Cambridge University Press, 1535 pp., <https://doi.org/10.1017/CBO9781107415324>.
- Janjić, Z. I., 1990: The step-mountain coordinate: Physical package. *Mon. Wea. Rev.*, **118**, 1429–1443, [https://doi.org/10.1175/1520-0493\(1990\)118<1429:TSMCPP>2.0.CO;2](https://doi.org/10.1175/1520-0493(1990)118<1429:TSMCPP>2.0.CO;2).
- , 2001: Nonsingular implementation of the Mellor-Yamada level 2.5 scheme in the NCEP Meso Model. NCEP Office Note 437, 61 pp.
- Jeong, J., and F. Hussain, 1995: On the identification of a vortex. *J. Fluid Mech.*, **285**, 69–94, <https://doi.org/10.1017/S0022112095000462>.
- Jerram, N., R. J. Perkins, J. C. H. Fung, M. J. Davidson, S. E. Belcher, and J. C. R. Hunt, 1995: Atmospheric flow through groups of buildings and dispersion from localized sources. *Wind Climate in Cities*, J. E. Cermak et al., Eds., Kluwer, 109–130.
- Jiménez, M. A., and J. Cuxart, 2005: Large-eddy simulations of the stable boundary layer using the standard Kolmogorov theory: Range of applicability. *Bound.-Layer Meteor.*, **115**, 241–261, <https://doi.org/10.1007/s10546-004-3470-4>.
- Johansson, C., A.-S. Smedman, U. Högström, J. G. Brasseur, and S. Khanna, 2001: Critical test of the validity of Monin–Obukhov similarity during convective conditions. *J. Atmos. Sci.*, **58**, 1549–1566, [https://doi.org/10.1175/1520-0469\(2001\)058<1549:CTOTVO>2.0.CO;2](https://doi.org/10.1175/1520-0469(2001)058<1549:CTOTVO>2.0.CO;2).
- Johnson, R. H., P. E. Ciesielski, and J. A. Cotturone, 2001: Multiscale variability of the atmospheric mixed layer over the western Pacific warm pool. *J. Atmos. Sci.*, **58**, 2729–2750, [https://doi.org/10.1175/1520-0469\(2001\)058<2729:MVOTAM>2.0.CO;2](https://doi.org/10.1175/1520-0469(2001)058<2729:MVOTAM>2.0.CO;2).
- Jonker, H. J. J., and M. A. Jiménez, 2014: Laboratory experiments on convective entrainment using a saline water tank. *Bound.-Layer Meteor.*, **151**, 479–500, <https://doi.org/10.1007/s10546-014-9909-3>.
- , M. van Reeuwijk, P. P. Sullivan, and E. G. Patton, 2012: Interfacial layers in clear and cloudy atmospheric boundary layers. *Proc. Seventh Int. Symp. on Turbulence, Heat and Mass Transfer*, Palermo, Italy, International Centre for Heat and Mass Transfer, <https://doi.org/10.1615/ICHMT.2012.ProcSevIntSympTurbHeatTransfPal.10>.
- , —, —, and —, 2013: On the scaling of shear-driven entrainment: A DNS study. *J. Fluid Mech.*, **732**, 150–165, <https://doi.org/10.1017/jfm.2013.394>.
- Jordan, C. F., 1969: Derivation of leaf area index from quality of light on the forest floor. *Ecology*, **50**, 663–666, <https://doi.org/10.2307/1936256>.
- Kahl, J. D., 1990: Characteristics of the low-level temperature inversion along the Alaskan Arctic coast. *Int. J. Climatol.*, **10**, 537–548, <https://doi.org/10.1002/joc.3370100509>.
- , D. A. Martinez, and N. A. Zaitseva, 1996: Long-term variability in the low-level inversion layer over the Arctic Ocean. *Int. J. Climatol.*, **16**, 1297–1313, [https://doi.org/10.1002/\(SICI\)1097-0088\(199611\)16:11<1297::AID-JOC86>3.0.CO;2-T](https://doi.org/10.1002/(SICI)1097-0088(199611)16:11<1297::AID-JOC86>3.0.CO;2-T).
- , N. A. Zaitseva, V. Khattatov, R. C. Schnell, D. M. Bacon, J. Bacon, V. Radionov, and M. C. Serreze, 1999: Radiosonde observations from the former Soviet “North Pole” series of drifting ice stations, 1954–90. *Bull. Amer. Meteor. Soc.*, **80**, 2019–2026, [https://doi.org/10.1175/1520-0477\(1999\)080<2019:ROFTFS>2.0.CO;2](https://doi.org/10.1175/1520-0477(1999)080<2019:ROFTFS>2.0.CO;2).
- Kaimal, J. C., and J. J. Finnigan, 1994: *Atmospheric Boundary Layer Flows*. Oxford University Press, 289 pp.
- , J. C. Wyngaard, Y. Izumi, and O. R. Coté, 1972: Spectral characteristics of surface-layer turbulence. *Quart. J. Roy. Meteor. Soc.*, **98**, 563–589, <https://doi.org/10.1002/qj.49709841707>.
- , —, D. A. Haugen, O. R. Coté, Y. Izumi, S. J. Caughey, and C. J. Readings, 1976: Turbulence structure in the convective boundary layer. *J. Atmos. Sci.*, **33**, 2152–2169, [https://doi.org/10.1175/1520-0469\(1976\)033<2152:TSITCB>2.0.CO;2](https://doi.org/10.1175/1520-0469(1976)033<2152:TSITCB>2.0.CO;2).
- Kanak, K. M., 2004: Douglas K. Lilly: A biography. *Atmospheric Turbulence and Mesoscale Meteorology: Scientific Research Inspired by Doug Lilly*. E. Fedorovich, R. Rotunno, and B. Stevens, Eds., Cambridge University Press, 1–14.
- Kanda, M., A. Inagaki, M. O. Letzel, S. Raasch, and T. Watanabe, 2004: LES study of the energy imbalance problem with eddy

- covariance fluxes. *Bound.-Layer Meteor.*, **110**, 381–404, <https://doi.org/10.1023/B:BOUN.0000007225.45548.7a>.
- Kang, Y., D. Belusic, and K. Smith-Miles, 2015: Classes of structures in the stable atmospheric boundary layer. *Quart. J. Roy. Meteor. Soc.*, **141**, 2057–2069, <https://doi.org/10.1002/qj.2501>.
- Kastner-Klein, P., R. Berkowicz, and R. E. Britter, 2004: The influence of street architecture on flow and dispersion in street canyons. *Meteor. Atmos. Phys.*, **87**, 121–131, <https://doi.org/10.1007/s00703-003-0065-4>.
- Katsaros, K. B., 1980: The aqueous thermal boundary layer. *Bound.-Layer Meteor.*, **18**, 107–127, <https://doi.org/10.1007/BF00117914>.
- , M. A. Donelan, and W. M. Drennan, 1993: Flux measurements from a Swath ship in SWADE. *J. Mar. Syst.*, **4**, 117–132, [https://doi.org/10.1016/0924-7963\(93\)90003-5](https://doi.org/10.1016/0924-7963(93)90003-5).
- , and Coauthors, 1994: Measurements of humidity and temperature in the marine environment during the HEXOS Main Experiment. *J. Atmos. Oceanic Technol.*, **11**, 964–981, [https://doi.org/10.1175/1520-0426\(1994\)011<0964:MOHATI>2.0.CO;2](https://doi.org/10.1175/1520-0426(1994)011<0964:MOHATI>2.0.CO;2).
- Katul, G., C.-I. Hsieh, G. Kuhn, and D. Ellsworth, 1997: Turbulent eddy motion at the forest-atmosphere interface. *J. Geophys. Res.*, **102**, 13 409–13 421, <https://doi.org/10.1029/97JD00777>.
- , and Coauthors, 1999: Spatial variability of turbulent fluxes in the roughness sublayer of an even-aged pine forest. *Bound.-Layer Meteor.*, **93**, 1–28, <https://doi.org/10.1023/A:1002079602069>.
- , A. G. Konings, and A. Porporato, 2011: Mean velocity profile in a sheared and thermally stratified atmospheric boundary layer. *Phys. Rev. Lett.*, **107**, 268502, <https://doi.org/10.1103/PhysRevLett.107.268502>.
- , D. Li, M. Chamecki, and E. Bou-Zeid, 2013: Mean scalar concentration profile in a sheared and thermally stratified atmospheric surface layer. *Phys. Rev.*, **87E**, 023004, <https://doi.org/10.1103/PhysRevE.87.023004>.
- Kawa, S. R., and R. Pearson Jr., 1989: An observational study of stratocumulus entrainment and thermodynamics. *J. Atmos. Sci.*, **46**, 2649–2651, [https://doi.org/10.1175/1520-0469\(1989\)046<2649:AOSOSE>2.0.CO;2](https://doi.org/10.1175/1520-0469(1989)046<2649:AOSOSE>2.0.CO;2).
- Kazil, J., H. Wang, G. Feingold, A. D. Clarke, J. R. Snider, and A. R. Bandy, 2011: Modeling chemical and aerosol processes in the transition from closed to open cells during VOCALS-REx. *Atmos. Chem. Phys.*, **11**, 7491–7514, <https://doi.org/10.5194/acp-11-7491-2011>.
- Keller, L. V., and A. A. Friedmann, 1924: Differentialgleichung für die turbulente Bewegung einer kompressiblen Flüssigkeit. *Proc. First Congress for Applied Mechanics*, Delft, Netherlands, International Union of Theoretical and Applied Mechanics, 395–405.
- Kellner, G., C. Wamser, and R. A. Brown, 1987: An observation of the planetary boundary layer in the marginal ice zone. *J. Geophys. Lett.*, **92**, 6955–6965, <https://doi.org/10.1029/JC092iC07p06955>.
- Kelly, M., J. C. Wyngaard, and P. P. Sullivan, 2009: Application of a subfilter-scale flux model over the ocean using OHATS field data. *J. Atmos. Sci.*, **66**, 3217–3225, <https://doi.org/10.1175/2009JAS2903.1>.
- Kemp, J. R., and D. J. Thomson, 1996: Diffusion in the stably stratified atmospheric boundary layer. *Atmos. Environ.*, **30**, 2911–2923, [https://doi.org/10.1016/1352-2310\(95\)00485-8](https://doi.org/10.1016/1352-2310(95)00485-8).
- Kent, E. C., and Coauthors, 2017: A call for new approaches to quantifying biases in observations of sea-surface temperature. *Bull. Amer. Meteor. Soc.*, **98**, 1601–1616, <https://doi.org/10.1175/BAMS-D-15-00251.1>.
- Khairoutdinov, M. F., S. K. Krueger, C.-H. Moeng, P. A. Bogenschutz, and D. A. Randall, 2009: Large eddy simulation of maritime deep tropical convection. *J. Adv. Model. Earth Syst.*, **1**, 15, <https://doi.org/10.3894/JAMES.2009.1.15>.
- Khanna, S., and J. G. Brasseur, 1997: Analysis of Monin-Obukhov similarity from large-eddy simulation. *J. Fluid Mech.*, **345**, 251–286, <https://doi.org/10.1017/S0022112097006277>.
- Khrgian, A. Kh., 1959: *Meteorology: A Historical Survey* (in Russian). Vol. I, 2nd rev. ed. Gidrometeorologicheskoe Izdatel'stvo, 270 pp.
- Kljun, N., M. W. Rotach, and H. P. Schmid, 2002: A 3-D backward Lagrangian footprint model for a wide range of boundary layer stratifications. *Bound.-Layer Meteor.*, **103**, 205–226, <https://doi.org/10.1023/A:1014556300021>.
- , P. Kastner-Klein, E. Fedorovich, and M. W. Rotach, 2004: Evaluation of Lagrangian footprint model using data from wind tunnel convective boundary layer. *Agric. For. Meteorol.*, **127**, 198–201, <https://doi.org/10.1016/j.agrformet.2004.07.013>.
- Kim, S. W., C.-H. Moeng, J. C. Weil, and M. C. Barth, 2005: Lagrangian particle dispersion modeling of the fumigation process using large-eddy simulation. *J. Atmos. Sci.*, **62**, 1932–1946, <https://doi.org/10.1175/JAS3435.1>.
- Kitaigorodskii, S. A., 1959: Contribution to theory of turbulent viscosity in wave motion. *Bull. (Izv.) Acad. Sci. USSR. Geophys. Ser.* **6**.
- , 1983: On the theory of the equilibrium range in the spectrum of wind-generated gravity waves. *J. Phys. Oceanogr.*, **13**, 817–827, [https://doi.org/10.1175/1520-0485\(1983\)013<0816:OTTOTE>2.0.CO;2](https://doi.org/10.1175/1520-0485(1983)013<0816:OTTOTE>2.0.CO;2).
- Kleissl, J., M. B. Parlange, and C. Meneveau, 2004: Field experimental study of dynamic Smagorinsky models in the atmospheric surface layer. *J. Atmos. Sci.*, **61**, 2296–2307, [https://doi.org/10.1175/1520-0469\(2004\)061<2296:FESODS>2.0.CO;2](https://doi.org/10.1175/1520-0469(2004)061<2296:FESODS>2.0.CO;2).
- Klipp, C., and L. Mahrt, 2004: Flux-gradient relationship, self-correlation and intermittency in the stable boundary layer. *Quart. J. Roy. Meteor. Soc.*, **130**, 2087–2104, <https://doi.org/10.1256/qj.03.161>.
- Kloesel, K. A., 1992: A 70-year history of marine stratocumulus cloud field experiments off the coast of California. *Bull. Amer. Meteor. Soc.*, **73**, 1581–1585, [https://doi.org/10.1175/1520-0477\(1992\)073<1581:AYHOMS>2.0.CO;2](https://doi.org/10.1175/1520-0477(1992)073<1581:AYHOMS>2.0.CO;2).
- Köhler, M., M. Ahlgrimm, and A. Beljaars, 2011: Unified treatment of dry convective and stratocumulus-topped boundary layers in the ECMWF model. *Quart. J. Roy. Meteor. Soc.*, **137**, 43–57, <https://doi.org/10.1002/qj.713>.
- Kolmogorov, A. N., 1941a: Local structure of turbulence in an incompressible fluid at very high Reynolds numbers. *Dokl. Akad. Nauk SSSR*, **30**, 299–303.
- , 1941b: Energy dissipation in locally isotropic turbulence. *Dokl. Akad. Nauk SSSR*, **32**, 19–21.
- , 1962: A refinement of previous hypotheses concerning the local structure of turbulence in a viscous incompressible fluid at high Reynolds number. *J. Fluid Mech.*, **13**, 82–85, <https://doi.org/10.1017/S0022112062000518>.
- Komen, G., P. E. M. Janssen, V. Makin, and W. Oost, 1998: On the sea state dependence of the Charnock parameter. *Global Atmos. Ocean Syst.*, **5**, 367–388.
- Kosović, B., 1997: Subgrid-scale modeling for large-eddy simulations of high-Reynolds-number boundary layers. *J. Fluid Mech.*, **336**, 151–182, <https://doi.org/10.1017/S0022112096004697>.

- , and J. A. Curry, 2000: A large eddy simulation of a quasi-steady, stably stratified atmospheric boundary layer. *J. Atmos. Sci.*, **57**, 1052–1068, [https://doi.org/10.1175/1520-0469\(2000\)057<1052:ALESSO>2.0.CO;2](https://doi.org/10.1175/1520-0469(2000)057<1052:ALESSO>2.0.CO;2).
- Koster, R. D., and P. C. D. Milly, 1997: The interplay between transpiration and runoff formulations in land surface schemes used with atmospheric models. *J. Climate*, **10**, 1578–1591, [https://doi.org/10.1175/1520-0442\(1997\)010<1578:TIBTAR>2.0.CO;2](https://doi.org/10.1175/1520-0442(1997)010<1578:TIBTAR>2.0.CO;2).
- , and Coauthors, 2004: Regions of coupling between soil moisture and precipitation. *Science*, **305**, 1138–1140, <https://doi.org/10.1126/science.1100217>.
- Kottmeier, C., J. Hartmann, C. Wamser, A. Bochert, C. Lüpkes, D. Freese, and W. Cohrs, 1994: *Radiation and Eddy Flux Experiment 1993 (REFLEX II)*. Reports on Polar Research, Vol. 133, Alfred Wegener Institute, 62 pp.
- Krettenauer, K., and U. Schumann, 1992: Numerical simulation of turbulent convection over wavy terrain. *J. Fluid Mech.*, **237**, 261–299, <https://doi.org/10.1017/S0022112092003410>.
- Krueger, S. K., G. T. McLean, and Q. Fu, 1995a: Numerical simulations of the stratus-to-cumulus transition in the subtropical marine boundary layer. Part I: Boundary-layer structure. *J. Atmos. Sci.*, **52**, 2839–2850, [https://doi.org/10.1175/1520-0469\(1995\)052<2839:NSOTST>2.0.CO;2](https://doi.org/10.1175/1520-0469(1995)052<2839:NSOTST>2.0.CO;2).
- , —, and —, 1995b: Numerical simulations of the stratus-to-cumulus transition in the subtropical marine boundary layer. Part II: Boundary-layer circulation. *J. Atmos. Sci.*, **52**, 2851–2868, [https://doi.org/10.1175/1520-0469\(1995\)052<2851:NSOTST>2.0.CO;2](https://doi.org/10.1175/1520-0469(1995)052<2851:NSOTST>2.0.CO;2).
- Kuettner, J. P., 1959: The band structure of the atmosphere. *Tellus*, **11**, 267–294, <https://doi.org/10.3402/tellusa.v11i3.9319>.
- , 1974: General description and central program of GATE. *Bull. Amer. Meteor. Soc.*, **55**, 712–719, [https://doi.org/10.1175/1520-0477\(1974\)055<0711:G>2.0.CO;2](https://doi.org/10.1175/1520-0477(1974)055<0711:G>2.0.CO;2).
- , and D. E. Parker, 1976: GATE: Report on the field phase. *Bull. Amer. Meteor. Soc.*, **37**, 11–27, <https://doi.org/10.1175/1520-0477-57.1.11>.
- Kuhlbrodt, E., and J. Reger, 1938: Die meteorologischen Beobachtungen. Methoden, Beobachtungsmaterial und Ergebnisse. German Atlantic Expedition *Meteor* 1925–1927, Wissenschaftliche Ergebnisse (Scientific Results), Vol. 14, Walter de Gruyter, 215–345.
- Kumar, V., J. Kleissl, C. Meneveau, and M. B. Parlange, 2006: Large-eddy simulation of a diurnal cycle of the atmospheric boundary layer: Atmospheric stability and scaling issues. *Water Resour. Res.*, **42**, <https://doi.org/10.1029/2005WR004651>.
- , G. Svensson, A. A. M. Holtslag, C. Meneveau, and M. Parlange, 2010: Impact of surface flux formulations and geostrophic forcing on large-eddy simulations of diurnal atmospheric boundary layer flow. *J. Appl. Meteor. Climatol.*, **49**, 1496–1516, <https://doi.org/10.1175/2010JAMC2145.1>.
- Kuo, H.-C., and W. H. Schubert, 1988: Stability of cloud-topped mixed layers. *Quart. J. Roy. Meteor. Soc.*, **114**, 887–916, <https://doi.org/10.1002/qj.49711448204>.
- Kustas, W. P., J. H. Prueger, J. I. MacPherson, M. Wolde, and F. Li, 2005: Effect of land use and meteorological conditions on local and regional momentum transport and roughness for Midwestern cropping systems. *J. Hydrometeorol.*, **6**, 825–839, <https://doi.org/10.1175/JHM460.1>.
- Kutzbach, G., 1979: *The Thermal Theory of Cyclones*. Amer. Meteor. Soc., 255 pp.
- Lamb, H., 1895: *Hydrodynamics*. Cambridge University Press, 604 pp.
- Lamb, R. G., 1978: A numerical simulation of dispersion from an elevated point source in the convective planetary boundary layer. *Atmos. Environ.*, **12**, 1297–1304, [https://doi.org/10.1016/0004-6981\(78\)90068-9](https://doi.org/10.1016/0004-6981(78)90068-9).
- , 1982: Diffusion in the convective boundary layer. *Atmospheric Turbulence and Air Pollution Modelling*, F. Nieuwstadt and H. van Dop, Eds., Reidel, 159–229.
- Lamaud, E., and M. Irvine, 2006: Temperature-humidity dissimilarity and heat-to-water-vapour transport above and within a pine forest canopy: The role of the Bowen ratio. *Bound.-Layer Meteorol.*, **120**, 87–109, <https://doi.org/10.1007/s10546-005-9032-6>.
- Langford, A. O., and Coauthors, 2017: Entrainment of stratospheric air and Asian pollution by the convective boundary layer in the southwestern U.S. *J. Geophys. Res. Atmos.*, **122**, 1312–1337, <https://doi.org/10.1002/2016JD025987>.
- Lareau, N. P., Y. Zhang, and S. A. Klein, 2018: Observed boundary layer controls on shallow cumulus at the ARM Southern Great Plains Site. *J. Atmos. Sci.*, **75**, 2235–2255, <https://doi.org/10.1175/JAS-D-17-0244.1>.
- Large, W. G., and S. Pond, 1981: Open ocean momentum-flux measurements in moderate to high winds. *J. Phys. Oceanogr.*, **11**, 324–336, [https://doi.org/10.1175/1520-0485\(1981\)011<0324:OOMFMI>2.0.CO;2](https://doi.org/10.1175/1520-0485(1981)011<0324:OOMFMI>2.0.CO;2).
- , J. C. McWilliams, and S. C. Doney, 1994: Oceanic vertical mixing: A review and a model with a nonlocal boundary layer parameterization. *Rev. Geophys.*, **32**, 363–403, <https://doi.org/10.1029/94RG01872>.
- Larsen, X. G., M. Kelly, and A. M. Sempreviva, 2014: On the temperature and humidity dissimilarity in the marine surface layer. *Bound.-Layer Meteorol.*, **151**, 273–291, <https://doi.org/10.1007/s10546-013-9896-9>.
- Launder, B. E., 2015: First steps in modelling turbulence and its origins: A commentary on Reynolds (1895) ‘On the dynamical theory of incompressible viscous fluids and the determination of the criterion.’ *Philos. Trans. Roy. Soc.*, **373A**, 20140231, <https://doi.org/10.1098/rsta.2014.0231>.
- Lawrence, D. M., K. W. Oleson, M. G. Flanner, C. G. Fletcher, P. J. Lawrence, S. Levis, S. C. Swenson, and G. B. Bonan, 2012: The CCSM4 Land Simulation, 1850–2005: Assessment of surface climate and new capabilities. *J. Climate*, **25**, 2240–2260, <https://doi.org/10.1175/JCLI-D-11-00103.1>.
- Leck, C., E. K. Bigg, D. S. Covert, J. Heintzenberg, W. Maenhaut, E. D. Nilsson, and A. Wiedensohler, 1996: Overview of the atmospheric research program during the International Ocean Expedition of 1991 (IAOE-1991) and its scientific results. *Tellus*, **48B**, 136–155, <https://doi.org/10.3402/tellusb.v48i2.15833>.
- , E. D. Nilsson, E. K. Bigg, and L. Bäcklin, 2001: The atmospheric program of the Arctic Ocean Expedition 1996 (AOE-1996): An overview of scientific objectives, experimental approaches and instruments. *J. Geophys. Res.*, **106**, 32 051–32 067, <https://doi.org/10.1029/2000JD900461>.
- Leclar, M. Y., and G. W. Thurtell, 1990: Footprint prediction of scalar fluxes using a Markovian analysis. *Bound.-Layer Meteorol.*, **52**, 247–258, <https://doi.org/10.1007/BF00122089>.
- , R. H. Shaw, G. Hartog, and H. H. Neumann, 1990: The influence of atmospheric stability on the budgets of the Reynolds stress and turbulent kinetic energy within and above a deciduous forest. *J. Appl. Meteorol.*, **29**, 916–933, [https://doi.org/10.1175/1520-0450\(1990\)029<0916:TIOASO>2.0.CO;2](https://doi.org/10.1175/1520-0450(1990)029<0916:TIOASO>2.0.CO;2).
- Lee, X., 2000: Air motion within and above forest vegetation in non-ideal conditions. *For. Ecol. Manage.*, **135**, 3–18, [https://doi.org/10.1016/S0378-1127\(00\)00294-2](https://doi.org/10.1016/S0378-1127(00)00294-2).

- Leith, C., 1990: Stochastic backscatter in a subgrid-scale model: Plane shear mixing layer. *Phys. Fluids*, **2**, 297–299, <https://doi.org/10.1063/1.857779>.
- LeMone, M. A., 1980: The marine boundary layer. *Workshop on the Planetary Boundary Layer*, J. C. Wyngaard, Ed., Amer. Meteor. Soc., 182–246.
- , and W. T. Pennell, 1976: The relationship of trade-wind cumulus distribution to subcloud-layer fluxes and structure. *Mon. Wea. Rev.*, **104**, 524–539, [https://doi.org/10.1175/1520-0493\(1976\)104<0524:TROTWC>2.0.CO;2](https://doi.org/10.1175/1520-0493(1976)104<0524:TROTWC>2.0.CO;2).
- , and R. J. Meitin, 1984: Three examples of fair-weather mesoscale boundary layer convection in the tropics. *Mon. Wea. Rev.*, **112**, 1985–1997, [https://doi.org/10.1175/1520-0493\(1984\)112<1985:TEOFWM>2.0.CO;2](https://doi.org/10.1175/1520-0493(1984)112<1985:TEOFWM>2.0.CO;2).
- , M. Zhou, C.-H. Moeng, D. H. Lenschow, L. J. Miller, and R. L. Grossman, 1999: An observational study of wind profiles in the baroclinic convective boundary layer. *Bound.-Layer Meteor.*, **90**, 47–82, <https://doi.org/10.1023/A:1001703303697>.
- , and Coauthors, 2000: Land–atmosphere interaction research, early results, and opportunities in the Walnut River watershed in southeast Kansas: CASES and ABLE. *Bull. Amer. Meteor. Soc.*, **81**, 757–779, [https://doi.org/10.1175/1520-0477\(2000\)081<0757:LIRERA>2.3.CO;2](https://doi.org/10.1175/1520-0477(2000)081<0757:LIRERA>2.3.CO;2).
- , and Coauthors, 2002: Late-morning warming and moistening of the convective boundary layer over the Walnut River watershed. *Bound.-Layer Meteor.*, **104**, 1–52, <https://doi.org/10.1023/A:1015569104180>.
- , K. Ikeda, R. L. Grossman, and M. W. Rotach, 2003: Horizontal variability of 2-m temperature at night during CASES-97. *J. Atmos. Sci.*, **60**, 2431–2449, [https://doi.org/10.1175/1520-0469\(2003\)060<2431:HVOMTA>2.0.CO;2](https://doi.org/10.1175/1520-0469(2003)060<2431:HVOMTA>2.0.CO;2).
- , F. Chen, J. G. Alfieri, M. Tewari, B. Geerts, Q. Miao, R. L. Grossman, and R. L. Coulter, 2007: Influence of land cover and soil moisture on the horizontal distribution of sensible and latent heat fluxes in southeast Kansas during IHOP_2002 and CASES-97. *J. Hydrometeor.*, **8**, 68–87, <https://doi.org/10.1175/JHM554.1>.
- Leng, G., L. R. Leung, and M. Huang, 2017: Significant impacts of irrigation water sources and methods on modeling irrigation effects in the ACME Land Model. *J. Adv. Model. Earth Syst.*, **9**, 1665–1683, <https://doi.org/10.1002/2016MS000885>.
- Lenschow, D. H., 1970: Airplane measurements of boundary layer structure. *J. Appl. Meteor.*, **9**, 874–884, [https://doi.org/10.1175/1520-0450\(1970\)009<0874:AMOPBL>2.0.CO;2](https://doi.org/10.1175/1520-0450(1970)009<0874:AMOPBL>2.0.CO;2).
- , and E. M. Agee, 1976: Preliminary results from the Air Mass Transformation Experiment (AMTEX). *Bull. Amer. Meteor. Soc.*, **57**, 1346–1355, <https://doi.org/10.1175/1520-0477-57.11.1346>.
- , B. Stankov, and L. Mahrt, 1979: The rapid morning boundary-layer transition. *J. Atmos. Sci.*, **36**, 2108–2124, [https://doi.org/10.1175/1520-0469\(1979\)036<2108:TRMBLT>2.0.CO;2](https://doi.org/10.1175/1520-0469(1979)036<2108:TRMBLT>2.0.CO;2).
- , J. C. Wyngaard, and W. T. Pennell, 1980: Mean-field and second-moment budgets in a baroclinic, convective boundary layer. *J. Atmos. Sci.*, **37**, 1313–1326, [https://doi.org/10.1175/1520-0469\(1980\)037<1313:MFA SMB>2.0.CO;2](https://doi.org/10.1175/1520-0469(1980)037<1313:MFA SMB>2.0.CO;2).
- , and Coauthors, 1988: Dynamics and Chemistry of Marine Stratocumulus (DYCOMS) Experiment. *Bull. Amer. Meteor. Soc.*, **69**, 1058–1067, [https://doi.org/10.1175/1520-0477\(1988\)069<1058:DACOMS>2.0.CO;2](https://doi.org/10.1175/1520-0477(1988)069<1058:DACOMS>2.0.CO;2).
- , M. Zhou, X. Zeng, L. Chen, and X. Xu, 2000: Measurements of fine-scale structure at the top of marine stratocumulus. *Bound.-Layer Meteor.*, **97**, 331–357, <https://doi.org/10.1023/A:1002780019748>.
- Leonard, A., 1974: Energy cascade in large eddy simulations of turbulent fluid flows. *Advances in Geophysics*, Vol. 18, Academic Press, 237–248.
- Lettau, H., 1949: Isotropic and non-isotropic turbulence in the atmospheric surface layer. Geophysical Research Paper 1, AFCRL, 86 pp.
- , 1950: A re-examination of the “Leipzig Wind Profile” considering some relations between wind and turbulence in the frictional layer. *Tellus*, **2**, 125–129, <https://doi.org/10.1111/j.2153-3490.1950.tb00321.x>.
- , 1957: Computation of heat budget constituents of the earth/air interface. *Exploring the Atmosphere’s First Mile*, Vol. I, H. Lettau and B. Davidson, Eds., Pergamon Press, 305–327.
- , and B. Davidson, Eds., 1957: *Proceedings of the Great Plains Turbulence Field Program 1 August to 8 September 1953 O’Neill, Nebraska*. Vol. II, *Exploring the Atmosphere’s First Mile*, Pergamon Press, 578 pp.
- Levis, S., G. B. Bonan, E. Kluzek, P. E. Thornton, A. Jones, W. J. Sacks, and C. J. Kucharik, 2012: Interactive crop management in the Community Earth System Model (CESM1): Seasonal influences on land–atmosphere fluxes. *J. Climate*, **25**, 4839–4859, <https://doi.org/10.1175/JCLI-D-11-00446.1>.
- Li, D., E. Bou-Zeid, M. Barlage, F. Chen, and J. A. Smith, 2013: Development and evaluation of a mosaic approach in the WRF-Noah framework. *J. Geophys. Res. Atmos.*, **118**, 11 918–11 935, <https://doi.org/10.1002/2013JD020657>.
- , G. G. Katul, and E. Bou-Zeid, 2015: Turbulent energy spectra and cospectra of momentum and heat fluxes in the stable atmospheric surface layer. *Bound.-Layer Meteor.*, **157**, 1–21, <https://doi.org/10.1007/s10546-015-0048-2>.
- Liebethal, C., B. Huwe, and T. Foken, 2005: Sensitivity analysis for two ground heat flux calculation approaches. *Agric. For. Meteorol.*, **132**, 253–262, <https://doi.org/10.1016/j.agrformet.2005.08.001>.
- Lilly, D. K., 1962: On the numerical simulation of buoyant convection. *Tellus*, **XIV**, 148–172, <https://doi.org/10.1111/j.2153-3490.1962.tb00128.x>.
- Lilly, D., 1966a: On the application of the eddy viscosity concept in the inertial sub-range of turbulence. NCAR Manuscript 123, 19 pp.
- , 1966b: On the stability of Ekman boundary flow. *J. Atmos. Sci.*, **23**, 481–494, [https://doi.org/10.1175/1520-0469\(1966\)023<0481:OTIOEB>2.0.CO;2](https://doi.org/10.1175/1520-0469(1966)023<0481:OTIOEB>2.0.CO;2).
- , 1967: The representation of small-scale turbulence in numerical simulation experiments. *Proc. IBM Scientific Computing Symp. on Environmental Science*, Thomas J. Watson I Research Center, Yorktown Heights, NY, 195–210.
- , 1968: Models of cloud-topped mixed layers under a strong inversion. *Quart. J. Roy. Meteor. Soc.*, **94**, 292–309, <https://doi.org/10.1002/qj.49709440106>.
- List, R. J., 1963: *Smithsonian Meteorological Tables*. 6th rev. ed. Smithsonian, 527 pp.
- Liu, S. and X. Liang, 2010: Observed diurnal cycle climatology of planetary boundary layer height. *J. Climate*, **23**, 5790–5809, <https://doi.org/10.1175/2010JCLI3552.1>.
- Liu, W. T., K. B. Katsaros, and J. A. Businger, 1979: Bulk parameterization of air-sea exchanges of heat and water vapor including the molecular constraints at the interface. *J. Atmos. Sci.*, **36**, 1722–1735, [https://doi.org/10.1175/1520-0469\(1979\)036<1722:BPOASE>2.0.CO;2](https://doi.org/10.1175/1520-0469(1979)036<1722:BPOASE>2.0.CO;2).
- Liu, X., F. Chen, M. Barlage, G. Zhou, and D. Niyogi, 2016: Noah-MP-Crop: Introducing dynamic crop growth in the Noah-MP land surface model. *J. Geophys. Res. Atmos.*, **121**, 13 953–13 972, <https://doi.org/10.1002/2016JD025597>.

- Lock, A. P., 2009: Factors influencing cloud area at the capping inversion for shallow cumulus clouds. *Quart. J. Roy. Meteor. Soc.*, **135**, 941–952, <https://doi.org/10.1002/qj.424>.
- , A. R. Brown, M. R. Bush, G. M. Martin, and R. N. B. Smith, 2000: A new boundary layer mixing scheme. Part I: Scheme description and single-column model tests. *Mon. Wea. Rev.*, **128**, 3187–3199, [https://doi.org/10.1175/1520-0493\(2000\)128<3187:ANBLMS>2.0.CO;2](https://doi.org/10.1175/1520-0493(2000)128<3187:ANBLMS>2.0.CO;2).
- Loewe, K., A. M. L. Ekman, M. Paukert, J. Sedlar, M. Tjernström, and C. Hoese, 2017: Modelling micro- and macrophysical contributors to the dissipation of an Arctic mixed-phase cloud during the Arctic Summer Cloud Ocean Study (ASCOS). *Atmos. Chem. Phys.*, **17**, 6693–6704, <https://doi.org/10.5194/acp-17-6693-2017>.
- Lothon, M., and Coauthors, 2014: The BLLAST field experiment: Boundary-Layer Late Afternoon and Sunset Turbulence. *Atmos. Chem. Phys.*, **14**, 10 931–10 960, <https://doi.org/10.5194/acp-14-10931-2014>.
- Loveland, T. R., J. W. Merchant, J. F. Brown, D. O. Ohlen, B. C. Reed, P. Olson, and J. Hutchinson, 1995: Seasonal land-cover regions of the United States. *Ann. Assoc. Amer. Geogr.*, **85**, 339–355, <https://doi.org/10.1111/j.1467-8306.1995.tb01798.x>.
- Lu, H., and F. Porté-Agel, 2010: A modulated gradient model for large-eddy simulation: Application to a neutral atmospheric boundary layer. *Phys. Fluids*, **22**, 015109, <https://doi.org/10.1063/1.3291073>.
- Ludwig, F. L., F. K. Chow, and R. L. Street, 2009: Effect of turbulence models and spatial resolution on resolved velocity and structure and momentum fluxes in large-eddy simulations of neutral boundary-layer flows. *J. Appl. Meteor. Climatol.*, **48**, 1161–1180, <https://doi.org/10.1175/2008JAMC2021.1>.
- Luhar, A. K., and R. E. Britter, 1989: A random walk model for dispersion in inhomogeneous turbulence in a convective boundary layer. *Atmos. Environ.*, **23**, 1911–1924, [https://doi.org/10.1016/0004-6981\(89\)90516-7](https://doi.org/10.1016/0004-6981(89)90516-7).
- , and B. L. Sawford, 1995: Lagrangian stochastic modeling of the coastal fumigation phenomenon. *J. Appl. Meteor.*, **34**, 2259–2277, [https://doi.org/10.1175/1520-0450\(1995\)034<2259:LSMOTC>2.0.CO;2](https://doi.org/10.1175/1520-0450(1995)034<2259:LSMOTC>2.0.CO;2).
- , and —, 2005: Micromixing modelling of concentration fluctuations in inhomogeneous turbulence in the convective boundary layer. *Bound.-Layer Meteor.*, **114**, 1–30, <https://doi.org/10.1007/s10546-004-1292-z>.
- , M. F. Hibberd, and M. S. Borgas, 2000: A skewed meandering plume model for concentration statistics in the convective boundary layer. *Atmos. Environ.*, **34**, 3599–3616, [https://doi.org/10.1016/S1352-2310\(00\)00111-4](https://doi.org/10.1016/S1352-2310(00)00111-4).
- Lumley, J. L., and H. A. Panofsky, 1964: *The Structure of Atmospheric Turbulence*. Interscience, 239 pp.
- Lundquist, J., 2003: Intermittent and elliptical inertial oscillations. *J. Atmos. Sci.*, **60**, 2661–2673, [https://doi.org/10.1175/1520-0469\(2003\)060<2661:IAEIOI>2.0.CO;2](https://doi.org/10.1175/1520-0469(2003)060<2661:IAEIOI>2.0.CO;2).
- Lundquist, K. A., F. K. Chow, and J. K. Lundquist, 2012: An immersed boundary method enabling large-eddy simulations of flow over complex terrain in the WRF model. *Mon. Wea. Rev.*, **140**, 3936–3955, <https://doi.org/10.1175/MWR-D-11-00311.1>.
- Luo, Y. Q., and Coauthors, 2012: A framework for benchmarking land models. *Biogeosciences*, **9**, 3857–3874, <https://doi.org/10.5194/bg-9-3857-2012>.
- Lüpkes, C., V. M. Gryanik, B. Witha, M. Gryschka, S. Raasch, and T. Gollnik, 2008: Modeling convection over arctic leads with LES and a non-eddy-resolving microscale model. *J. Geophys. Res.*, **113**, C09028, <https://doi.org/10.1029/2007JC004099>.
- , T. Vihma, E. Jakobson, G. König-Langlo, and A. Tetzlaff, 2010: Meteorological observations from ship cruises during summer to the central Arctic: A comparison with reanalysis data. *Geophys. Res. Lett.*, **37**, L09810, <https://doi.org/10.1029/2010GL042724>.
- , M. Vladimir, V. M. Gryanik, J. Hartmann, and E. L. Andreas, 2012: A parametrization, based on sea ice morphology, of the neutral atmospheric drag coefficients for weather prediction and climate models. *J. Geophys. Res.*, **117**, D13112, <https://doi.org/10.1029/2012JD017630>.
- Maggioni, V., and P. R. Houser, 2017: Soil moisture data assimilation. *Data Assimilation for Atmospheric, Oceanic and Hydrologic Applications*, Vol. III, S. Park and L. Xu, Eds., Springer, 195–217, https://doi.org/10.1007/978-3-319-43415-5_9.
- Mahfouf, J. F., 1991: Analysis of soil moisture from near-surface parameters: A feasibility study. *J. Appl. Meteor.*, **30**, 1534–1547, [https://doi.org/10.1175/1520-0450\(1991\)030<1534:AOSMFN>2.0.CO;2](https://doi.org/10.1175/1520-0450(1991)030<1534:AOSMFN>2.0.CO;2).
- , E. Richard, and P. Mascart, 1987: The influence of soil and vegetation on the development of mesoscale circulations. *J. Appl. Meteor. Climatol.*, **26**, 1483–1495, [https://doi.org/10.1175/1520-0450\(1987\)026<1483:TIOSAV>2.0.CO;2](https://doi.org/10.1175/1520-0450(1987)026<1483:TIOSAV>2.0.CO;2).
- Mahrt, L., 1996: The bulk aerodynamic formulation over heterogeneous surfaces. *Bound.-Layer Meteor.*, **78**, 87–119, <https://doi.org/10.1007/BF00122488>.
- , 1999: Stratified atmospheric boundary layers. *Bound.-Layer Meteor.*, **90**, 375–396, <https://doi.org/10.1023/A:1001765727956>.
- , 2000: Surface heterogeneity and vertical structure of the boundary layer. *Bound.-Layer Meteor.*, **96**, 33–62, <https://doi.org/10.1023/A:1002482332477>.
- , 2014: Stably stratified atmospheric boundary layers. *Annu. Rev. Fluid Mech.*, **46**, 23–45, <https://doi.org/10.1146/annurev-fluid-010313-141354>.
- , and M. Ek, 1993: Spatial variability of turbulent fluxes and roughness lengths in HAPEX-MOBILHY. *Bound.-Layer Meteor.*, **65**, 381–400, <https://doi.org/10.1007/BF00707034>.
- , J. I. MacPherson, and R. Desjardins, 1994: Observations of fluxes over heterogeneous surfaces. *Bound.-Layer Meteor.*, **67**, 345–367, <https://doi.org/10.1007/BF00705438>.
- , X. Lee, A. Black, H. Neumann, and R. M. Staebler, 2000: Nocturnal mixing in a forest subcanopy. *Agric. For. Meteorol.*, **101**, 67–78, [https://doi.org/10.1016/S0168-1923\(99\)00161-6](https://doi.org/10.1016/S0168-1923(99)00161-6).
- , E. Moore, D. Vickers, and N. O. Jensen, 2001: Dependence of turbulent and mesoscale velocity variances on scale and stability. *J. Appl. Meteor.*, **40**, 628–641, [https://doi.org/10.1175/1520-0450\(2001\)040<0628:DOTAMV>2.0.CO;2](https://doi.org/10.1175/1520-0450(2001)040<0628:DOTAMV>2.0.CO;2).
- , J. Sun, S. P. Oncley, and T. W. Horst, 2014: Transient cold air drainage down a shallow valley. *J. Atmos. Sci.*, **71**, 2534–2544, <https://doi.org/10.1175/JAS-D-14-0010.1>.
- Malkus, J. S., 1956: On the maintenance of the trade winds. *Tellus*, **8**, 335–350, <https://doi.org/10.1111/j.2153-3490.1956.tb01231.x>.
- , 1958: On the structure of the trade wind moist layer. *Papers in Physical Oceanography and Meteorology*, Vol. XIII, No. 2, MIT/WHOI, 47 pp.
- , 1962: Large scale interactions. *Physical Oceanography*, M. N. Hill, Ed., *The Sea—Ideas and Observations on Progress in the Study of the Seas*, Vol. 1, Pergamon Press, 88–294.
- , and H. Riehl, 1964: *Cloud Structure and Distribution over the Tropical Pacific Ocean*. University of California Press, 229 pp.
- Manabe, S., 1969: Climate and the ocean circulation: I. The atmospheric circulation and the hydrology of the earth's surface. *Mon. Wea. Rev.*, **97**, 739–774, [https://doi.org/10.1175/1520-0493\(1969\)097<0739:CATOC>2.3.CO;2](https://doi.org/10.1175/1520-0493(1969)097<0739:CATOC>2.3.CO;2).

- Mann, J., and D. H. Lenschow, 1994: Errors in airborne flux measurements. *J. Geophys. Res.*, **99**, 14 519–14 526, <https://doi.org/10.1029/94JD00737>.
- Mason, P. J., 1988: The formation of aeriially-averaged roughness lengths. *Quart. J. Roy. Meteor. Soc.*, **114**, 399–420, <https://doi.org/10.1002/qj.49711448007>.
- , and S. H. Derbyshire, 1990: Large eddy simulation of the stably-stratified atmospheric boundary layer. *Bound.-Layer Meteor.*, **53**, 117–162, <https://doi.org/10.1007/BF00122467>.
- , and D. J. Thomson, 1992: Stochastic backscatter in large-eddy simulations of boundary layers. *J. Fluid Mech.*, **242**, 51–78, <https://doi.org/10.1017/S0022112092002271>.
- Mauder, M., R. L. Desjardins, and J. I. MacPherson, 2008: Creating surface flux maps from airborne measurements: Applications to the Mackenzie area GEWEX Study MAGS 1999. *Bound.-Layer Meteor.*, **129**, 431–450, <https://doi.org/10.1007/s10546-008-9326-6>.
- Mauritsen, T., and G. Svensson, 2007: Observations of stably stratified shear-driven atmospheric turbulence at low and high Richardson numbers. *J. Atmos. Sci.*, **64**, 645–655, <https://doi.org/10.1175/JAS3856.1>.
- , —, and B. Grisogono, 2005: Wave Flow Simulations Over Arctic Leads. *Bound.-Layer Meteor.*, **117**, 259–273, <https://doi.org/10.1007/s10546-004-1427-2>.
- , —, S. Zilitinkevich, I. Esau, L. Enger, and B. Grisogono, 2007: A total turbulent energy closure model for neutral and stably stratified atmospheric boundary layers. *J. Atmos. Sci.*, **64**, 4113–4126, <https://doi.org/10.1175/2007JAS2294.1>.
- Maxwell, R. M., and N. L. Miller, 2005: Development of a coupled land surface and groundwater model. *J. Hydrometeorol.*, **6**, 233–247, <https://doi.org/10.1175/JHM422.1>.
- Maykut, G. A., A. S. Thorndike, and N. Untersteiner, 1972: AIDJEX Scientific Plan. AIDJEX Bulletin, No. 15, Jet Propulsion Laboratory, Pasadena, CA, 38–42, http://psc.apl.washington.edu/nonwp_projects/aidjex/files/AIDJEX-15.pdf.
- McAdie, A., 1915: The theory and practise of frost fighting. *Sci. Mon.*, **1**, 292–301.
- McCumber, M.C. and R. A. Pielke, 1981: Simulation of the effects of surface fluxes of heat and moisture in a mesoscale numerical model: 1. Soil layer. *J. Geophys. Res.*, **86**, 9929–9938, <https://doi.org/10.1029/JC086iC10p09929>.
- McFarquhar, G. M., and Coauthors, 2011: Indirect and Semi-Direct Aerosol Campaign: The impact of Arctic aerosols on clouds. *Bull. Amer. Meteor. Soc.*, **92**, 183–201, <https://doi.org/10.1175/2010BAMS2935.1>.
- McGavin, R. E., and M. J. Vetter, 1963: Radio refractometry and its potential for humidity studies. *Applications*, Vol. 2, *Humidity and Moisture Measurement and Control in Science and Industry*, Reinhold, 553–560.
- McGibbon, J., and C. S. Bretherton, 2017: Skill of ship-following large-eddy simulations in reproducing MAGIC observations across the northeast Pacific stratocumulus to cumulus transition region. *J. Adv. Model. Earth Syst.*, **9**, 810–831, <https://doi.org/10.1002/2017MS000924>.
- McGillis, W. R., and Coauthors, 2004: Air–sea CO₂ exchange in the equatorial Pacific. *J. Geophys. Res.*, **109**, C08S02, <https://doi.org/10.1029/2003JC002256>.
- McNider, R. T., D. E. England, M. J. Friedman, and X. Shi, 1995: Predictability of the stable atmospheric boundary layer. *J. Atmos. Sci.*, **52**, 1602–1614, [https://doi.org/10.1175/1520-0469\(1995\)052<1602:POTSAB>2.0.CO;2](https://doi.org/10.1175/1520-0469(1995)052<1602:POTSAB>2.0.CO;2).
- Mejninger, W. M. L., A. E. Green, O. K. Hartogensis, W. Kohsiek, J. C. R. Hoedjes, R. M. Zuurbier, and H. A. R. DeBruin, 2002a: Determination of area-averaged water vapour fluxes with a large aperture scintillometer over a heterogeneous surface—Flevoland field experiment. *Bound.-Layer Meteor.*, **105**, 63–83, <https://doi.org/10.1023/A:1019683616097>.
- , O. K. Hartogensis, W. Kohsiek, J. C. B. Hoedjes, R. M. Zuurbier, and H. A. R. DeBruin, 2002b: Determination of area-averaged sensible heat fluxes with a large aperture scintillometer over a heterogeneous surface—Flevoland field experiment. *Bound.-Layer Meteor.*, **105**, 37–62, <https://doi.org/10.1023/A:1019647732027>.
- Melfi, S. H., and S. P. Palm, 2012: Estimating the orientation and spacing of midlatitude linear convective boundary layer features: Cloud streets. *J. Atmos. Sci.*, **69**, 352–364, <https://doi.org/10.1175/JAS-D-11-070.1>.
- Mellado, J. P., 2017: Cloud-top entrainment in stratocumulus clouds. *Annu. Rev. Fluid Mech.*, **49**, 145–169, <https://doi.org/10.1146/annurev-fluid-010816-060231>.
- Mellor, G., and T. Yamada, 1974: A hierarchy of turbulence closure models for planetary boundary layer. *J. Atmos. Sci.*, **31**, 1791–1806, [https://doi.org/10.1175/1520-0469\(1974\)031<1791:AHOTCM>2.0.CO;2](https://doi.org/10.1175/1520-0469(1974)031<1791:AHOTCM>2.0.CO;2).
- , and —, 1982: Development of a turbulence closure model for geophysical fluid problems. *Rev. Geophys.*, **20**, 851–875, <https://doi.org/10.1029/RG020i004p00851>.
- Meneveau, C., and J. Katz, 2000: Scale invariance and turbulence models for large-eddy simulations. *Annu. Rev. Fluid Mech.*, **32**, 1–32, <https://doi.org/10.1146/annurev.fluid.32.1.1>.
- , T. S. Lund, and W. H. Cabot, 1996: A lagrangian dynamic subgrid-scale model of turbulence. *J. Fluid Mech.*, **319**, 353–385, <https://doi.org/10.1017/S0022112096007379>.
- Mestayer, P. G., and S. Anquetin, 1995: Climatology of cities. *Diffusion and Transport of Pollutants in Atmospheric Mesoscale Flow Fields*, F.-S. Rys and A. Gyr, Eds., Atmospheric Sciences Library, Kluwer Academic Publishers, 165–189.
- Miguez-Macho, G., Y. Fan, C. P. Weaver, R. Walko, and A. Robock, 2007: Incorporating water table dynamics in climate modeling: 2. Formulation, validation, and soil moisture simulation. *J. Geophys. Res.*, **112**, D13108, <https://doi.org/10.1029/2006JD008112>.
- Mildner, P., 1932: Über Reibung in einer speziellen Luftmasse. *Beitr. Phys. Atmos.*, **19**, 151–158.
- Miller, M. A., and B. A. Albrecht, 1995: Surface-based remote sensing of mesoscale cloud structure during ASTEX. *J. Atmos. Sci.*, **52**, 2809–2826, [https://doi.org/10.1175/1520-0469\(1995\)052<2809:SBOOMC>2.0.CO;2](https://doi.org/10.1175/1520-0469(1995)052<2809:SBOOMC>2.0.CO;2).
- Mintz, Y., 1982: The sensitivity of numerically simulated climates to land surface conditions. *Land Surface Processes in Atmospheric General Circulation Models*, P. S. Eagleson, Ed., Cambridge University Press, 109–111.
- Mirocha, J., J. K. Lundquist, and B. Kosović, 2010: Implementation of a nonlinear subfilter turbulence stress model for large-eddy simulation in the Advanced Research WRF model. *Mon. Wea. Rev.*, **138**, 4212–4228, <https://doi.org/10.1175/2010MWR3286.1>.
- , G. Kirkil, E. Bou-Zeid, F. K. Chow, and B. Kosović, 2013: Transition and equilibration of neutral atmospheric boundary layer flow in one-way nested large-eddy simulations using the Weather Research and Forecasting model. *Mon. Wea. Rev.*, **141**, 918–940, <https://doi.org/10.1175/MWR-D-11-00263.1>.
- , B. Kosović, and G. Kirkil, 2014: Resolved turbulence characteristics in large-eddy simulations nested within mesoscale simulations using the Weather Research and Forecasting model. *Mon. Wea. Rev.*, **142**, 806–831, <https://doi.org/10.1175/MWR-D-13-00064.1>.

- Misra, P. K., 1982: Dispersion of nonbuoyant particles inside a convective boundary layer. *Atmos. Environ.*, **16**, 239–243, [https://doi.org/10.1016/0004-6981\(82\)90438-3](https://doi.org/10.1016/0004-6981(82)90438-3).
- Mitchell, K. E., and Coauthors, 2004: The multi-institution North American Land Data Assimilation System (NLDAS): Utilizing multiple GICP products and partners in a continental distributed hydrological modeling system. *J. Geophys. Res.*, **109**, D07S90, <https://doi.org/10.1029/2003JD003823>.
- Miura, Y., 1986: Aspect ratios of longitudinal rolls and convective cells observed during cold air outbreaks. *J. Atmos. Sci.*, **43**, 26–39, [https://doi.org/10.1175/1520-0469\(1986\)043<0026:AROLRA>2.0.CO;2](https://doi.org/10.1175/1520-0469(1986)043<0026:AROLRA>2.0.CO;2).
- Miyake, M., and G. McBean, 1970: On the measurement of vertical humidity transport over land. *Bound.-Layer Meteor.*, **1**, 88–101, <https://doi.org/10.1007/BF00193907>.
- Moene, A. F., and D. Schüttemeyer, 2008: The effects of surface heterogeneity on the temperature-humidity correlation and the relative transport efficiency. *Bound.-Layer Meteor.*, **129**, 99–113, <https://doi.org/10.1007/s10546-008-9312-z>.
- Moeng, C.-H., 1984: A large-eddy simulation model for the study of planetary boundary-layer turbulence. *J. Atmos. Sci.*, **41**, 2052–2062, [https://doi.org/10.1175/1520-0469\(1984\)041<2052:ALESMF>2.0.CO;2](https://doi.org/10.1175/1520-0469(1984)041<2052:ALESMF>2.0.CO;2).
- , and J. C. Wyngaard, 1989: Evaluation of turbulent transport and dissipation closures in second-order modeling. *J. Atmos. Sci.*, **46**, 2311–2330, [https://doi.org/10.1175/1520-0469\(1989\)046<2311:EOTTAD>2.0.CO;2](https://doi.org/10.1175/1520-0469(1989)046<2311:EOTTAD>2.0.CO;2).
- , and P. P. Sullivan, 1994: A comparison of shear- and buoyancy-driven boundary layer flows. *J. Atmos. Sci.*, **51**, 999–1022, [https://doi.org/10.1175/1520-0469\(1994\)051<0999:ACOSAB>2.0.CO;2](https://doi.org/10.1175/1520-0469(1994)051<0999:ACOSAB>2.0.CO;2).
- , and —, 2015: Large eddy simulation. *Encyclopedia of Atmospheric Science*, Vol. 4, G. North, J. Pylie, and F. Zhang, Eds., Academic Press, 232–240.
- , and Coauthors, 1996: Simulation of a stratocumulus-topped planetary boundary layer: Intercomparison among different numerical codes. *Bull. Amer. Meteor. Soc.*, **77**, 261–278, [https://doi.org/10.1175/1520-0477\(1996\)077<0261:SOASTP>2.0.CO;2](https://doi.org/10.1175/1520-0477(1996)077<0261:SOASTP>2.0.CO;2).
- , J. Dudhia, J. Klemp, and P. Sullivan, 2007: Examining two-way grid nesting for large eddy simulation of the PBL using the WRF model. *Mon. Wea. Rev.*, **135**, 2295–2311, <https://doi.org/10.1175/MWR3406.1>.
- Mohn, H., 1905: *Meteorology*. Vol. VI, *The Norwegian North Polar Expedition: 1893–1896, Scientific Results*, J. Dybwad, 659 pp.
- Moin, P., and K. Mahesh, 1998: Direct numerical simulation: A tool in turbulence research. *Annu. Rev. Fluid Mech.*, **30**, 539–578, <https://doi.org/10.1146/annurev.fluid.30.1.539>.
- Monin, A. S., 1959: Smoke propagation in the surface layer of the atmosphere. *Advances in Geophysics*, Vol. 6, Academic Press, 331–341.
- , and A. M. Obukhov, 1954: Basic laws of turbulent mixing in the ground layer of the atmosphere. *Akad. Nauk. SSSR. Geofiz. Inst. Tr.*, **151**, 163–187.
- , and A. M. Yaglom, 1971: *Statistical Fluid Mechanics: Mechanics of Turbulence*. Vol. I, MIT Press, 784 pp.
- Montgomery, R. B., 1940: Observations of vertical humidity distribution above the ocean surface and their relation to evaporation. *Papers in Physical Oceanography and Meteorology*, Vol. 7, MIT/WHOI, 30 pp.
- Morison, J., M. G. McPhee, and G. A. Maykut, 1987: Boundary layer, upper ocean, and ice observations in the Greenland Sea marginal ice zone. *J. Geophys. Res.*, **92**, 6987–7011, <https://doi.org/10.1029/JC092iC07p06987>.
- , and Coauthors, 1993: The LeadEx Experiment. *Eos, Trans. Amer. Geophys. Union*, **74**, 393–400, <https://doi.org/10.1029/93EO00341>.
- Morrison, H., G. de Boer, G. Feingold, J. Harrington, M. D. Shupe, and K. Sulia, 2011: Resilience of persistent Arctic mixed-phase clouds. *Nat. Geosci.*, **5**, 10–17, <https://doi.org/10.1038/ngeo1332>.
- Mortarini, L., M. Stefanello, G. Degrazia, D. Roberti, S. T. Castelli, and D. Anfossi, 2016: Characterization of wind meandering in low-wind-speed conditions. *Bound.-Layer Meteor.*, **161**, 165–182, <https://doi.org/10.1007/s10546-016-0165-6>.
- Muñoz-Esparza, D., J. K. Lundquist, J. A. Sauer, and B. Kosović, 2017: Coupled mesoscale-LES modeling of a diurnal cycle during the CWEX-13 field campaign: From weather to boundary-layer eddies. *J. Adv. Model. Earth Syst.*, **9**, 1572–1594, <https://doi.org/10.1002/2017MS000960>.
- Nadeau, D. F., E. R. Pardyjak, C. W. Higgins, and M. B. Parlange, 2013: Similarity scaling over a steep alpine slope. *Bound.-Layer Meteor.*, **147**, 401–419, <https://doi.org/10.1007/s10546-012-9787-5>.
- Nakanishi, M., and H. Niino, 2006: An improved Mellor–Yamada level 3 model: Its numerical stability and application to a regional prediction of advecting fog. *Bound.-Layer Meteor.*, **119**, 397–407, <https://doi.org/10.1007/s10546-005-9030-8>.
- , and —, 2009: Development of an improved closure model for the atmospheric boundary layer. *J. Meteor. Soc. Japan*, **87**, 895–912, <https://doi.org/10.2151/jmsj.87.895>.
- Neggers, R. A., M. Köhler, and A. C. Beljaars, 2009: A dual mass flux framework for boundary layer convection. Part I: Transport. *J. Atmos. Sci.*, **66**, 1465–1487, <https://doi.org/10.1175/2008JAS2635.1>.
- Neiburger, M., D. S. Johnson, and C.-W. Chien, 1961: Studies of the structure of the atmosphere over the eastern Pacific Ocean in Summer. University of California Publications in Meteorology, Vol. 1, No. 1, University of California Press, 94 pp.
- Newman, A. J., N. Mizukami, M. P. Clark, A. W. Wood, B. Nijssen, and G. Nearing, 2017: Benchmarking of a physically based hydrologic model. *J. Hydrometeorol.*, **18**, 2215–2225, <https://doi.org/10.1175/JHM-D-16-0284.1>.
- Nicholls, S., 1984: The dynamics of stratocumulus: Aircraft observations and comparisons with a mixed layer model. *Quart. J. Roy. Meteor. Soc.*, **110**, 783–820, <https://doi.org/10.1002/qj.49711046603>.
- , and M. A. LeMone, 1980: The fair-weather boundary layer in GATE: The relationship of subcloud fluxes and structure to the distribution and enhancement of cumulus clouds. *J. Atmos. Sci.*, **37**, 2051–2067, [https://doi.org/10.1175/1520-0469\(1980\)037<2051:TFWBLLI>2.0.CO;2](https://doi.org/10.1175/1520-0469(1980)037<2051:TFWBLLI>2.0.CO;2).
- , and J. D. Turton, 1986: An observational study of the structure of stratiform cloud layers: Part II. Entrainment. *Quart. J. Roy. Meteor. Soc.*, **112**, 461–480, <https://doi.org/10.1002/qj.49711247210>.
- Nieuwstadt, F. T. M., 1980: application of mixed-layer similarity to the observed dispersion from a ground-level source. *J. Appl. Meteorol.*, **19**, 157–162, [https://doi.org/10.1175/1520-0450\(1980\)019<0157:AOMLST>2.0.CO;2](https://doi.org/10.1175/1520-0450(1980)019<0157:AOMLST>2.0.CO;2).
- , 1984: The turbulent structure of the stable, nocturnal boundary layer. *J. Atmos. Sci.*, **41**, 2202–2216, [https://doi.org/10.1175/1520-0469\(1984\)041<2202:TTSOTS>2.0.CO;2](https://doi.org/10.1175/1520-0469(1984)041<2202:TTSOTS>2.0.CO;2).
- , 1998: Turbulence and similarity theory meteorology and engineering. *Clear and Cloudy Boundary Layers: Proceedings of the Colloquium “Clear and Cloudy Boundary Layers,”* P. Duynkerke and A. Holtslag, Eds., Royal Netherlands Academy of Arts and Sciences, 43–66.

- , and A. P. van Ulden, 1978: A numerical study of vertical dispersion of passive contaminants from a continuous source in the atmospheric surface layer. *Atmos. Environ.*, **12**, 2119–2124, [https://doi.org/10.1016/0004-6981\(78\)90166-X](https://doi.org/10.1016/0004-6981(78)90166-X).
- , P. J. Mason, C.-H. Moeng, and U. Schumann, 1992: Large-eddy simulation of the convective boundary layer: A comparison of four computer codes. *Turbulent Shear Flows*, Vol. 8, F. Durst et al., Eds., 343–367, https://doi.org/10.1007/978-3-642-77674-8_24.
- Niu, G. Y., and Coauthors, 2011: The community Noah land surface model with multiparameterization options (Noah-MP): 1. Model description and evaluation with local-scale measurements. *J. Geophys. Res.*, **116**, D12109, <https://doi.org/10.1029/2010JD015139>.
- Noh, Y., W. G. Cheon, S. Y. Hong, and S. Raasch, 2003: Improvement of the K-profile model for the planetary boundary layer based on large eddy simulation data. *Bound.-Layer Meteor.*, **107**, 401–427, <https://doi.org/10.1023/A:1022146015946>.
- Noilhan, J., and S. Planton, 1989: A simple parameterization of land surface processes for meteorological models. *Mon. Wea. Rev.*, **117**, 536–549, [https://doi.org/10.1175/1520-0493\(1989\)117<0536:ASPOLS>2.0.CO;2](https://doi.org/10.1175/1520-0493(1989)117<0536:ASPOLS>2.0.CO;2).
- Oberbeck, A., 1888: On the phenomena of motion in the atmosphere. *Sitzungsberichte der Königlich Preussischen Akademie der Wissenschaften*, Deutsche Akademie der Wissenschaften zu Berlin, 383–395.
- O'Brien, J. J., 1970: A note on the vertical structure of the eddy exchange coefficient. *J. Atmos. Sci.*, **27**, 1213–1215, [https://doi.org/10.1175/1520-0469\(1970\)027<1213:ANOTVS>2.0.CO;2](https://doi.org/10.1175/1520-0469(1970)027<1213:ANOTVS>2.0.CO;2).
- Obukhov, A. M., 1941: Energy distribution in the spectrum of a turbulent flow. *Izv. Akad. Nauk SSSR, Ser. Geogr. Geofiz.*, **4–5**, 453–466.
- , 1946: Turbulence in thermally inhomogeneous atmosphere. *Tr. Inst. Teoret. Geofiz. Akad. Nauk SSSR*, **1**, 95–115.
- , 1971: Turbulence in an atmosphere with a non-uniform temperature. *Bound.-Layer Meteor.*, **2**, 7–29, <https://doi.org/10.1007/BF00718085>.
- Oke, T. R., 1982: The energetic basis of the urban heat island. *Quart. J. Roy. Meteor. Soc.*, **108**, 1–24, <https://doi.org/10.1002/qj.49710845502>.
- Oleson, K. W., and Coauthors, 2010: Technical description of version 4.0 of the Community Land Model (CLM). NCAR Tech. Note NCAR/TN-478+STR, 257 pp., <https://doi.org/10.5065/D6FB50WZ>.
- , and Coauthors, 2013: Technical description of version 4.5 of the Community Land Model (CLM). NCAR Tech. Note NCAR/TN-503+STR, 420 pp., <https://doi.org/10.5065/D6RR1W7M>.
- , G. B. Bonan, J. Feddema, M. Vertenstein, and C. S. B. Grimmond, 2008: An urban parameterization for a global climate model. Part I: Formulation and evaluation for two cities. *J. Appl. Meteor. Climatol.*, **47**, 1038–1060, <https://doi.org/10.1175/2007JAMC1597.1>.
- Oncley, S. P., and Coauthors, 2007: The energy balance experiment EBEX-2000. Part I: Overview and energy balances. *Bound.-Layer Meteor.*, **126**, 185–202, <https://doi.org/10.1007/s10546-007-9161-1>.
- Ookouchi, Y., M. Segal, R. C. Kessler, and R. A. Pielke, 1984: Evaluation of soil moisture effects on the generation and modification of mesoscale circulations. *Mon. Wea. Rev.*, **112**, 2281–2292, [https://doi.org/10.1175/1520-0493\(1984\)112<2281:EOSMEO>2.0.CO;2](https://doi.org/10.1175/1520-0493(1984)112<2281:EOSMEO>2.0.CO;2).
- Orszag, S. A., and G. S. Patterson, 1972: Numerical simulation of three-dimensional homogeneous isotropic turbulence. *Phys. Rev. Lett.*, **28**, 76–79, <https://doi.org/10.1103/PhysRevLett.28.76>.
- Paeschke, W., 1937: Experimentelle Untersuchungen zum Rauigkeits- und Stabilitätsproblem in der bodennahen Luftschicht. *Beitr. Phys. Atmos.*, **24**, 163–189.
- Paluch, I. R., D. H. Lenschow, S. Siems, S. McKeen, G. L. Kok, and R. D. Schillawski, 1994: Evolution of the subtropical marine boundary layer: comparison of soundings over the eastern Pacific from FIRE and HaRP. *J. Atmos. Sci.*, **51**, 1465–1479, [https://doi.org/10.1175/1520-0469\(1994\)051<1465:EOTSMB>2.0.CO;2](https://doi.org/10.1175/1520-0469(1994)051<1465:EOTSMB>2.0.CO;2).
- Pan, H. L., and L. Mahrt, 1987: Interaction between soil hydrology and boundary-layer development. *Bound.-Layer Meteor.*, **38**, 185–202, <https://doi.org/10.1007/BF00121563>.
- Panofsky, H. A., 1963: Determination of stress from wind and temperature measurements. *Quart. J. Roy. Meteor. Soc.*, **89**, 85–94, <https://doi.org/10.1002/qj.49708937906>.
- , H. Tennekes, D. H. Lenschow, and J. C. Wyngaard, 1977: The characteristics of turbulent velocity components in the surface layer under convective conditions. *Bound.-Layer Meteor.*, **11**, 355–361, <https://doi.org/10.1007/BF02186086>.
- Park, S., and C. S. Bretherton, 2009: The University of Washington shallow convection and moist turbulence schemes and their impact on climate simulations with the Community Atmosphere Model. *J. Climate*, **22**, 3449–3469, <https://doi.org/10.1175/2008JCLI2557.1>.
- Pasquill, F., 1972: Some aspects of boundary layer description. *Quart. J. Roy. Meteor. Soc.*, **98**, 469–494, <https://doi.org/10.1002/qj.49709841702>.
- , and F. B. Smith, 1983: *Atmospheric Diffusion*. 3rd ed. Wiley, 437 pp.
- Passalacqua P, F. Porté-Agel, E. Foufoula-Georgiou, and C. Paola, 2006: Application of dynamic subgrid-scale concepts from large-eddy simulation to modeling landscape evolution. *Water Resour. Res.*, **42**, W06D11, <https://doi.org/10.1029/2006WR004879>.
- Patton, E. G., and J. J. Finnigan, 2013: Canopy turbulence. *Overview and Fundamentals*, Vol. 1, *Handbook of Environmental Fluid Dynamics*, H. J. S. Fernando, Ed., CRC Press, 311–328.
- , and Coauthors, 2011: The Canopy Horizontal Array Turbulence Study. *Bull. Amer. Meteor. Soc.*, **92**, 593–611, <https://doi.org/10.1175/2010BAMS2614.1>.
- , P. P. Sullivan, R. H. Shaw, J. J. Finnigan, and J. C. Weil, 2016: Atmospheric stability influences on coupled boundary layer canopy turbulence. *J. Atmos. Sci.*, **73**, 1621–1647, <https://doi.org/10.1175/JAS-D-15-0068.1>.
- Paulson, C. A., 1970: The mathematical representation of wind speed and temperature profiles in the unstable atmospheric surface layer. *J. Appl. Meteor.*, **9**, 857–861, [https://doi.org/10.1175/1520-0450\(1970\)009<0857:TMROWS>2.0.CO;2](https://doi.org/10.1175/1520-0450(1970)009<0857:TMROWS>2.0.CO;2).
- Pearson, H. J., J. S. Puttock, and J. C. R. Hunt, 1983: A statistical model of fluid-element motions and vertical diffusion in a homogeneous stratified turbulent flow. *J. Fluid Mech.*, **129**, 219–249, <https://doi.org/10.1017/S0022112083000749>.
- Pergaud, J., V. Masson, S. Malardel, and F. Couvreur, 2009: A parameterization of dry thermals and shallow cumuli for mesoscale numerical weather prediction. *Bound.-Layer Meteor.*, **132**, 83–106, <https://doi.org/10.1007/s10546-009-9388-0>.
- Persson, P. O. G., 2012: Onset and end of the summer melt season over sea ice: Thermal structure and surface energy perspective from SHEBA. *Climate Dyn.*, **39**, 1349–137, <https://doi.org/10.1007/s00382-011-1196-9>.

- , and T. Vihma, 2017: The atmosphere over sea ice. *Sea Ice*, 3rd ed. D. N. Thomas, Ed., John Wiley & Sons, <https://doi.org/10.1002/9781118778371.ch6>.
- , C. W. Fairall, E. L. Andreas, P. S. Guest, and D. K. Perovich, 2002: Measurements near the Atmospheric Surface Flux Group tower at SHEBA: Near-surface conditions and surface energy budget. *J. Geophys. Res.*, **107**, 8045, <https://doi.org/10.1029/2000JC000705>.
- Phelps, G. T., and S. Pond, 1971: Spectra of the temperature and humidity fluctuations and of the fluxes of moisture and sensible heat in the marine boundary layer. *J. Atmos. Sci.*, **28**, 918–928, [https://doi.org/10.1175/1520-0469\(1971\)028<0918:SOTTAH>2.0.CO;2](https://doi.org/10.1175/1520-0469(1971)028<0918:SOTTAH>2.0.CO;2).
- Phillips, N. A., 1986: Turbulent mixing near the ground for nested grid model. National Meteorological Center, National Weather Service/NOAA Office Note 318, 19 pp.
- Physick, W., 1976: A numerical model of the sea-breeze phenomenon over a lake or gulf. *J. Atmos. Sci.*, **33**, 2107–2135, [https://doi.org/10.1175/1520-0469\(1976\)033<2107:ANMOTS>2.0.CO;2](https://doi.org/10.1175/1520-0469(1976)033<2107:ANMOTS>2.0.CO;2).
- , and N. J. Tapper, 1990: A numerical study of circulations induced by a dry salt lake. *Mon. Wea. Rev.*, **118**, 1029–1042, [https://doi.org/10.1175/1520-0493\(1990\)118<1029:ANSOCI>2.0.CO;2](https://doi.org/10.1175/1520-0493(1990)118<1029:ANSOCI>2.0.CO;2).
- Pielke, R. A., and Coauthors, 1992: A comprehensive meteorological modeling system—RAMS. *Meteor. Atmos. Phys.*, **49**, 69–91, <https://doi.org/10.1007/BF01025401>.
- , T. J. Lee, J. H. Copeland, J. L. Eastman, C. L. Ziegler, and C. A. Finley, 1997: Use of USGS-provided data to improve weather and climate simulations. *Ecol. Appl.*, **7**, 3–21, [https://doi.org/10.1890/1051-0761\(1997\)007\[0003:UOUPDT\]2.0.CO;2](https://doi.org/10.1890/1051-0761(1997)007[0003:UOUPDT]2.0.CO;2).
- Pierrehumbert, R. T., and S. E. Widnall, 1982: The two- and three-dimensional instabilities of a spatially periodic shear layer. *J. Fluid Mech.*, **114**, 59–82, <https://doi.org/10.1017/S0022112082000044>.
- Pithan, F., B. Medeiros, and T. Mauritsen, 2014: Mixed-phase clouds cause climate model biases in Arctic wintertime temperature inversion. *Climate Dyn.*, **43**, 289–303, <https://doi.org/10.1007/s00382-013-1964-9>.
- Plant, W. J., 1982: A relationship between wind stress and wave slope. *J. Geophys. Res.*, **87**, 1961–1967, <https://doi.org/10.1029/JC087iC03p01961>.
- Pleim, J. E., 2007: A combined local and nonlocal closure model for the atmospheric boundary layer. Part I: Model description and testing. *J. Appl. Meteor. Climatol.*, **46**, 1383–1395, <https://doi.org/10.1175/JAM2539.1>.
- Pond, S., G. T. Phelps, J. E. Paquin, G. McBean, and R. W. Stewart, 1971: Measurements of the turbulent fluxes of momentum, moisture, and sensible heat over the ocean. *J. Atmos. Sci.*, **28**, 901–917, [https://doi.org/10.1175/1520-0469\(1971\)028<0901:MOTTFO>2.0.CO;2](https://doi.org/10.1175/1520-0469(1971)028<0901:MOTTFO>2.0.CO;2).
- Porté-Agel, F., 2004: A scale-dependent dynamic model for scalar transport in large-eddy simulations of the atmospheric boundary layer. *Bound.-Layer Meteor.*, **112**, 81–105, <https://doi.org/10.1023/B:BOUN.0000020353.03398.20>.
- , C. Meneveau, and M. B. Parlange, 2000: A scale-dependent dynamic model for large-eddy simulation: application to a neutral atmospheric boundary layer. *J. Fluid Mech.*, **415**, 261–284, <https://doi.org/10.1017/S0022112000008776>.
- , M. Pahlow, C. Meneveau, and M. B. Parlange, 2001: Atmospheric stability effect on subgrid-scale physics for large-eddy simulation. *Adv. Water Resour.*, **24**, 1085–1102, [https://doi.org/10.1016/S0309-1708\(01\)00039-2](https://doi.org/10.1016/S0309-1708(01)00039-2).
- Poulos, G., and Coauthors, 2002: CASES-99—A comprehensive investigation of the stable nocturnal boundary layer. *Bull. Amer. Meteor. Soc.*, **83**, 555–581, [https://doi.org/10.1175/1520-0477\(2002\)083<0555:CACIOT>2.3.CO;2](https://doi.org/10.1175/1520-0477(2002)083<0555:CACIOT>2.3.CO;2).
- Prandtl, L., 1905: Über Flüssigkeitsbewegung bei sehr kleiner Reibung. *Verhaglungen des Dritten Internationalen Mathematiker-Kongresses in Heidelberg 1904*, A. Krazer, Ed., Teubner, 484–491.
- , 1925: Bericht über Untersuchungen zur ausgebildeten Turbulenz. *Z. Angew. Math. Mech.*, **5**, 136–139, <https://doi.org/10.1002/zamm.19250050212>.
- , 1932: Meteorologische Anwendung der Strömungslehre. *Beitr. Z. Phys. Atmos.*, **19**, 188–202.
- Prenni, A. J., and Coauthors, 2007: Can ice-nucleating aerosols affect Arctic seasonal climate? *Bull. Amer. Meteor. Soc.*, **88**, 541–550, <https://doi.org/10.1175/BAMS-88-4-541>.
- Priestley, C. H. B., and W. C. Swinbank, 1947: Vertical transport of heat by turbulence in the atmosphere. *Proc. Roy. Soc. London*, **189**, 543–561, <https://doi.org/10.1098/rspa.1947.0057>.
- Randall, D. A., 1980: Conditional instability of the first kind up-side-down. *J. Atmos. Sci.*, **37**, 125–130, [https://doi.org/10.1175/1520-0469\(1980\)037<0125:CIOTFK>2.0.CO;2](https://doi.org/10.1175/1520-0469(1980)037<0125:CIOTFK>2.0.CO;2).
- , and Coauthors, 2003: Confronting models with data: The GEWEX cloud systems study. *Bull. Amer. Meteor. Soc.*, **84**, 455–469, <https://doi.org/10.1175/BAMS-84-4-455>.
- , and Coauthors, 2019: 100 years of Earth system model development. *A Century of Progress in Atmospheric and Related Sciences: Celebrating the American Meteorological Society Centennial*, Meteor. Monogr., No. 59, Amer. Meteor. Soc., 10.1175/AMSMONOGRAPHS-D-18-0018.1.
- Rasmussen, R., and Coauthors, 2011: High-resolution coupled climate runoff simulations of seasonal snowfall over Colorado: A process study of current and warmer climate. *J. Climate*, **24**, 3015–3048, <https://doi.org/10.1175/2010JCLI3985.1>.
- Rauber, R. M., and Coauthors, 2007: Rain in shallow cumulus over the ocean: The RICO campaign. *Bull. Amer. Meteor. Soc.*, **88**, 1912–1928, <https://doi.org/10.1175/BAMS-88-12-1912>.
- Raupach, M. R., and A. S. Thom, 1981: Turbulence in and above plant canopies. *Annu. Rev. Fluid Mech.*, **13**, 97–129, <https://doi.org/10.1146/annurev.fl.13.010181.000525>.
- , R. A. Antonia, and S. Rajagopalan, 1991: Rough-wall turbulent boundary layers. *Appl. Mech. Rev.*, **44**, 1–25, <https://doi.org/10.1115/1.3119492>.
- , J. J. Finnigan, and Y. Brunet, 1996: Coherent eddies and turbulence in vegetation canopies: The mixing-layer analogy. *Bound.-Layer Meteor.*, **78**, 351–382, <https://doi.org/10.1007/BF00120941>.
- Reynolds, O., 1883: An experimental investigation of the circumstances which determine whether the motion of water shall be direct or sinuous and the law of resistance in parallel channels. *Philos. Trans. Roy. Soc.*, **174A**, 935–982, <https://doi.org/10.1098/rstl.1883.0029>.
- , 1895: On the dynamical theory of incompressible viscous fluids and the determination of the criterion. *Philos. Trans. Roy. Soc.*, **186A**, 123–164, <https://doi.org/10.1098/rsta.1895.0004>.
- Reynolds, W. C., 1976: Computation of turbulent flows. *Annu. Rev. Fluid Mech.*, **8**, 183–209, <https://doi.org/10.1146/annurev.fl.08.010176.001151>.
- Richardson, L. F., 1920: The supply of energy from and to atmospheric eddies. *Proc. Roy. Soc. London*, **97A**, 354–373, <https://doi.org/10.1098/rspa.1920.0039>.
- , 1922: *Weather Prediction by Numerical Process*. Cambridge University Press, 236 pp.
- , 1926: Atmospheric diffusion shown on a distance-neighbour graph. *Philos. Trans. Roy. Soc.*, **110A**, 709–737, <https://doi.org/10.1098/rspa.1926.0043>.

- Richter, D. H., and P. P. Sullivan, 2014: The sea spray contribution to sensible heat flux. *J. Atmos. Sci.*, **71**, 640–654, <https://doi.org/10.1175/JAS-D-13-0204.1>.
- Richter, J. P., 1970: *The Notebooks of Leonardo da Vinci: Compiled and Edited from the Original Manuscripts*. Dover Publications, 866 pp.
- Rieder, K. F., J. A. Smith, and R. A. Weller, 1994: Observed directional characteristics of wind, wind stress, and surface waves on the open ocean. *J. Geophys. Res.*, **99**, 22 589–22 596, <https://doi.org/10.1029/94JC02215>.
- Riehl, H., C. Yeh, J. S. Malkus, and N. E. LaSeur, 1951: On the heat balance and maintenance of the circulation in the trades. *Quart. J. Roy. Meteor. Soc.*, **77**, 598–626, <https://doi.org/10.1002/qj.49707733405>.
- Roach, W. T., R. Brown, S. J. Caughey, B. A. Crease, and A. Slingo, 1982: A field study of nocturnal stratocumulus: I. Mean structure and budgets. *Quart. J. Roy. Meteor. Soc.*, **108**, 103–123, <https://doi.org/10.1002/qj.49710845507>.
- Robinson, I. S., 2004: *Measuring the Oceans from Space: The Principles and Methods of Satellite Oceanography*. Geophysical Sciences, Springer-Praxis, 669 pp.
- Rodell, M., and Coauthors, 2004: The global land data assimilation system. *Bull. Amer. Meteor. Soc.*, **85**, 381–394, <https://doi.org/10.1175/BAMS-85-3-381>.
- Romanov, I. P., Yu. B. Konstantinov, and N. A. Kornilov, 1997: *Ice Drift Stations “North Pole” (1937–1991)* (in Russian). 2nd ed. Gidrometeoizdat, 226 pp.
- Rosero, E., Z. L. Yang, L. E. Gulden, G. Y. Niu, and D. J. Gochis, 2009: Evaluating enhanced hydrological representations in Noah-LSM over transition zones: Implications for model development. *J. Hydrometeor.*, **10**, 600–622, <https://doi.org/10.1175/2009JHM1029.1>.
- Rossby, C.-G., 1927: The theory of atmospheric turbulence: an historical resumé and an outlook. *Mon. Wea. Rev.*, **55**, 6–10, [https://doi.org/10.1175/1520-0493\(1927\)55<6:TTOATH>2.0.CO;2](https://doi.org/10.1175/1520-0493(1927)55<6:TTOATH>2.0.CO;2).
- , and R. B. Montgomery, 1935: The layer of frictional influence in wind and ocean currents. *Papers in Physical Oceanography and Meteorology*, Vol. 3, No. 3, MIT/WHOI, 3, No. 3, <https://doi.org/10.1575/1912/1157>.
- Rothermel, J., and E. M. Agee, 1980: Aircraft investigation of mesoscale cellular convection during AMTEX 1975. *J. Atmos. Sci.*, **37**, 1027–1040, [https://doi.org/10.1175/1520-0469\(1980\)037<1027:AIOMCC>2.0.CO;2](https://doi.org/10.1175/1520-0469(1980)037<1027:AIOMCC>2.0.CO;2).
- Rouse, J. W., R. H. Haas, J. A. Schell, D. W. Deering, and J. C. Harlan, 1974: Monitoring the vernal advancement and retrogradation (greenwave effect) of natural vegetation. NASA/GSFC Type III Final Rep., 8 pp., <https://ntrs.nasa.gov/archive/nasa/casi.ntrs.nasa.gov/19740022555.pdf>.
- Rowntree, P. R., and J. A. Bolton, 1983: Simulation of the atmospheric response to soil moisture anomalies over Europe. *Quart. J. Roy. Meteor. Soc.*, **109**, 501–526, <https://doi.org/10.1002/qj.49710946105>.
- Ruffieux, D., P. O. G. Persson, C. W. Fairall, and D. E. Wolfe, 1995: Ice pack and lead surface energy budgets during LEADDEX 1992. *J. Geophys. Res.*, **100**, 4593–4612, <https://doi.org/10.1029/94JC02485>.
- Saito, K., and Coauthors, 2006: The operational JMA non-hydrostatic mesoscale model. *Mon. Wea. Rev.*, **134**, 1266–1298, <https://doi.org/10.1175/MWR3120.1>.
- Salesky, S. T., M. Chamecki, and E. Bou-Zeid, 2017: On the nature of the transition between rolls and cellular organization in the convective boundary layer. *Bound.-Layer Meteor.*, **163**, 41–68, <https://doi.org/10.1007/s10546-016-0220-3>.
- Sawford, B. L., 2004: Micro-mixing modelling of scalar fluctuations for plumes in homogeneous turbulence. *Flow Turbul. Combust.*, **72**, 133–160, <https://doi.org/10.1023/B:APPL.0000044409.74300.db>.
- Schalkwijk, J., H. J. J. Jonker, A. P. Siebesma, and E. V. Meijgaard, 2015: Weather forecasting using GPU-based large-eddy simulations. *Bull. Amer. Meteor. Soc.*, **96**, 715–723, <https://doi.org/10.1175/BAMS-D-14-00114.1>.
- Schmauss, A., 1920: Seewind ohne See. *Meteor. Z.*, **37**, 154–155.
- Schmid, H. P., 1994: Source areas for scalars and scalar fluxes. *Bound.-Layer Meteor.*, **67**, 293–318, <https://doi.org/10.1007/BF00713146>.
- Schotland, R. M., 1955: The measurement of wind velocity by sonic means. *J. Meteor.*, **12**, 386–390, [https://doi.org/10.1175/1520-0469\(1955\)012<0386:TMOWVB>2.0.CO;2](https://doi.org/10.1175/1520-0469(1955)012<0386:TMOWVB>2.0.CO;2).
- Schröder, D., T. Vihma, A. Kerber, and B. Brümmer, 2003: On the parameterization of turbulent surface fluxes over heterogeneous sea ice surfaces. *J. Geophys. Res.*, **108**, 3195, <https://doi.org/10.1029/2002JC001385>.
- Schuepp, P. H., M. Y. Leclerc, J. I. McPherson, and R. L. Desjardins, 1990: Footprint prediction of scalar fluxes from analytical solutions of the diffusion equations. *Bound.-Layer Meteor.*, **50**, 355–373, <https://doi.org/10.1007/BF00120530>.
- , J. I. McPherson, and R. L. Desjardins, 1992: Adjustment of footprint correction for airborne flux mapping over the FIFE site. *J. Geophys. Res.*, **97**, 18 455–18 466, <https://doi.org/10.1029/92JD00884>.
- Schytt, V., 1983: Ymer-80: A Swedish expedition to the Arctic Ocean. *Geogr. J.*, **149**, 22–28, <https://doi.org/10.2307/633339>.
- Scorer, R. S., 1978: *Natural Aerodynamics*. Ellis Horwood, 488 pp.
- Sedlar, J., and Coauthors, 2011: A transitioning Arctic surface energy budget: The impacts of solar zenith angle, surface albedo and cloud radiative forcing. *Climate Dyn.*, **37**, 1643–1660, <https://doi.org/10.1007/s00382-010-0937-5>.
- Seifert, A., T. Heus, R. Pincus, and B. Stevens, 2015: Large-eddy simulation of the transient and near-equilibrium behavior of precipitating shallow convection. *J. Adv. Model. Earth Syst.*, **7**, 1918–1937, <https://doi.org/10.1002/2015MS000489>.
- Sellers, P. J., Y. Mintz, Y. E. A. Sud, and A. Dalcher, 1986: A simple biosphere model (SiB) for use within general circulation models. *J. Atmos. Sci.*, **43**, 505–531, [https://doi.org/10.1175/1520-0469\(1986\)043<0505:ASBMFU>2.0.CO;2](https://doi.org/10.1175/1520-0469(1986)043<0505:ASBMFU>2.0.CO;2).
- , F. G. Hall, G. Asrar, D. E. Strebel, and R. E. Murphy, 1992: An overview of the First International Satellite Land Surface Climatology Project (ISLSCP) field experiment (FIFE). *J. Geophys. Res.*, **97**, 18 345–18 371, <https://doi.org/10.1029/92JD02111>.
- Serreze, M. C., J. D. Kahl, and R. C. Schnell, 1992: Low-level temperature inversions of the Eurasian Arctic and comparisons with Soviet drifting station data. *J. Climate*, **5**, 615–629, [https://doi.org/10.1175/1520-0442\(1992\)005<0615:LLTIOT>2.0.CO;2](https://doi.org/10.1175/1520-0442(1992)005<0615:LLTIOT>2.0.CO;2).
- Suuffert, G., P. Gross, C. Simmer, and E. F. Wood, 2002: The influence of hydrologic modeling on the predicted local weather: Two-way coupling of a mesoscale weather prediction model and a land surface hydrologic model. *J. Hydrometeor.*, **3**, 505–523, [https://doi.org/10.1175/1525-7541\(2002\)003<0505:TIOHMO>2.0.CO;2](https://doi.org/10.1175/1525-7541(2002)003<0505:TIOHMO>2.0.CO;2).
- Sfyri, E., M. W. Rotach, I. Stiperski, F. Bosveld, M. Lehner, and F. Obleitner, 2018: Scalar-flux similarity in the layer near the surface over mountainous terrain. *Bound.-Layer Meteor.*, **169**, 11–46, <https://doi.org/10.1007/s10546-018-0365-3>.
- Shah, S., and E. Bou-Zeid, 2014: Direct numerical simulations of turbulent Ekman layers with increasing static stability:

- Modifications to the bulk structure and second-order statistics. *J. Fluid Mech.*, **760**, 494–539, <https://doi.org/10.1017/jfm.2014.597>.
- Shapiro, A., and E. Fedorovich, 2008: Coriolis effects in homogeneous and inhomogeneous katabatic flows. *Quart. J. Roy. Meteor. Soc.*, **134**, 353–370, <https://doi.org/10.1002/qj.217>.
- , —, and S. Rahimi, 2016: A unified theory for the Great Plains nocturnal low-level jet. *J. Atmos. Sci.*, **73**, 3037–3057, <https://doi.org/10.1175/JAS-D-15-0307.1>.
- Sharma, V., M. B. Parlange, and M. Calaf, 2017: Perturbations to the spatial and temporal characteristics of the diurnal-varying atmospheric boundary layer due to an extensive wind farm. *Bound.-Layer Meteor.*, **162**, 255–282, <https://doi.org/10.1007/s10546-016-0195-0>.
- Shaw, R. H., and U. Schumann, 1992: Large-eddy simulation of turbulent flow above and within a forest. *Bound.-Layer Meteor.*, **61**, 47–64, <https://doi.org/10.1007/BF02033994>.
- , and E. G. Patton, 2003: Canopy element influences on resolved- and subgrid-scale energy within a large-eddy simulation. *Agric. For. Meteorol.*, **115**, 5–17, [https://doi.org/10.1016/S0168-1923\(02\)00165-X](https://doi.org/10.1016/S0168-1923(02)00165-X).
- , J. Tavangar, and D. P. Ward, 1983: Structure of the Reynolds stress in a canopy layer. *J. Appl. Meteor.*, **22**, 1922–1931, [https://doi.org/10.1175/1520-0450\(1983\)022<1922:SOTRSI>2.0.CO;2](https://doi.org/10.1175/1520-0450(1983)022<1922:SOTRSI>2.0.CO;2).
- , G. Hartog, and H. H. Neumann, 1988: Influence of foliar density and thermal stability on profiles of Reynolds stress and turbulence intensity in a deciduous forest. *Bound.-Layer Meteor.*, **45**, 391–409, <https://doi.org/10.1007/BF00124010>.
- , Y. Brunet, J. J. Finnigan, and M. R. Raupach, 1995: A wind tunnel study of air flow in waving wheat: Two-point velocity statistics. *Bound.-Layer Meteor.*, **76**, 349–376, <https://doi.org/10.1007/BF00709238>.
- , E. G. Patton, and J. J. Finnigan, 2013: Coherent eddy structures over plant canopies. *Coherent Flow Structures at Earth's Surface*, John Wiley & Sons, 149–159, <https://doi.org/10.1002/9781118527221.ch10>.
- Shi, X., F. K. Chow, R. L. Street, and G. H. Bryan, 2018a: An evaluation of LES turbulence models for scalar mixing in the stratocumulus-capped boundary layer. *J. Atmos. Sci.*, **75**, 1499–1507, <https://doi.org/10.1175/JAS-D-17-0392.1>.
- , H. L. Hagan, F. K. Chow, G. H. Bryan, and R. L. Street, 2018b: Large-eddy simulation of the stratocumulus-capped boundary layer with explicit filtering and reconstruction turbulence modeling. *J. Atmos. Sci.*, **75**, 611–637, <https://doi.org/10.1175/JAS-D-17-0162.1>.
- Shin, H. H., and J. Dudhia, 2016: Evaluation of PBL parameterization in WRF at sub-kilometer resolution: Turbulence statistics in the convective boundary layer. *Mon. Wea. Rev.*, **144**, 1161–1177, <https://doi.org/10.1175/MWR-D-15-0208.1>.
- Shupe, M. D., 2011: Clouds at Arctic Atmospheric Observatories, Part II: Thermodynamic phase characteristics. *J. Appl. Meteor. Climatol.*, **50**, 645–661, <https://doi.org/10.1175/2010JAMC2468.1>.
- , P. O. G. Persson, I. M. Brooks, M. Tjernström, J. Sedlar, T. Mauritsen, S. Sjogren, and C. Leck, 2013: Cloud and boundary layer interactions over the Arctic sea-ice in late summer. *Atmos. Chem. Phys.*, **13**, 9379–9400, <https://doi.org/10.5194/acp-13-9379-2013>.
- Siebesma, A. P., and Coauthors, 2003: A large eddy simulation intercomparison study of shallow cumulus convection. *J. Atmos. Sci.*, **60**, 1201–1219, [https://doi.org/10.1175/1520-0469\(2003\)60<1201:ALESIS>2.0.CO;2](https://doi.org/10.1175/1520-0469(2003)60<1201:ALESIS>2.0.CO;2).
- , P. M. Soares, and J. Teixeira, 2007: A combined eddy-diffusivity mass-flux approach for the convective boundary layer. *J. Atmos. Sci.*, **64**, 1230–1248, <https://doi.org/10.1175/JAS3888.1>.
- Simpson, J. E., 1982: Gravity currents in the laboratory, atmosphere, and ocean. *Annu. Rev. Fluid Mech.*, **14**, 213–234, <https://doi.org/10.1146/annurev.fl.14.010182.001241>.
- Smagorinsky, J., 1963: General circulation experiments with the primitive equation. *Mon. Wea. Rev.*, **91**, 99–165, [https://doi.org/10.1175/1520-0493\(1963\)091<0099:GCEWTP>2.3.CO;2](https://doi.org/10.1175/1520-0493(1963)091<0099:GCEWTP>2.3.CO;2).
- Smirnova, T. G., J. M. Brown, and S. G. Benjamin, 1997: Performance of different soil model configurations in simulating ground surface temperature and surface fluxes. *Mon. Wea. Rev.*, **125**, 1870–1884, [https://doi.org/10.1175/1520-0493\(1997\)125<1870:PODSMC>2.0.CO;2](https://doi.org/10.1175/1520-0493(1997)125<1870:PODSMC>2.0.CO;2).
- Smith, S. D., 1980: Wind stress and heat flux over the ocean in gale force winds. *J. Phys. Oceanogr.*, **10**, 709–726, [https://doi.org/10.1175/1520-0485\(1980\)010<0709:WSAHFO>2.0.CO;2](https://doi.org/10.1175/1520-0485(1980)010<0709:WSAHFO>2.0.CO;2).
- , and Coauthors, 1992: Sea surface wind stress and drag coefficients: The HEXOS results. *Bound.-Layer Meteor.*, **60**, 109–142, <https://doi.org/10.1007/BF00122064>.
- Soares, P. M. M., P. M. A. Miranda, A. P. Siebesma, and J. Teixeira, 2004: An eddy-diffusivity/mass-flux parameterization for dry and shallow cumulus convection. *Quart. J. Roy. Meteor. Soc.*, **130**, 3365–3384, <https://doi.org/10.1256/qj.03.223>.
- Sommeria, G., 1976: Three-dimensional simulation of turbulent processes in an undisturbed trade-wind boundary layer. *J. Atmos. Sci.*, **33**, 216–241, [https://doi.org/10.1175/1520-0469\(1976\)033<0216:TDSOTP>2.0.CO;2](https://doi.org/10.1175/1520-0469(1976)033<0216:TDSOTP>2.0.CO;2).
- , and M. A. LeMone, 1978: Direct testing of a three-dimensional model of the planetary boundary layer against experimental data. *J. Atmos. Sci.*, **35**, 25–39, [https://doi.org/10.1175/1520-0469\(1978\)035<0025:DTOATD>2.0.CO;2](https://doi.org/10.1175/1520-0469(1978)035<0025:DTOATD>2.0.CO;2).
- Sorbjan, Z., 1989: *Structure of the Atmospheric Boundary Layer*. Prentice Hall, 317 pp.
- Sorteberg, A., V. Kattsov, J. E. Walsh, and T. Pavlova, 2007: The Arctic surface energy budget as simulated with the IPCCAR4 AOGCMs. *Climate Dyn.*, **29**, 131–156, <https://doi.org/10.1007/s00382-006-0222-9>.
- Sotiropoulou, G., J. Sedlar, M. Tjernström, M. D. Shupe, I. M. Brooks, and P. O. G. Persson, 2014: The thermodynamic structure of summer Arctic stratocumulus and the dynamic coupling to the surface. *Atmos. Chem. Phys.*, **14**, 12 573–12 592, <https://doi.org/10.5194/acp-14-12573-2014>.
- Sotiropoulou, G. M., and Coauthors, 2016: Arctic Cloud Summer Experiment (ACSE): Boundary layer and cloud characteristics over ice and open-water, during the melt and freeze-up seasons. *J. Climate*, **29**, 8721–8744, <https://doi.org/10.1175/JCLI-D-16-0211.1>.
- Spalart, P. R., and J. H. Watmuff, 1993: Experimental and numerical study of a turbulent boundary layer with pressure gradients. *J. Fluid Mech.*, **249**, 337–371, <https://doi.org/10.1017/S002211209300120X>.
- Steenefeld, G. J., B. J. H. van de Wiel, and A. A. M. Houtslag, 2006: Modeling the evolution of the atmospheric boundary layer coupled to the surface for three contrasting nights in CASES-99. *J. Atmos. Sci.*, **63**, 920–935, <https://doi.org/10.1175/JAS3654.1>.
- Stevens, B., C.-H. Moeng, and P. P. Sullivan, 1999: Large-eddy simulations of radiatively driven convection: Sensitivity to the representation of small scales. *J. Atmos. Sci.*, **56**, 3963–3894, [https://doi.org/10.1175/1520-0469\(1999\)056<3963:LESORD>2.0.CO;2](https://doi.org/10.1175/1520-0469(1999)056<3963:LESORD>2.0.CO;2).
- , and Coauthors, 2003: Dynamics and Chemistry of Marine Stratocumulus—DYCOMS-II. *Bull. Amer. Meteor. Soc.*, **84**, 579–594, <https://doi.org/10.1175/BAMS-84-5-579>.

- , and Coauthors, 2005a: Evaluation of large-eddy simulations via observations of nocturnal marine stratocumulus. *Mon. Wea. Rev.*, **133**, 1443–1462, <https://doi.org/10.1175/MWR2930.1>.
- , G. Vali, K. Comstock, R. Wood, M. C. van Zanten, P. H. Austin, C. S. Bretherton, and D. H. Lenschow, 2005b: Pockets of open cells (POCs) and drizzle in marine stratocumulus. *Bull. Amer. Meteor. Soc.*, **86**, 51–57, <https://doi.org/10.1175/BAMS-86-1-51>.
- Stith, J., and Coauthors, 2019: 100 years of progress in atmospheric observing systems. *A Century of Progress in Atmospheric and Related Sciences: Celebrating the American Meteorological Society Centennial, Meteor. Monogr.*, No. 59, Amer. Meteor. Soc., <https://doi.org/10.1175/AMSMONOGRAPHS-D-18-0006.1>.
- Stoll, R., and F. Porté-Agel, 2009: Surface heterogeneity effects on regional-scale fluxes in stable boundary layers: Surface temperature transitions. *J. Atmos. Sci.*, **66**, 412–536, <https://doi.org/10.1175/2008JAS2668.1>.
- Stommel, H., 1947: Entrainment of air into a cumulus cloud. *J. Meteor.*, **4**, 91–94, [https://doi.org/10.1175/1520-0469\(1947\)004<0091:EOAIAC>2.0.CO;2](https://doi.org/10.1175/1520-0469(1947)004<0091:EOAIAC>2.0.CO;2).
- Stramler, K., A. D. Del Genio, and W. B. Rossow, 2011: Synoptically driven Arctic winter states. *J. Atmos. Sci.*, **24**, 1747–1762, <https://doi.org/10.1175/2010JCLI3817.1>.
- Strang, E. J., and J. S. Fernando, 2001: Vertical mixing and transports through a stratified shear layer. *J. Phys. Oceanogr.*, **31**, 2026–2048, [https://doi.org/10.1175/1520-0485\(2001\)031<2026:VMATTA>2.0.CO;2](https://doi.org/10.1175/1520-0485(2001)031<2026:VMATTA>2.0.CO;2).
- Stuart, J. T., 1967: On finite amplitude oscillations in laminar mixing layers. *J. Fluid Mech.*, **29**, 417–440, <https://doi.org/10.1017/S0022112067000941>.
- Stull, R. B., 1976: The energetics of entrainment across a density interface. *J. Atmos. Sci.*, **13**, 1260–1266, [https://doi.org/10.1175/1520-0469\(1976\)033<1260:T0E0AD>2.0.CO;2](https://doi.org/10.1175/1520-0469(1976)033<1260:T0E0AD>2.0.CO;2).
- , 1988: *An Introduction to Boundary Layer Meteorology*. Kluwer Academic, 666 pp.
- Sukoriansky, S., and B. Galperin, 2013: An analytical theory of the buoyancy–Kolmogorov subrange transition in turbulent flows with stable stratification. *Philos. Trans. Roy. Soc. London*, **371A**, <https://doi.org/10.1098/rsta.2012.0212>.
- Sullivan, P. P., and J. C. McWilliams, 2002: Turbulent flow over water waves in the presence of stratification. *Phys. Fluids*, **14**, 1182–1195, <https://doi.org/10.1063/1.1447915>.
- , and —, 2010: Dynamics of winds and currents coupled to surface waves. *Annu. Rev. Fluid Mech.*, **42**, 19–42, <https://doi.org/10.1146/annurev-fluid-121108-145541>.
- , and E. G. Patton, 2011: The effect of mesh resolution on convective boundary layer statistics and structures generated by large-eddy simulation. *J. Atmos. Sci.*, **68**, 2395–2415, <https://doi.org/10.1175/JAS-D-10-05010.1>.
- , J. C. McWilliams, and C.-H. Moeng, 1994: A subgrid-scale model for large-eddy simulation of planetary boundary-layer flows. *Bound.-Layer Meteor.*, **71**, 247–276, <https://doi.org/10.1007/BF00713741>.
- , T. W. Horst, D. H. Lenschow, C.-H. Moeng, and J. C. Weil, 2003: Structure of subfilter-scale fluxes in the atmospheric surface layer with applications to large-eddy simulation modeling. *J. Fluid Mech.*, **482**, 101–139, <https://doi.org/10.1017/S0022112003004099>.
- , J. B. Edson, T. S. Hristov, and J. C. McWilliams, 2008: Large-eddy simulations and observations of atmospheric marine boundary layers above nonequilibrium surface waves. *J. Atmos. Sci.*, **65**, 1225–1245, <https://doi.org/10.1175/2007JAS2427.1>.
- , J. C. McWilliams, and E. G. Patton, 2014: Large eddy simulation of marine atmospheric boundary layers above a spectrum of moving waves. *J. Atmos. Sci.*, **71**, 4001–4027, <https://doi.org/10.1175/JAS-D-14-0095.1>.
- , J. C. Weil, E. G. Patton, H. J. J. Jonker, and D. V. Mironov, 2016: Turbulent winds and temperature fronts in large-eddy simulations of the stable atmospheric boundary layer. *J. Atmos. Sci.*, **73**, 1815–1840, <https://doi.org/10.1175/JAS-D-15-0339.1>.
- , J. B. Edson, T. W. Horst, J. C. Wyngaard, and M. Kelly, 2006: Subfilter-scale fluxes in the marine surface layer: Results from the Ocean Horizontal Array Turbulence Study (OHATS). *17th Symp. on Boundary Layers and Turbulence*, San Diego, CA, Amer. Meteor. Soc., 4.1, <https://ams.confex.com/ams/pdfpapers/110884.pdf>.
- Sun, J., 1999: Diurnal variations of thermal roughness height over a grassland. *Bound.-Layer Meteor.*, **92**, 407–427, <https://doi.org/10.1023/A:1002071421362>.
- , L. Mahrt, R. M. Banta, and Y. L. Pichugina, 2012: Turbulence regimes and turbulence intermittency in the stable boundary layer during CASES-99. *J. Atmos. Sci.*, **69**, 338–351, <https://doi.org/10.1175/JAS-D-11-082.1>.
- , —, C. Nappo, and L. H. Lenschow, 2015: Wind and temperature oscillations generated by wave–turbulence interactions in the stably stratified boundary layer. *J. Atmos. Sci.*, **72**, 1484–1503, <https://doi.org/10.1175/JAS-D-14-0129.1>.
- , D. H. Lenschow, L. Mahrt, M. A. LeMone, and L. Mahrt, 2016: The role of large-coherent-eddy transport in the atmospheric surface layer based on CASES-99 observations. *Bound.-Layer Meteor.*, **160**, 83–111, <https://doi.org/10.1007/s10546-016-0134-0>.
- Svensson, G., and Coauthors, 2011: Evaluation of the diurnal cycle in the atmospheric boundary layer over land as represented by a variety of single-column models: The second GABLS experiment. *Bound.-Layer Meteor.*, **140**, 177–206, <https://doi.org/10.1007/s10546-011-9611-7>.
- Sverdrup, H. U., 1922: Meteorology on Captain Amundsen’s present Arctic expedition. *Mon. Wea. Rev.*, **50**, 74–75, [https://doi.org/10.1175/1520-0493\(1922\)50<74:MOCAPA>2.0.CO;2](https://doi.org/10.1175/1520-0493(1922)50<74:MOCAPA>2.0.CO;2).
- , 1925: The North-Polar cover of cold air. *Mon. Wea. Rev.*, **53**, 471–475, [https://doi.org/10.1175/1520-0493\(1925\)53<471:TNCOCA>2.0.CO;2](https://doi.org/10.1175/1520-0493(1925)53<471:TNCOCA>2.0.CO;2).
- , M. W. Johnson, and R. H. Fleming, 1942: *The Oceans: Their Physics, Chemistry, and General Biology*. Prentice Hall, 1087 pp.
- Swinbank, W. C., 1951: The measurement of vertical transfer of heat and water vapor and momentum in the lower atmosphere with some results. *J. Meteor.*, **8**, 135–145, [https://doi.org/10.1175/1520-0469\(1951\)008<0135:TMOVTO>2.0.CO;2](https://doi.org/10.1175/1520-0469(1951)008<0135:TMOVTO>2.0.CO;2).
- , 1964: The exponential wind profile. *Quart. J. Roy. Meteor. Soc.*, **90**, 119–135, <https://doi.org/10.1002/qj.49709038402>.
- , and A. J. Dyer, 1967: An experimental study in micrometeorology. *Quart. J. Roy. Meteor. Soc.*, **93**, 494–500, <https://doi.org/10.1002/qj.49709339808>.
- Sykes, R. I., and D. S. Henn, 1992: Large-eddy simulations of concentration fluctuations in a dispersing plume. *Atmos. Environ.*, **26A**, 3127–3144, [https://doi.org/10.1016/0960-1686\(92\)90470-6](https://doi.org/10.1016/0960-1686(92)90470-6).
- , W. S. Lewellen, and S. F. Parker, 1984: A turbulent-transport model for concentration fluctuations and fluxes. *J. Fluid Mech.*, **139**, 193–218, <https://doi.org/10.1017/S002211208400032X>.

- Tapp, M. C., and P. W. White, 1976: A non-hydrostatic mesoscale model. *Quart. J. Roy. Meteor. Soc.*, **102**, 277–296, <https://doi.org/10.1002/qj.49710243202>.
- Taylor, G. I., 1915: Eddy motion in the atmosphere. *Philos. Trans. Roy. Soc.*, **215A**, 1–26, <https://doi.org/10.1098/rsta.1915.0001>.
- , 1916: Skin friction of the wind on the earth's surface. *Proc. Roy. Soc. London*, **92A**, 196–199, <https://doi.org/10.1098/rspa.1916.0005>.
- , 1921: Diffusion by continuous movements. *Proc. London Math. Soc.*, **20**, 196–211.
- , 1935: Statistical theory of turbulence, I-IV. *Philos. Trans. Roy. Soc.*, **151A**, 421–478.
- Taylor, A. C., R. J. Beare, and D. J. Thomson, 2014: Simulating dispersion in the evening-transition boundary layer. *Bound.-Layer Meteor.*, **153**, 389–407, <https://doi.org/10.1007/s10546-014-9960-0>.
- Telford, J. W., and J. Warner, 1962: On the measurement from an aircraft of buoyancy and vertical air velocity in cloud. *J. Atmos. Sci.*, **19**, 415–423, [https://doi.org/10.1175/1520-0469\(1962\)019<0415:OTMFAA>2.0.CO;2](https://doi.org/10.1175/1520-0469(1962)019<0415:OTMFAA>2.0.CO;2).
- , and —, 1964: Fluxes of heat and vapor in the lower atmosphere derived from aircraft observations. *J. Atmos. Sci.*, **21**, 539–548, [https://doi.org/10.1175/1520-0469\(1964\)021<0539:FOHAVI>2.0.CO;2](https://doi.org/10.1175/1520-0469(1964)021<0539:FOHAVI>2.0.CO;2).
- Tennekes, H., 1970: Free convection in the turbulent Ekman layer of the atmosphere. *J. Atmos. Sci.*, **27**, 1027–1034, [https://doi.org/10.1175/1520-0469\(1970\)027<1027:FCITTE>2.0.CO;2](https://doi.org/10.1175/1520-0469(1970)027<1027:FCITTE>2.0.CO;2).
- Terai, C., C. S. Bretherton, R. Wood, and G. Painter, 2014: Aircraft observations of five pockets of open cells sampled during VOCALS REX. *Atmos. Chem. Phys.*, **14**, 8071–8088, <https://doi.org/10.5194/acp-14-8071-2014>.
- Thomas, C., and T. Foken, 2007: Organised motion in a tall spruce canopy: Temporal scales, structure spacing and terrain effects. *Bound.-Layer Meteor.*, **122**, 123–147, <https://doi.org/10.1007/s10546-006-9087-z>.
- , J. G. Martin, B. E. Law, and K. Davis, 2013: Toward biologically meaningful net carbon exchange estimates for tall, dense canopies: Multi-level eddy covariance observations and canopy coupling regimes in a mature Douglas-fir forest in Oregon. *Agric. For. Meteorol.*, **173**, 14–27, <https://doi.org/10.1016/j.agrformet.2013.01.001>.
- Thomson, D. J., 1987: Criteria for the selection of stochastic models of particle trajectories in turbulent flows. *J. Fluid Mech.*, **180**, 529–556, <https://doi.org/10.1017/S0022112087001940>.
- , 1990: A stochastic model for the motion of particle pairs in isotropic high Reynolds number turbulence, and its application to the problem of concentration variance. *J. Fluid Mech.*, **210**, 113–153, <https://doi.org/10.1017/S0022112090001239>.
- Thomson, W., 1887: On the propagation of laminar motion through a turbulently moving inviscid liquid. *London Edinburgh Dublin Philos. Mag. J. Sci.*, **24**, 342–353, <https://doi.org/10.1080/14786448708628110>.
- Tjernström, M., 2005: The summer Arctic boundary layer during the Arctic Ocean Experiment 2001 (AOE-2001). *Bound.-Layer Meteor.*, **117**, 5–36, <https://doi.org/10.1007/s10546-004-5641-8>.
- , 2007: Is there a diurnal cycle in Arctic summer cloud-capped boundary layer? *J. Atmos. Sci.*, **64**, 3970–3986, <https://doi.org/10.1175/2007JAS2257.1>.
- , and R. G. Graversen, 2009: The vertical structure of the lower Arctic troposphere analysed from observations and ERA-40 reanalysis. *Quart. J. Roy. Meteor. Soc.*, **135**, 431–433, <https://doi.org/10.1002/qj.380>.
- , C. Leck, P. O. G. Persson, M. L. Jensen, S. P. Oncley, and A. Targino, 2004: The summertime Arctic atmosphere: Meteorological measurements during the Arctic Ocean Experiment (AOE-2001). *Bull. Amer. Meteor. Soc.*, **85**, 1305–1322, <https://doi.org/10.1175/BAMS-85-9-1305>.
- , and Coauthors, 2005: Modeling the Arctic boundary layer: An evaluation of six ARCMIP regional-scale models with data from the SHEBA project. *Bound.-Layer Meteor.*, **117**, 337–381, <https://doi.org/10.1007/s10546-004-7954-z>.
- , J. Sedlar, and M. Shupe, 2008: How well do regional climate models reproduce radiation and clouds in the Arctic? An evaluation of ARCMIP simulations. *J. Appl. Meteor. Climatol.*, **47**, 2405–2422, <https://doi.org/10.1175/2008JAMC1845.1>.
- , and Coauthors 2014: The Arctic Summer Cloud Ocean Study (ASCOS): Overview and experimental design. *Atmos. Chem. Phys.*, **14**, 2823–2869, <https://doi.org/10.5194/acp-14-2823-2014>.
- Tomas, J. M., M. J. B. M. Pourquie, and H. J. J. Jonker, 2016: Stable stratification effects on flow and pollutant dispersion in boundary layers entering a generic urban environment. *Bound.-Layer Meteor.*, **159**, 221–239, <https://doi.org/10.1007/s10546-015-0124-7>.
- Tong, C., J. C. Wyngaard, S. Khanna, and J. G. Brasseur, 1998: Resolvable- and subgrid-scale measurement in the atmospheric surface layer: Technique and issues. *J. Atmos. Sci.*, **55**, 3114–3126, [https://doi.org/10.1175/1520-0469\(1998\)055<3114:RASSMI>2.0.CO;2](https://doi.org/10.1175/1520-0469(1998)055<3114:RASSMI>2.0.CO;2).
- , —, and J. G. Brasseur, 1999: Experimental study of the subgrid-scale stresses in the atmospheric surface layer. *J. Atmos. Sci.*, **56**, 2277–2292, [https://doi.org/10.1175/1520-0469\(1999\)056<2277:ESOTSS>2.0.CO;2](https://doi.org/10.1175/1520-0469(1999)056<2277:ESOTSS>2.0.CO;2).
- Troen, I., and L. Mahrt, 1986: A simple model of the atmospheric boundary layer; sensitivity to surface evaporation. *Bound.-Layer Meteor.*, **37**, 129–148, <https://doi.org/10.1007/BF00122760>.
- Tseng, Y.-H., C. Meneveau, and M. B. Parlange, 2006: Modeling flow around bluff bodies and predicting urban dispersion using large eddy simulation. *Environ. Sci.*, **40**, 2653–2662, <https://doi.org/10.1021/es051708m>.
- Twine, T. E., and Coauthors, 2000: Correcting eddy-covariance flux underestimates over a grassland. *Agric. For. Meteorol.*, **103**, 279–300, [https://doi.org/10.1016/S0168-1923\(00\)00123-4](https://doi.org/10.1016/S0168-1923(00)00123-4).
- Untersteiner, N., 1979: A review of the AIDJEX Project, 1970–77. *Polar Rec.*, **19**, 363–367, <https://doi.org/10.1017/S0032247400002114>.
- , and F. I. Badgley, 1965: The roughness parameters of sea ice. *J. Geophys. Sci.*, **70**, 4573–4577, <https://doi.org/10.1029/JZ070i018p04573>.
- USWB, 1918: Free-air data at Broken Arrow, Okla., Drexel, Nebr., Ellendle, N. Dak., and Royal Center, Ind. Aerological stations: July, August, and September 1918. *Mon. Wea. Rev.*, **46** (Suppl. 14), 5–8.
- Uttal, T., and Coauthors, 2002: The surface heat budget of the Arctic Ocean. *Bull. Amer. Meteor. Soc.*, **83**, 255–276, [https://doi.org/10.1175/1520-0477\(2002\)083<0255:SHBOTA>2.3.CO;2](https://doi.org/10.1175/1520-0477(2002)083<0255:SHBOTA>2.3.CO;2).
- Vali, G., R. D. Kelly, J. French, S. Haimov, D. Leon, R. E. McIntosh, and A. Pazmany, 1998: Finescale structure and microphysics of coastal stratus. *J. Atmos. Sci.*, **55**, 3540–3564, [https://doi.org/10.1175/1520-0469\(1998\)055<3540:FSAMOC>2.0.CO;2](https://doi.org/10.1175/1520-0469(1998)055<3540:FSAMOC>2.0.CO;2).
- van der Dussen, J. J., and Coauthors, 2013: The GASS/EUCLIPSE model intercomparison of the stratocumulus transition as observed during ASTEX: LES results. *J. Adv. Model. Earth Syst.*, **5**, 483–499, <https://doi.org/10.1002/jame.20033>.
- van de Wiel, B. J. H., R. J. Ronda, A. F. Moene, H. A. R. De Bruin, and A. A. M. Holtslag, 2002: Intermittent turbulence and oscillations in the stable boundary layer over land. Part I: A bulk

- model. *J. Atmos. Sci.*, **59**, 942–958, [https://doi.org/10.1175/1520-0469\(2002\)059<0942:ITAOIT>2.0.CO;2](https://doi.org/10.1175/1520-0469(2002)059<0942:ITAOIT>2.0.CO;2).
- , A. Moene, G. Hartogenesis, H. D. Bruin, and A. A. M. Holtslag, 2003: Intermittent turbulence in the stable boundary layer over land. Part III: A classification for observations during CASES-99. *J. Atmos. Sci.*, **60**, 2509–2522, [https://doi.org/10.1175/1520-0469\(2003\)060<2509:ITTSB>2.0.CO;2](https://doi.org/10.1175/1520-0469(2003)060<2509:ITTSB>2.0.CO;2).
- , —, G. J. Steeneveld, P. Baas, F. C. Bosveld, and A. A. M. Holtslag, 2010: A conceptual view on inertial oscillations and nocturnal low-level jets. *J. Atmos. Sci.*, **67**, 2679–2689, <https://doi.org/10.1175/2010JAS3289.1>.
- van Haren, L., and F. T. M. Nieuwstadt, 1989: The behavior of passive and buoyant plumes in a convective boundary layer, as simulated with a large-eddy model. *J. Appl. Meteor.*, **28**, 818–832, [https://doi.org/10.1175/1520-0450\(1989\)028<0818:TBOPAB>2.0.CO;2](https://doi.org/10.1175/1520-0450(1989)028<0818:TBOPAB>2.0.CO;2).
- van Hooff, J. A., S. Popinet, C. C. van Heerwaarden, S. J. A. van der Linden, S. R. de Roode, and B. J. H. van de Wiel, 2018: Towards adaptive grids for atmospheric boundary-layer simulations. *Bound.-Layer Meteor.*, **167**, 421–443, <https://doi.org/10.1007/s10546-018-0335-9>.
- van Ulden, A. P., 1978: Simple estimates for vertical dispersion from sources near the ground. *Atmos. Environ.*, **12**, 2125–2129, [https://doi.org/10.1016/0004-6981\(78\)90167-1](https://doi.org/10.1016/0004-6981(78)90167-1).
- van Zanten, M., and Coauthors, 2010: Controls on precipitation and cloudiness in simulations of trade-wind cumulus as observed during RICO. *J. Adv. Model. Earth Sys.*, **3**, M04001, <https://doi.org/10.1029/2011MS000056>.
- Venkatram, A., 1983: On dispersion in the convective boundary layer. *Atmos. Environ.*, **17**, 529–533, [https://doi.org/10.1016/0004-6981\(83\)90126-9](https://doi.org/10.1016/0004-6981(83)90126-9).
- , 1992: Vertical dispersion of ground-level releases in the surface boundary layer. *Atmos. Environ.*, **26A**, 947–949, [https://doi.org/10.1016/0960-1686\(92\)90253-H](https://doi.org/10.1016/0960-1686(92)90253-H).
- , D. Strimaitis, and D. Dicristofaro, 1984: A semiempirical model to estimate vertical dispersion of elevated releases in the stable boundary layer. *Atmos. Environ.*, **18**, 923–928, [https://doi.org/10.1016/0004-6981\(84\)90068-4](https://doi.org/10.1016/0004-6981(84)90068-4).
- Vercauteren, N., and R. Klein, 2015: A clustering method to characterize intermittent bursts of turbulence and interactions with submeso motions in the stable boundary layer. *J. Atmos. Sci.*, **72**, 1504–1517, <https://doi.org/10.1175/JAS-D-14-0115.1>.
- , L. Mahrt, and R. Klein, 2016: Investigation of interactions between scales of motion in the stable boundary layer. *Quart. J. Roy. Meteor. Soc.*, **142**, 2424–2433, <https://doi.org/10.1002/qj.2835>.
- Verkaik, J. W., and A. A. M. Holtslag, 2007: Wind profiles, momentum fluxes, and roughness lengths at Cabauw revisited. *Bound.-Layer Meteor.*, **122**, 701–719, <https://doi.org/10.1007/s10546-006-9121-1>.
- Verlinde, J., and Coauthors, 2007: The Mixed-Phase Arctic Cloud Experiment. *Bull. Amer. Meteor. Soc.*, **88**, 205–221, <https://doi.org/10.1175/BAMS-88-2-205>.
- Veron, F., 2015: Ocean spray. *Annu. Rev. Fluid Mech.*, **47**, 507–538, <https://doi.org/10.1146/annurev-fluid-010814-014651>.
- Vickers, D., and C. K. Thomas, 2014: Observations of the scale-dependent turbulence and evaluation of the flux–gradient relationship for sensible heat for a closed Douglas-fir canopy in very weak wind conditions. *Atmos. Chem. Phys.*, **14**, 9665–9676, <https://doi.org/10.5194/acp-14-9665-2014>.
- , L. Mahrt, and D. Belusic, 2008: Particle simulations of dispersion using observed meandering and turbulence. *Acta Geophys.*, **56**, 234–256, <https://doi.org/10.2478/s11600-007-0041-3>.
- Vignon, E., and Coauthors, 2017: Stable boundary-layer regimes at Dome C, Antarctica: Observation and analysis. *Quart. J. Roy. Meteor. Soc.*, **143**, 1241–1253, <https://doi.org/10.1002/qj.2998>.
- Vihma, T., J. Jaagus, E. Jakobson, and T. Palo, 2008: Meteorological conditions in the Arctic Ocean in spring and summer 2007 as recorded on the drifting ice station Tara. *Geophys. Res. Lett.*, **35**, L18706, <https://doi.org/10.1029/2008GL034681>.
- Viterbo, P., and A. C. Beljaars, 1995: An improved land surface parameterization scheme in the ECMWF model and its validation. *J. Climate*, **8**, 2716–2748, [https://doi.org/10.1175/1520-0442\(1995\)008<2716:AILSPS>2.0.CO;2](https://doi.org/10.1175/1520-0442(1995)008<2716:AILSPS>2.0.CO;2).
- von Ficker, H., 1936: Die Passatinversion. Veröffentlichungen des Meteorologischen Instituts der Universität Berlin, Vol I, Heft 4, 33 pp.
- von Kármán, T., 1931: Mechanische Ähnlichkeit und Turbulenz. *Proc. Third Int. Congress on Applied Mechanics*, Vol. 1, Stockholm, Sweden, 85–93.
- Wakefield, J. S., and W. H. Schubert, 1976: Design and execution of the Marine Stratocumulus Experiment. Colorado State University Atmospheric Science Paper 256, 74 pp.
- , and —, 1981: Mixed-layer simulation of eastern North Pacific stratocumulus. *Mon. Wea. Rev.*, **109**, 1952–1968, [https://doi.org/10.1175/1520-0493\(1981\)109<1952:MLMSOE>2.0.CO;2](https://doi.org/10.1175/1520-0493(1981)109<1952:MLMSOE>2.0.CO;2).
- Walko, R. L., W. R. Cotton, and R. A. Pielke, 1992: Large-eddy simulations of the effects of hilly terrain on the convective boundary layer. *Bound.-Layer Meteor.*, **58**, 133–150, <https://doi.org/10.1007/BF00120755>.
- Wang, H., G. Feingold, R. Wood, and J. Kazil, 2010: Modelling microphysical and meteorological controls on precipitation and cloud cellular structures in Southeast Pacific stratocumulus. *Atmos. Chem. Phys.*, **10**, 6347–6362, <https://doi.org/10.5194/acp-10-6347-2010>.
- Warren, S. G., C. J. Hahn, J. London, R. M. Chervin, and R. L. Jenne, 1986: Global distribution of total cloud cover and cloud type amounts over land. NCAR Tech. Note NCAR/TN-273+STR, 29 pp., <https://doi.org/10.5065/D6GH9FXB>.
- , —, —, —, and —, 1988: Global distribution of total cloud cover and cloud type amounts over the ocean. NCAR Tech. Note NCAR/TN-317+STR, 41 pp., <https://doi.org/10.5065/D6QC01D1>.
- Webster, C. J., 1954: The Soviet expedition to the Central Arctic. *Arctic*, **7**, 58–80, <https://doi.org/10.14430/arctic3830>.
- Weckwerth, T. W., J. W. Wilson, R. M. Wakimoto, and N. A. Crook, 1997: Horizontal convective rolls: Determining the environmental conditions supporting their existence and characteristics. *Mon. Wea. Rev.*, **125**, 505–526, [https://doi.org/10.1175/1520-0493\(1997\)125<0505:HCRDTE>2.0.CO;2](https://doi.org/10.1175/1520-0493(1997)125<0505:HCRDTE>2.0.CO;2).
- , and Coauthors, 2004: An overview of the International H₂O Project (IHOP 2002) and some preliminary highlights. *Bull. Amer. Meteor. Soc.*, **85**, 253–277, <https://doi.org/10.1175/BAMS-85-2-253>.
- Weil, J. C., 1988: Dispersion in the convective boundary layer. *Lectures on Air Pollution Modeling*, A. Venkatram and J. C. Wyngaard, Eds., Amer. Meteor. Soc., 167–227.
- , 1990: A diagnosis of the asymmetry in top-down and bottom-up diffusion using a Lagrangian stochastic model. *J. Atmos. Sci.*, **47**, 501–515, [https://doi.org/10.1175/1520-0469\(1990\)047<0501:ADOTAI>2.0.CO;2](https://doi.org/10.1175/1520-0469(1990)047<0501:ADOTAI>2.0.CO;2).
- , 2013: Atmospheric dispersion. *Handbook of Environmental Fluid Dynamics*, Vol. 2, H. J. S. Fernando, Ed., CRC Press, 163–174.

- , and T. W. Horst, 1992: Footprint estimates for atmospheric flux measurements in the convective boundary layer. *Precipitation Scavenging and Atmosphere-Surface Exchange*, Vol. 2, S. E. Schwartz and W. G. N. Slinn, Eds., Hemisphere Publishing, 717–728.
- , W. H. Snyder, R. E. Lawson Jr., and M. S. Shipman, 2002: Experiments on buoyant plume dispersion in a laboratory convection tank. *Bound.-Layer Meteor.*, **102**, 367–414, <https://doi.org/10.1023/A:1013874816509>.
- , P. P. Sullivan, and C.-H. Moeng, 2004: The use of large-eddy simulations in Lagrangian particle dispersion models. *J. Atmos. Sci.*, **61**, 2877–2887, <https://doi.org/10.1175/JAS-3302.1>.
- , —, E. G. Patton, and C.-H. Moeng, 2012: Statistical variability of dispersion in the convective boundary layer: Ensembles of simulations and observations. *Bound.-Layer Meteor.*, **145**, 185–210, <https://doi.org/10.1007/s10546-012-9704-y>.
- , —, G. Patton, and A. Wyszogrodski, 2017: Concentration fluctuations and variability at local and regional scales: Use of a Lagrangian two-particle dispersion model coupled with LES fields. *Air Pollution Modeling and its Application XXV*, C. Mensink and G. Kallos, Eds., Springer, 281–285.
- Weligepolage, K., A. S. M. Gieske, C. van der Tol, J. Timmermans, and Z. Su, 2012: Effect of sub-layer corrections on the roughness parameterization of a Douglas fir forest. *Agric. For. Meteorol.*, **162–163**, 115–126, <https://doi.org/10.1016/j.agrformet.2012.04.017>.
- Whiteman, C. D., T. Haiden, B. Pospichal, S. Eisenbach, and R. Steinacker, 2004: Minimum temperatures, diurnal temperature ranges, and temperature inversions in limestone sinkholes of different sizes and shapes. *J. Appl. Meteorol.*, **43**, 1224–1236, [https://doi.org/10.1175/1520-0450\(2004\)043<1224:MTDTRA>2.0.CO;2](https://doi.org/10.1175/1520-0450(2004)043<1224:MTDTRA>2.0.CO;2).
- Wieringa, J., 1976: An objective exposure correction method for average wind speeds measured at a sheltered location. *Quart. J. Roy. Meteor. Soc.*, **102**, 241–253, <https://doi.org/10.1002/qj.49710243119>.
- , 1980: A reevaluation of the Kansas mast influence on measurements of stress and cup anemometer overspeeding. *Bound.-Layer Meteorol.*, **18**, 411–430, <https://doi.org/10.1007/BF00119497>.
- Willis, G. E., and J. W. Deardorff, 1974: A laboratory model of the unstable boundary layer. *J. Atmos. Sci.*, **31**, 1297–1307, [https://doi.org/10.1175/1520-0469\(1974\)031<1297:ALMOTU>2.0.CO;2](https://doi.org/10.1175/1520-0469(1974)031<1297:ALMOTU>2.0.CO;2).
- , and —, 1976: A laboratory model of diffusion into the convective planetary boundary layer. *Quart. J. Roy. Meteor. Soc.*, **102**, 427–445, <https://doi.org/10.1002/qj.49710243212>.
- , and —, 1978: A laboratory study of dispersion from an elevated source within a modeled convective planetary boundary layer. *Atmos. Environ.*, **12**, 1305–1312, [https://doi.org/10.1016/0004-6981\(78\)90069-0](https://doi.org/10.1016/0004-6981(78)90069-0).
- , and —, 1981: A laboratory study of dispersion from a source in the middle of the convectively mixed layer. *Atmos. Environ.*, **15**, 109–117, [https://doi.org/10.1016/0004-6981\(81\)90001-9](https://doi.org/10.1016/0004-6981(81)90001-9).
- , and —, 1983: On plume rise within the convective boundary layer. *Atmos. Environ.*, **17**, 2435–2447, [https://doi.org/10.1016/0004-6981\(83\)90068-9](https://doi.org/10.1016/0004-6981(83)90068-9).
- , and —, 1987: Buoyant plume dispersion and inversion entrainment in and above a laboratory mixed layer. *Atmos. Environ.*, **21**, 1725–1735, [https://doi.org/10.1016/0004-6981\(87\)90111-9](https://doi.org/10.1016/0004-6981(87)90111-9).
- Wilson, T. H., and R. G. Fovell, 2018: Modeling the evolution and life cycle of radiative cold pools and fog. *Wea. Forecasting*, **33**, 203–220, <https://doi.org/10.1175/WAF-D-17-0109.1>.
- Wilson, J. D., and B. L. Sawford, 1997: Review of Lagrangian stochastic models for trajectories in the turbulent atmosphere. *Bound.-Layer Meteorol.*, **84**, 411–425, <https://doi.org/10.1023/A:1000474206967>.
- Wood, E. F., D. P. Lettenmaier, and V. G. Zartarian, 1992: A land-surface hydrology parameterization with subgrid variability for general circulation models. *J. Geophys. Res.*, **97**, 2717–2728, <https://doi.org/10.1029/91JD01786>.
- , and Coauthors, 1998: The Project for Intercomparison of Land-surface Parameterization Schemes (PILPS) Phase 2 (c) Red-Arkansas River basin experiment: 1. Experiment description and summary intercomparisons. *Global Planet. Change*, **19**, 115–135, [https://doi.org/10.1016/S0921-8181\(98\)00044-7](https://doi.org/10.1016/S0921-8181(98)00044-7).
- Wood, N., and P. J. Mason, 1991: The influence of static stability on the effective roughness lengths for momentum and heat flux. *Quart. J. Roy. Meteor. Soc.*, **117**, 1025–1056, <https://doi.org/10.1002/qj.49711750108>.
- Wood, R., C. S. Bretherton, D. Leon, A. D. Clarke, P. Zuidema, G. Allen, and H. Coe, 2011a: An aircraft case study of the spatial transition from closed to open mesoscale cellular convection over the southeast Pacific. *Atmos. Chem. Phys.*, **11**, 2341–2370, <https://doi.org/10.5194/acp-11-2341-2011>.
- , and Coauthors, 2011b: The VAMOS Ocean-Cloud-Atmosphere-Land Study Regional Experiment (VOCALS-REx): Goals, platforms, and field operations. *Atmos. Chem. Phys.*, **11**, 627–654, <https://doi.org/10.5194/acp-11-627-2011>.
- Woodcock, A., 1941: Soaring over the open sea. *Sci. Mon.*, **25**, 226–232.
- Wyant, M. C., C. S. Bretherton, H. A. Rand, and D. E. Stevens, 1997: Numerical simulations and a conceptual model of the subtropical marine stratocumulus to trade cumulus transition. *J. Atmos. Sci.*, **54**, 168–192, [https://doi.org/10.1175/1520-0469\(1997\)054<0168:NSAACM>2.0.CO;2](https://doi.org/10.1175/1520-0469(1997)054<0168:NSAACM>2.0.CO;2).
- Wyngaard, J. C., 1981: The effects of probe-induced flow distortion on atmospheric turbulence measurements. *J. Appl. Meteorol.*, **20**, 784–794, [https://doi.org/10.1175/1520-0450\(1981\)020<0784:TEOPIF>2.0.CO;2](https://doi.org/10.1175/1520-0450(1981)020<0784:TEOPIF>2.0.CO;2).
- , 1988: Introduction. *Lectures on Air Pollution Modeling*, A. Venkatram and J. C. Wyngaard, Eds., Amer. Meteor. Soc., 1–7.
- , 2004: Towards numerical modeling in the “terra incognita.” *J. Atmos. Sci.*, **61**, 1816–1826, [https://doi.org/10.1175/1520-0469\(2004\)061<1816:TNMITT>2.0.CO;2](https://doi.org/10.1175/1520-0469(2004)061<1816:TNMITT>2.0.CO;2).
- , 2010: *Turbulence in the Atmosphere*. Cambridge University Press, 393 pp.
- Wyser, K., and Coauthors, 2008: An evaluation of Arctic cloud and radiation processes during the SHEBA year: Simulation results from 8 Arctic regional climate models. *Climate Dyn.*, **30**, 203–223, <https://doi.org/10.1007/s00382-007-0286-1>.
- Xue, M., and Coauthors, 2001: The Advanced Regional Prediction System (ARPS): A multi-scale nonhydrostatic atmospheric simulation and prediction tool. Part II: Model physics and applications. *Meteor. Atmos. Phys.*, **76**, 143–165, <https://doi.org/10.1007/s007030170027>.
- Yague, C., S. Viana, G. Maqueda, and J. M. Redondo, 2006: Influence of stability on the flux-profile relationships for wind speed, θ_m , and temperature, θ_n for the stable atmospheric boundary layer. *Nonlinear Processes Geophys.*, **13**, 185–203, <https://doi.org/10.5194/npg-13-185-2006>.
- Yamada, T., and G. Mellor, 1975: A simulation of the Wangara atmospheric boundary layer data. *J. Atmos. Sci.*, **32**, 2309–2329, [https://doi.org/10.1175/1520-0469\(1975\)032<2309:ASOTWA>2.0.CO;2](https://doi.org/10.1175/1520-0469(1975)032<2309:ASOTWA>2.0.CO;2).

- Yan, H., and R. A. Anthes, 1988: The effect of variations in surface moisture on mesoscale circulations. *Mon. Wea. Rev.*, **116**, 192–208, [https://doi.org/10.1175/1520-0493\(1988\)116<0192:TEOVIS>2.0.CO;2](https://doi.org/10.1175/1520-0493(1988)116<0192:TEOVIS>2.0.CO;2).
- Young, G. S., D. A. R. Kristovich, M. R. Hjelmfelt, and R. C. Foster, 2002: Rolls, streets, waves, and more: A review of quasi-two-dimensional structures in the atmospheric boundary layer. *Bull. Amer. Meteor. Soc.*, **83**, 997–1001, [https://doi.org/10.1175/1520-0477\(2002\)083<0997:RSWAMA>2.3.CO;2](https://doi.org/10.1175/1520-0477(2002)083<0997:RSWAMA>2.3.CO;2).
- Zappa, C. J., M. L. Banner, H. Schultz, J. R. Gemmrich, R. P. Morison, D. A. LeBel, and T. Dickey, 2012: An overview of sea state conditions and air-sea fluxes during RaDyO. *J. Geophys. Res.*, **117**, C00H19, <https://doi.org/10.1029/2011JC007336>.
- Zhang, C., R. H. Shaw, and K. T. Paw U, 1992: Spatial characteristics of turbulent coherent structures within and above an orchard canopy. *Precipitation Scavenging And Atmosphere-Surface Exchange*, S. E. Schwartz and W. G. N. Slinn, Eds., CRC Press, 603–1172.
- Zhang, D.-L., and R. A. Anthes, 1982: A high-resolution model of the planetary boundary layer—Sensitivity tests and comparisons with SESAME-79 data. *J. Appl. Meteor.*, **21**, 1594–1609, [https://doi.org/10.1175/1520-0450\(1982\)021<1594:AHRMOT>2.0.CO;2](https://doi.org/10.1175/1520-0450(1982)021<1594:AHRMOT>2.0.CO;2).
- Zhang, G., F. Chen, and Y. Gan, 2016: Assessing uncertainties in the Noah-MP ensemble simulations of a cropland site during the Tibet Joint International Cooperation program field campaign. *J. Geophys. Res. Atmos.*, **121**, 9576–9596, <https://doi.org/10.1002/2016JD024928>.
- Zhang, J. A., P. G. Black, J. R. French, and W. M. Drennan, 2008: First direct measurements of enthalpy flux in the hurricane boundary layer: The CBLAST results. *Geophys. Res. Lett.*, **35**, L14813, <https://doi.org/10.1029/2008GL034374>.
- Zhou, B., and F. K. Chow, 2011: Large-eddy simulation of the stable boundary layer with explicit filtering and reconstruction turbulence modeling. *J. Atmos. Sci.*, **68**, 2142–2155, <https://doi.org/10.1175/2011JAS3693.1>.
- , J. S. Simon, and F. K. Chow, 2014: The convective boundary layer in the terra incognita. *J. Atmos. Sci.*, **71**, 2545–2563, <https://doi.org/10.1175/JAS-D-13-0356.1>.
- , M. Xue, and K. Zhu, 2017: A grid-refinement-based approach for modeling the convective boundary layer in the gray zone: A pilot study. *J. Atmos. Sci.*, **74**, 3497–3513, <https://doi.org/10.1175/JAS-D-16-0376.1>.
- Zhu, P., and Coauthors, 2005: Intercomparison and interpretation of single-column model simulations of a nocturnal stratocumulus-topped marine boundary layer. *Mon. Wea. Rev.*, **133**, 2741–2758, <https://doi.org/10.1175/MWR2997.1>.
- , B. A. Albrecht, V. P. Ghate, and Z. Zhu, 2010: Multiple-scale simulations of stratocumulus clouds. *J. Geophys. Res.*, **115**, D23201, <https://doi.org/10.1029/2010JD014400>.
- Zilitinkevich, S. S., 1970: *Dynamics of the Atmospheric Boundary Layer*. Leningrad Gidrometeor., 291 pp.
- , T. Elperin, N. Kleerorin, I. Rogachevskii, and I. Esau, 2013: A hierarchy of energy- and flux-budget (EFB) turbulence closure models for stably-stratified geophysical flows. *Bound.-Layer Meteor.*, **146**, 341–373, <https://doi.org/10.1007/s10546-012-9768-8>.